microRNAs in the interaction between osteoarthritis and muscle atrophy

Thesis submitted in accordance with the requirements of the University of Liverpool for the degree of Doctor in Philosophy by:

Emily Shorter

October 2022

Abstract

Musculoskeletal tissue dysfunction is the leading cause of frailty, falls, and decreased quality of life in older people. Osteoarthritis (OA), the most common chronic joint disorder, was initially characterised by deterioration of the articular cartilage, but is now considered to be a disease of the entire joint. Linked to the joint, peri-articular muscles also play a major role in joint function and stability. Muscle atrophy is defined as the loss of muscle mass and strength with age. Despite the high prevalence of both muscle atrophy and OA in older populations, little is known about the interaction between the two disorders - in particular the molecular interaction and involvement of post-transcriptional regulators, such as miRNAs.

The following research uses molecular and histological techniques to characterise OA-associated muscle atrophy, and whether treatment with miR-378a-3p – a sarcopenia associated myomiR - may restore musculoskeletal tissue function *in vivo*. Results show that peri-articular quadriceps muscles experience significant atrophy in response to mechanical loading-induced OA. These quadriceps muscles are characterised by overexpression of muscle atrophy marker 'ATROGIN-1', downregulation of miR-378a-3p, and concurrent upregulation of its target gene 'P62'.

This research also proposes the CD1 strain of mice as a novel model of spontaneous OA, demonstrating significant development of articular cartilage lesions at 6-months of age in this model. Muscle atrophy is also shown at this age in the gastrocnemius muscles, which significantly correlates with OA severity in the joint. Moreover, the quadriceps exhibit a decrease in miR-378a-3p expression, similar to that of the loading model.

Intravenous treatment with a miR-378a-3p inhibitor in older mice with load-induced OA resulted in a 25% less severe OA and a 9-12% increase in muscle fiber CSA, compared to treatment with a control microRNA. The improvement in muscle health, observed histologically as increased fiber CSA, was also reflected behaviourally with improved grip strength. Absence of changes in subchondral bone with miR-378a-3p treatment compared to control indicates that miR-378a-3p may help to protect the bone against the effects of the load-induced OA.

Finally, to investigate genetic dysregulation in human OA, p-value based meta-analyses were used to discover significantly differentially expressed OA-associated microRNAs and genes in human OA cartilage vs healthy controls. Experimental confirmation of these bioinformatic analyses, using mass spectrometry data, revealed 7 proteins that are significantly differentially expressed in human OA cartilage. Ultimately, this will allow for future research to focus on genes that may be of higher importance to OA pathogenesis and assess their suitability as drug targets or disease biomarkers.

Overall, this research is the first to characterise muscle atrophy in non-surgical murine models of OA and provides evidence that OA and muscle atrophy are intricately linked. Moreover, it demonstrates the potential of microRNA-based therapies for age-related musculoskeletal diseases.

Contents

List of Figures

List of Tables

List of Abbreviations

Abbreviations	Full Description
AC	Articular cartilage
ACL	Anterior cruciate ligament
ACLT	Anterior cruciate ligament transection
ANOVA	Analysis of variance
CO_2	Carbon Dioxide
COL2	Collagen type II
CSA	Cross-sectional area
DAPI	4′,6-diamidino-2-phenylindole
DMEM	Dulbecco's Modified Eagle Medium
DMM	Destabilisation of the medial meniscus
DNA	Deoxyribonucleic acid
ECM	Extracellular matrix
EDTA	Ethylenediaminetetraacetic acid
GAGs	Glycosaminoglycans
Gastroc	Gastrocnemius muscles
IL	Interleukin
IPA	Ingenuity pathway analysis
LF	Lateral femur
LT	Lateral tibia
MCL	Medial collateral ligament
MF	Medial femur

mg	Milligram
miRNA	microRNA
mL	Milliliter
mm	Millimeter
MMP	Matrix metalloproteinase
mRNA	Messenger RNA
MT	Medial tibia
myomiR	Muscle specific microRNAs
O_2	Oxygen
OA	Osteoarthritis / osteoarthritic
OARSI	Osteoarthritis Research Society International
OCT	Optimal cutting temperature compound
PBS	Phosphate-buffered saline
PCL	Posterior cruciate ligament
PTOA	Post-traumatic OA
qRT-PCR	Quantitative real-time polymerase chain reaction
Quad	Quadricep muscle
RNA	Ribonucleic acid
RNase	Ribonuclease
Tol Blue	Toludine blue stain
type I	Slow-twitch muscle fibers
type IIb	Fast-twitch muscle fibers

Acknowledgements

I would firstly like to thank my supervisory team for their continuous support over the last 4 years - it has truly been a collaborative process. Dr Blandine Poulet introduced me to histology and *in vivo* models, Dr Kasia Whysall has answered all my many microRNA-related questions, and Professor George Bou-Gharios helped me to understand the extracellular matrix and all it's complexity. I am so grateful for all of their help and expertise and hope to keep the collaboration going in the next step of my academic career.

My lovely family also deserve a huge thank you for their unconditional support and encouragement in all my endeavours – PhD included! My parents have always provided a safe and loving environment for me to pursue my interests and I truly could not have done this without them! My wonderful partner, Dennis, has always been my biggest advocate (and spell checker!) and I'm so grateful for all his support and love over the last 10 years. Our two cats, Buddy and Badger, also deserve a special mention, their mischief has been a source of endless entertainment. My sister, Hannah, is always dependable for some comedic relief – I am a very proud older sister!

Finally, a big thank you to the Institute of Life Course and Medical Sciences and the Biotechnology and Biological Sciences Research Council for funding my PhD project. I will really miss Liverpool but am excited to start the next chapter of my career!

Chapter 1: Introduction

1.1 The Healthy Joint

1.1.1. Structure and Function

The knee joint consists of the tibiofemoral, the patellofemoral and the proximal tibiofibular joint. Its complex structure consists of an interplay between the femur, tibia, patella and fibula as well as its ligaments, tendons, meniscus, muscles and joint capsule (Hirschmann and Müller, 2015). It is a gliding hinge joint with its principle kinematics being: rolling, gliding and rotation. The joint has six degrees of freedom for rotation and translation - flexion-extension, internal-external tibial rotation, abduction-adduction, medial-lateral joint space opening, anterior-posterior displacement, and compression-distraction (Noyes et al., 1991). A number of ligaments and muscles provide stability in all directions to the knee joint which is optimally adapted for carrying a large portion of our body weight and allows a wide range of motion for flexion–extension. A diagram of the knee joint and its various tissues is shown in figure 1.1.

The articulation between the femur and tibia bears most of the body weight, while the articulation between the patella and femur creates a frictionless transfer over the knee of the forces generated by contraction of the quadriceps femoris muscle (Whitesides, 2001). The intercondylar articular cavity of the knee is enclosed by a fibrous joint capsule. Primary stabilisation of the knee is achieved through the ligaments. The medial and lateral collateral ligaments reinforce the joint and the two stronger cruciate ligaments prevent excessive displacement of the tibia in relation to the femur (Abulhasan and Grey, 2017). Two fibrocartilaginous menisci are positioned between the medial and lateral femoral condyles and the tibia and work to accommodate changes in the shape of the articular surfaces during activity. Moreover, articular cartilage covers both the femoral and tibial condyles and provides a frictionless surface that allows joint movement (Abulhasan and Grey, 2017).

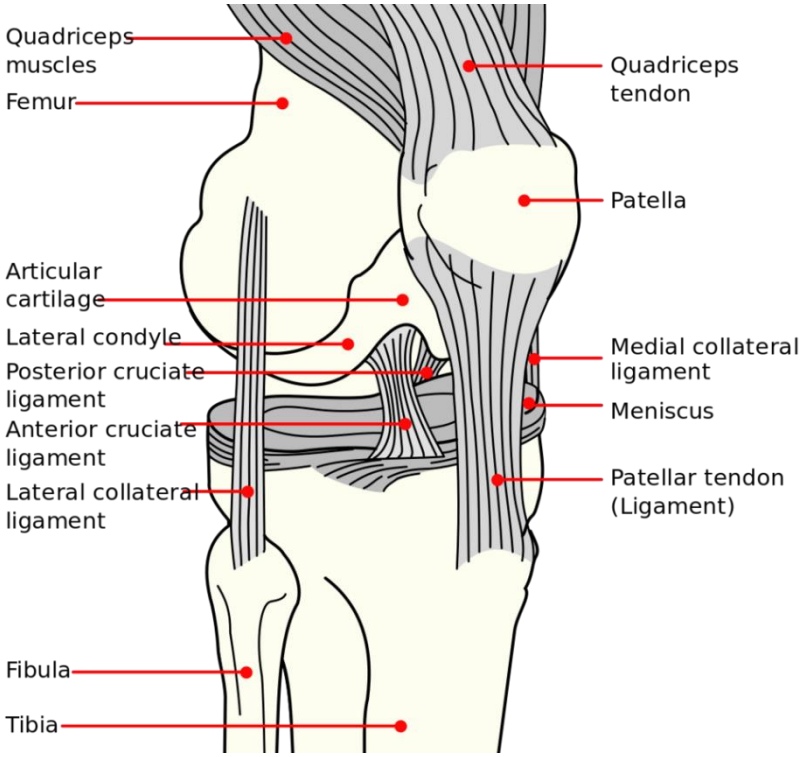

Figure 1.1: A diagram of a healthy knee joint and its constituent tissues. *The diagram was obtained from 'WikiMSK' and is subject to the compatible CC-BY-SA license.*

Attached to the knee joint is the periarticular skeletal muscles - one of the most dynamic and plastic tissues of the human body (Kim et al., 2016). Skeletal muscle is a striated tissue designed to accomplish the task of generating contraction, force and movement. Briefly, skeletal muscle is a highly organised tissue containing several bundles of muscle fibers – otherwise known as myofibers – contained in a connective tissue sheath known as a perimysium. Each myofiber contains several myofibrils which are, in turn, composed of sarcomeres - the smallest functional unit of striated muscle tissue. The ordered structure of each sarcomere is based on the ordered alignment of two sets of filaments: thick filaments composed of myosin and myosin binding proteins, and thin filaments composed of actin, nebulin and regulatory proteins (Bottinellia and Reggiani, 2000). As the muscle is attached to the bone tendons, its contraction leads to movement of that bone which allows for the performance of specific movements as well as structural support (Dave et al., 2021).

1.1.2. Articular Cartilage

Articular cartilage is a highly specialized, avascular, connective tissue in the joint. Its principal function is to provide a smooth, lubricated surface for articulation and to facilitate the transmission of mechanical load. It is composed of a dense extracellular matrix (ECM) with a sparse distribution of highly specialised cells called chondrocytes, which are the only cell type of the cartilage (Fox et al., 2009). Articular cartilage has an organized layered structure that is divided into four zones: superficial, middle, deep, and calcified (Pearle et al., 2005). Chondrocytes proliferate and secrete ECM to maintain the cartilage. The cartilage ECM is composed primarily of the network type II collagen, which provides tensile support for the tissue, and an interlocking mesh of fibrous proteins and proteoglycans, hyaluronic acid, and chondroitin sulfate (Gao et al., 2014). Aggrecan, a negatively charged proteoglycan, attracts water molecules and enables the shock absorbing capability of cartilage upon mechanical loading (Maldonado and Nam et al., 2013). Aggrecan itself is composed of chondroitin sulfate and keratan sulfate that bind to the linear core protein and connect to the hyaluronic acid backbone (Guilak et al., 2018). Chondroitin sulfate is the most abundant constituent of cartilage proteoglycan and is a member of sulfated glycosaminoglycans (GAGs) - long unbranched polysaccharides. Hyaluronic acid is another GAG which provides lubrication and viscoelasticity of the joint's synovial fluid (Gupta et al., 2019). Finally, fibronectin is a glycoprotein whose roles range from being a component of the cell matrix adhesion complex to enabling ECM organisation (Chevalier, 1993). Maintenance of the ECM and its components is a delicate balance that is mediated by a number of proteases produced by chondrocytes. The chondrocytes respond to external stimuli (such as mechanical force), proliferate, and secrete ECM to maintain the articular cartilage.

1.1.3. Peri-articular Muscles

Skeletal muscle is a highly organised, innervated, and voluntary muscle type with a high energy requirement. It is one of the most dynamic and plastic tissues of the human body, comprising approximately 40 % of total body weight (Kim et al., 2016). Skeletal

muscle is a striated tissue designed to accomplish the task of generating contraction, force and movement. Each muscle consists of a bundle of muscle fibers (called myofibers) that themselves consist of many myofibrils. These myofibrils are, in turn, composed of sarcomeres - the smallest functional unit of striated muscle tissue. The ordered structure of each sarcomere is based on the ordered alignment of two sets of filaments: thick filaments composed of myosin and myosin binding proteins, and thin filaments composed of actin, nebulin and regulatory proteins (Bottinellia and Reggiani, 2000).

One of the hallmarks of adult skeletal muscle is its ability to regenerate, a process largely driven by the interaction between satellite cells and their niche – a particular microenvironment within the skeletal muscle. Satellite cells are typically quiescent and lie between the basal lamina, where they are anchored by an actin cytoskeleton, and the sarcolemma (Blanco-Bose et al., 2001). The niche where the satellite cells are sequestered is composed of growth factors, ECM proteins, fibroadipogenic progenitors, chemokines, and matrix metalloproteinases (Dumont et al., 2015). A hierarchy of transcription factors – such as MYF5 and MYOD1 - regulate the myogenic lineage, which are activated in response to muscle injury. These environmental cues trigger activation of satellite cells, where they differentiate to mature fibers and replace the damaged ones (Mukund and Subramaniam, 2020). There are a variety of transcription factors that regulate the myogenic lineage. For example, The myogenic regulatory factors (MRFs) Myf5, MyoD, myogenin and MRF4 are members of the basic helix-loop-helix family of transcription factors that control the determination and differentiation of skeletal muscle cells (Hernández-Hernández et al., 2017). The terminal differentiation of muscle cells starts when Pax3+ and/or Pax7+ progenitors begin to express Myf5 or MyoD as committed myoblasts. These myoblasts gradually express myogenin (MyoG) and form single-nucleated nascent myotubes with myosin heavy chain (MHC+). Myotube fusion to form multinucleated myotubes is then initiated by insulin-like growth factor-I (IGF-I), TGF-β1 inhibitor, and myostatin inhibitors (Jiwlawat et al., 2018). A diagram of these main transcription factors alongside muscle lineage is depicted in figure 1.2.

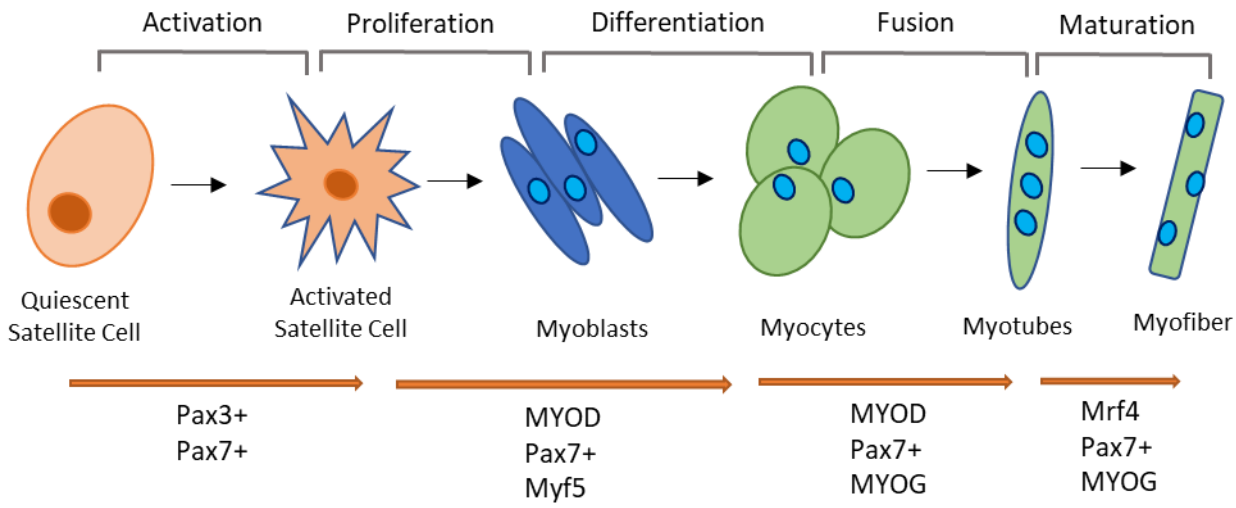

Figure 1.2: A diagram of the main transcription factors involved in the activation and differentiation of quiescent satellite cells into mature myofibers. *Satellite cells remain quiescent and are characterized by expression of PAX7. Terminal differentiation occurs when PAX7+ progenitors begin to express Myf5 or MyoD as committed myoblasts. A hierarchy of myogenic regulatory factors then leads to the formation of mature myofibers.*

Two muscle groups that are integral to the stability of the knee joint are the gastrocnemius and quadriceps muscles. The gastrocnemius is a biarticular muscle that acts not only as a plantar flexor, but also as a knee flexor, meaning that it is an antagonist during knee extension (Suzuki et al., 2014). The medial and lateral head of the gastrocnemius muscles originates from the medial and lateral epicondyles of the femur, respectively. The tendon and muscle fibers of both head also take originate from the joint capsule of the knee. The muscles then insert at the calcaneus bone via the Achilles tendon (Andjelkov et al., 2016). The quadriceps consist of the rectus femoris, the vastus lateralis, the vastus intermedius, and the vastus medialis. The three vastus muscles act as knee extensors whilst the rectus femoris also flexes the hip. The vastus medialis extends and externally rotates the thigh and inserts into, and stabilizes, the patella via the quadricep tendon (Waligora et al., 2009). These muscle groups are depicted in figure 1.2.

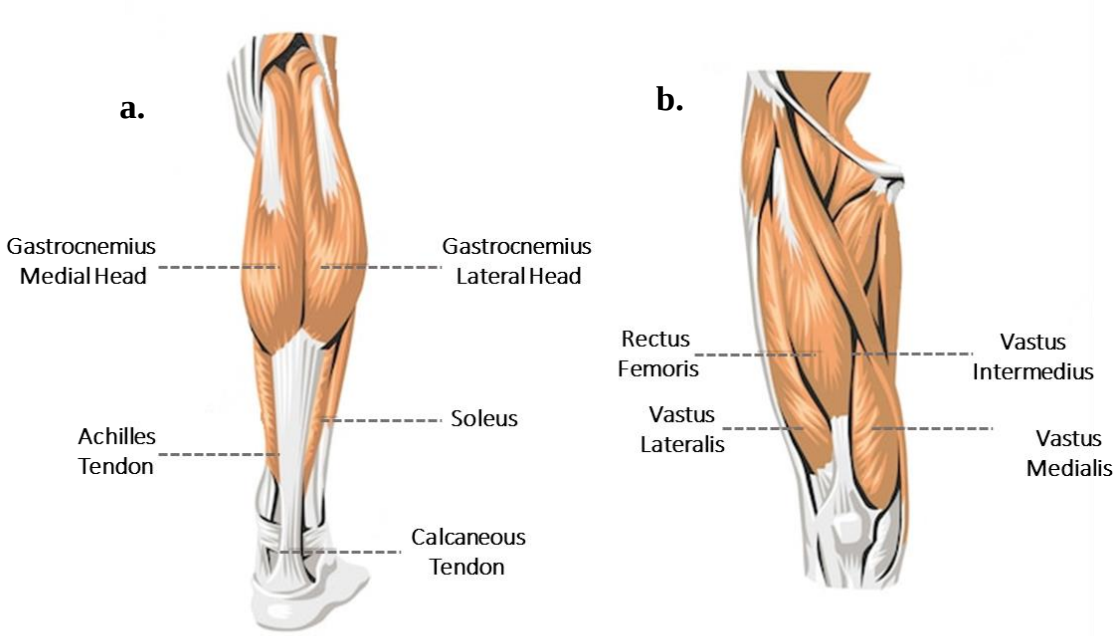

Figure 1.3: A diagram of the peri-articular muscles. *(a) The two gastrocnemius muscles, soleus, Achilles tendon, and calcaneous tendon. (b) The rectus femoris, and vastus muscles of the Quadriceps. The diagram was obtained from 'Adobe Stock' and is subject to the compatible CC-BY-SA license.*

1.1.4 Other Joint Tissues

Healthy joints allow the movement of bones that surround the joint whilst bearing the loads against gravity caused by the movement. The bones are maintained in place and stabilised by four main ligaments: the anterior cruciate ligament (ACL), the posterior cruciate ligament (PCL), the medial collateral ligament (MCL) and the lateral collateral ligament (LCL) (Frank, 2004). The medial compartment of the joint is tightly fixed between the two strongest ligaments, the PCL and the MCL system, including the posterior oblique ligament (POL) with the meniscus (Hirschmann and Müller, 2015). Menisci are fibrocartilaginous and act as shock absorbers and stabilisers (Messner et al., 1998) and are attached to the tibial surface by meniscotibial ligaments (Frank, 2004). In addition, the entire knee joint is surrounded by a joint capsule which is lined by a synovial fluid-filled membrane. This synovial membrane acts as a transport medium as well as to reduce friction (Smith, 2011). Finally, tendons connect the bone to the muscle providing more stability for movement and joint function (Woo et al., 2006).

1.2 Joint Disease and Ageing

1.2.1 Aetiology

Osteoarthritis (OA) is the most common musculoskeletal disorder and cause of chronic disability in adults (Man and Mologhianu, 2014). Although ageing is a major OA risk factor, obesity, joint injury, and genetics also contribute to its development (Johnson et al., 2014). Primary – or idiopathic - OA is the most common subset of the disease and is develops in the absence of a predisposing trauma. For example, obesity can lead to increased or abnormal joint load, and thus the development of OA. In fact, individuals with obesity and/or metabolic syndrome have a greater risk of developing OA, implicating the metabolic syndrome as a modulator of the effects of mechanical loading on joint degeneration (Courties et al., 2015). Secondary – or post-traumatic OA (PTOA) - arises after joint injury and repetitive joint trauma associated with recurrent instability (Punzi et al., 2016). For example, patients exhibiting ACL injuries have a very high risk (50-90%) of developing PTOA. The main characteristic of both idiopathic and post-traumatic OA is the deterioration of the articular cartilage – of which chondrocytes are the only cell type. The primary function of chondrocytes is to maintain homeostasis of the extracellular matrix (ECM) by balancing anabolism and catabolism of its components, which mainly consists of collagen and proteoglycans. These ECM components are responsible for the biomechanical properties of cartilage – i.e. its ability to disperse pressure and shear stress as the joint moves. As such, upon cartilage degeneration, you see a drastic loss in joint function, leading to pain and immobility.

In early stages of OA, hypertrophic chondrocytes express collagen type X. These hypertrophic, terminally differentiated chondrocytes are characterized by an enlarged size, high expression of collagen type X (COL10A1), runt-related transcription factor 2 (RUNX2), matrix metalloproteinases (MMPs), and disintegrin and metalloproteinase with thrombospondin motifs (ADAMTSs) and low expression of collagen type II (COL2A1) (Mackie et al., 2011). The MMPs and ADAMTSs are

upregulated in hypertrophic chondrocytes are considered the main enzymes responsible for degradation of aggrecan and collagens in cartilage (Okada et al., 2001). This breakdown of proteoglycans leads to a reduction in the compressive stiffness of the tissue that accelerates the rate of collagen loss associated with OA (Falah et al., 2010). MMP induced cartilage degradation is in part mediated by inflammatory cytokines, such as IL-1β, TNF-α, and IL-6, secreted by chondrocytes and synoviocytes (Kapoor et al., 2011). Moreover, chondrocytes can undergo cellular senescence - a state of stable proliferation arrest – where their accumulation and secretion of inflammatory factors can contribute to breakdown of the ECM (McCulloch et al., 2017). These ECM changes during OA are depicted in figure 1.3.

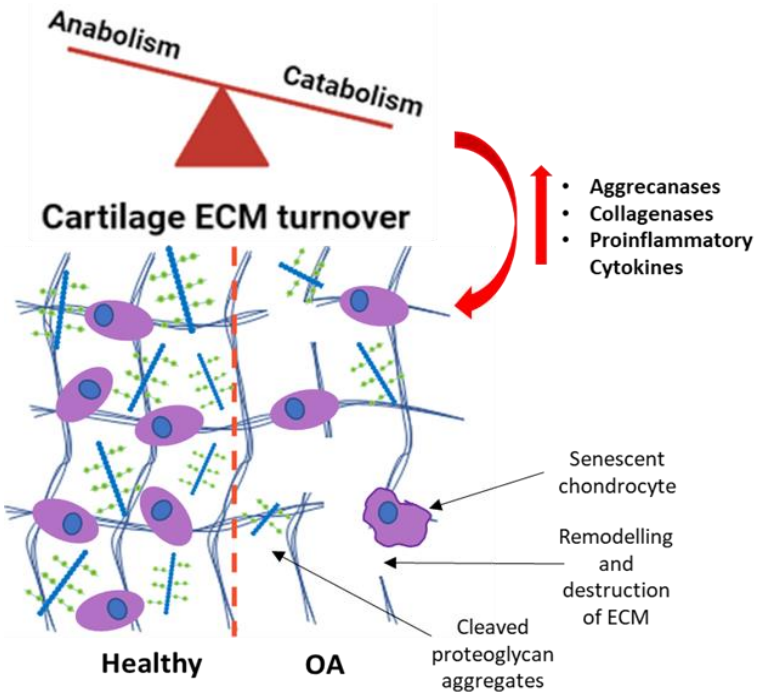

Figure 1.4: A schematic representation of the ECM structure in healthy vs OA cartilage. *During OA there is an increase in catabolic enzymes and factors (such as aggrecanases, collagenases, and cytokines) which lead to destruction and remodeling of the ECM.*

It is not known what initiates the imbalance between the degradation and the repair of cartilage, with research suggesting it could be either mechanical loading-induced damage or inflammation. For example, research demonstrates a release of peptides from matrix components, e.g., fibronectin fragments, subsequent to the development of overloading-induced articular lesions. This provides evidence of a damaged ECM as a result of mechanical overloading (Loeser et al., 2014). These fibronectin fragments bind to integrins and toll like receptors and lead to an increased expression of proinflammatory cytokines such as IL-1, -6, -8 and TNF-α as well as MMPs, leading to further destruction and breakdown of the ECM (Hwang et al., 2015). This highlights how complex the mechanisms behind ECM degradation are and makes it hard to elucidate the initiating factors. Lots of studies have therefore focused on targeting genes encoding ECM degrading enzymes in order to prevent its destruction during OA.

Cartilage deterioration is not the only disease characteristic of OA, with others including: low-grade synovial inflammation, subchondral bone remodelling, meniscal tears, hyperplasia, and osteophyte formation (Pollard et al., 2008). Biomechanical stress, pro-inflammatory mediators, and proteases are all known contributors to the disease pathogenesis of OA (Kapoor et al., 2011) (Troeberg and Nagase, 2011; (Heijink et al., 2012). It is a combination of these factors that is thought to lead to the primary and secondary changes that occur in the cartilage, synovium, joint capsule, ligaments, and periarticular muscles (Aigner and Schmitz, 2011). This wide spectrum of OA characteristics has led to the recent proposal that OA be defined as a condition that effects the entire joint, as opposed to just the loss of articular cartilage (Loeser et al., 2012). A depiction of the OA-associated joint changes is shown in figure 1.2.

Linked to the joint, periarticular muscles also play a major role in joint function during movement and in joint stability, but their relationship with OA has been seldom explored. Muscle atrophy is defined as the loss of muscle mass and strength with age. This reduction in muscle mass and strength is attributed to a loss of myofibers, atrophy of remaining fibers, reduction of muscle quality and defective muscle regeneration

(reviewed in Brown and Goljanek-Whysall (2015). The consequences of muscle atrophy are similar to that of OA, with the functional decline leading to a number of adverse health outcomes, including loss of function, disability, and frailty. Muscle aging is characterised by a reduction in muscle fiber number as well as atrophy of the remaining fibers. Moreover, a decline in its regenerative capacity, primarily caused by a reduction in the number and function of the muscle satellite cells – the tissue's resident stem cell niche – is often a characteristic of the disease (Walston, 2014). However, the aetiology of muscle atrophy is complex and involves factors such as: increased production of catabolic cytokines, decreased physical activity, and loss of α-motor neurons (Marzetti et al., 2009). The myofibers of skeletal muscle are classified as either slow-twitch (type I) or fast-twitch (type IIb) fibers, with the former utilising aerobic (oxidative phosphorylation) respiration and the latter utilising anaerobic metabolism (glycolysis) (Schiaffino and Reggiani, 2011). Ageing is associated with a preferential loss of the smaller fast twitch fibers (Canepari et al., 2010), resulting in reduced contractile force and increased contractile weakness, as well as the progressive loss of muscle mass (Ohlendieck, 2011). Myofiber loss can be accompanied by inflammation and age-associated fibro-adipose conversion of satellite cells leading to accumulation of connective tissue and fibrosis (Molina et al., 2021; Parker, 2015; depicted in figure 1.2).

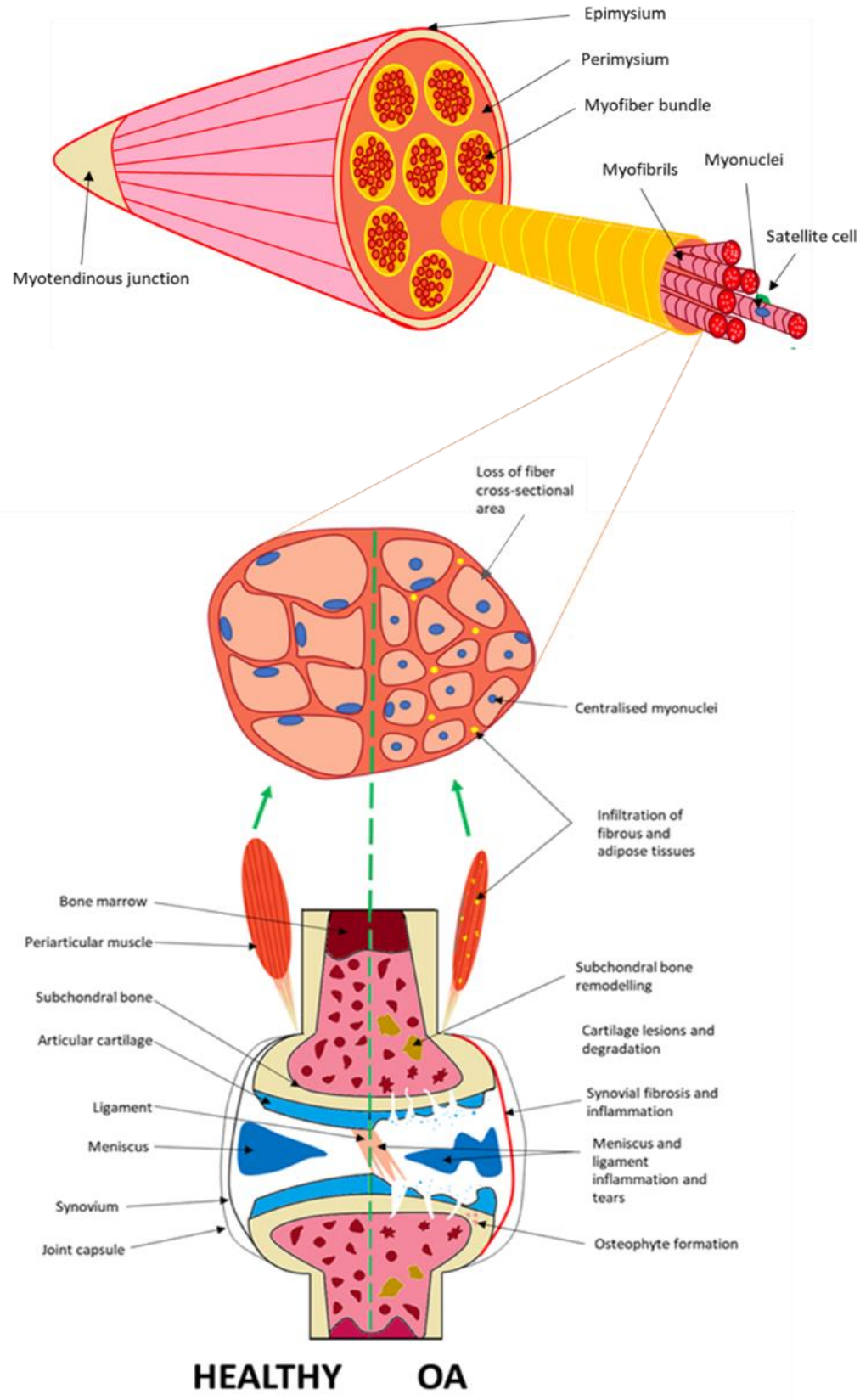

Figure 1.5: A diagram depicting the pathophysiological changes that occur in the knee joint and surrounding peri-articular muscles during OA. *Diagram includes the synovium, joint capsule, meniscus, ligaments, articular cartilage, subchondral bone, peri-articular muscles, and bone and the changes that occur in these tissues with OA.*

1.2.2 The Relationship Between Osteoarthritis and Muscle Atrophy

The progressive loss of periarticular muscle mass and function has consequences on joint stability and health. Muscle atrophy is inevitably associated with ageing, and, more recently, it has been demonstrated in patients with OA (Narici et al., 2010; de Souza Silva et al., 2018; Larsson et al., 2019; Veronese et al., 2021; Kim et al., 2022). Until recently, research investigating the association of muscle atrophy with OA has been scarce. Currently, more and more data support the relationship between joint health and the surrounding skeletal muscle, as reviewed in a recent review by Shorter et al. (2021), however, functional and mechanistic studies are still lacking.

Muscle contractility is required for joint formation already during embryogenesis (Kahn et al., 2009) and muscle weakness is an important determinant of pain and disability during OA (Fisher et al., 1997). Several studies have shown that a decrease in lower limb lean mass is frequent in OA patients (Toda et al., 2000) and this is associated with a greater risk of falls (O'Reilly et al., 1998) (Segal et al., 2010) (Conroy et al., 20120). Progressive muscle weakness in OA is also associated with muscle fibre atrophy, with studies demonstrating 12–19% reduction in cross-sectional area in the quadriceps of patients with hip and knee OA (Arokoski et al., 2002; Ikeda et al., 2005). Another study subjected 117 patients with symptomatic knee OA to magnetic resonance imaging of the knee. They found that a larger cross-sectional area of the *vastus medialis* is associated with a decreased rate of tibial cartilage volume loss, reduced risk of knee replacement, and reduced pain in OA patients (Wang et al., 2012). Moreover, dystrophic mice show significant articular cartilage degeneration, along with a spectrum of degenerative musculoskeletal abnormalities (Isaac et al., 2013).

On the other hand, a large longitudinal cohort study found that, in 1653 subjects without radiographic knee OA (ROA) at baseline, an increased risk of ROA was not associated with sarcopenia alone, but rather with sarcopenic and body composition–based obesity (Misra et al., 2019). Conversely, Lee et al (2016) suggested that skeletal muscle mass of the lower limbs shows a higher correlation with knee OA than that of

the lower and upper limbs combined. Therefore, a statistical association between the risk of knee OA and sarcopenia may be observed, if the assessment of skeletal muscle mass focuses on the lower limbs. A study investigating the association of pain and ROA on muscle mass, strength, quality, and risk of falls in older adults showed that hip and knee ROA are not significantly associated with changes in muscle strength and quality, despite the association of self-reported lower extremity joint pain, stiffness and dysfunction with declines in the aforementioned muscle parameters in older women. As such, it was concluded that pain may be the underlying mechanism via which OA leads to functional decline of muscle (Scott et al., 2012).

One of the main limitations of muscle research is a lack of a clear definition of the diagnostic criteria of sarcopenia. In recent years, many definitions of sarcopenia have been proposed, each one recommending diagnostic criteria based on muscle mass combined with measures of muscle strength, function or physical performance (Cruz-Jentoft et al., 2019). It is therefore crucial that criteria for the definition of sarcopenia are established and adopted in order for research to obtain results that are clinically relevant.

Another limitation of research in this area is the lack of a clear method to correlate the development of OA and incidence of sarcopenia. The current method used by research to investigate this relationship is to separately assess the OA severity grade and the lean body mass (LBM) of the area of interest (Papalia et al., 2014). Moreover, most of the research into OA and sarcopenia focuses on whether or not there is a correlation between the two disorders and has yet to fully investigate the molecular mechanisms behind the observed changes. It has been suggested that myokines, muscle-produced cytokines, peptides and growth factors communicate with the surrounding articular components such as the synovium, cartilage and bone through paracrine mediation, and thus may affect the signalling cascades implicated in OA (Krishnasamy et al., 2018).

These limitations make it difficult to determine whether OA and sarcopenia are co-existing conditions with shared risk factors or whether the relationship is causal. To

overcome this, researchers conducted a systematic analysis to combine all relevant studies into one statistical test – detailed in an abstract by Amirthalingam et al. (2019). They identified 15 studies that investigated the association of sarcopenia and OA-related knee structural changes, all of which were deemed to be of low to moderate quality. Although they concluded that sarcopenia is associated with knee structural changes predictive of knee osteoarthritis, their data has yet to be published. In the meantime, more high-quality studies are required to understand the role of sarcopenia in pathogenesis of knee OA.

1.2.2.1 Molecular mechanisms of OA-associated muscle atrophy

Research into the molecular interactions between muscle and joint tissues during OA has been severely lacking. Potentially mechanical signals from loading may induce biomechanical interplay – or cross-talk – between the tissues. This was demonstrated in other tissues of the musculoskeletal system, with research into osteoporosis suggesting that bone and muscles are secretory organs involved in autocrine, paracrine, and endocrine communication. This study postulated that this biochemical interaction may occur at the muscle fiber insertion sites along the periosteal interface (Isaacson et al., 2014). More support for the interaction between bone and muscle comes from research which found that bone remodelling - a key characteristic of OA - is often a response of muscular activity (Judex and Rubin, 2010). Moreover, the muscle secretome includes proteins that are known to exert effects on the bone, such as osteoglycin and osteoactivin (as reviewed by Tagliaferri et al., 2015). As well as affecting bone, proteins secreted from muscle cells have also been shown to exert effects on chondrocytes in culture. Cairns et al., 2010 showed that chondrocytes co-cultured with C2C12 muscle cells showed enhanced ECM production as well as resistance to IL1b induced chondrocyte damage. Furthermore, chondrocytes secrete osteoinhibitor molecules and Indian hedgehog signalling molecules which can promote both muscle and bone metabolisms (Tagliaferri et al., 2015). For example, research found an upregulation of Indian hedgehog (Ihh) expression by chondrocytes during myogenesis (Bren-Mattison et al., 2011). Moreover, BDNF, which serves a key role in maintaining the population of muscle progenitors in adult muscle, has receptors in osteoblasts and chondrocytes (Camerino et al., 2012). Therefore, the role of

cartilage and muscle in the 'musculoskeletal control loop' is a very interesting, but understudied, topic. Research in this area consists of a few *in vitro* and in animal studies ultimately showing that muscle cells may play an important role in regulating cartilage gene expression.

Of the studies exploring molecular mechanisms underlying muscle atrophy in OA, most have focused on inflammatory mediators as the molecular link between muscle function and OA. For example, Levinger et al. (2011) observed increased protein abundance of p65 NF-κB, STAT-3 and JNK in the *vastus lateralis* in patients with knee OA compared with a control group – indicating inflammation. This inflammation was shown to have an impact on the muscle function, with significantly reduced muscle strength in the OA group.

The muscle quality of this quadriceps muscle was also investigated in a study by Noehren et al. (2018) who conducted the first cellular-level analysis of the *vastus lateralis* in adults with moderate knee OA. Results of this study showed significant pathogenic fibrosis in the muscle of OA patients. Moreover, aberrant collagen deposition was noted in the extracellular matrix of OA muscle, which was significantly associated with decreased satellite cell density, as well as muscle strength. Increased expression levels of both CCN2 and TGFβ mRNAs were correlated positively to the amount of collagen deposition and inversely correlated with muscle strength. However, they showed that despite quadriceps weakness, there was no significant difference in muscle fiber CSA or fiber type-specific CSA. Finally, results indicated a muscle fibre type shift in the OA group, with significantly more type IIa/x hybrid fibres and fewer type I fibres in OA muscles relative to controls. Despite the limitations of this study, including low sample sizes and its cross-sectional nature, the data provide excellent molecular insight into the pathology of muscle changes that occur during OA. Nonetheless, there remains a large insufficiency of research in this area, making it essential that future studies focus on elucidating the mechanisms behind potential cross-talk between the joint and skeletal muscle in order to develop more targeted therapeutic approaches.

Although studies have demonstrated reduced muscle quality and strength in OA, it has not yet been determined as to whether muscle changes precede OA, or vice versa. It has been suggested that the disuse of an OA affected joint, due to the pain of movement, may be the primary cause of the reduction in muscle strength associated with OA (Pisters et al., 2014). To add to the complexity, data from a study investigating muscle atrophy in an anterior cruciate ligament transection (ACLT) model of OA suggest that disuse does not fully explain the muscle atrophy observed in OA (de Souza Silva et al., 2018). Results of this research show that 3-month-old rats in the OA group display the same pattern of movement as those of SHAM group (i.e., rats submitted to surgery without ALCT). Despite the similar locomotion (measured as spontaneous exploratory velocity and distance), the gastrocnemius cross-sectional area was reduced by approximately 10% in the OA group. It was concluded, therefore, that muscle atrophy may be a consequence of chronic, low-grade inflammation associated with OA, rather than solely joint disuse. However, the authors did acknowledge that the rats in the OA group displayed significantly increased nociception towards the end of the study, suggesting that the extended experimental period could have allowed for the detection of reduction in joint use. These studies suggest that it may be a vicious cycle in that there is an early loss of muscle with OA, as well as later disuse-related muscle atrophy.

Although it research suggests that skeletal muscle atrophy plays an important role in OA development and/or progression, there are still large gaps in our knowledge, especially regarding molecular mechanisms. A decline in lower limb muscle strength is associated with knee or hip osteoarthritis in a pathological network of pain, altered joint stability, maladapted postures and defective neuromuscular communication (Veronese et al., 2018). At the cellular levels, chondrocytes and myoblasts share common pathways, and the close anatomical location of both cell types also suggest the possibility of paracrine communication. One of the ways that you can modulate

1.3. microRNAs

1.3.1 Biogenesis and Mechanisms of Action

miRNAs are a class of small non-coding RNA molecules, approximately 22 nucleotides long, which bind to messenger RNAs (mRNAs), induce degradation or inhibit protein translation, and thus work to post-transcriptionally regulate gene expression (Horak et al., 2016). In animals, the first stage in miRNA synthesis involves the cleavage of the primary transcript (pri-miRNA) by the RNase III-type protein Drosha, a process which forms a long, hair-pin shaped transcript called precursor-miRNA (pre-miRNA) (Wahid et al., 2010). Pre-miRNAs are recognized by Exportin-5 (EXP-5), and, in complex with Ran-GTP, are transported to the cytosol through the nuclear pore complex (NPCF) where they are then cleaved near the terminal loop by 'Dicer'. The resulting miRNA duplexes unwind, with the mature miRNA strand binding to proteins of the Agonaute-subfamily, thus assembling into the 'RNA-induced silencing complex' (RISC) (Kim et al., 2009). Mature miRNAs then bind - via RISC - to complementary messenger RNA (mRNA) sequences of target genes, inducing either endonucleolytic cleavage or translational repression of the mRNAs depending on the degree of complementarity between the miRNA and mRNA sequences (Gregory et al., 2005). A fully complementary interaction induces AGO2 endonuclease activity and subsequent mRNA cleavage (Jo et al., 2015). However, this interaction destabilises the association between AGO and the 3′ end of the miRNA, resulting in its degradation. In animal cells, the majority of interactions between the miRNA and mRNA are not fully complementary, preventing AGO2 endonuclease activity (Jonas et al., 2015). Instead, when this occurs, AGO2 acts as a mediator of RNA interference, similar to the non-endonucleolytic AGO family members (O'Brien et al., 2018). An overview of the miRNA mechanism of action is depicted in figure 1.5.

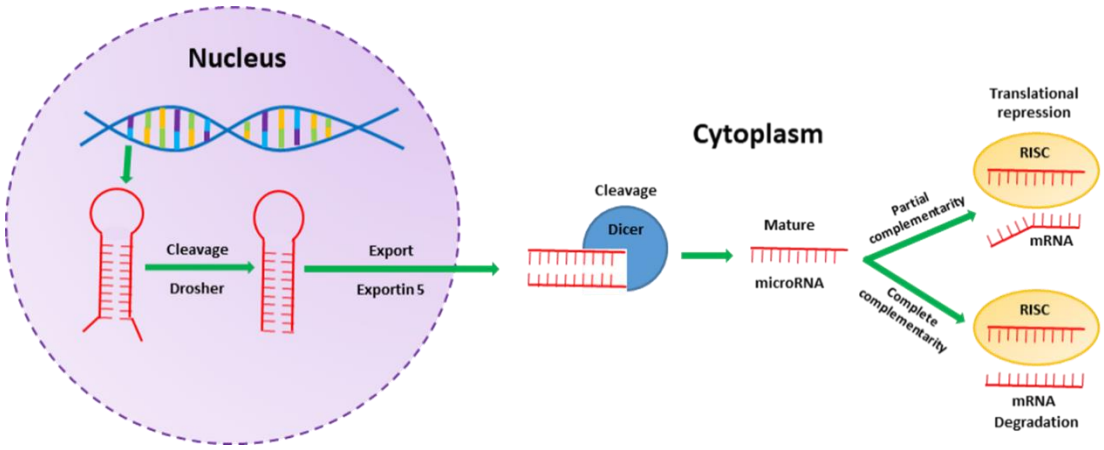

Figure 1.6: A diagram depicting the biogenesis and mechanisms of action by which miRNAs repress or degrade target mRNAs. *The miRNA is transcribed to generate a primary microRNA (pri-miRNA) precursor molecule that undergoes nuclear cleavage to form a precursor microRNA (pre-miRNA). The pre-miRNA is cleaved in the cytoplasm, by the microprocessor complex comprised of DGCR8 and Drosha, to create a microRNA duplex containing the mature miRNA. The duplex unwinds and the mature miRNA assembles into RISC. The miRNA base-pairs with target mRNA to direct gene silencing via mRNA cleavage or translation repression based on the level of complementarity between the miRNA and the mRNA target.*

miRNAs have also been implicated more recently in post-transcriptional upregulation. This occurs in response to specific cellular conditions, sequences, and cofactors, upon partial binding of the miRNA to the target mRNA, and can be either direct (activation) or indirect (lack of repression) (Vasudevan et al., 2012). An example of indirect upregulation is the regulation of mRNA expression by both AU-rich element (ARE)-binding negative feedback inhibitors (such as TTP and HUR) as well as miRNAs. This coordinated regulation leads to competition for the target site, thus resulting in mRNA stabilisation. This is supported by the finding that many target mRNAs have AU-rich sequences in the 3' UTR upon which miRNAs bind. This means that the miRNAs can compete with the negative feedback inhibitors (such as TTP, HUR etc.), leading to mRNA stabilisation.

1.3.2. miRNA dysregulation in articular cartilage

miRNAs are dynamically regulated with research demonstrating their varying expression levels during different disease states (Alexander and Kunkel, 2015) and specific enrichment in certain tissues - such as that of the joint (Jones et al., 2009; Yin et al., 2017). Moreover, studies report that specific miR-target mRNAs interactions may regulate all major known contributors to the onset of the senescent phenotype, such as DNA damage, telomere shortening, protein mis-folding, oxidative stress (Williams et al., 2017). Due to this, recent research has begun to investigate whether restoring physiologic levels of specific miRNAs in these tissues can work to - at least partially - restore its function (Rupaimoole and Slack, 2017). Investigating the use of miRNA therapies in disorders such as OA is particularly important given that the only current treatment options for the condition are pain and symptom management and eventual joint replacement therapy (Hermann et al., 2018). It is anticipated that deciphering the underlying molecular mechanisms of the disorder, in particular the associated genetic and epigenetic dysregulation, will lead to the development of novel interventions to delay the need for invasive and transient total joint replacement procedures.

One of the most well-studied miRNAs in OA research to date is miR-140, a cartilage specific miRNA (Tuddenham et al., 2006) that was first implicated in OA pathogenesis in a study by Miyaki et al. (2009). In this study, miRNAs specifically expressed in chondrocytes were identified by performing miRNA microarrays and quantitative PCR (qPCR) analysis of primary chondrocytes from articular cartilage and comparing them to that of mesenchymal stem cells (MSCs). Several miRNAs were found to have significantly higher expression levels in primary articular chondrocytes compared with undifferentiated MSCs – the largest difference of which was observed for miR-140. qPCR of miR-140 together with OA related marker genes (Col2a1, ADAMTS-5, MMP-13, and Sox9) found that the expression of ADAMTS-5, a protein that plays a central role in the degradation of collagen and aggrecan, was significantly increased in OA cartilage. Conversely, the expression of Col2a1 – a gene encoding the pro-alpha1(II) chain of type II collagen - was decreased. The group further investigated the function of this miRNA in miR-140 null mice created via

targeted deletion (Miyaki et al., 2010). They found that 3-month old miR-140−/− mice showed age-related OA-like proteoglycan loss (indicated by reduced Safranin O staining) and fibrillation of articular cartilage. By 8 months old, the miR-140−/− mice showed overt cartilage degradation compared to the age-matched wild-type mice, including: severe proteoglycan loss, a roughened articular surface, and fibrillation. Since then, numerous studies have corroborated the association between dysregulation of miR-140 – and its various isomers - and OA development and progression (Araldi and Schipani, 2010) (Zhang et al., 2013) (Si et al., 2017) (Woods et al., 2020). Moreover, multiple targets of miR-140 have been identified as having an important role in the progression of OA and are involved in pathways ranging from inflammation and senescence to chondrocyte hypertrophy and ECM breakdown, for example: MMP-13, ADAMTS-5, and insulin-like growth factor-binding protein (IGFBP)-5 (reviewed by Duan et al., 2020).

A more recent family of miRNAs implicated in OA are the miR-29 family (Le et al., 2014), consisting of miR-29a, miR-29b1/2, and miR-29c, which were identified as being significantly overexpressed 1 and 3 days after the destabilisation of the medial meniscus in a mouse model (Le et al., 2016). Amongst the target genes of miR-29 are collagens and TGF-β (Maurer et al., 2010; and Smyth et al., 2022), making it a positive regulator of chondrocytes. Moreover, overexpression and knockdown of SOX9 - a critical transcription factor regulating chondrocyte differentiation - in SW1353 cells resulted in a decrease and increase in miR-29 family expression, respectively. It was concluded that SOX9 appears to be a negative regulator of miR-29 expression in chondrocytes (Lee et al., 2016). This study also looked at the effect of inflammatory cytokines on the miRNA expression, finding that in micromass culture, IL-1 increased the expression of all mature miR-29 family members. Recent research has supported the involvement of miR-29a in OA pathogenesis, using a luciferase reporter assay to identify Bax, a pro-apoptotic protein of the Bcl-2 family, as a direct target of miR-29a (Miao et al., 2019). The group also investigated the miRNA in an IL-1β induced chondrocyte-like ATDC5 apoptosis model, finding that a miR-29a mimic and inhibitor decreased and increased Bax protein levels, respectively, in IL-1β treated cells compared to the corresponding controls. However, in direct contrast to the study by Le et al. (2016), only miR-29a expression levels were significantly decreased in

cultured cells from OA patients, whereas the expression of the other miRNA family members remained unchanged.

In contrast to miR-29 which is regulated by IL-1 in chondrocytes, miR-93-5p has been shown to reduce the expression of inflammatory cytokines, including IL-1β, TNF-α, and IL-6 (Yan et al., 2017). In terms of its role in OA, miR-93-5p was found to be significantly under expressed in the cartilage tissue of patients with OA, as well as in IL-1β–treated normal chondrocytes. Additionally, the overexpression of miR-93-5p was shown to inhibit the cartilage matrix degradation characteristic of OA (Xue et al., 2019). This study was supported by Ding et al. (2019) who demonstrated an inhibitory effect of miR-93 on inflammatory cytokine production in chondrocytes transiently transfected with a miR-93 mimic.

Research into the role of miRNAs in OA cartilage are often conflicting. For example, one study showed miR-146 to be downregulated in OA cartilage compared to normal cartilage, with its overexpression being found to downregulate interleukin-1beta (IL-1β) induced TNF-α production (Jones et al., 2009). However, results from research by Yamasaki et al. (2009), directly contradict these findings, suggesting that miR-146 is expression is not only induced by stimulation of IL-1β, but that the miRNA is also significantly expressed in low grade OA cartilage. This is supported by research which found that miR-146a was upregulated in articular chondrocytes in response to IL-1β treatment *in vitro*, as well as *in vivo* in the knee joints of rats that have undergone destabilisation of the medial meniscus (Li et al., 2012). This discrepancy may be due to the study methodology, in particular the samples used. It appears that Jones et al. (2009) compared human OA cartilage to that of post-mortem patients with no previous history of OA. However, the study by Yamasaki et al. (2009) does not specify whether the 'normal' cartilage samples used in their cell culture experiments were from patients with no history of OA, only that they were considered macroscopically 'normal'. This is an important point to clarify as studies have shown that 'normal' cartilage away from the OA lesion has a distinct transcriptome and histology to that of a joint completely unaffected by OA. For example, Weaver et al. (2005) showed that microscopic changes occur in cartilage showing no macroscopic change. They concluded that these data are compatible with a model of early OA with increased

production of cytokines and expression of their receptors, particularly in the superficial and middle cartilage zones. This highlights the need to consider the samples used and where they come from when investigating OA pathogenesis, whether it be molecularly or histologically.

Another miRNA to emerge as being important in the development of OA is miR-199a-5p. Previous (unpublished) *in vivo* data from our lab shows that mice subject to repetitive joint loading and injected with miR-199a-5p have higher lesion severity scores than those injected with a scramble. This higher cartilage lesion severity was also demonstrated in the limbs of the non-loaded control groups. Previous research has also shown that miR-199a significantly inhibits early chondrogenesis, measured by the reduced expression of early chondrogenesis marker genes: cartilage oligomeric matrix protein, type II collagen, and Sox9. Conversely, anti-miR-199a was shown to increase the expression of these genes (Lin et al., 2009). miR-199a-5p has many predicted and experimentally confirmed targets that are integral to cartilage homeostasis (Kozomara et al., 2019). For example, sirtuin 1 (SIRT1) is a protein that is present in the nuclei of chondrocytes in all layers of the cartilage tissue as well as in synovial tissues (Takayama et al., 2009). Expression of the SIRT1 protein has been shown to be downregulated in degenerated human OA cartilage and is negatively correlated with OA severity (Fujita et al., 2011). SIRT1 has been implicated in promoting the chondrogenic differentiation of mesenchymal stem cells (MSCs) via the activation of Y box protein 9 (SOX9) – a critical transcription factor in adult cartilage development (Lefebvre and Dvir-Ginzberg, 2017). Another miR-199a-5p target gene that has a pivotal role in articular cartilage, subchondral bone, and synovium tissue during OA progression is TGF-β (Shen et al., 2014), which has also been shown to be upregulated in the muscle of OA patients (Noehren et al., 2018). miR-199 has also been identified as upregulated in the femorotibial joint during ageing and following the DMM OA model in mice (House et al., 2016). Moreover, recent research has shown that silencing miR-199a-5p protects the articular cartilage in a rat model of OA, leading to improved gait and chondrocyte survival (Lu et al., 2022). This was theorised to be through mitogen-stimulated protein kinase 4 (MAOK4) which was validated as a miR-199 target by a dual luciferase assay.

1.3.3 miRNA dysregulation in the synovium

Though the above studies provide excellent insight into the role that miRNAs play in OA pathogenesis, it is now widely accepted that OA does not only affect the articular cartilage (Loeser et al., 2012). Therefore, investigating the involvement of miRNAs in the different joint components, and their interactions with one and other, is crucial for a more in-depth understanding of the molecular mechanisms underlying OA. To date, there is little OA research looking at miRNAs in the synovium, with most research focusing on rheumatoid arthritis (Hong et al., 2017; Kuo et al., 2017; Maeda et al., 2017; Hussain et al., 2018; Wang et al., 2022) of which synovitis is a characteristic symptom.

However, one study utilised IL-1β treated explant cultures of OA synovial and cartilage tissue to try and determine the origin of circulating miRNAs in synovial fluid (Li et al., 2016). The findings of this study showed that stimulation of OA cartilage explants with IL-1β only resulted in a significant change in expression of a few of the miRs investigated, with reductions being observed in miR-23a-3p, 27a-3p and 27b-3p. Conversely, IL-1β stimulation of the synovial explants resulted in a significant increase in the expression of the above miRs, as well as miRs 24-3p, 29c-3p, 186-5p, 378a-5p, suggesting that IL-1β may enhance the expression of miRNAs in the synovium and not in the cartilage. Of these miRs, miR-23a-3p and 27b-3p were found in the supernatant of the cell culture to a significant degree, suggesting that they may be released into the synovial fluid during inflammation. This positive regulation of microRNA expression suggests that their knockdown, via antamonirs etc, may help to restore tissue function in OA. This study is also particularly interesting given that IL-1β is widely used in OA research to model the inflammatory component of the OA phenotype.

Future research may therefore need to consider the potential differing responses of the various joint components to inflammatory cytokines when investigating miRNAs in OA. Despite the differing expression levels of certain miRNAs between the cartilage and synovium, some miRs appear to play a similar role in both tissues. For example,

recent research found that miR-29a knockdown in synovial fibroblasts resulted in high expressions of the pro-inflammatory TGF-β1, as well as collagen III, MMP9, MMP13, and ADAMTS5 (Ko et al., 2017). Moreover, in collagenase-mediated OA pathogenesis, miR-29a-overexpressing transgenic mice had mitigated articular cartilage loss, determined by histological analysis, as well as gait aberrance of injured joints, determined by measuring the print area, maximum intensity, contact area, and contact intensity of the paws (Ko et al., 2017). Moreover, intra-articular administration of miR-29a precursor lessened the collagenase aggravation of excessive synovial remodelling reactions and thereby sustained joint tissue integrity. The role of microRNAs in synovial pathology associated with osteoarthritis has recently been reviewed by Tavallaee et al. (2020). The researchers detailed microRNAs that were found to be involved in regulating the activity of fibroblast-like synoviocytes (FLS) and concluded that the miRNAs contribute to synovial homeostasis, inflammation, fibrosis, angiogenesis, cell survival and cell apoptosis, contributing to OA synovial pathology.

1.3.3 miRNA dysregulation in skeletal muscle

There have been multiple studies that have focused on the role of miRNAs in muscle development, regeneration, and disease. A recent systematic review identified 13 and 10 significantly dysregulated miRNAs in human and rodent sarcopenia, respectively (Yanai et al., 2020). Moreover, their dysregulation was associated with the expression of many signalling molecules, including: PRKAA1, PFKFB3, TGF-βR2, VEGFA, Pol I R1A, UBTF, SIRT1, NGF, and PITX1.

One well studied miRNA in relation to muscle atrophy is miR-181a. A previous study by Soriano-Arroquia et al. (2016) found that overexpression of miRNA-181a significantly decreased myotube diameter *in vitro*, which was then mediated by inhibiting its target SIRT1. Conversely, its knockdown led to an increase in myotube diameter in C2C12 cells. As previously mentioned, miR-199a-5p is another miRNA that has been predicted to target SIRT1. In muscle, this miR has been shown to regulate myogenic differentiation by acting downstream of Srf, which targets multiple factors in the WNT signalling pathway (Lamon et al., 2017). Moreover, miR-199a-5p

expression is increased in human dystrophic muscle and its overexpression in zebrafish muscle leads to major and lethal disruption of the myofibers (Alexander et al., 2013). Most recently, Kanakis et al. (2021) demonstrated miR-199a's dysregulation in muscle atrophy with both small RNA-sequencing and PCR validation. Subsequent bioinformatic analyses revealed that miR-199a – as well miRs-15a, -34a, -122 and - were predicted to target a variety of genes that regulate striated muscle cell apoptosis and histone methylation, which is associated with epigenetic regulation of embryonic myogenesis (Jin et al., 2016). They also showed that these miRs share a variety of common predicted myomiR gene targets that are implicated in skeletal muscle physiology. They concluded that the four selected miRs can serve as a complement of known myomiRs and form a promising set to monitor skeletal muscle development.

Another miRNA whose downregulation has recently been implicated in muscle atrophy is miR-378a-3p. Research investigating this miR has demonstrated its role in delaying satellite cell activation and differentiation in transgenic murine models (Zeng et al., 2016). Even more recently, Li et al. (2018) identified miR-378 as a regulator of autophagy and apoptosis – processes in the metabolic regulation of cell death. They proposed that the miR enhances autophagy and suppressing apoptosis by directly targeting phosphoinositide-dependent protein kinase 1 (PDPK1) and Caspase 9 (CASP9). This proposed role that miR-378 plays in autophagy is supported by the fact that multiple of its target genes are associated with the pathway. For example, microtubule-associated protein 1 light chain 3β (LC3B), a target gene of miR-378, is a ubiquitin-like molecule that is conjugated to phosphatidylethanolamine and forms LC3-II upon autophagic stimulation (Klionsky et al., 2007). LC3-II then localises to autophagic structures including: phagophores, autophagosomes, and autolysosomes (Ju et al., 2010). P62 is another target gene of miR-378 that has been found to be upregulated in the skeletal muscle of mice with reduced miR-378a-3p expression (Li et al., 2018). The accumulation of p62 protein is primarily used as a reporter of autophagy activity (Liu et al., 2016), strengthening the theorised role of miR-378a-3p in the pathway. Interestingly, P62 is also a target gene of miR-199a, the miRNA shown to inhibit chondrogenesis in murine prechondrogenic ATDC5 cells (Lin et al., 2009),

suggesting that autophagy may be a common pathway in both OA and skeletal muscle maintanence.

In vitro studies investigating muscle atrophy-associated miRNA dysregulation often use mimic and/or antagomir transfection to knock down/overexpress the miR of interest. From this, one can analyse myotube size as well as gene and protein expression to confirm predicted targets and investigate associated pathways. miRNA-203a-3p, -434-3p, - 455-3p, and -672-5p have all been implicated in sarcopenia using this methodology. Knockdown of miRNA-203a-3p and overexpression of miRNA-434-3p in skeletal muscle cells induced and inhibited apoptosis, respectively (Okugawa et al., 2019). Overexpression of miRNA-455-3p resulted in a significant increase in myotube diameter, which was suggested to be due to inhibited expression levels of PITX1 and RXRB that are involved in muscle dystrophy and aging (Jung et al., 2017).

Whilst multiple studies have focused on the role of miRNAs in muscle development and regeneration, very few functional studies exist that have characterised the role of miRNAs in muscle atrophy during ageing or OA. For example, only one miRNA, miR-141, has been suggested to have a function in the ageing of the multiple tissues of the musculoskeletal system (Fariyike et al., 2019). It should also be noted that Soares et al. (2014) demonstrated that miRNA function is context dependent in different models of muscle atrophy; therefore, a question arises whether the miR-associated mechanisms of muscle atrophy during ageing are similar or different to those observed during muscle atrophy in OA. An overview of the microRNAs detailed in the previous subchapters as being dysregulated during OA, the direction of expression and their target genes are detailed in figure 1.6.

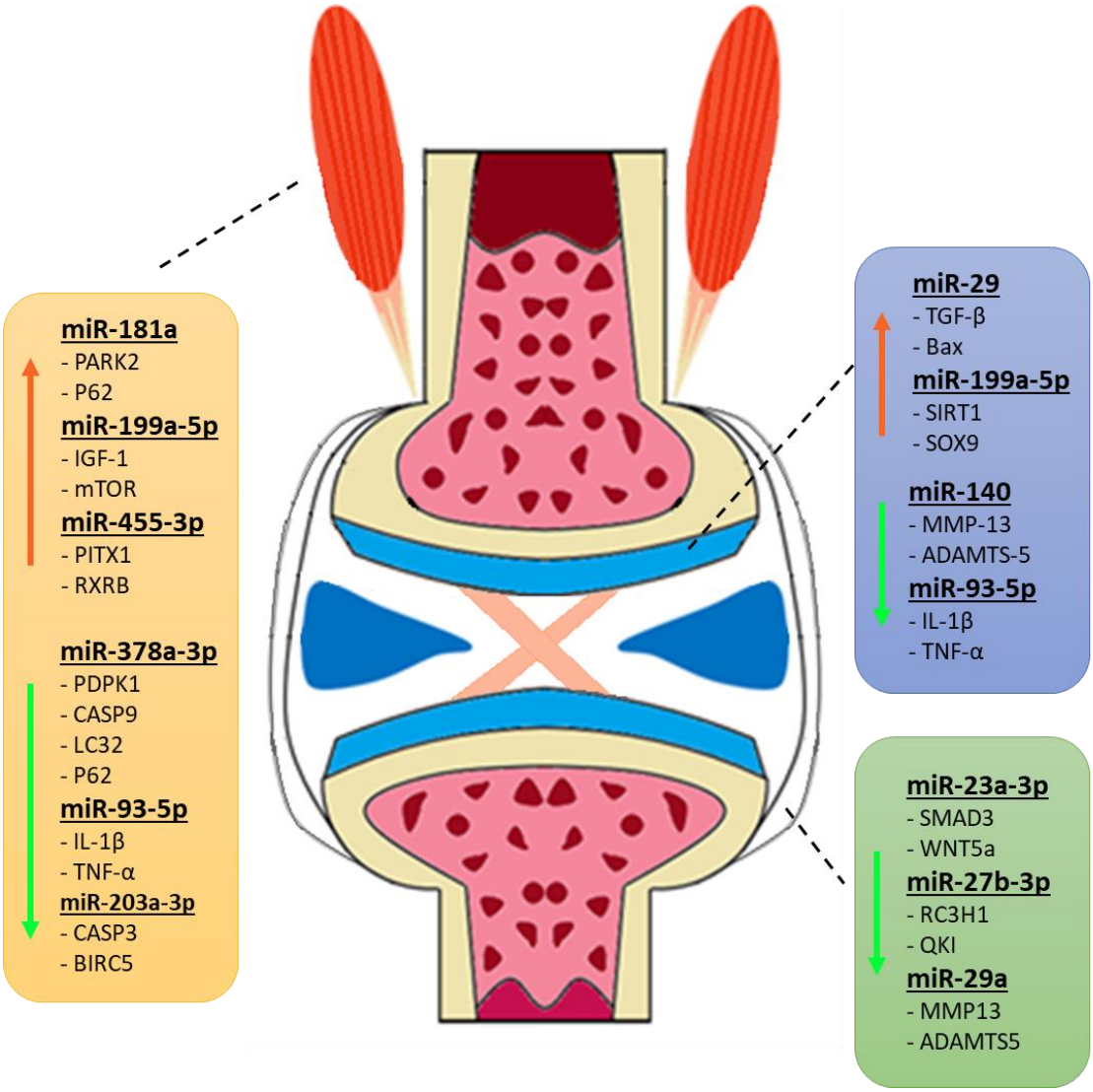

Figure 1.7: A diagram depicting some important microRNAs that research has shown have differential expression levels in OA *(blue and green) and muscle atrophy (orange) and the tissue in which they are expressed (articular cartilage (blue), synovium (green), and skeletal muscle (orange). Their validated targets are displayed along with the direction of expression in the tissue with OA.*

1.3.4 miRNAs as therapeutics

In general, miRNA therapeutic approaches can be divided into two different categories: miRNA inhibition therapies and miRNA replacement therapies. The former can be utilised when the upregulation of a specific miRNA has been shown to contribute to the disease pathology, whereas the latter supplements lower levels of miRNAs (Rothschild, 2014). The primary method of miRNA replacement therapy involves the use of oligonucleotide mimics that possess the same sequence as the mature endogenous miRNA that is intended to be supplemented (Bader et al., 2011). The double-stranded mimic – more commonly used than the less potent single-stranded mimic - is composed of a guide and passenger strand, the sequences of which are identical and complementary to the mature miRNA respectively (Zhang et al., 2013). As the name suggests, these mimics were developed to perform the same functions as naturally occurring miRNAs, whereby they enter the RNA-induced silencing complex (RISC), pair with complementary mRNAs and subsequently inhibit gene expression (Wang, 2010). Conversely, inhibition therapies work by repressing target miRNAs, preventing the interaction between miRNA and mRNA in the RNA-induced silencing complex (RISC) (Shah et al., 2016). Several different methods can achieve miRNA inhibition, the most common of which are antisense oligonucleotides (antagomirs) and miRNA sponges. Antagomirs induce the degradation of the miRNA by annealing to the mature miRNA guide strand, whereas miRNA sponges contain multiple tandem binding sites to target miRNA, saturate the RISC complex and repress the activity toward naturally occurring mRNA (Krützfeldt et al., 2005) (Ebert et al., 2007). The use of these miRNA therapies has many potential advantages over other approaches, including the fact that miRNAs are able to target over 100 transcripts, and therefore as therapeutic agents could target multiple genes involved in a specific disease process (Felekkis et al., 2010). Furthermore, miRNAs as therapeutic molecules can act upon, and silence, targets that would be inaccessible by traditional drug molecules – for example non-enzymatic proteins (Lam et al., 2015). The therapeutic advances of miRNA therapies have been reviewed recently in a paper by Chakraborty et al., 2021).

Despite the exciting potential of these miRNA therapies, there are intrinsic challenges

associated with the approaches that somewhat limits their clinical translation. For example, the rapid degradation of naked RNA particles *in vivo* by enzymes such as serum RNase A-type nucleases is one of the key limitations of miRNA inhibition therapies for use in any disorder (Rupaimoole et al., 2011). However, research has overcome this via the use of chemical modifications of the antagomir to increase the stability, binding affinity and nuclease resistance. For example, fluoro or locked nucleic acid (LNA) allows for effective RNase H-mediated cleavage of the target mRNA (Burnett and Rossi, 2012). Even though some toxicity has been observed previously (Deleavey and Damha, 2012), the effectiveness of LNA modifications is exemplified by the fact that they are found in the FDA-approved oligonucleotide cancer drug, Fomivirsen (Moreno and Pego, 2014). Furthermore, research has recently demonstrated the efficacy of using a small-molecule inhibitor that blocks RNase L to stabilise miRNA mimics (Nogimori et al., 2019).

Another challenge for the clinical translation of miRNA therapies is the development of methods to successfully deliver miRNA inhibitors or mimics to the target regions without compromising the miRNAs integrity. There are several strategies that could potentially deliver therapeutic miRNAs to diseased tissues, all of which can be broadly categorised into the classes 'local' and 'systemic' (Chen et al., 2015). In order for a therapeutic miRNA to be successfully delivered to the target tissue, and reach the cytoplasm of the target cells, it first needs to exit the circulatory system, cross the cell membrane, and escape from endosomal vesicles (Broderick and Zamore, 2011). As the local delivery of therapeutic miRNA is limited to the eyes, skin and mucous membranes, the use of miRNA therapeutics for musculoskeletal tissues would have to rely on systemic delivery systems, all of which come with their own associated challenges. For example, lipid-based delivery systems can be used whereby the miRNA is encapsulated in lipid forming vesicles - lipoplexes – which prevents the miRNA from being filtrated by the kidneys, as well as enhancing intracellular delivery (Yang et al., 2015). However, a major disadvantage of this technique is that they are prone to non-specific binding to serum proteins, making their half-lives less than several hours once administered. Research has therefore focused on increasing their stability by conjugating the lipids with hydrophilic and flexible polyethylene glycol (PEG) (Bikram et al., 2005). Viral-based systems are another focus of research into

miRNA delivery systems, and can overcome the low transfection efficiency that is associated with the use of lipoplexes (and other non-viral delivery systems) and allow for the constant expression of the required miRNA or antagomir. However, viral vectors have high immunogenicity which causes the inflammatory system of the individual receiving the treatment to degenerate the transduced tissue. Furthermore, toxin production, insertional mutagenesis, and the limited transgenic capacity size of the vectors limit their applications for miRNA therapeutics (Gardlík et al., 2005).

OA is a progressive and debilitating disease and the most common cause of chronic disability in adults. Despite this, pain management and total joint replacement procedures are the only current treatment options for the disease. Recent research into OA has therefore focused on the development of novel interventions to delay the need for invasive total joint replacement procedures. The use of miRNA therapeutics in OA is a promising avenue of research, with many recent studies suggesting that their use may overcome the limitations of many traditional therapies. However, as mentioned above, many limitations to the therapeutic use of miRNAs have yet to be overcome. Moreover, experiments using more relevant animal OA models and large-scale clinical trials should be conducted in order to comprehensively evaluate the efficacy of miRNA therapeutics in OA

1.4 Aims and Hypotheses

The main aims of this project were to:

1. Characterise OA-associated muscle atrophy in models of murine OA.
2. Identify differentially expressed microRNAs and mRNAs in OA-associated muscle atrophy that could be used as therapeutic agents to restore joint and muscle health.
3. Use microRNA therapy to restore skeletal muscle health and determine whether this prevents the progression of load-induced OA.
4. Perform systematic analyses to identify and prioritise microRNAs and mRNAs that are most important to OA development.

I hypothesise that:

1. Both idiopathic and loading-induced murine models of OA will exhibit OA-associated peri-articular muscle atrophy.
2. microRNA dysregulation is, at least partially, responsible for OA-associated muscle atrophy.
3. OA severity can be indirectly ameliorated by treatment with myomiRs to restore muscle health and, thus, joint stability.

Chapter 2: General Methods

2.1. Animal Husbandry and Murine Tissue Collection

All mice were kept in polypropylene cages of 2–6 littermates, subjected to 12h:12h light/dark cycles at 21±2°C, and fed standard RM1 maintenance diet ad libitum (No.1; Special Diet Services, Witham UK). All procedures complied with Animals (Scientific Procedures) Act 1986 and local ethics committee. All experiments were performed under the project licence 'PP3119883'. Mice for all experiments were culled by a rising concentration of carbon dioxide for immediate tissue collection, and storage at -80^{o}C.

Firstly, skin was removed to reveal the skeletal muscle and the hind foot pinned to a polystyrene board facing upwards. For dissection of the gastrocnemius muscle, small forceps were inserted under the Achilles tendon and used to slide along the bone to separate the muscles up to the knee joint. The pocket formed between the biceps femoris and the gastrocnemius is removed to reveal the gastrocnemius muscle in full. The gastrocnemius is then separated from surrounding muscles (soleus and plantaris muscles) and removed from the limb. Likewise, the quadriceps muscle is dissected by using forceps to glide under the femoris tendon, avoiding the patella ligament as to not disrupt the knee joint structure. After muscle dissection, hindlimbs were detached near the hip joint. Remaining muscles surrounding the knee joint and femur and tibia were carefully trimmed and removed. Knee joints were fixed in 10% neutral buffered formalin for 24 hours, washed in water and stored in 70% ethanol.

2.2. *In Vivo* Procedures

2.2.1. Non-Invasive Mechanical Joint Loading

For the model of mechanical loading-induced OA, the right knee joints of the mice were loaded repetitively as described previously by Poulet et al. (2011). Briefly, axial compressive loads were applied by an ElectroForce 3100 machine (TA Instruments, USA) via custom-made cups which hold knee and ankle joints flexed and the tibia vertically. Single loading patterns were used in which peak loads of 9N were applied for 0.05 seconds, with a rise and fall time each of 0.025 seconds and a baseline hold

time of 9.9 seconds. Mice underwent forty cycles per loading episode which were repeated on alternate days, 3 times each week, for 2 weeks. The left limb was used as a contralateral control.

2.2.2. Measurement of Grip Strength

To measure grip strength of all limbs in murine models of OA, a test meter (BIOSEB; EB Instruments) was used (Mandillo et al., 2008). During the grip strength test, the mice were handled by their tails and placed over the grid until all paws grasped the grid. The tail was then pulled horizontally until the mouse released hold entirely. Three separate readings were recorded and averaged in Newtons, then converted to grams for analysis. All measurements were normalised to the mouse weight on the day of the recording.

2.2.3. Intravenous Treatment with miR-378a-3p

For miR-378a-3p expression manipulation, mice were injected intravenously with 100ul of a 500nmol stock solution of miR-378a-3p or a control miRNA (2mg/kg body weight; as specified in Whysall et al. (2020)) every two weeks during the 12-week post-loading period with either a miR-378a-3p mimic or control miRNA 'cel-239b' (Dharmacon). miRNA and control mimics were conjugated to cholesterol and the sequences were as follows:

Cel-239b control mimic:

Active: 5'- P.U.U.G.U.A.C.U.A.C.A.C.A.A.A.A.G.U.A.C.U.G

Passenger: 5'-Cholesterol.G.U.A.C.U.U.U.U.G.U.G.U.A.G.U.A.C.A.A.U.U

miR-378a-3p mimic:

Active: 5'-P.A.C.G.G.A.C.U.U.G.G.A.G.U.C.A.G.A.A.G.G

Passenger: 5' Cholesterol.U.U.C.U.G.A.C.U.C.C.A.A.G.U.C.C.A.G.U.U.U

2.3. Ex Vivo Tissue Culture

For ex vivo tissue culture, knee joints from both hindlimbs were then harvested aseptically and dissected sagittally into two halves to allow penetration of the treatment into the joint. Each half was placed into a 24-well-plate with 500ul of Dulbecco′s Modified Eagle′s Medium/Nutrient Mixture F-12 Ham (Sigma-Alrdich). All media was kept serum and antibiotic free.

2.4. Histology

2.4.1. Skeletal Muscle

For each mouse, the gastrocnemius and quadriceps muscles from one hindlimb was processed for histology whilst the other was used for RNA isolation for downstream qRT-PCR. Muscles for RNA extraction were snap frozen in RNAse and DNAse free eppendorfs. Muscles for histological analysis were cut in half laterally and placed on an electron microscopy cork disc (FisherScientific). The samples were covered completely in Optimal Cutting Temperature (OCT) compound and then immediately placed in ispopentane chilled in liquid nitrogen for cryoprotection. Muscles were then stored at -80◦C until sectioning. After removal from the -80◦C freezer, muscles were incubated at -20◦C for at least 30 minutes prior to sectioning. 10um sections of muscle were cut using a cryostat (Leica CM1860), fixed using ice cold methanol, and stained with a 1:1000 dilution of rhodamine wheat germ agglutinin (WGA; 5 µg/mL; Vector Laboratories, UK) for 10 minutes. Vectashield HardSet Antifade Mounting Medium with DAPI (Vectorlabs, UK) was used to coverslip the section and protect against photobleaching. Entire sections were imaged either using a Ziesslsm800 confocal microscope or Axio Scan.Z1 slide scanner (Zeiss, UK) and the fiber cross-sectional area subsequently analysed with Myovision software (Wen et al., 2017). Nuclei were visualised with DAPI and numbers of centralised myonuclei were manually counted and divided by the section area (mm^2).

2.4.1.2. Analysis of Fiber Cross-Sectional Area

For analysis of fiber cross-sectional area in the gastrocnemius and quadriceps muscles, myovision software was used (Wen et al., 2017). MyoVision is an automated image analysis program to quantify muscle immunofluorescent microscopy images. CZA files of entire muscle sections were opened in Zen Blue (Zeiss) where then smaller images throughout the section were captured and saved as a TIFF file. A minimum of 3 images across the section were used for muscle fiber analysis. TIFF files were loaded into the Myovision software. Minimum and maximum area was set to 50 and 5000, respectively. Pixel scale was set to the 'scaling per pixel' value obtained from the Zen Blue 'info' tab on the image being loaded. Once the image is completed regions for exclusion are highlighted with the 'exclude region' button. An example image analysis in myovision is depicted below (figure 2.1). Once the image analysis has completed, the data (fiber cross-sectional area and minimum feret's diameter) can be exported. This analysis is repeated for each image of the section and then data combined to obtain an average cross-sectional area and minimum feret's diameter across the section.

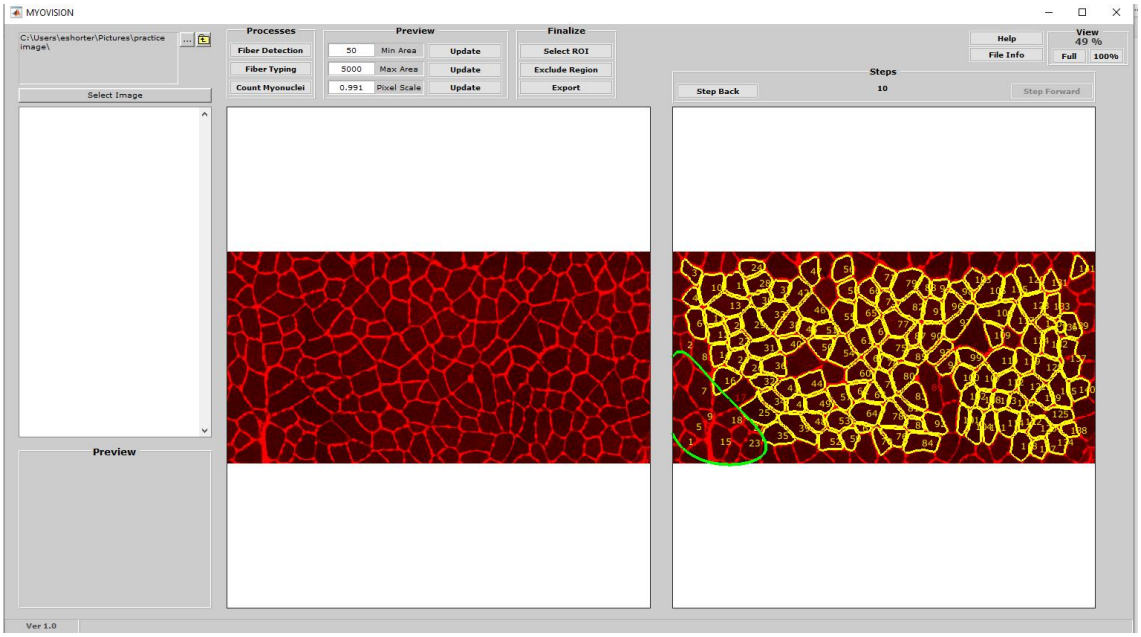

Figure 2.1: A screenshot of the Myovision software used for analysis of the muscle fiber cross-sectional area. *Fibers highlighted in yellow have been analysed and those circled in green are excluded from analysis. Excluded regions included areas where there was cryodamage or faint staining that may prevent accurate measurement of fiber size.*

2.4.2. Knee joints

Joints were fixed in 10% neutral buffered formalin, stored in 70% ethanol, and then decalcified with 10% formic acid (Sigma) for 1-2 weeks., dehydrated, and processed for wax embedding. Serial coronal 6µm thick sections were cut across the entire joint and a quarter of the sections were selected at regular intervals across the joint (every 20 µms) and stained with toluidine blue (0.1% in 0.1M solution of acetate buffer, pH 5.6) and counterstained with 0.2% fast green to stain for collagen.

Toluidine blue was used for histological examination for OARSI cartilage scoring. Initially, Slides were dewaxed and hydrated with xylene (x2), 100% ethanol, 90% ethanol, 70% ethanol, and distilled water. Slides were then pre-conditioned with sodium acetate buffer (0.1M, pH 5.6) for 1 minute and stained with toluidine blue (0.1% toluidine blue in 0.1M solution of acetate buffer, pH 5.6) for 15 minutes. After two washes with distilled water, slides were counterstained with 0.2% fast green for 5 seconds. Slides were washed with distilled water, and then dehydrated with acetone (x2) and xylene (x2) before being mounted with DPX (Sigma) and coverslipped. Slides were imaged with a standard brightfield microscope (Nikon Eclipse Ci).

Mouse knee joints were graded using the OARSI cartilage scoring system (Glasson et al., 2010). In brief: grade 0 for normal articular cartilage, grade 1 for lesions in the superficial zone, grade 2 for lesions in the intermediate zone, grade 3 for lesions down to the tidemark and up to 20% of articular cartilage loss, grade 4 for 20-50% of articular cartilage loss, grade 5 for 50-80% of articular cartilage loss, and grade 6 for greater than 80% of articular cartilage loss and bone exposure (Glasson et al., 2010). Toluidine blue slides of the entire knee joint were scored for cartilage lesion severity in each knee compartment: medial tibia (MT), medial femur (MF), lateral tibia (LT) and lateral femur (LF). Using these calculations, the average mean and maximum lesion scores was calculated for each compartment and for the whole knee joint of each mouse. Summed scores of all the compartments were also calculated from the mean and maximum scores. Statistical analysis was completed using GraphPad Prism (version 6, USA).

2.5. Micro computed tomography (µCT) for analysis of subchondral and trabecular bone.

Mice cadaveric knee joints were analysed with micro computed tomography (µCT) to quantify subchondral and trabecular bone thickness, joint space mineralisation, and trabecular number (as depicted in figure 4.1-3). After fixation in neutral buffered formalin for 2-3 days, knee joints of the mice were scanned with a 4.5µm isotropic voxel size (50kV, 200µA respectively, 0.5mm Aluminium filter; 0.6° rotation angle, no frame averaging) using a Skyscan 1172 µCT scanner (Skyscan, Belgium). Scans were reconstructed with NRecon software (Bruker) using an algorithm that included ring artefact reduction, beam-hardening correction, and misalignment compensation. Coronal images were used for analysis of the tibial epiphysis. The medial and lateral femoral condyles were analysed from sagittal sections. For both the tibia and femur, the subchondral and trabecular bone were selected individually as regions of interest (Keenan et al., 2020). For joint space analysis, regions of interests were hand-drawn. This included the menisci (lateral and medial) and other mineralised tissues that were not part of the tibial or femoral bones (Ramos-Mucci et al., 2022). These regions of interests were analysed using 3D algorithms in CTAn (Skyscan, Belgium) to provide the mineralised tissue volume (measured as Bone Volume on CTAn). The task lists performed on the batman software for measuring the subchondral and trabecular bone thickness, joint space mineralisation, and trabecular number and separation are detailed in supplementary table 2.

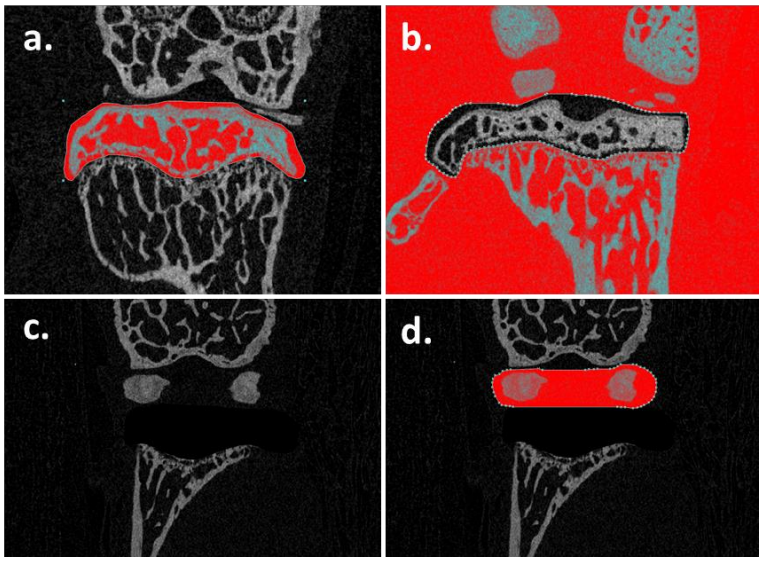

Figure 2.2: Analysis of joint space mineralisation. *(a) The tibial epiphysis is selected excluding the femur, growth plate and menisci. (b) The subtractive function isolates everything but the tibial epiphysis. (c) The subtractive image is selected. (d) Mineralisation in the joint space is selected.*

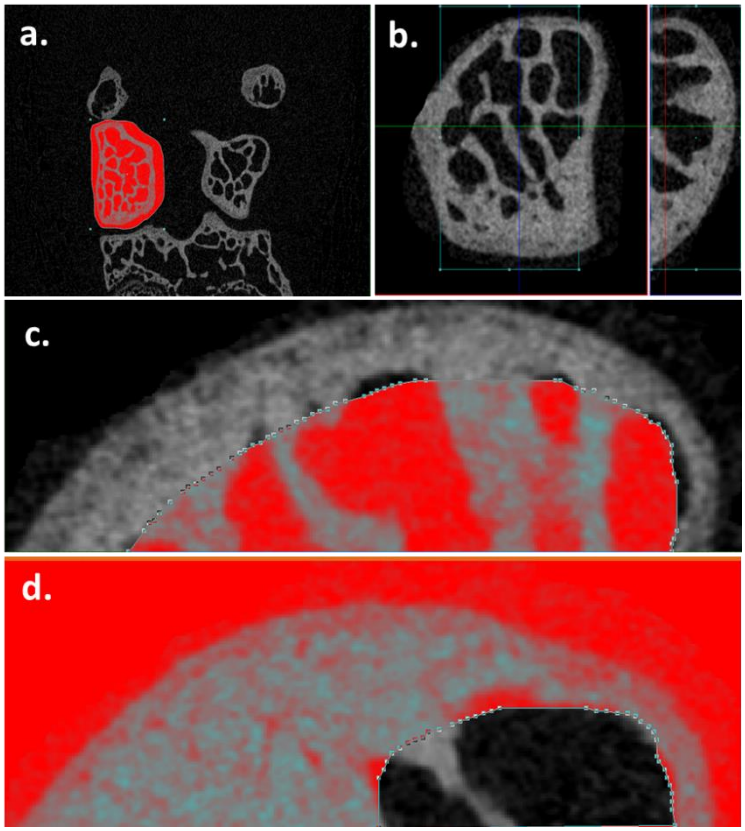

Figure 2.3: Analysis of trabeculae and subchondral bone for femoral condyles. *(a) Select the medial and lateral chondyles without the meniscus. (b) Reorient and save the chondyles in a saggital view. (c) Select the trabecular region of the lateral and medial chondyles from the saggital image. (d) Subtract the trabecular region, isolating the subchondral bone.*

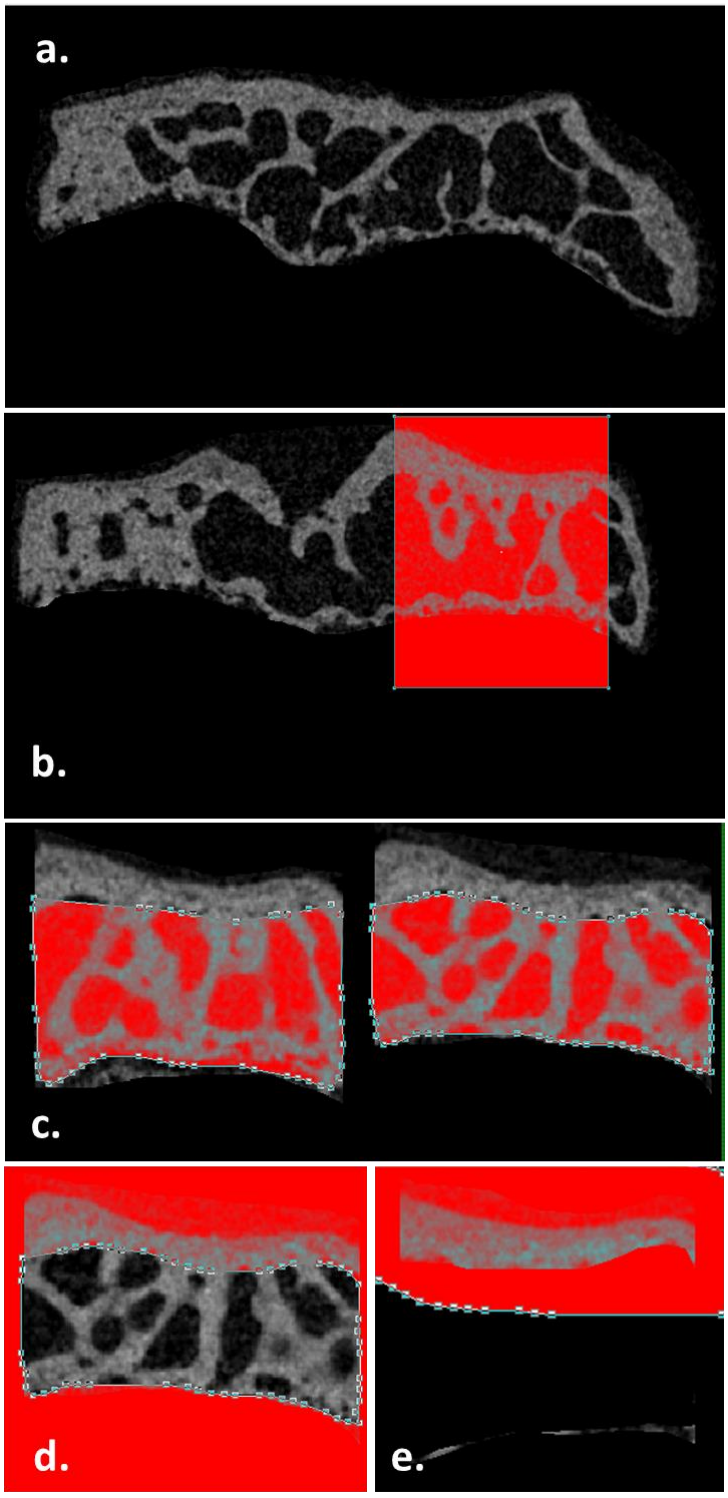

Figure 4.3: Analysis of trabeculae and subchondral bone for tibial condyles. *(a) Select the whole tibial epiphysis. (b) Select and save the medial and lateral chondyles. (c) Select the trabecular region of the lateral and medial chondyles. (d) Subtract the trabecular region, leaving the subchondral bone. (e) Isolate the subchondral bone.*

2.6. RNA isolation

Muscle and knee samples were powdered on dry ice using a hammer and kept in Trizol (Invitrogen) at -70°C until needed. For RNA extraction, 0.3 volumes of Chloroform (Sigma-Aldrich) were added to the Trizol-tissue solution per 1 volume of Trizol initially used. Following centrifugation, the RNA-containing aqueous phase was removed and incubated with 0.3 volumes of isopropanol (ThermoFisher) per 1 volume of Trizol. The RNA pellet was washed with 75% Ethanol (Sigma-Aldrich), air-dried, and re-suspended in 20µL of nuclease-free water (Ambion). RNA quality and concentration were determined by NanoDrop 2000 (ThermoFisher).

2.7. cDNA Synthesis

For Real-Time quantitative PCR, cDNA synthesis (mRNA) was performed using 500 ng RNA and SuperScript II (Thermo Fisher Scientific), and cDNA synthesis (miRNA) was performed using 100 ng RNA and miRscript RT kit II (Qiagen) according to the manufacturer's protocol.

2.7.1. mRNA

1 µl of 50 µM random hexamers, RNAse-free water and 500 ng of RNA were mixed to a total volume of 11 µl and run in a thermocycler for 10 minutes at 65˚C. The reaction was then stopped by putting samples on ice and 9µl of a master mix containing 4 µl of 5X First-Strand Buffer, 2 µl 0.1 M DTT, 1 µl 10 mM dNTPs, 1 µl Superscript II RT and 1 µl RNAse inhibitor (40 U/µL) was added to each reaction to make the total volume 20 µl. Subsequently, samples were run at 42˚C for 60 minutes in a thermocycler and, after run, each sample was diluted 8 times by adding 160 µl of RNA-free for a total volume of 180 µl.

2.7.2 miRNA

RNAse-free water and 100 ng of RNA were mixed to obtain a total volume of 12 µl. Then, 8 µl of a master mix containing 5 µl 5X HiSpec Buffer, 2 µl 10X miScript Nucleics Mix and 1 µl of miScript Reverse Transcriptase was added per reaction. Samples were run for 60 minutes at 37˚C and 5 minutes at 95˚C in a thermocycler. Finally, each sample was diluted 7 times by adding 140 µl of RNA-free for a total volume of 160 µl.

2.8. Quantitative Real-Time PCR (qRT-PCR)

qPCR analysis was performed using SsoAdvanced Universal SYBR Green Supermix (BioRad) in a 20 µL reaction mixture. For mRNAs, a master mix containing 6 µL of SybrGreen, 8ul DEPC treated water,1 µL of 10 µM forward and reverse primers mix, and 5 µL of cDNA were added per reaction. For miRNAs, a master mix containing 11ul DEPC treated water, 5 µL of SybrGreen, 1 µL of miScript Universal Primer, 1 µL of miRNA primer, and 2 µL of cDNA were added per reaction. For all qPCRs, each sample was included in triplicates and a negative control without cDNA was also included per qPCR plate. Expression relative to 18S (mRNA) or SNORD68 (miRNA) was calculated using delta Ct method. The qPCR conditions were: 95 °C for 30 seconds, 55 °C (miRNA) or 58-60 °C (mRNA) for 30 seconds, and 72 °C 30 seconds (38 times repetitions). Moreover, a hot start steps of 95 °C for 15 seconds was added at the beginning of the qPCR run. Melt curves were obtained in instances where new primers required testing whereby the temperature was increased from 65°C to 95°C in 0.5-degree increments. Primers for miRNAs, ATROGIN-1, and MURF1 were bought pre-designed from Qiagen's miRscript and RT2 range whereby the gene/miRNA of interest was identified on GeneGlobe. 18S primers were designed via NCBI nucleotide BLAST (NCBI resource coordinators, 2016). The designed primers had a melting temperature (Tm) of 50-65◦C, an amplicon size of 75-200 base pairs, and a GC content of 40-60%. Designed primers were then ordered using SigmaAaldrich's custom DNA oligo tool. All other primers were bought pre-designed from Sigma Aldrich's 'KiCqStart® SYBR® Green Primers' range. All primers were diluted to a working

stock concentration of 10μM. The housekeeping primers (18S and SNORD-68) were chosen based on their consistent expression across all conditions and treatment groups. The 2–ΔΔCt method was used to calculate the relative expression of mRNAs and microRNAs compared to the housekeeping gene. Firstly, triplicate values were averaged for each sample. Then the average CT value of the housekeeping gene was subtracted from that of the gene of interest for each sample. These values are then log transformed to give the relative fold change prior to statistical analysis.

2.8.1. Primer Sequences

Table 1.1 The 18S primer sequence used in this thesis.

Primer	Forward Sequence (5'-3')	Reverse Sequence (5'-3')
18S	GGAAAGCAGACATCGACCTCA	AGTTCTCCAGCCCTCTTGGT

Table 1.2 Sigma Aldrich's 'KiCqStart' catalogue details for mRNA primers used in this thesis.

Primer	RefSeq ID
ATROGIN-1	NM_026346
MURF-1	NM_001039048
P62	NM_011018
NRF1	NM_001164227

Table 1.3 Qiagen miRScript catalogue details for all miRNA primers used in this thesis.

Primer	Catalogue ID
miR-24	MS00005922
miR-199a-5p	MS00032529
miR-378a-3p	MS00032781
SNORD-68	MS00017752

2.9. Bioinformatic Analyses

2.9.1. Ingenuity Pathway Analysis

Qiagen's Ingenuity Pathway Analysis (IPA) was used to find significantly enriched pathways in various list of genes throughout this thesis. For IPA, core expression analysis is selected and only experimentally observed interactions are used. Species is set to human only and tissues and cell lines set to tissues and primary cells.

2.9.2. Meta Analyses

For this project p-value based meta-analyses methodologies were used as it enables the combination of results when effect size estimates and/or standard errors from individual studies are not freely available. Meta-analyses were performed on p-values and directions of effects, providing the miRNA or mRNA was identified as being significantly dysregulated in ≥3 independent studies, as previously described (Schulz et al., 2019). To do so, a customised R studio script was used to transform p values into signed z-scores using Stouffer's method (Stouffer et al., 1949; Zaykin et al., 2011) which were then converted to positive or negative values depending on the direction of expression (R script can be found in supplementary table 5). Z-scores for each miRNA/mRNA were combined by calculating a weighted sum, with weights being proportional to the square root of the effective sample size of the study.

2.9.3 Overlap Analyses

All overlap analyses were performed using the R package 'GeneOverlap' (Shen et al., 2022). Given two gene lists, this package tests the significance of their overlap in comparison with a genomic background. In this case, all human protein coding genes were used as background for the analysis. Significance was assessed using a two-tailed Fisher's exact test with Benjamini-Hochberg false discovery rate (FDR) correction.

2.10. Statistical analysis and normality of data testing

Normality and statistical analysis were calculated using GraphPad Prism (GraphPad v8). Normality of data was tested using a Shapiro-Wilk test where a p-value ≤ 0.05 indicated statistical significance. For all other statistical analyses, a p-value ≤ 0.05 also indicated statistical significance.

To determine any significance between the means of two groups, a student´s t-test was used. For more than two groups, a one-way variance analysis (ANOVA) was used. If comparisons were being made between different time points within the same group, the analysis was paired. Likewise, a paired test was used when comparing mechanically loaded vs contralateral control tissue within the same mouse. For all other analyses, unpaired tests were used. In instances where data did not fit a normal distribution, non-parametric tests were applied. All data throughout the thesis is displayed graphically as mean $\pm$ range with all data points per group included.

Chapter 3:

Characterising the relationship between muscle atrophy and osteoarthritis, and involvement of miRNAs, in a mechanical loading-induced and spontaneous model of murine OA

3.1. Introduction

Musculoskeletal tissue dysfunction is the leading cause of frailty, falls, and decreased quality of life in older people (Greco et al., 2019). The loss of muscle mass, strength, and function during ageing, known collectively as sarcopaenia, is a major factor in the frailty of the elderly, and is a condition that is becoming increasingly prevalent as the population distribution shifts towards an older mean age (Cesari et al., 2014). OA is another form of musculoskeletal dysfunction (Cross et al., 2014). Despite the high prevalence of both muscle atrophy and OA in older populations, little is known about the interaction between these two diseases, as discussed in a recent review by Shorter et al. (2019). Research has previously suggested that muscle atrophy directly affects joint stability, with loss of mobility leading to gradual degeneration of articular cartilage (Bennell et al., 2013). Conversely, it has been proposed that the disuse of an OA affected joint, due to the pain of movement, may be the primary cause of the reduction in muscle strength associated with OA (Pisters et al., 2014). Whether muscle atrophy precedes OA, or *vice versa*, changes in gene expression and epigenetic modifications are anticipated to be important contributors to the process.

Murine models are often used to investigate pathological changes that occur in the joint and surrounding tissues during OA. Murine models of OA can be broadly categorised into either induced or spontaneous models, with the latter being subcategorised into naturally occurring and genetically modified models. Spontaneous models are the hallmark of primary OA, and often more closely simulate the progression of human primary OA (Kuyinu et al., 2016). The STR/ort model is the most used genetically modified model of spontaneous OA and exhibit human-like cartilage lesions at approximately 12 to 20 weeks of age (Mason et al., 2001; Staines et al., 2017). Altered biomechanical loading is another way to induce OA, with researchers often using surgical methods to impair joint stability. Destabilisation of the medial meniscus or transection of the anterior cruciate ligament are the main two methods to do this and consistently result in cartilage degeneration and OA development. However, these methods may have detrimental effects on periarticular tissues (Poulet et al., 2016) and rely on the researcher having micro-surgical skills. No OA animal model is entirely predictive of idiopathic OA in the aging human

population, and often require long time points to observe OA development. Surgical procedures also run the risk of introducing infection into the joint, with the associated inflammation affecting experimental results. Non-invasive models (such as mechanical joint loading) overcome these limitations and can create injury with more precision and reproducibility than other induced models. Articular cartilage lesions have been demonstrated histologically in mice that have undergone a single mechanical loading episode. When the loading is repeated three times a week for 2 weeks, these lesions spontaneously progress and worsen (Poulet et al., 2011). Studies have previously characterised this mechanical loading model histologically. In particular, the regimen used in this experiment has been shown to induce reproducible cartilage lesions in the lateral femur, localised medial osteophyte formation, synovial hyperplasia and fibrosis, and OA-like cruciate ligament changes (Poulet et al., 2011).

As previously mentioned, miRNAs are emerging as powerful regulatory molecules and are found to be dysregulated in different diseases – such as degenerative musculoskeletal diseases (Zheng et al., 2021). For example, in muscle, miRNAs have been shown to regulate myogenesis, through the control of satellite cell quiescence, proliferation, and terminal differentiation (Brzeszczyńska et al., 2020), with the dysregulation of such processes leading to muscle atrophy. However, there is no consensus on how miRNA dysregulation may alter muscle atrophy. Moreover, even less is known about the role of miRNA dysregulation in muscle atrophy associated with other pathophysiologies, such as OA. The fact that both muscle atrophy and OA are both multifactorial disorders add to this complexity. One of these factors is abnormal mechanical load, which may modulate the disease states of both joint and muscle tissues. To date, there have been multiple studies identifying specific miRNAs as being mechanoresponsive in cartilage, bone, and muscle (Dunn et al., 2009; Guan et al., 2011; Guo et al., 2015; Yu et al., 2015; Chen et al., 2020; Wang et al., 2021; Shang et al., 2021). These studies suggest that specific mechanoresponsive miRNAs may regulate processes such as chondrogenic proliferation and differentiation and myoblast maturation (Guan et al., 2011; Rhim et al., 2020).

3.1.1. Aims

Studies looking at the molecular changes in response to mechanical loading using this mechanical load-induced murine model are lacking. Moreover, the effect of mechanical joint loading on the neighboring periarticular muscle tissues is unknown. Despite previous research showing the development of OA in CD1 mice by 6 months (data unpublished), later time points have not been investigated. OA-associated muscle atrophy in these mice has also not been investigated.

Therefore, the aim of this study was to utilise histological and molecular techniques to characterise the muscle phenotype, and miRNA dysregulation, in spontaneous and mechanical load-induced models of OA. Another aim was to investigate specific pathways that may be enriched in the validated target genes of miRNAs that we find to be dysregulated in these models.

3.2. Materials and Methods

3.2.1. Animals and Experimental Groups

All mice were kept in polypropylene cages of 2–6 littermates, subjected to 12-hour light/dark cycles at 21±2°C, and fed standard RM1 maintenance diet ad libitum (No.1; Special Diet Services, Witham UK). All procedures complied with Animals (Scientific Procedures) Act 1986 and local ethics committee. At the end of the experiments, mice were culled via asphyxiation by a rising CO2 concentration.

Male outbred CD-1 mice (Charles River, UK) were used as a spontaneous model of OA and were culled at either 3-months (n=9), 4-months (n=5), 6-months (n=10), or 8-months (n=6). For the model of mechanical load-induced OA, 12-week-old male mice were subjected to a two-week regimen of non-invasive mechanical loading (see general methods for detailed protocol) and left to age for 12 weeks post-loading (n=22).

3.2.2. Histology

Methods to determine skeletal muscle and knee joint phenotypes is detailed in the general methodology chapter. In brief, 10um sections of muscle were stained with a 1:1000 dilution of rhodamine wheat germ agglutinin and imaged either using a Ziesslsm800 confocal microscope or Axio Scan.Z1 slide scanner (Zeiss, UK). The fiber cross-sectional area and minimum ferret's diameter was analysed with Myovision software (Wen et al., 2017).

Serial coronal 6µm thick sections of knee joints were cut across the entire joint and a quarter of the sections were selected, stained with toluidine blue (0.1% in 0.1M solution of acetate buffer, pH 5.6), and counterstained with 0.2% fast green. Toluidine blue slides of the entire knee joint were scored for cartilage lesion severity in each knee compartment: medial tibia (MT), medial femur (MF), lateral tibia (LT) and lateral femur (LF) using the OARSI grading system (Glasson et al., 2010). Using these calculations, the average mean and maximum lesion scores was calculated for each compartment and for the whole knee joint of each mouse. Summed scores of all the compartments were also calculated from the mean and maximum scores.

3.2.3. cDNA Synthesis and qRT-PCR

For miRNA expression analysis, total RNA was isolated and purified using the Trizol method, as detailed in the general methodology chapter. Reverse transcription of total RNA containing miRNAs was performed with miScript II RT kit (Qiagen, UK). qPCR was performed on a Rotor-Gene Q™ (Qiagen) instrument in a 20 µL reaction mixture. qPCR conditions were: 95 ◦C for 30 s, 55 ◦C for 30 s and 72 ◦C for 30 s (40 cycles) using a hot start step of 95 ◦C for 15 s. Specific primers for miR-199a-3p, miR-378a-3p, miR-24, SNORD-68, ATROGIN-1, MURF-1, P62, NRF1, and 18S (tables 1.1-1.3) were used for the qPCR whereby SNORD-68 was used as the housekeeping gene. The results were analysed using the delta CT method (Livak and Schmittgen, 2001).

3.2.4. Ingenuity Pathway Analysis

Qiagen's Ingenuity Pathway Analysis (IPA) was used to find significantly enriched pathways in a list of validated miR-378a-3p target genes obtained from miRTarBase (Huang et al., 2022). Parameters for the analysis are detailed in chapter 2.9.1.

3.2.5. Statistical analysis and normality of data testing

Normality and statistical analysis were calculated using GraphPad Prism (GraphPad v8). Normality of data was tested using a Shapiro-Wilk test where a p-value ≤ 0.05 indicated statistical significance. For all other statistical analyses, a p-value ≤ 0.05 also indicated statistical significance. Statistical analysis of the fiber cross-sectional area, OARSI severity, and gene expression between CD1 age groups involved conducting an analysis of variance (ANOVA) ($p \leq 0.05$). For analysis of fiber cross-sectional area, OARSI severity, and gene expression in the loaded *vs* contralateral control limb in the load-induced model, a paired t-test was utilized. Data is displayed graphically as mean $\pm$ range with all data points per group included.

3.3. Results

3.3.1. CD1 mice exhibit significant spontaneous OA at 6-months and 8-months old compared to their younger counterparts

CD1 mice showed minimal OA at 3-months, mild to moderate OA at 4-months, and moderate to severe OA at 6- and 8-months old (figure 3.1). Analysis of the maximum lesion severity of each age group finds the largest increase in OA occurs between 3- and 6-months old ($p<0.0001$). The summed maximum lesion severity also reflects this, with the largest increase in severity occurring between 3- vs 6-month-old, and 3- vs 8-month-old mice ($p<0.001$). Mean and summed mean lesion severity scores also show a significant increase in severity between 3 and 6-month-old and 3 and 8-month-old mice ($p<0.01$). OA severity appears to plateau between 6- and 8-months-old where there is no significant increase in maximum or mean lesion severity across the joint.

Maximum lesion severity in the younger 3- and 4-month-old mice is much less variable (grade 0-2) than the older 6- and 8-month-old mice (grade 2-6).

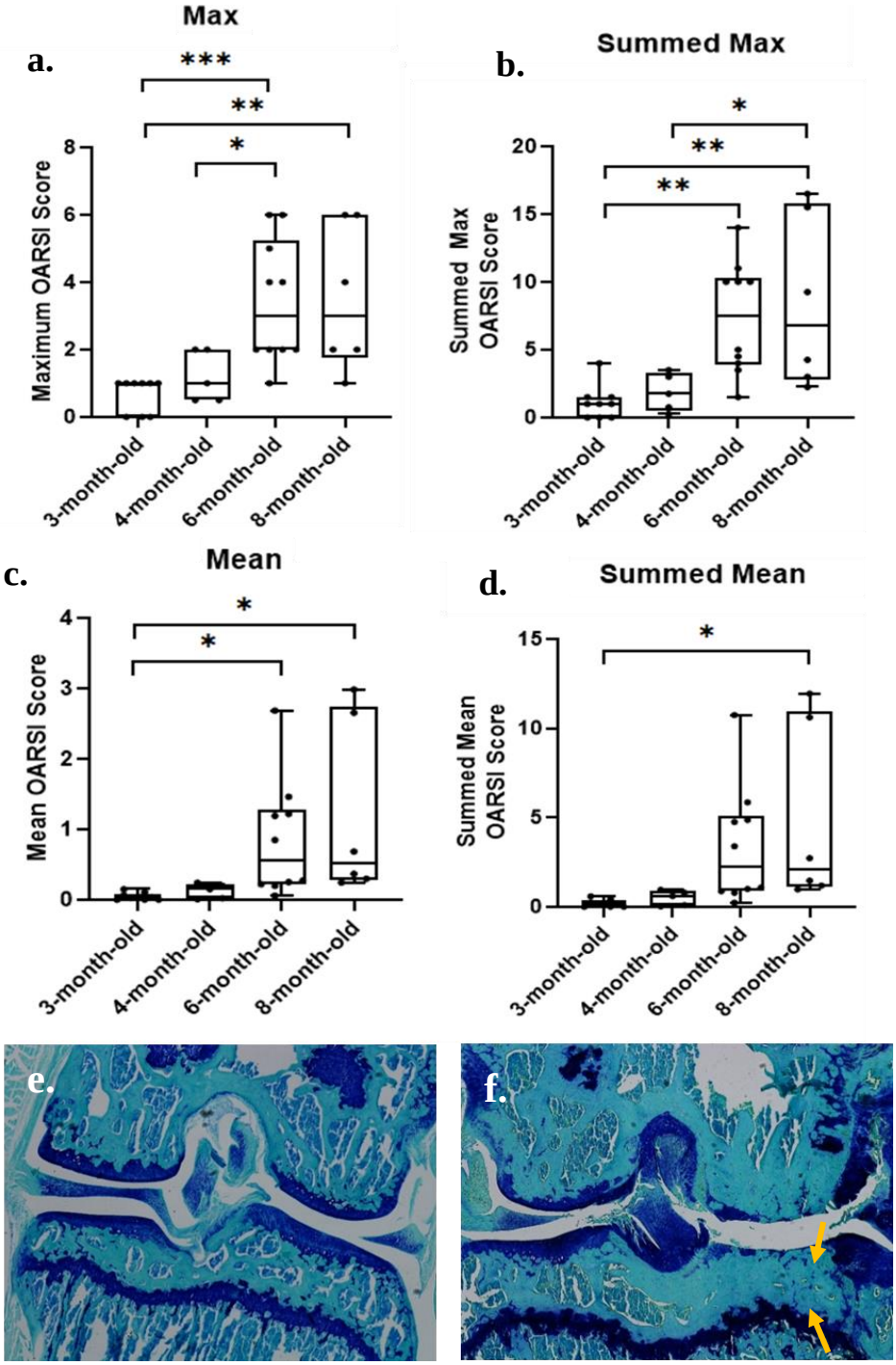

Figure 3.1: Joint histology in CD1 mice with spontaneous OA. *(a-d)) Mean, maximum, and summed mean and maximum lesion severity across all joint compartment combined. (e) An OARSI grade 0, 3-month-old CD1 joint stained with toluidine blue demonstrating no cartilage lesions. (f) An OARSI grade 6, 8-month-old CD1 joint stained with toluidine blue with complete cartilage loss in the medial compartments. Student's unpaired t-test. Yellow arrows are highlighting the complete loss of articular cartilage in the medial tibia and femur. *p<0.05, **p<0.01, ***p<0.001. MT= medial tibia., MF = medial femur, LT = lateral tibia, LF = lateral femur. Data is displayed graphically as mean ± range with all data points per group included. 3-months (n=9), 4-months (n=5), 6-months (n=10), or 8-months (n=6).*

3.3.2. Markers of muscle atrophy are increased in the quadriceps of older CD1 mice

Muscle Atrophy F-box gene (Atrogin-1) and Muscle RING-finger protein-1 (MURF-1) expression showed a trend in increased expression in the quadriceps and gastrocnemius of the older CD1 mice (6 and 8-month old; n=16) compared to the younger 3- and 4-month-old mice (n=14), depicted in figure 3.2 (a-d). This was only significant in the quadriceps where Atrogin-1 was found to be significantly increased in the older mice (figure 3.2 (c); p=0.0294, approximately +1.6 fold-change).

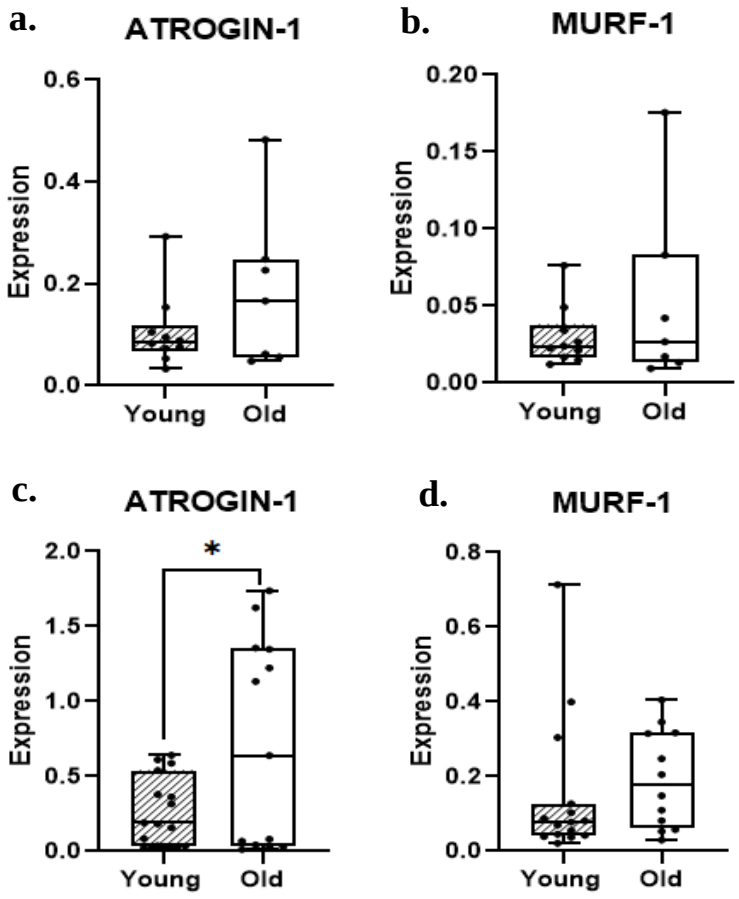

Figure 3.2: Expression of muscle atrophy markers in mice with spontaneous OA. *(a-b) Atrogin-1 and Murf-1 expression in the gastrocnemius muscles of 'young'(n=14) vs 'old' (n=16) CD1 mice. (c-d) Atrogin-1 and Murf-1 expression in the quadriceps muscles of 'young' vs 'old' CD1 mice. 'Expression' refers to the CT expression value of the mRNA relative to the housekeeping gene '18S'. Student's unpaired t-test. *p<0.05. Data is displayed graphically as mean ± range with all data points per group included.*

3.3.3. Older CD1 mice have significantly reduced fiber cross sectional area in the gastrocnemius, which correlates with OA lesion severity.

Fiber cross-sectional area in the gastrocnemius was significantly reduced at 6- and 8-months-old, compared to the 3- and 4-month-old mice. Although there was a trend of reduced CSA in the quadriceps, this was not significant. The maximum lesion severity across the entire joint (average of all compartments) negatively correlated significantly with fiber CSA in the gastrocnemius (figure 3.4; p=0.0054), but not the quadriceps (figure 3.3 (c)).

There was no significant difference in the fiber cross-sectional area means between the 3- and 4-month-old mice. There is a significant decline in fiber cross-sectional area between 3-month-old and 6-month-old mice (p=0.0489) and 4-month-old and 6-month-old mice (p=0.0013). There was an even larger decrease in fiber CSA between the 4-month-old and 8-month-old mice (p=0.0005). Despite an apparent decline in fiber CSA between the 6-month-old and 8-month-old mice, this was not found to be significant.

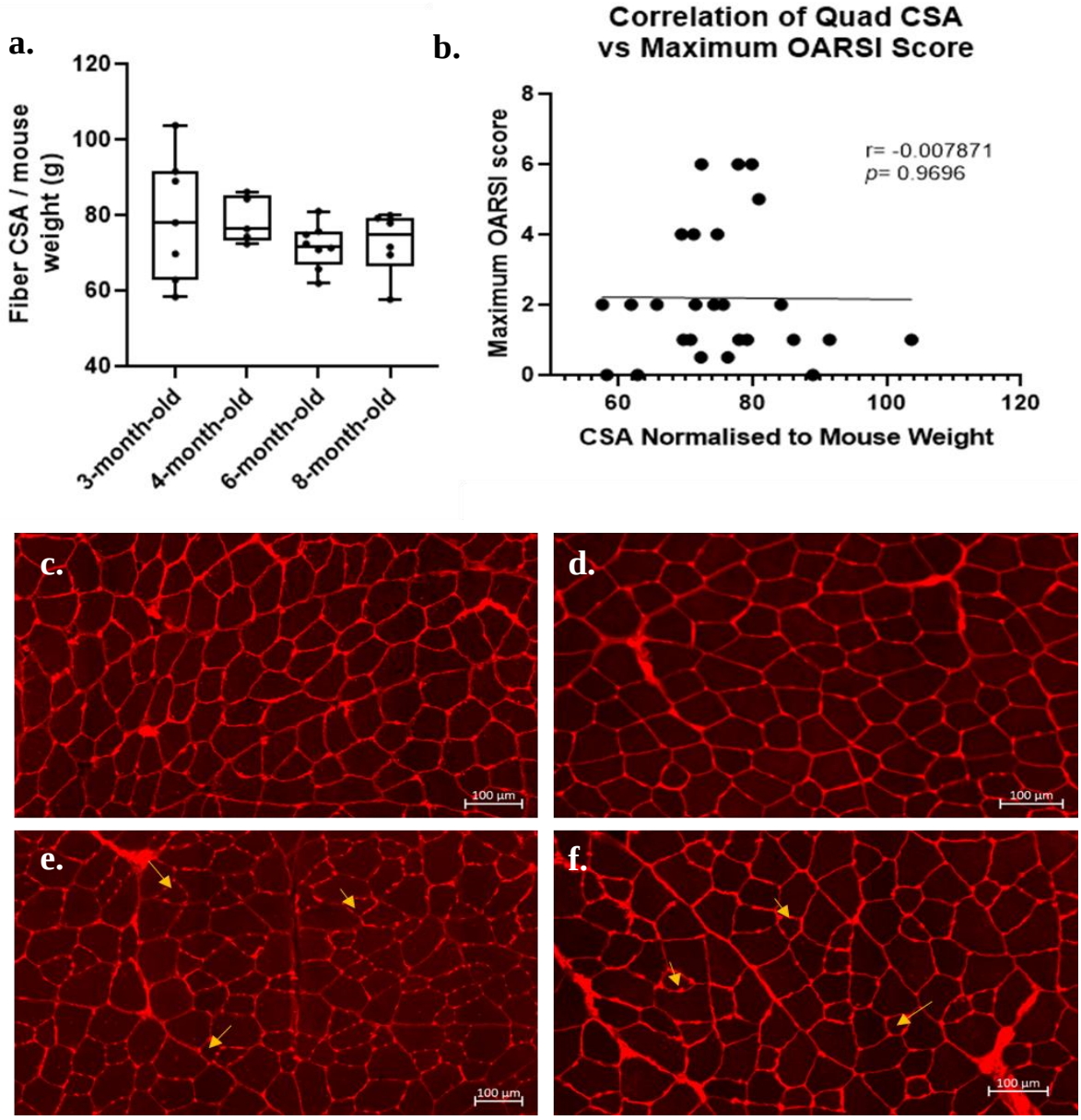

Figure 3.3: Quadriceps histology in the CD1 model of spontaneous OA. *(a) Fiber cross-sectional area normalized to mouse weight in the quadriceps of CD1 mice aged 3-, 4-, 6-, and 8-months-old. (b) Pearson's correlation of fiber cross-sectional area (normalized to mouse weight) and the maximum OARSI score in the joint. (c-f) representative cross-sections of the quadriceps muscles of 3-, 4-, 6-, and 8-month-old CD1 mice, respectively. Yellow arrows indicate smaller muscle fibers throughout the section. Student's unpaired t-test. * p<0.05, **p<0.01, ***p<0.001. Data is displayed graphically as mean ± range with all data points per group included. 3-months (n=9), 4-months (n=5), 6-months (n=10), or 8-months (n=6). 3-months (n=9), 4-months (n=5), 6-months (n=10), or 8-months (n=6). Scale bar shown in all cross-sectional images is 100um.*

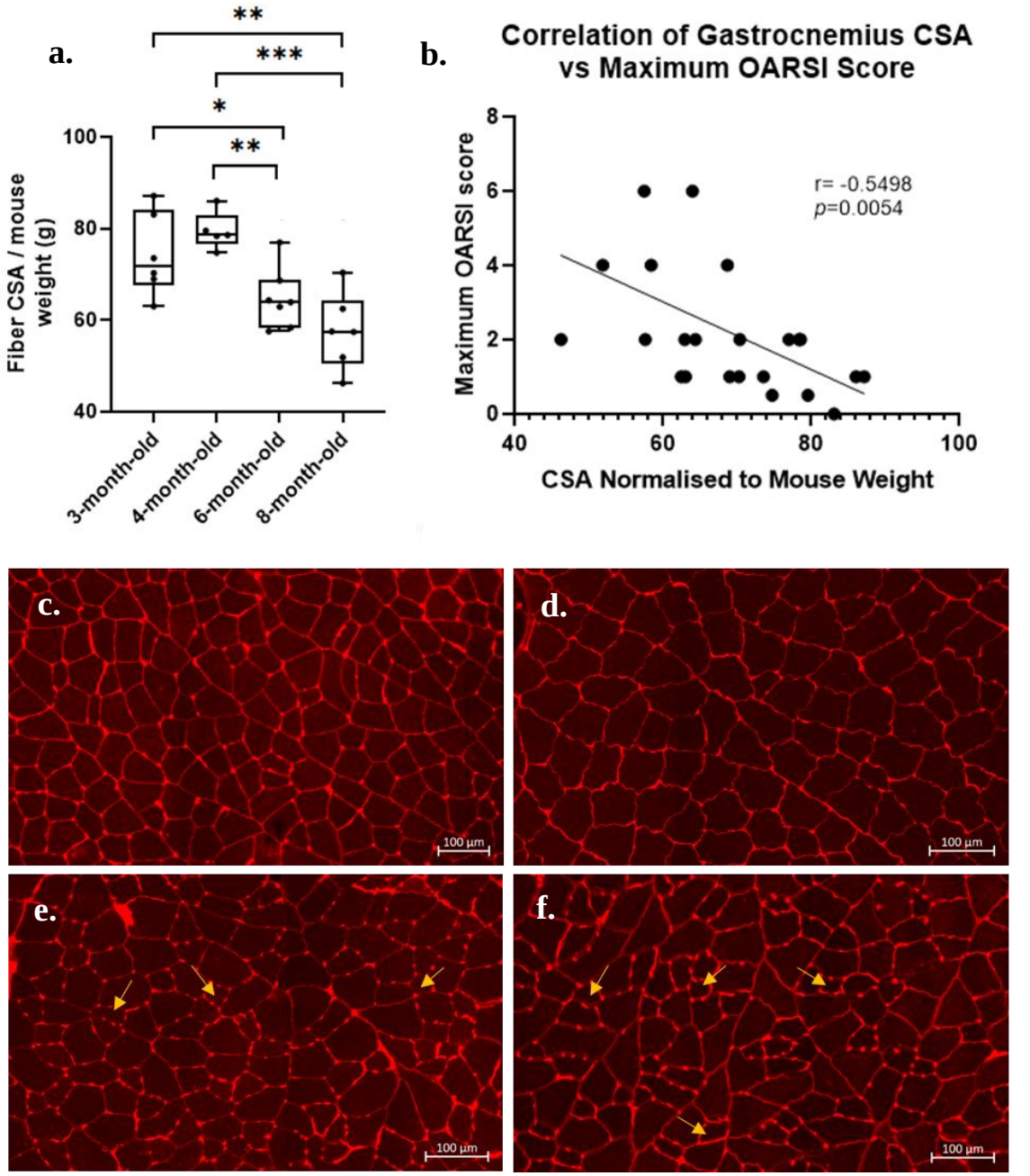

Figure 3.4: Gastrocnemius histology in the CD1 model of spontaneous OA. *(a) Fiber cross-sectional area normalized to mouse weight in the gastrocnemius of CD1 mice aged 3-, 4-, 6-, and 8-months-old. (b) Pearson's correlation of fiber cross-sectional area (normalized to mouse weight) and the maximum OARSI score in the joint. (c-f) representative cross-sections of the gastrocnemius muscles of 3-, 4-, 6-, and 8-month-old CD1 mice, respectively. Yellow arrows indicate smaller muscle fibers throughout the section. ANOVA test of mean variance. * $p<0.05$, ** $p<0.01$, *** $p<0.001$. Data is displayed graphically as mean $\pm$ range with all data points per group included. 3-months (n=9), 4-months (n=5), 6-months (n=10), or 8-months (n=6).*

3.3.4. miR-24a and miR-378a-3p were downregulated in the old CD1 gastrocnemius and quadriceps, respectively.

microRNAs that have been previously implicated in muscle atrophy and ageing - miR-378a-3p, miR-199a-5p, and miR-24a - were quantified in the quadriceps and gastrocnemius muscles of the CD1 mice with spontaneous OA (figure 3.5). miR-199a-5p was not significantly dysregulated in the young (3- and 4-month-old; n=14) *vs* old (6- and 8-month-old; n=16) quadriceps or gastrocnemius muscles. miR-24a was downregulated in both the quadriceps and the gastrocnemius, though it was only significant in the gastrocnemius (p=0.0287, fold-change of -1.6). miR-378a-3p was very variable in the old gastrocnemius muscle but was significantly downregulated in the quadriceps of the older CD1 mice (p=0.0382, fold-change of -3).

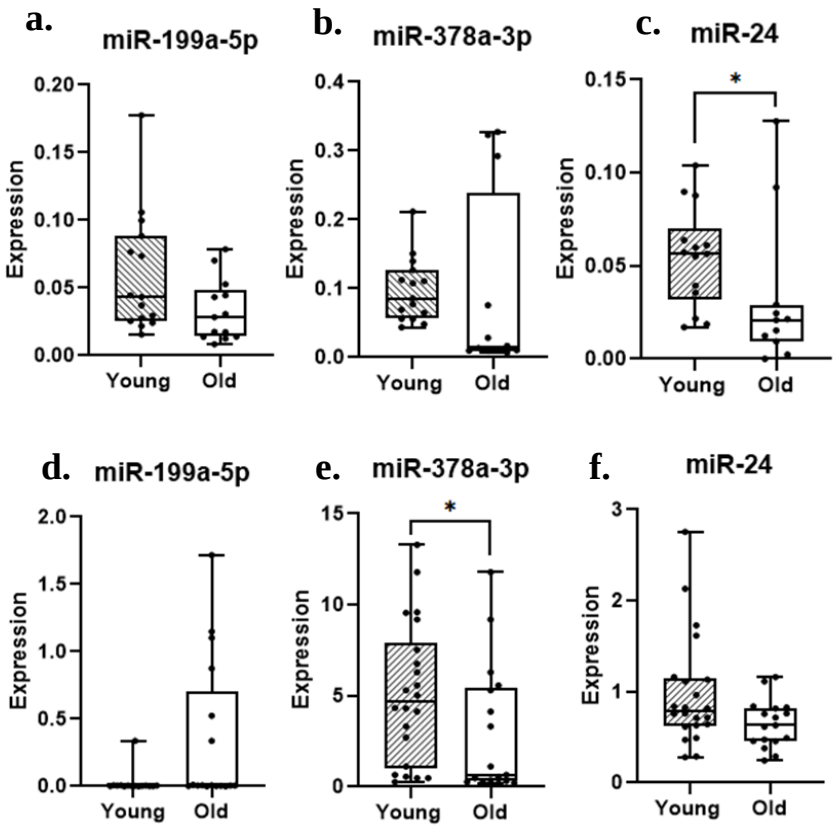

Figure 3.5: miRNA expression in spontaneous OA skeletal muscle. *(a-c) miR-199a-5p, -378a-3p, and -24 expression in the gastrocnemius muscles of old (n=16)* vs *young (n=14) CD1 mice. (d-f) miR-199a-5p, -378a-3p, and -24 expression in the quadriceps muscles of old vs young CD1 mice. 'Expression' refers to the CT expression value of the microRNA relative to the housekeeping miR 'SNORD-68'. Student's unpaired t-test *p<0.05. Data is displayed graphically as mean ± range with all data points per group included.*

3.3.5. C57BL/6 mice show a significant reduction in fiber cross-sectional area and increase in centralised myonuclei in the quadriceps of the limb with mechanical load-induced OA compared to contralateral controls.

Fiber cross-sectional area in the quadriceps show significant reduction in the limb subjected to non-invasive mechanical joint loading compared to the non-loaded contralateral control limb (figure 3.6 (a); n=15, $p<0.05$). This was not reflected in the minimal Feret's diameter measurements of the quadricep fibers, which found no significant difference between the loaded and non-loaded limbs (figure 3.6 (b); $p=0.1646$). The numbers of centralised myonuelci per mm^2 in the quadriceps was found to be significantly increased in the loaded limb compared to contralateral controls (figure 3.6 (c); n=10, $p<0.05$).

In the gastrocnemius, no significant differences in minimum Feret's diameter or centralised myonuclei were observed in the loaded limb compared to the non-loaded contralateral control (figure 3.7 (b-c); $p=0.1335$ and $p=0.5216$, respectively). Despite an apparent reduction in fiber CSA in the gastrocnemius of the loaded limb, this was not found to be statistically significant (figure 3.7(a); n=12, $p=0.3822$).

Muscle-specific E3 ubiquitin ligase atrophy gene-1 (ATROGIN-1) and muscle atrophy F-box and muscle ring-finger protein 1 (MURF-1) expression quantification showed no differences in the control vs loaded limb (figure 3.6(g-h) and 3.7(g-h)) in either the quadriceps (n=5; $p=0.5186$ and $p=0.1319$, respectively) or gastrocnemius muscles (n=5; $p=0.9722$ and $p=0.2445$, respectively).

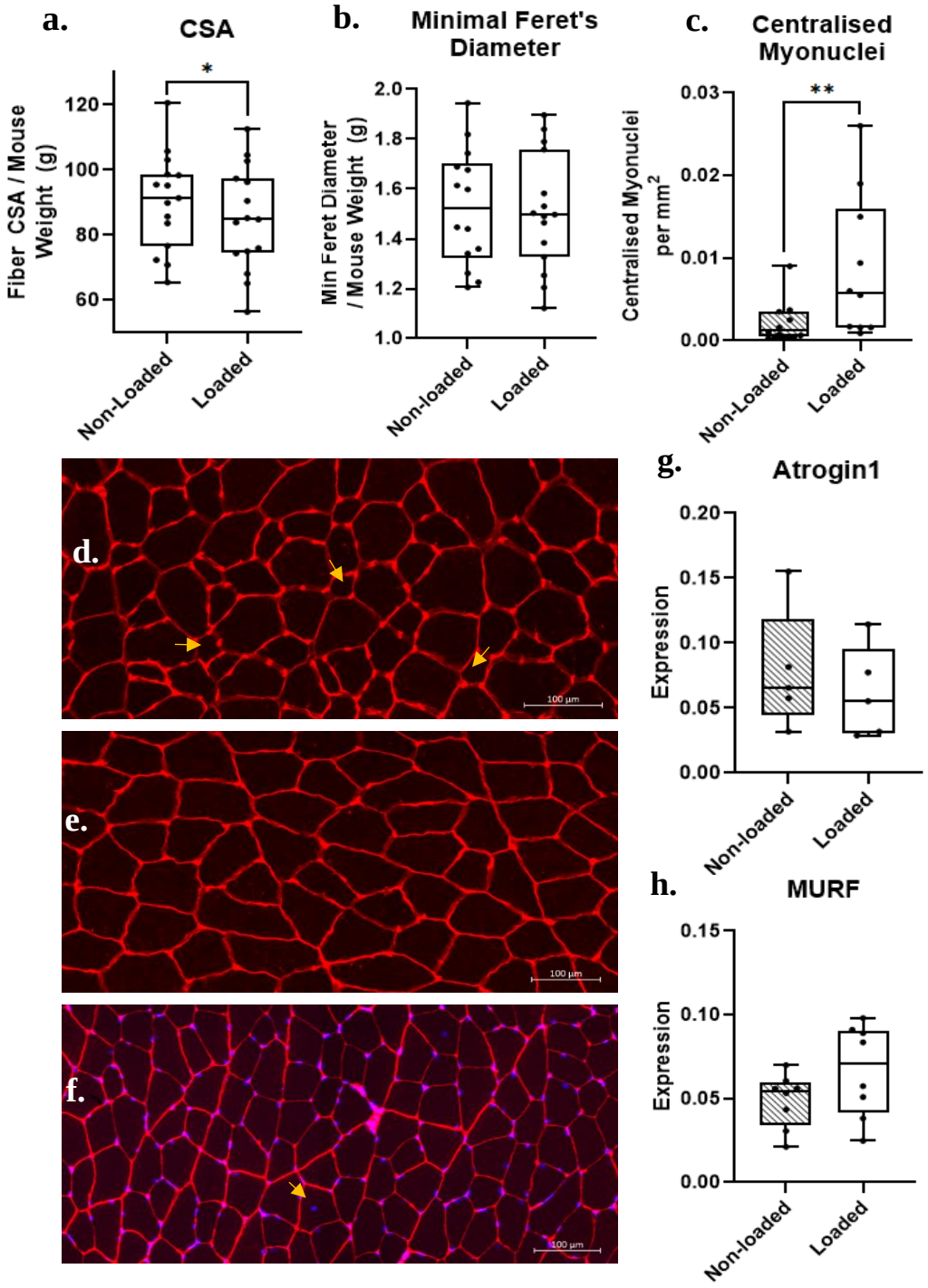

Figure 3.6: Quadricep histology in a mechanical load-induced OA model. *(a) Fiber cross-sectional area normalized to the mouse weight in the quadriceps of the limb with post-traumatic OA compared to contralateral control limbs (n=15). (b) The minimal Feret's diameter of the quadricep fibers normalized to the mouse weight. (c) Number of centralised myonuclei per mm^2 across the quadricep section. (d) A representative image of the quadriceps fibers of the limb with post-traumatic OA, with yellow arrows indicating smaller muscle fibers throughout the section. (e) A representative image of the quadriceps of the non-loaded contralateral control limb from the same mouse. (f) An image of a quadricep section where one of the fibers is shown by the yellow arrow to have a centralized myonuclei. (g-h) MURF1 and ATROGIN1 expression as determined by qRT-PCR. *p<0.05 paired student's t-test. Data is displayed graphically as mean ± range with all data points per group included.*

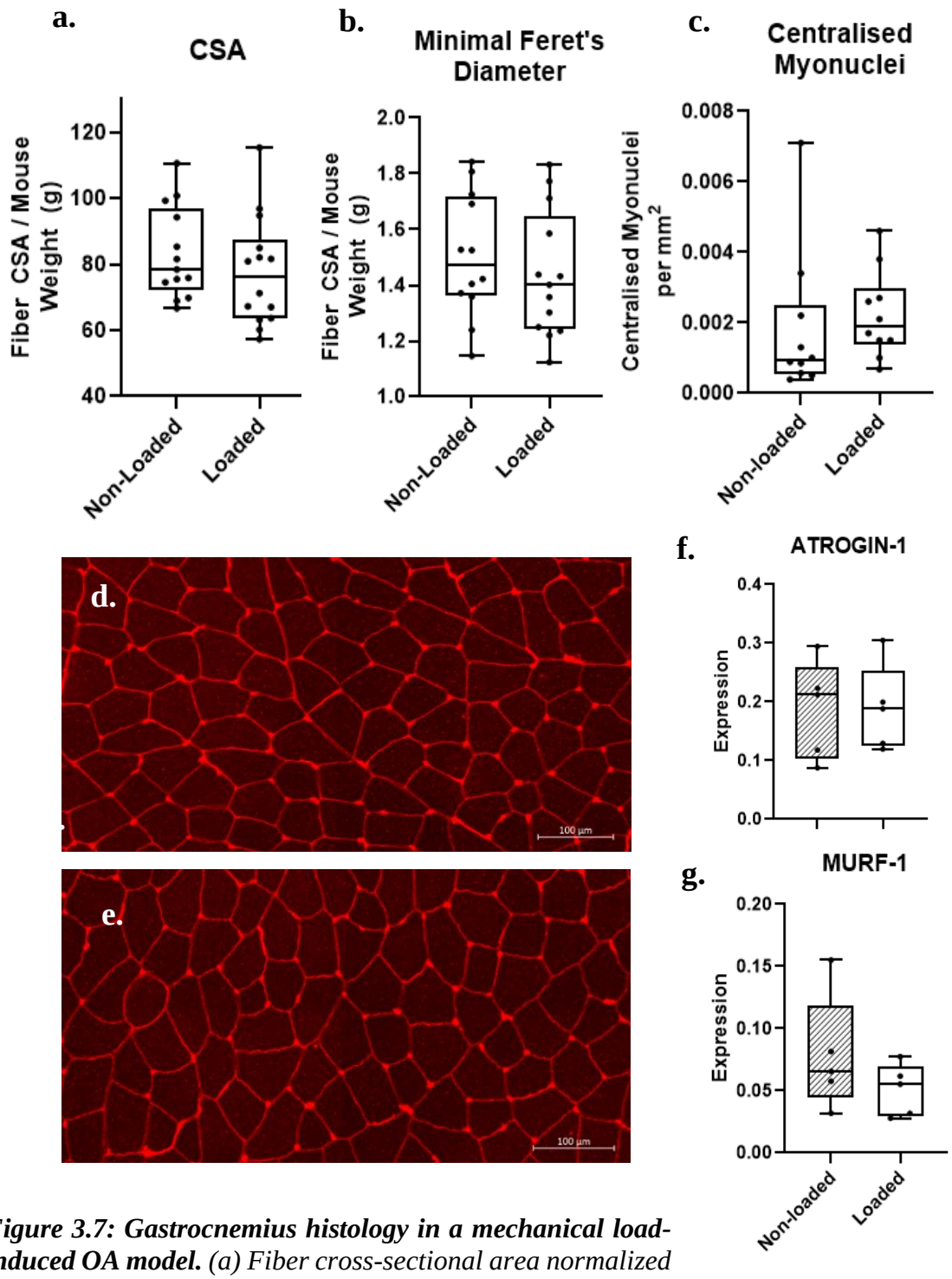

Figure 3.7: Gastrocnemius histology in a mechanical load-induced OA model. *(a) Fiber cross-sectional area normalized to the mouse weight in the limb with post-traumatic OA control limbs (n=12). (b) The minimal Feret's diameter of the gastrocnemius fibers normalized to the mouse weight. (c) Number of centralised myonuclei per mm^2 across the gastrocnemius section. (d) A representative image of the gastrocnemius fibers of the limb with post-traumatic OA, (e) A representative image of the gastrocnemius of the non-loaded contralateral control limb from the same mouse. (f-g) MURF1 and ATROGIN1 expression as determined by qRT-PCR. *$p<0.05$ paired student's t-test. Data is displayed graphically as mean $\pm$ range with all data points per group included.*

3.3.6. miRNA expression in the gastrocnemius and quadriceps show downregulation of miR-378a-3p in mechanical load-induced OA.

miR-378a-3p, miR-199a-5p, and miR-24a expression was quantified in the gastrocnemius and quadriceps muscles of the C57BL/6 mice with mechanical load-induced OA. miR-199a-5p and miR-24a showed a trend of downregulation but were not significantly dysregulated in the quadriceps or gastrocnemius muscles of the loaded limb *vs* the contralateral control limb (figure 3.8 (a-f)). miR-378a-3p was significantly downregulated in the quadriceps of the loaded limb *vs* the contralateral control limb (p=0.0391, fold-change of -1).

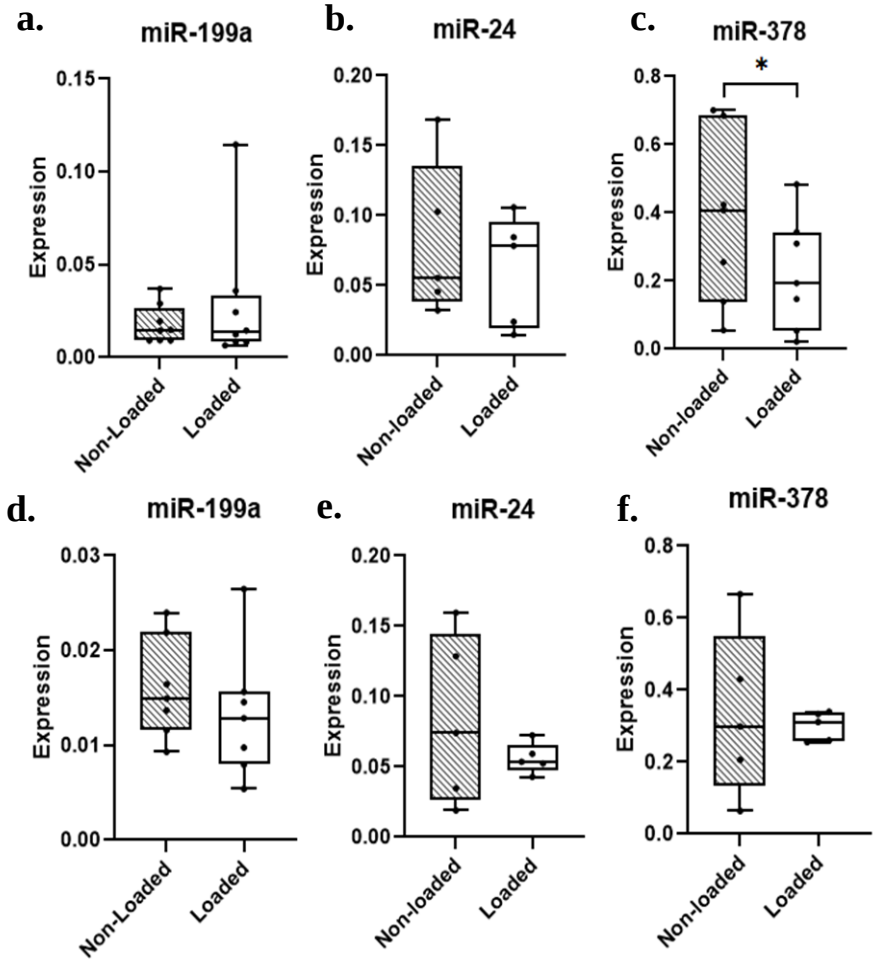

Figure 3.8: miRNA expression in the skeletal muscles of mice with mechanical load-induced OA. *(a-c) miR-199a-5p, -24, and -378a-3p expression in the quadriceps muscles of the limb with post-traumatic OA (n=5) vs the non-loaded contralateral control limb (n=5). (d-f) miR-199a-5p, -378a-3p, and -24 in the gastrocnemius muscles of the limb with post-traumatic OA vs the non-loaded contralateral control limb. 'Expression' refers to the CT expression value of the microRNA relative to the housekeeping miR 'SNORD-68'. Student's paired t-test *p<0.05. Data is displayed graphically as mean ± range with all data points per group included.*

3.3.7. IPA reveals autophagy as the most significantly enriched pathway from a list of experimentally validated miR-378a-3p target genes.

In order to investigate which genes, and their pathways, were targeted by miR-378a-3p, IPA was used. This determined the most significantly enriched pathways in a list of validated miR-378a-3p target genes. From the 201 pathways that resulted from this analysis, autophagy was the most significant. 31 genes from the miR-378a-3p target gene list were associated with autophagy (figure 3.9). All significantly enriched pathways identified by IPA are detailed in supplementary table 1. SQSTM1 – otherwise known as P62 – was one of the 31 miR-378a-3p target genes that were found to be involved in the autophagy pathway and is a classic reporter of autophagy activity.

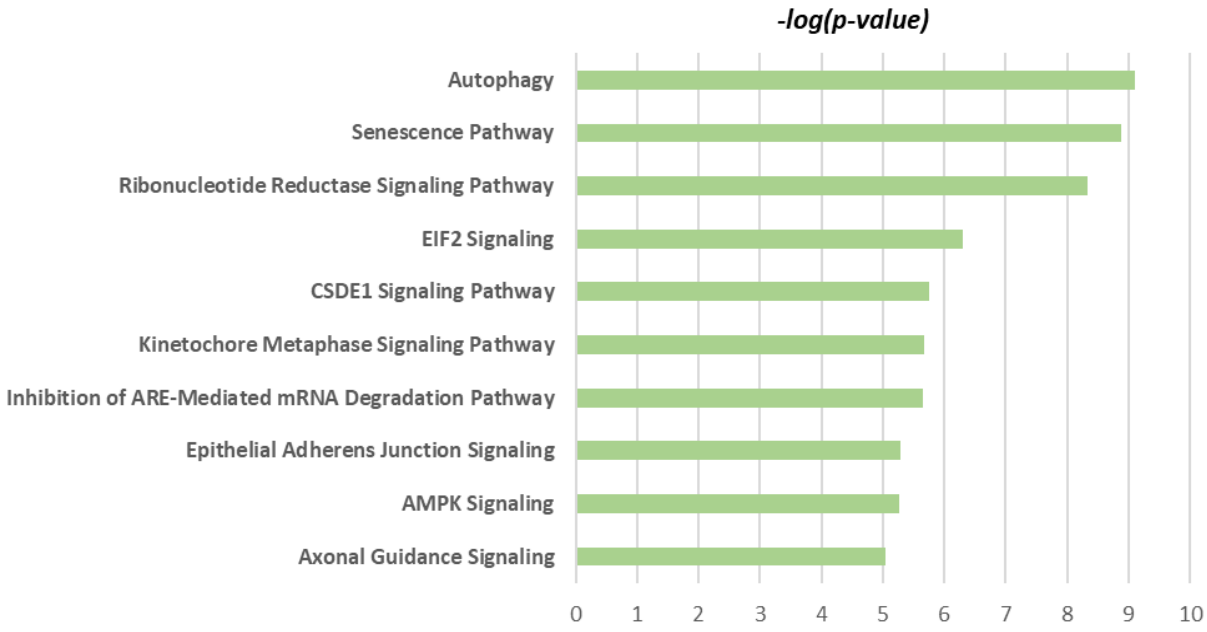

Figure 3.9: The top 10 canonical pathways, determined by Ingenuity Pathway Analysis (IPA), that were significantly enriched in a list of miR-378a-3p validated target genes.

3.3.8. P62 is upregulated in both the quadriceps of the loaded limb.

qRT-PCR analysis of the quadriceps from the limb subjected to mechanical loading revealed a significant upregulation in P62 expression (p=0.0466, fold-change of +1.2) a target gene of miR-378a-3p that was found to be downregulated in the same tissue (figure 3.10). No upregulation of P62 was observed in the gastrocnemius of the limb subjected to mechanical joint loading.

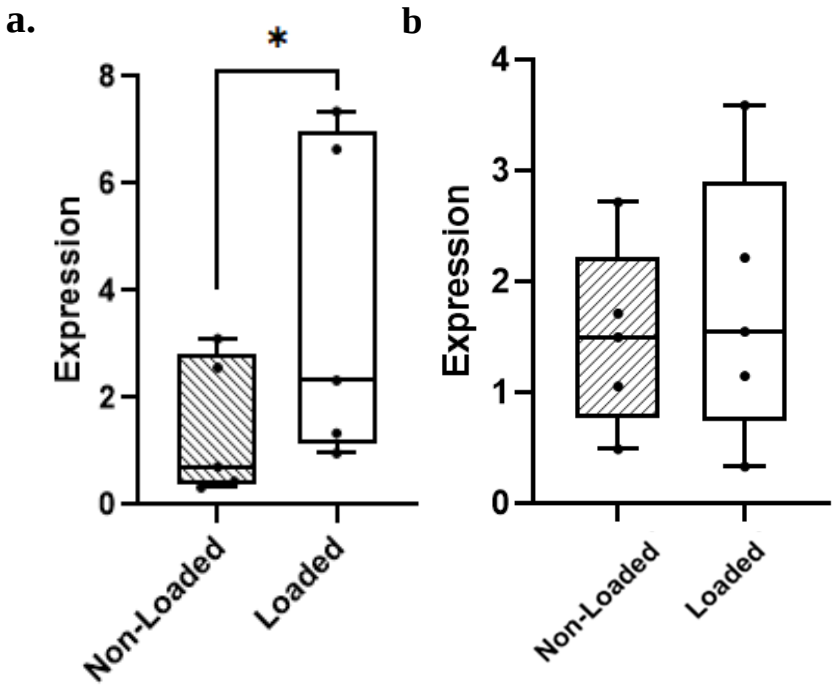

Figure 3.10: P62 expression in the quadriceps (a) and gastrocnemius (b) of the limb with mechanical loading-induced OA compared to the contralateral control limb. *'Expression' refers to the CT expression value of the microRNA relative to the housekeeping miR 'SNORD-68'. Student's unpaired t-test. * p<0.05. Data is displayed graphically as mean ± range with all data points per group included.*

3.4. Discussion

This study aimed to characterise the peri-articular muscle phenotype in a range of murine models of OA. Results show that the quadriceps muscles experience significant atrophy in response to mechanical loading-induced OA. These quadriceps muscles are characterised by overexpression of muscle atrophy marker 'ATROGIN-1', downregulation of miR-378a-3p, and concurrent upregulation of its target gene 'P62'. This research also proposes the CD1 strain of mice as a novel model of spontaneous OA, demonstrating significant development of articular cartilage lesions at 6-months of age. Muscle atrophy is also shown at this age in the gastrocnemius muscles, which significantly correlates with OA severity in the joint. Moreover, the quadriceps exhibit a decrease in miR-378a-3p expression, similar to that of the mechanical loading model. This ultimately supports the relationship between OA and muscle atrophy, suggesting that induction of load-induced or spontaneous OA is linked to sarcopenia in the muscles surrounding the joint. Autophagy was also implicated in this OA-associated muscle atrophy and was enriched in a list of miR-378a-3p target genes, highlighting it as a potential therapeutic target.

CD1 mice were used to investigate spontaneous OA, with 6-month-old mice demonstrating significant OA development. This provides further evidence that the CD1 strain of mice can be used as a model of spontaneous OA. The potential of CD1 mice as a spontaneous OA model was first proposed by Dr Ramos-Mucci and Professor Frank Beier, who showed significant increases in OA severity by 6-months-old in CD1 mice, as measured by OARSI scoring and joint space mineralization (data unpublished). The early development of severe OA lesions may make CD1 mice a potentially very advantageous model as a major drawback of current spontaneous models is the time required for the injury to develop. The CD1 mice in this study all showed mild lesions (grade 1-2) by 4-months of age. This is comparable to the STR/ort model that are the most used genetically modified model of spontaneous OA. STR/ort mice develop OA spontaneously and exhibit human-like cartilage lesions at approximately 12 to 20 weeks of age (Mason et al., 2001), as well as ossification of the medial meniscus (Walton, 1977) and medial collateral ligament calcification (Walton, 1977).

By 6-months of age, CD1 mice in this study exhibited significant OA lesions, though the severity was quite variable between mice (ranging from grade 2-6).

Molecular analysis of the muscles of these CD1 mice identified upregulation of muscle-specific E3 ubiquitin ligase atrophy gene-1 (ATROGIN-1) and muscle atrophy F-box and muscle ring-finger protein 1 (MURF-1) in the older group. This suggests that the muscle changes observed in this model may be due, at least in part, to dysregulation of the ubiquitin–proteasome-dependent pathway (Kitajima et al., 2020) and supports previous research finding its marked increase in skeletal muscle atrophy (Bodine et al., 2001). This finding, along with the large reduction in fiber cross-sectional area in the gastrocnemius muscles of the old CD1 mice, indicate potential sarcopenia in these muscles with age and OA. However, this increased expression of ATROGIN-1 and MURF-1 was only significant in the quadriceps - the muscle that showed no significant reduction in fiber cross-sectional area with age. Potentially, muscle atrophy markers could be expressed early in the atrophy process and stabilize by the time that muscle atrophy can be observed histologically. This is also the case for the model of load-induced, where there was no upregulation in muscle atrophy markers.

This study found that the muscles that experience the most atrophy – at least as observed histologically – differs depending on the model. In the CD1 model of spontaneous OA, the gastrocnemius showed the most significant reduction in fiber cross-sectional area. Conversely, the quadriceps muscles exhibited the most significant downregulation of fiber cross-sectional area in the mechanical loading model of OA, whilst the gastrocnemius showed no decrease. A reason for this discrepancy may lie in the roles of the specific muscles play in movement of the limb and how these are influenced by the position of the limb during the application of mechanical loading regimen. The position of the quadricep during the mechanical loading may put particular strain on quadricep tendon, and subsequently the quadricep, as the knee joint is required to be in deep flexion whilst in the loading cups (Poulet et al., 2011). The gastrocnemius, however, is posterior and may not be under so much mechanical strain during the process. This may help to explain the more severe effect of mechanical joint loading on the quadricep muscles in this model. In the spontaneous OA model, the gastrocnemius experienced significantly more atrophy. As the CD1

model used in this study did not undergo any treatment, you would expect them to experience sarcopenia in the muscles that are involved in normal ambulation following disuse of the limb. This is supported by studies that have found that the gastrocnemius is particularly important in ambulation and wheel running in rodents (Baltgalvis et al., 2012) and is the most affected muscles in mouse models of muscular dystrophy (Garlich et al., 2010). Future research should consider this disparity in which muscles develop atrophy when assessing which of these two models to use in experiments.

Three miRNAs (-378a-3p, -199a-5p, and -24) were selected for expression analyses in this study based on their previous association with sarcopenia (Kanakis et al., 2021; Soriano-Arroquia et al., 2021; Proctor and Goljanek-Whysall, 2017). Downregulation of miR-378a-3p was found in the peri-articular muscles of both the load-induced and spontaneous models. Interestingly, miR-378a-3p was downregulated in the quadriceps of both models regardless of the fact that the quadriceps fiber cross-sectional area in the spontaneous model wasn't significantly reduced. As miR-378a-3p was reduced in the quadriceps despite no observed histological atrophy may be another indicator that molecular dysregulation occurs earlier in the process of sarcopenia development. As such, it may also be a useful biomarker for the disorder, which is something that future research should investigate. IPA analysis was used to investigate the pathways enriched in its validated target genes, including P62, and found that autophagy was the most significantly enriched. qPCR analysis of P62 expression in these muscles revealed its significant upregulation, providing further experimental evidence that it is a miR-378a-3p target. P62 is an autophagosome cargo protein that targets other proteins that bind to it for selective autophagy, making it a classic reporter of autophagy activity (Lui et al., 2016). Autophagy is a pathway known to be involved in sarcopenia development, and research has shown P62 to be prominently accumulated in cell cytosol of sarcopenic muscle (Sakura et al., 2016). Inefficient autophagy has been attributed a major role in the age-related accumulation of damaged cellular components, such as undegradable lysosome-bound lipofuscin, protein aggregates, and damaged mitochondria (Terman and Brunk, 2006). This makes autophagy, and P62, an potential target for OA-associated muscle atrophy that should be investigated further. In particular, immunohistochemistry for the protein in muscle samples would provide a better idea of its expression and localization in the tissue.

miR-24 was also found to be downregulated, but only in the gastrocnemius of mice with spontaneous OA. Age-related changes in miR-24 and its target gene Prdx6 have been shown to contribute to defective function of myogenic progenitors and muscle regeneration during aging (Soriano-Arroquia et al., 2021). This research proposed that upregulation of miR-24 induces senescence and decreases myogenic potential early in muscle wasting, and it is subsequently downregulated in ageing as a compensatory mechanism. The downregulation in the older CD1 gastrocnemius may therefore indicate a more aged phenotype in these muscles.

Future research would benefit from investigating whether these miRNAs are implicated in the dysfunction of multiple skeletal tissues, and therefore whether they can be used to simultaneous target multiple disorders (such as OA and muscle wasting). The next two chapters start to explore this further, specifically investigating the effect of miR-378a-3p in the joint and peri-articular muscle tissues.

3.4.1. Future Directions

The mice used in these models were relatively young – with the oldest being the 8-month-old CD1 mice. As mentioned, muscle atrophy markers were not significantly overexpressed in the muscles that were shown to have reduced fiber cross-sectional area. Therefore, future studies should look at longer time points to see whether the muscles exhibit higher expression of atrophy markers at later ages. It should also be noted that there are other markers of muscle atrophy that were not investigated in this experiment, for example, FOXO transcription factors (Sanchez et al., 2014). The main molecular pathways of sarcopenia should also be investigated in more depth to see if one is more enriched in spontaneous versus load-induced OA. For example, it appears that, at least in the CD1 model of spontaneous OA, there is a dysregulation of the ubiquitin–proteasome-dependent pathway. However, in the load-induced model, research may find that the muscle degradation is driven by a different proteolytic or oxidative stress-associated pathway.

Though a few genes and miRNAs were investigated in these muscles, it is by no way a comprehensive view of their transcriptome during ageing/atrophy. Research would

benefit from conducting RNA-seq on the peri-articular muscles and joint tissues in CD1 mice to gain more insight into the molecular underpinnings of OA-associated muscle atrophy in this model. Previous studies have also suggested that changes in muscle quality precedes the loss of absolute performance and often occurs without muscle atrophy in CD1 mice (Hill et al., 2020). This suggests that using fiber CSA as an indicator of muscle atrophy may not be the best measure- However, as *in vivo* muscle strength was not assessed – via techniques such as grip strength – it is not possible to confirm whether the observed reduction in fiber CSA correlates with loss of muscle performance.

Conclusions regarding whether muscle wasting precedes OA, or vice versa, cannot be determined from the results of this study alone. There are a couple of theories as to the pathogenesis of OA associated muscle atrophy. Potentially, disuse of an OA affected joint, due to the pain of movement, may be the primary cause of the reduction in muscle strength associated with OA. A reduced mechanical load on the skeletal muscle is one of the key external factors that leads to muscle atrophy, as reviewed in a recent paper by Nunes et al. (2021). Conversely, increased mechanical load is one of the main causes of OA (Chang et al., 2019; Zhu et al., 2020). With a reduction in load attenuating its progression (He et al., 2020). One way to assess this would be to measure the gait of the mice as they age and develop OA. A previous study by Poulet et al. (2014) showed that reduced paw area and treadmill task noncompliance are the most effective measures of OA onset and progression in the STR/ort model of spontaneous OA. Reduced paw area in the OA-affected limb would provide evidence that any observed muscle atrophy would be due to its disuse. It is anticipated that if gait would have been measured in these CD1 and loaded models of OA, similar results would be observed.

3.5. Conclusions

This research is the first to characterise muscle atrophy in non-surgical murine models of OA and provides evidence that OA and muscle atrophy are intricately linked. These data provide a good basis for future research to investigate the specific mechanisms of OA-associated muscle atrophy.

Chapter 4:

Investigating the effect of intravenous miR-378a-3p mimic treatment on joint and muscle health in a murine model of mechanical load-induced OA.

4.1 Introduction

Muscle atrophy and osteoarthritis (OA) are highly prevalent ageing-associated conditions but seldom is known about their interaction. As previously mentioned, the progressive loss of periarticular muscle mass and function has consequences on joint stability and health, and *vice versa*. Muscle atrophy is inevitably associated with ageing, and, more recently, it has been demonstrated in patients with OA. The reduction in muscle mass and strength is attributed to myofibre atrophy, reduction of muscle quality, and defective muscle regeneration – reviewed by Brown and Goljanek-Whysall (2015).

The importance of muscle heath on joint physiology is exemplified by multiple studies. For example, muscle contractility has been shown to be required for joint formation already during embryogenesis (Shwartz et al., 2009), and muscle weakness is an important determinant of pain and disability during OA (Fisher et al., 1997). Several studies have shown that a decrease in lower limb lean mass is frequent in OA patients (Toda et al., 2000), and this is associated with a greater risk of falls (O'Reilly et al., 1998; Segal et al., 2010; Conroy et al., 2012). Another study subjected 117 patients with symptomatic knee OA to magnetic resonance imaging of the knee. They found that a larger cross-sectional area of the *vastus medialis* is associated with a decreased rate of tibial cartilage volume loss, reduced risk of knee replacement, and reduced pain in OA patients (Wang et al., 2012). Moreover, dystrophic mice show significant articular cartilage degeneration, along with a spectrum of degenerative musculoskeletal abnormalities (Isaac et al., 2013).

Despite accumulating evidence supporting the interaction between OA and muscle atrophy, research has yet to determine whether muscle changes precede OA, or vice versa. To date, most research have correlated measures of muscle pathology (such as: grip strength, muscle fiber size, and muscle mass) with radiographic knee OA/pain in patients presenting with either muscle atrophy or OA. To my knowledge, there is only one paper suggesting a molecular interaction between the two neighbouring tissues during human OA (Noehren et al., 2018). This research proposed that impaired satellite cell density, high profibrotic gene expression, and a slow-to-fast fiber type

transition may contribute to reduced muscle quality in OA. However, human tissue is often obtained from the joint or *vastus lateralis* of patients in late-stage OA/muscle atrophy which is a large limitation of research in the field. Murine models can overcome this and really help to understand the underlying mechanisms behind their development and interaction.

Research has also implicated miRNAs as integral factors in the maintenance of both muscle and joint health. In the muscle, they have been shown to act as regulators of myogenesis, differentiation, and atrophy (Wang et al., 2013). In the joint, miRNAs have been shown to regulate the production of cartilage degrading enzymes, inhibit the expression of cartilage matrix components, increase the production of proinflammatory cytokines, facilitate chondrocyte apoptosis, and suppress autophagy, as reviewed in a paper by Panagopoulos and Lambrou (2018).

miR-378a in particular has been shown to be downregulated in muscle of humans during ageing (Drummond et al., 2008) and has been shown to control myogenesis, metabolism and autophagy (Proctor et al., 2017; Li et al., 2018; Carrer et al., 2012). The previous chapter of this thesis also finds its downregulation in both spontaneous and load-induced OA-associated muscle atrophy. Indeed, molecules regulating miR-378 have been patented for the use in regulating metabolism in different tissues, including skeletal muscle (patent number WO2011153542A3). Although there has been very little research on the role of this miRNA in OA, changes to the regulation of cellular metabolism via autophagy have been noted during OA pathogenesis – as reviewed by Duan et al (2020). Moreover, miR-378-3p has been detected in synovium in late-stage OA patients (Li et al., 2018; Cheng et al., 2017). Together, these data indicate a potential common mechanism, via miR-378, underlying musculoskeletal tissues homeostasis.

4.2. Aims and Hypotheses

Whilst multiple studies have focused on the role of miRNAs in muscle development and regeneration, very few functional studies exist that have characterised the role of miRNAs in muscle atrophy during ageing or OA. As such, this study aims to investigate whether miR-378a-3p could be used as a therapeutic agent to treat muscle

atrophy in a model of mechanical load-induced OA. Moreover, this research will explore the effect of this miRNA on the bone and joint tissues of these mice to obtain a more comprehensive view of its role in the musculoskeletal system.

4.3. Materials and Methods

4.3.1. Animals and Experimental Groups

All mice were kept in polypropylene cages of 2–6 littermates, subjected to 12-hour light/dark cycles at 21±2°C, and fed standard RM1 maintenance diet *ad libitum*. All procedures complied with Animals (Scientific Procedures) Act 1986 and local ethics committee. At the end of the experiments, mice were culled via asphyxiation by a rising CO2 concentration. Mice were kept at the Biomedical Services Unit (BSU) of the University of Liverpool and monitored daily for any health and welfare issues.

In order to induce OA, 36-week-old male C57BL/6 mice (n=21) were subjected to a two-week regimen of non-invasive mechanical loading (see general methods (2.2.1) for detailed protocol) and left to age for 12 weeks post-loading.

For miR-378a-3p expression manipulation, mice were injected intravenously with 100ul of a 500nmol stock solution of miR-378a-3p (n=11) or a control miRNA (n=10) (2mg/kg body weight; as specified in Whysall et al. (2020)) every two weeks during the 12-week post-loading period with either a miR-378a-3p mimic or control miRNA ‘cel-239b’ (Dharmacon). Non-loaded control mice were used for grip strength analyses. For this group, 36-week-old C57BL/6 mice were aged for 2 weeks and then injected intravenously with the miR-378a-3p mimic (n=5) and control microRNA (n=5) every 2 weeks for 10 weeks. These mice were culled the day after their last injection. miRNA and control mimics were conjugated to cholesterol and the sequences are as follows:

Cel-239b control mimic:

Active: 5’- P.U.U.G.U.A.C.U.A.C.A.C.A.A.A.A.G.U.A.C.U.G
Passenger: 5’-Cholesterol.G.U.A.C.U.U.U.U.G.U.G.U.A.G.U.A.C.A.A.U.U

miR-378a-3p mimic:

Active: 5’-P.A.C.G.G.A.C.U.U.G.G.A.G.U.C.A.G.A.A.G.G
Passenger: 5’ Cholesterol.U.U.C.U.G.A.C.U.C.C.A.A.G.U.C.C.A.G.U.U.U

12 weeks after loading the mice were euthanised and their knee joints, gastrocnemius, and quadriceps muscles dissected. A detailed description of this dissection procedure can be found in Chapter 2 ‘General Methodology’.

4.3.2. Measurement of Grip Strength

Every two weeks throughout the 12-week post-loading period, and on alternate weeks to the miRNA injections, a grip strength test meter (BIOSEB; EB Instruments) was used to measure the grip strength of all limbs (Mandillo et al., 2008). During the grip strength test, the mice were handled by their tails and placed over the grid until all paws grasped the grid. The tail was then pulled horizontally until the mouse released hold entirely. Three separate readings were recorded and averaged in Newtons, then converted to grams for analysis. All measurements were normalised to the mouse weight on the day of the recording.

4.3.3. Ex Vivo Tissue Culture

C57BL/6 mice (n=7, 16-week-old males) were euthanised via asphyxiation by a rising CO2 concentration. Knee joints from both hindlimbs were then harvested aseptically and dissected sagittally into two halves. Each half was placed into a 24-well-plate with 500ul of Dulbecco′s Modified Eagle′s Medium/Nutrient Mixture F-12 Ham (Sigma-Alrdich). All media was kept serum and antibiotic free. The joint tissue was left

overnight and then treated with 10ul of a 500nmol miR-378a-3p mimic or control miRNA (see 'Animals and Experimental Groups' for mimic details). Joints were left in for 24 hours in the miR-378a-3p or control treated media for 24 hours and were then snap frozen in liquid nitrogen for downstream RNA analyses.

4.3.4. Micro computed tomography (µCT) for analysis of subchondral and trabecular bone.

Mice cadaveric knee joints were analysed with micro computed tomography (µCT) to quantify subchondral and trabecular bone thickness, joint space mineralisation, and trabecular number. A detailed description of the methodology can be found in chapter 2.5.

4.3.5. Histology

Methods to determine skeletal muscle and knee joint phenotypes is detailed in the general methodology chapter. In brief, 10um sections of muscle were stained with a 1:1000 dilution of rhodamine wheat germ agglutinin and imaged either using a Ziesslsm800 confocal microscope or Axio Scan.Z1 slide scanner (Zeiss, UK). The fiber cross-sectional area and minimum ferret's diameter was analysed with Myovision software (Wen et al., 2017).

Serial coronal 6µm thick sections of knee joints were cut across the entire joint and a quarter of the sections were selected, stained with toluidine blue (0.1% in 0.1M solution of acetate buffer, pH 5.6), and counterstained with 0.2% fast green. Toluidine blue slides of the entire knee joint were scored for cartilage lesion severity in each knee compartment: medial tibia (MT), medial femur (MF), lateral tibia (LT) and lateral femur (LF) using the OARSI grading system (Glasson et al., 2010). Using these calculations, the average mean and maximum lesion scores was calculated for each compartment and for the whole knee joint of each mouse. Summed scores of all the compartments were also calculated from the mean and maximum scores.

4.3.6. cDNA synthesis and qRT-PCR

For miR expression analysis, total RNA was isolated and purified using the Trizol method, as detailed in the general methodology chapter. Reverse transcription of total RNA containing miRNAs was performed with miScript II RT kit (Qiagen, UK). qPCR was performed on a Rotor-Gene Q™ (Qiagen) instrument in a 20 µL reaction mixture. qPCR conditions were: 95 ◦C for 30 s, 55 ◦C for 30 s and 72 ◦C for 30 s (40 cycles) using a hot start step of 95 ◦C for 15 s. Specific primers for miR-199a-3p, miR-378a-3p, miR-24, SNORD-68, ATROGIN-1, MURF-1, P62, NRF1, and 18S (table 1.1-3) were used for the qPCR whereby SNORD-68 was used as the housekeeping gene. The results were analysed using the delta CT method.

4.3.7. Statistical analysis and normality of data testing

Normality and statistical analysis were calculated using GraphPad Prism (GraphPad v8). Normality of data was tested using a Shapiro-Wilk test where a p-value ≤ 0.05 indicated statistical significance. For all other statistical analyses, a p-value ≤ 0.05 also indicated statistical significance. For statistical analysis of the fiber cross-sectional area, OARSI severity, and gene expression in the loaded *vs* contralateral control limbs, paired t-test was used. For the bone and joint space pathology quantified by *µCT* analysis, a ratio of the non-loaded:loaded limb values was calculated for each treatment group. A t-test was then used to compare the differences between the means of the miR-378a-3p treated and control groups. Comparisons between miRNA treated and control treated groups involved an unpaired t-test. A repeated measure ANOVA was used to analyse differences between the mean grip strength values of the miR-378a-3p treated and control treated group. A t-test was used to determine whether the means within each group at different time points were significantly different from each other.

4.4. Results

4.4.1. Mice treated with miR-378a-3p have significantly increased grip strength after loading than those treated with a control microRNA.

Grip strength was measured prior to, and in the 12 weeks following, the mechanical loading regime (figure 4.4(a) and 4.5(a-b)). Two weeks after loading, and after one round of IV injections, the mice of both miR-378a-3p and control treatment groups experienced a significant reduction in grip strength ($p<0.0001$). After two rounds of IV injections, there was a slight drop in grip strength of the control miRNA-treated group, though this was not significant. A significant increase in grip strength in the miR-378a-3p treated group was observed after three injections ($p=0.01$). This gap between the miR-378a-3p and control treated group continued to widen with each subsequent injection ($p=0.007$, $p=0.003$, and $p=0.0001$, after 4, 5, and 6 injections, respectively).

Along with the changes in grip strength between each treatment groups, the changes within each group throughout the course of the treatment was also assessed. This revealed that mice treated with the miR-378a-3p mimic and control miRNA both had reduced grip strength after 6 injections compared to the first injection (figure 4.5(a-b)). However, this was more acute in the control treated group that experienced a 32.3% reduction in grip strength ($p=0.0006$) compared to the miR-378a-3p treated group which experienced a 14.5% reduction ($p=0.002$).

In the non-loaded control group, there was no observed differences in grip strength between the miR-378a-3p and control miR treated groups (figure 4.4(b)). Moreover, the drastic reduction in grip strength that occurred after loading in the group subject to mechanical joint loading was not present in the control group (figures 4.6(a-b)).

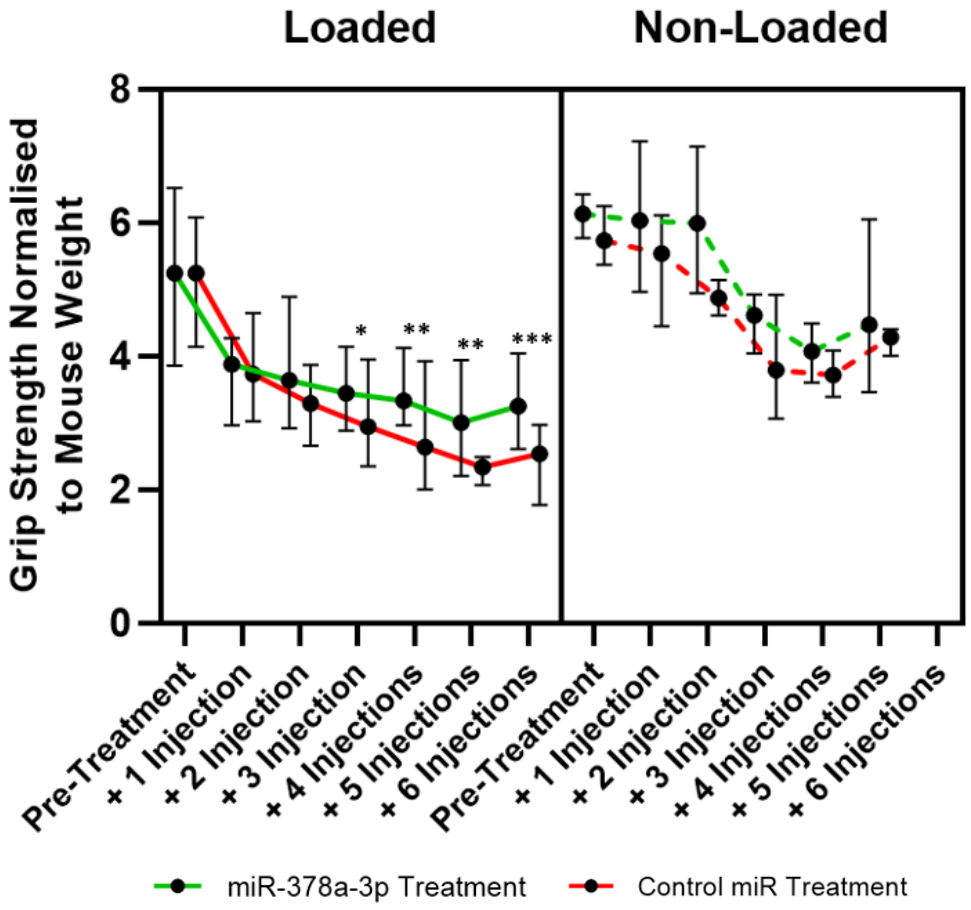

Figure 4.1: Grip strength in mice treated with a miR-378a-3p mimic vs control miRNA. *(a) Grip strength was measured prior to, and every 2 weeks after, mechanical joint loading. Mice were culled 12 weeks after joint loading where they received 6 injections of their respective treatments – miR-378a-3p mimic (n=11) or a control microRNA (n=10). (b) Grip strength of the control mice were measured every 2 weeks after 2 weeks of ageing instead of loading. These mice were culled immediately after their last injection of either a miR-378a-3p mimic (n=5) or a control microRNA (n=5). Differences in mean grip strength between the miR-378a-3p and control treated groups was determined by a student's t-test. *p<0.05, **p<0.01, ***p<0.001. Data is displayed graphically as mean ± range with all data points per group included.*

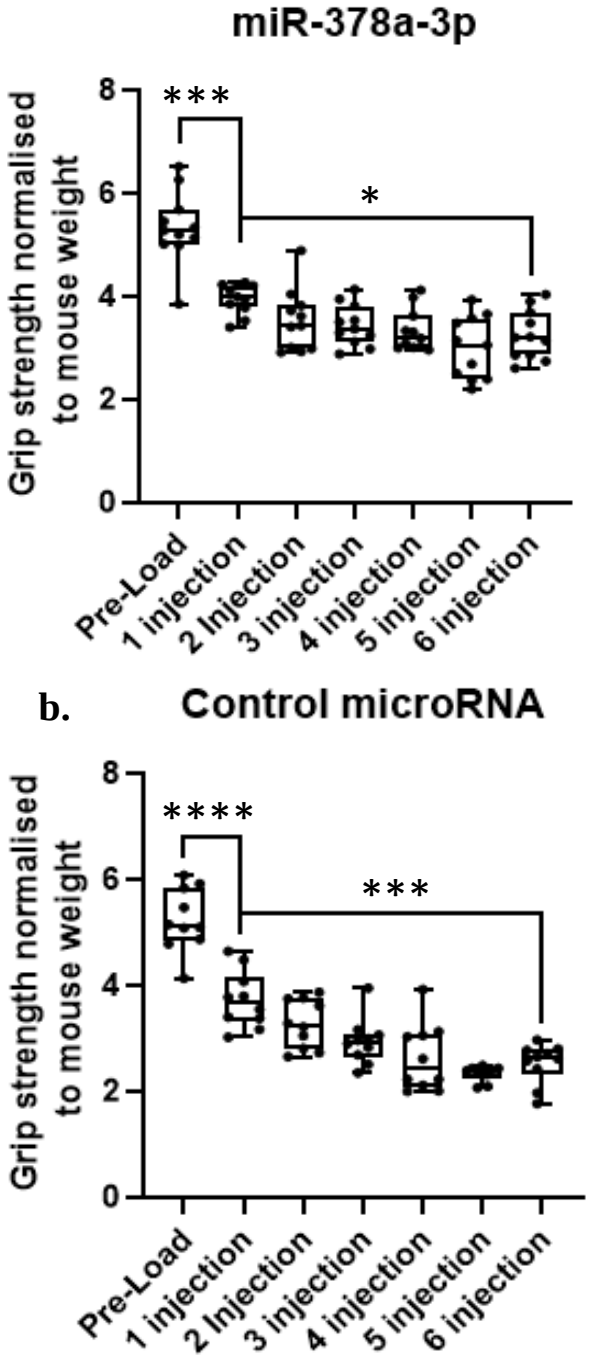

Figure 4.2: Grip strength reduction over 12 weeks in mice subjected to mechanical joint loading and treated with a miR-378a-3p mimic and control miRNA. *(a) Grip strength in mice treated with a miR-378a-3p mimic (n=11). (b) Grip strength in mice treated with a control miRNA (n=10). Grip strength was measured prior to, and every 2 weeks after, mechanical joint loading. Mice were culled 12 weeks after joint loading where they received 6 injections of their respective treatments. Differences in mean grip strength before and after loading and after the first and last treatment was determined by a student's t-test within each treatment group., **p<0.01, ***p<0.001 ****p<0.0001. Data is displayed graphically as mean ± range with all data points per group included.*

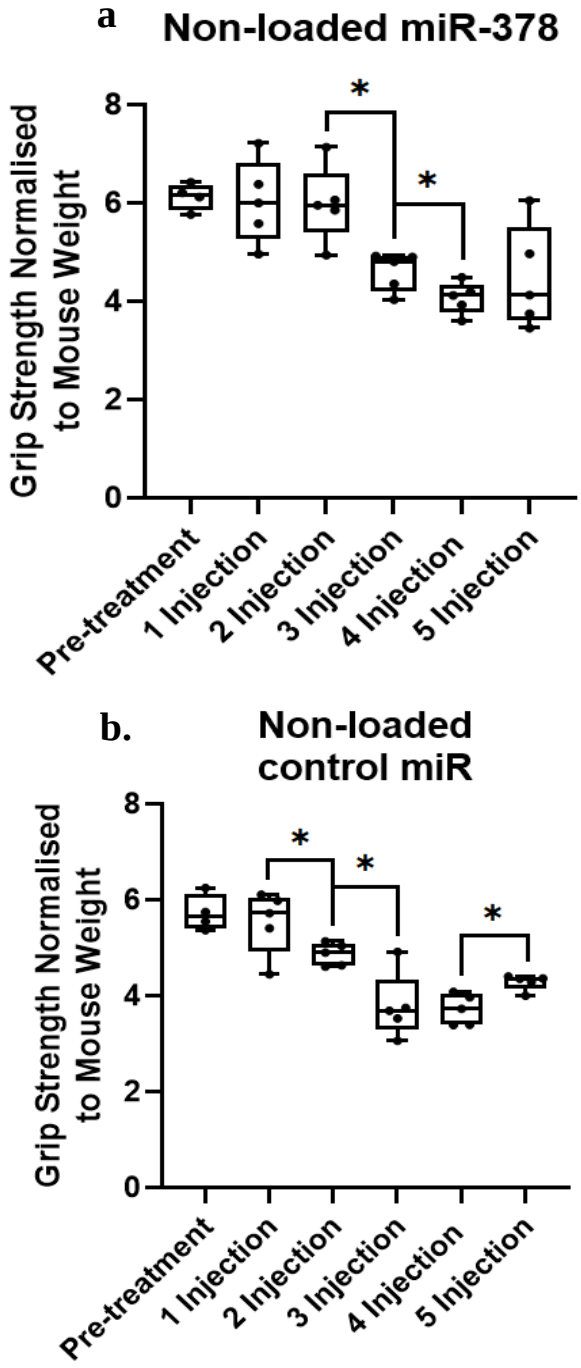

Figure 4.3: Grip strength reduction over 10 weeks in non-loaded mice treated with a miR-378a-3p mimic and control miRNA. *(a) Grip strength in mice treated with a miR-378a-3p mimic (n=5). (b) Grip strength in mice treated with a control miRNA (n=5). Grip strength was measured prior to, and every 2 weeks after, mechanical joint loading. Mice were culled 12 weeks after joint loading where they received 6 injections of their respective treatments. Differences in mean grip strength before and after loading and after the first and last treatment was determined by a student's t-test within each treatment group., **p<0.01, ***p<0.001 ****p<0.0001. Data is displayed graphically as mean ± range with all data points per group included.*

4.4.2. Mice treated with a miR-378a-3p mimic show a trend of increased fiber CSA and minimum ferret diameter in both loaded and non-loaded gastrocnemius muscles compared to the control treated mice.

Fiber cross-sectional area in the gastrocnemius of mice treated with the miR-378a-3p mimic had a larger average fiber cross-sectional area in both the loaded and non-loaded limbs (figure 4.7(a)). There is a 9.4% increase in gastrocnemius fiber CSA in the non-loaded miR-378a-3p treated group (n=11) compared to the control miRNA group, though this was not siginficant (n=10) (p= 0.4896). This is similar in the loaded limbs, where the average fiber CSA is 9.8% larger in the miR-378a-3p treated group (p=0.4311). There was also no significant effect of loading in either the miR-378a-3p (p=0.6491) or the control miRNA treated groups (p=0.6665). Overall, treatment with the miR-378a-3p mimic seems to increase the average fiber CSA by 9-13% depending on the muscle analysed. There is, however, no significant correlation between fiber CSA and OARSI severity in either the miR-379a-3p (p=0.3699, r=0.3184) or control miRNA group (p=0.6506, r= -0,190) (figure 4.7(e-f)).

4.4.3. The average quadriceps fiber CSA in mice treated with a control miRNA is significantly reduced in the loaded compared to the non-loaded limb, whereas those treated with miR-378a-3p have no significant difference.

There was a trend of smaller fiber CSA in the loaded limbs of both miR-378a-3p (n=11) and control treated (n=10) groups. However, this was only significant in the quadriceps of the mice treated with the control miRNA (fiber 4.8(a); p=0.0174). The minimum feret diameter reflected this, where the only difference between loaded and contralateral limbs was also seen in the quadriceps of the control miRNA treated group (p=0.0142). There is, however, no significant correlation between fiber CSA and OARSI severity in either the miR-379a-3p (p=0.3505, r=0.3308) or control miRNA group (p=0.8655, r=-0.07946) (figure 4.7(e-f)).

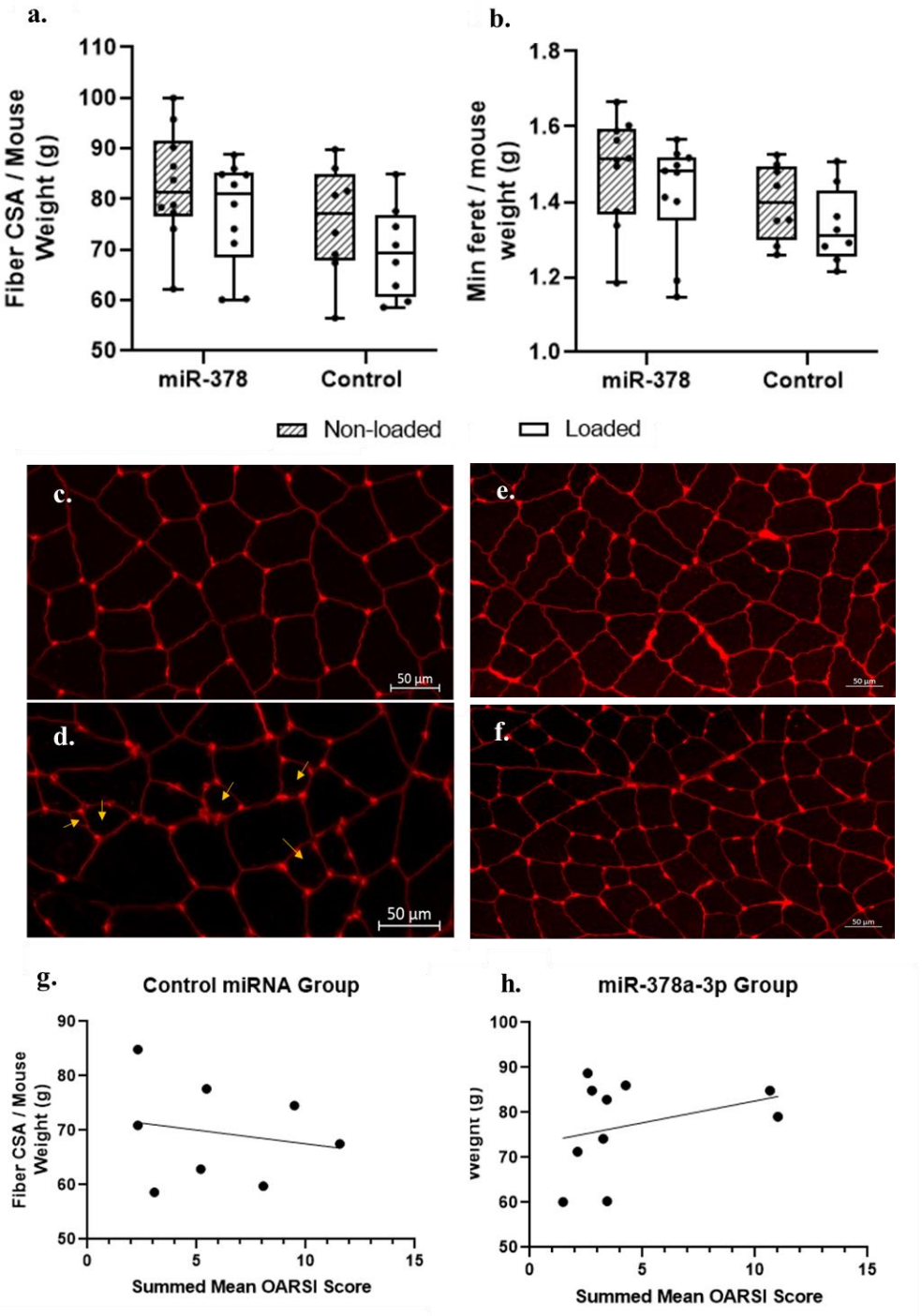

Figure 4.4: Histology of the gastrocnemius muscles in mice treated with a miR-378a-3p mimic or control miRNA *(a) Gastrocnemius fiber cross-sectional area in the miR-378a-3p treated mice (n=11) and the control miRNA treated mice (n=10). (b) Gastrocnemius minimum feret's diameter in the miR-378a-3p treated mice and the control miRNA treated mice. (c) Representative image of a gastrocnemius cross-section from a non-loaded limb treated with a control miR. (d) Representative image of a gastrocnemius cross-section from a loaded limb treated with a control miR.(e) Representative image of a gastrocnemius cross-section from a non-loaded limb treated with a miR-378a-3p mimic. (f) Representative image of a gastrocnemius cross-section from loaded limb treated with a miR-378a-3p mimic. Yellow arrows show smaller fibers interspersed throughout the section. Both images were taken from gastrocnemius muscles of the same mouse. (g-h) Pearson's correlation of gastrocnemius fiber CSA with summed mean OARSI score in the miR-378a-3p and control groups. Shaded boxes represent the non-loaded limb, non-shaded boxes represent the loaded limb. Data is displayed graphically as mean ± range with all data points per group included.*

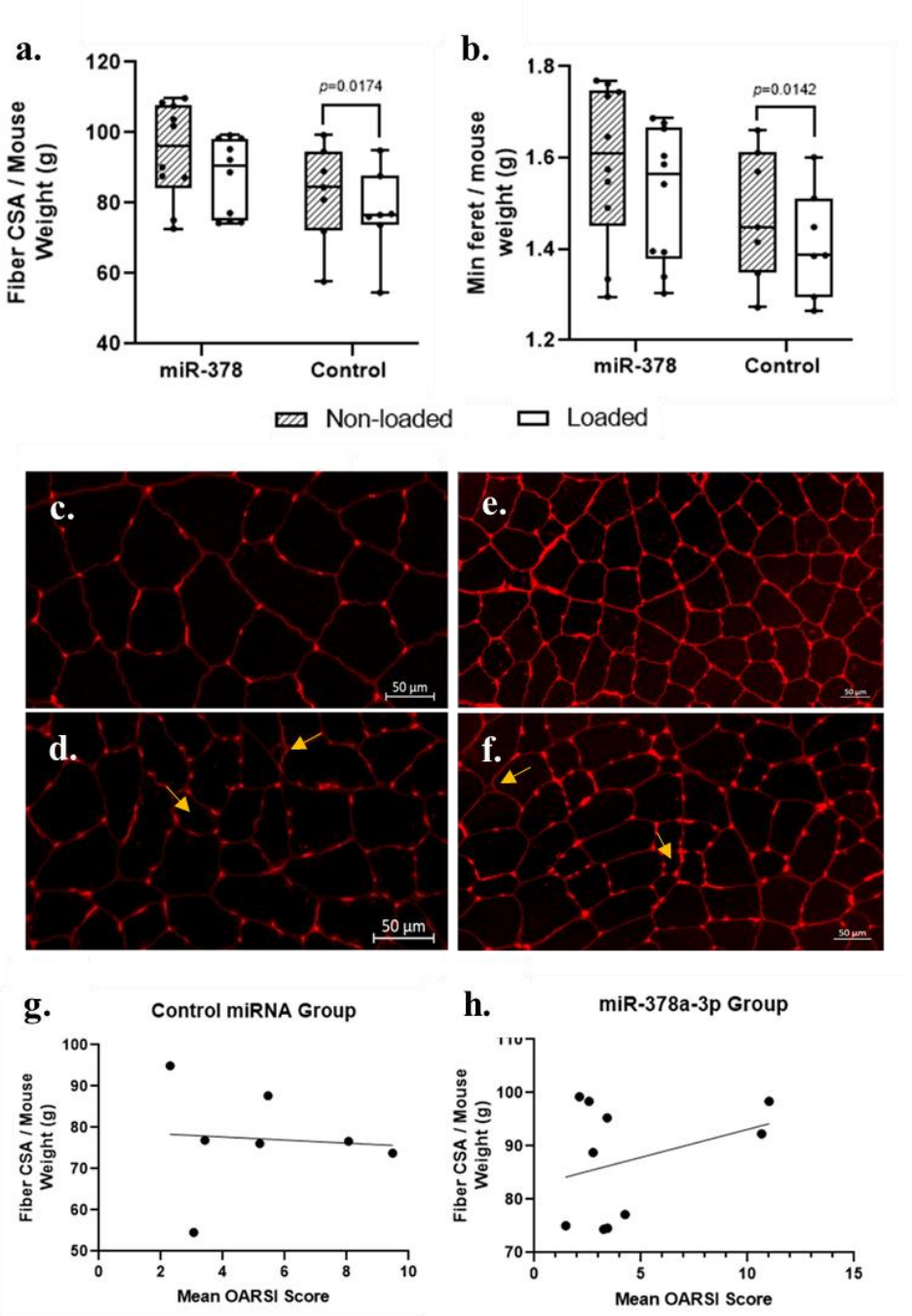

Figure 4.5: Histology of the quadriceps muscles in mice treated with a miR-378a-3p mimic or control miRNA. *(a) Quadriceps fiber cross-sectional area in the miR-378a-3p treated mice (n=11) and the control miRNA treated mice (n=10). (b) Quadriceps minimum feret's diameter in the miR-378a-3p treated mice and the control miRNA treated mice (c) Representative image of a quadriceps cross-section from a non-loaded limb treated with a control miR. (d) Representative image of a quadriceps cross-section from a loaded limb treated with a control miR (e) Representative image of a quadriceps cross-section from a non-loaded limb treated with a miR-378a-3p mimic.. (f) Representative image of a quadriceps cross-section from a loaded limb treated with a miR-378a-3p mimic.. The fibers overall appear smaller and the yellow arrows show smaller fibers interspersed throughout the section. Both images were taken from quadriceps muscles of the same mouse. (e-f) Pearson's correlation of quadriceps fiber CSA with summed mean OARSI score in the miR-378a-3p and control groups. Shaded boxes represent the non-loaded limb, non-shaded boxes represent the loaded limb. Data is displayed graphically as mean ± range with all data points per group included.*

4.4.4. ATROGIN-1 and MURF-1 expression are unaffected by loading in either treatment groups.

ATROGIN-1 and MURF expression was measured, via qRT-PCR, in the gastrocnemius and quadricep muscles of mice treated with the miR-378a-3p mimic and control miRNA. Mice treated with the miR-378a-3p mimic had increased expression of both ATROGIN-1 and MURF-1, though this was only significant in the gastrocnemius (figure 4.9(a)). Loading appeared to have no effect on the expression of ATROGIN-1 or MURF-1 in either muscle/treatment group.

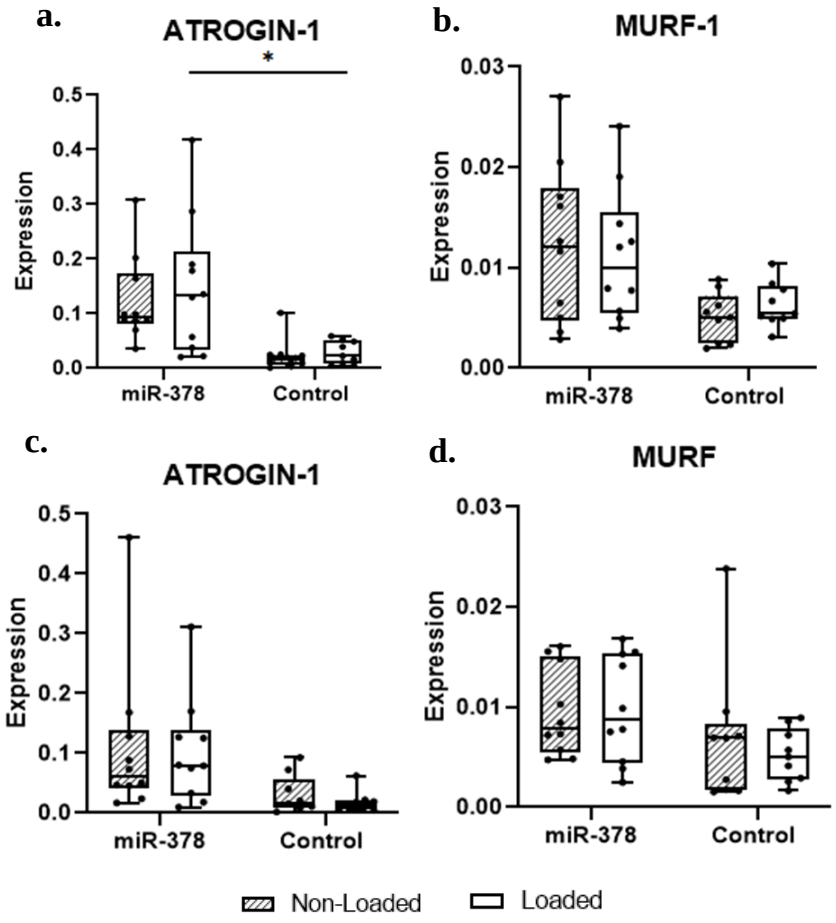

Figure 4.6: qRT-PCR quantification of muscle atrophy markers in the muscles of mice with mechanical load-induced OA and treated with a miR-378a-3p mimic or control miRNA*. (a-b) ATROGIN-1 and MURF-1 expression in the gastrocnemius of the miR-378a-3p treated mice (n=11) and the control miRNA treated mice (n=11). (c-d) ATROGIN-1 and MURF-1 expression in the quadriceps of the miR-378a-3p treated mice and the control miRNA treated mice. Shaded boxes represent the non-loaded limb and the non-shaded box represents the loaded limb. 'Expression' refers to the CT expression value of the mRNA relative to the housekeeping gene '18S'. *p<0.05. **p<0.01. Data is displayed graphically as mean ± range with all data points per group included.*

4.4.5. Expression of miR-378a-3p target genes – P62 and NRF1 - are unaffected by loading in either treatment groups.

P62 and NRF1 expression was measured, via qRT-PCR, in the gastrocnemius and quadricep muscles of mice treated with the miR-378a-3p mimic and control miRNA. Loading appeared to have no effect on the expression of ATROGIN-1 or MURF-1 in either muscle/treatment group. Moreover, there was no increased expression in either gene between miR-378a-3p or control miRNA treated mice.

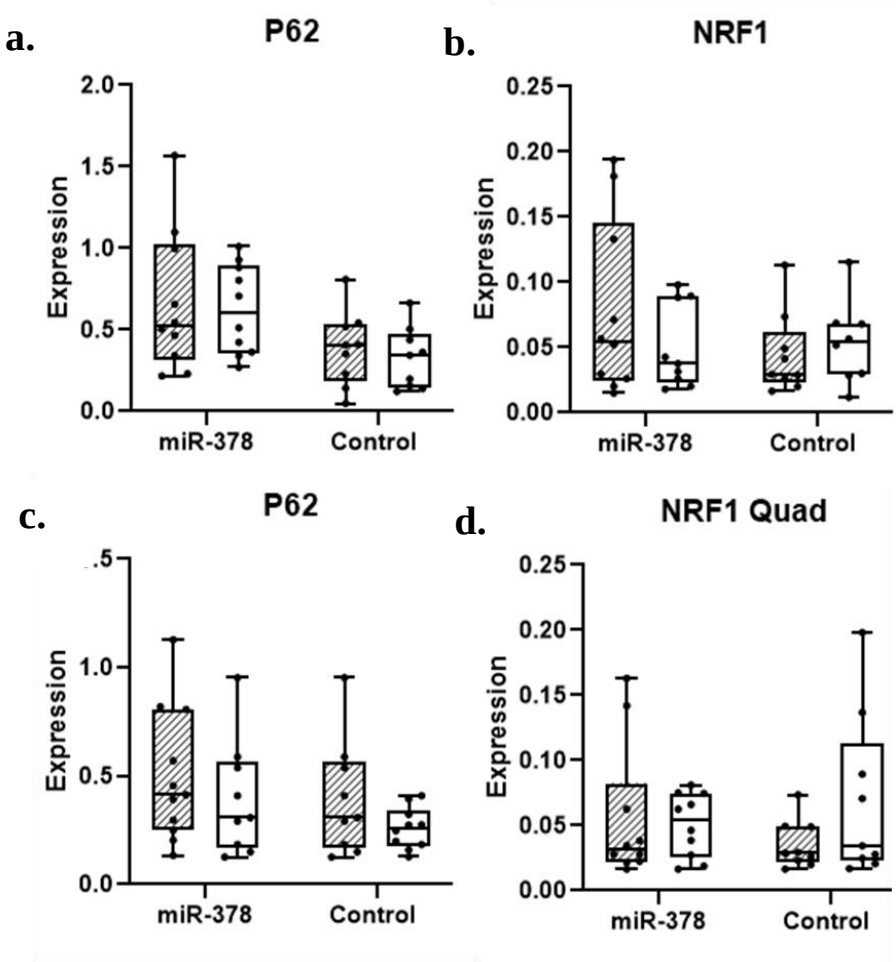

***Figure 4.7*: (a-b) P62 and NRF1 expression in the gastrocnemius of the miR-378a-3p treated mice and the control miRNA treated mice.** *(a-b)) P62 and NRF1 expression in the gastrocnemius of the miR-378a-3p treated mice (n=11) and the control miRNA treated mice (n=10). (c-d) P62 and NRF1 expression in the quadriceps of the miR-378a-3p treated mice (n=11) and the control miRNA treated mice (n=10). Shaded boxes represent the non-loaded limb and the non-shaded box represents the loaded limb. 'Expression' refers to the CT expression value of the mRNA relative to the housekeeping gene '18S'. Data is displayed graphically as mean ± range with all data points per group included*

4.4.6 OARSI lesion severity is lower in the group treated with a miR-378a-3p mimic compared to a control miRNA, but not significantly.

Both treatment groups (miR-378a-3p mimic and control miRNA) showed quite variable OA lesion severity in the loaded limb. Summed mean and maximum values across all compartments of the loaded limb (medial tibia/femur and lateral tibia/femur) were calculated to give a more comprehensive view of OA severity across the entire joint. The summed mean severity scores showed a 24.5% increase in lesion severity in the loaded limb of the mice treated with a control miRNA, though this was not significant (p=0.2527). This was also reflected in the maximum summed lesion severity scores, where there was an increased, but not a significant, severity in the control group compared to the miR-378a-3p treated group (figure 4.11(b)). Lesions were mostly located in the lateral femur, as is typical of this model (figure 4.11(c-d)).

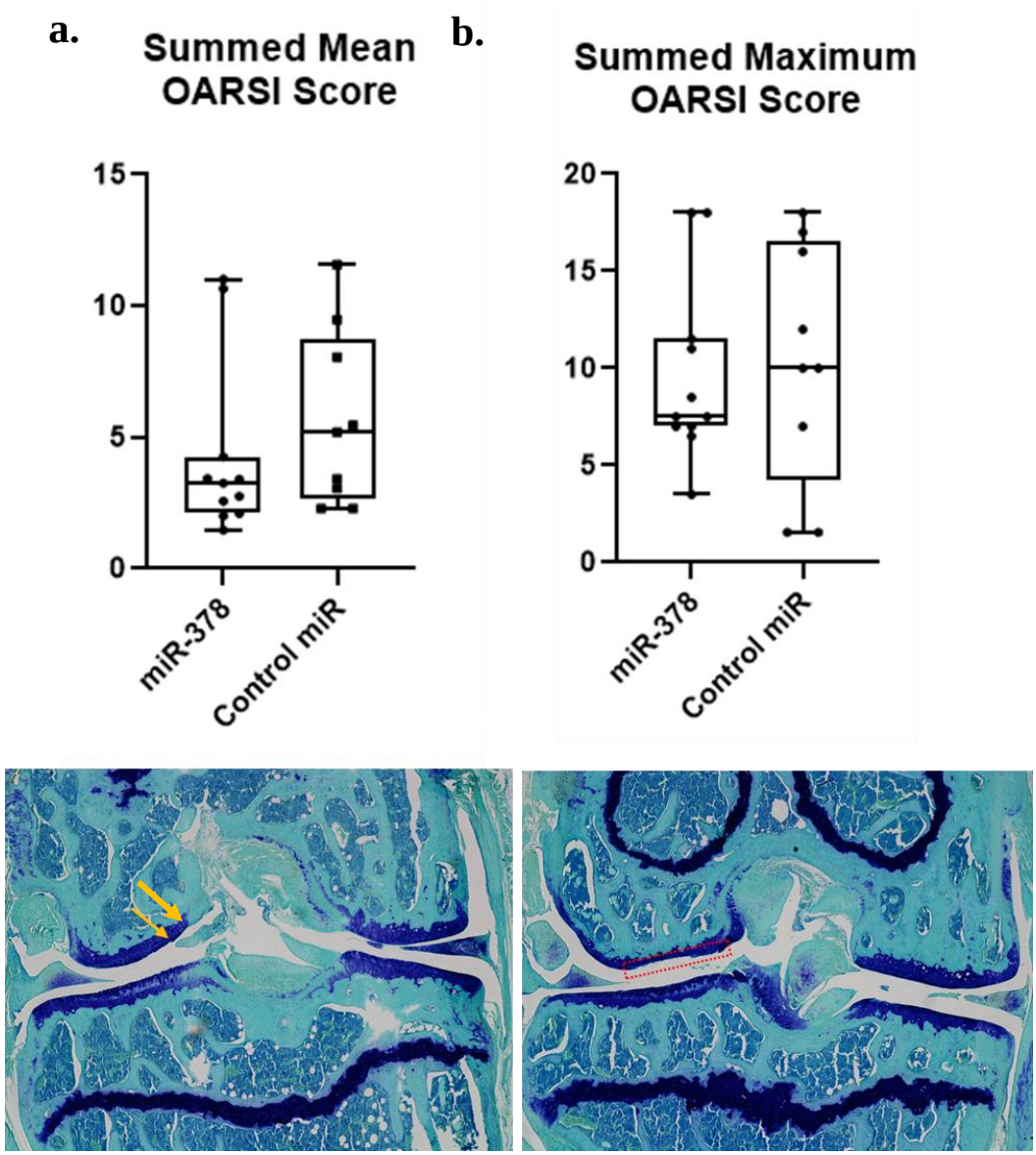

Figure 4.8: Joint histology in mice with load-induced treated with a miR-378a-3p mimic or control miRNA *(a-b) Summed mean and summed maximum lesion severity across all joint compartments combined. (c) An example image of a loaded joint, in mice treated with a miR-378a-3p mimic, with mild grade one lesions (yellow arrow) and slight loss of toluidine blue staining in the lateral compartments. (d) More severe cartilage loss in the lateral femur of a mouse treated with a control microRNA. This is characteristic of this mechanical loading model of load-induced OA (highlighted with a red box). Data is displayed graphically as mean ± range with all data points per group included. miR-378a-3p group (n=11) and control miR treated group (n=10).*

4.4.7 Joint space mineralisation is significantly higher in the loaded limb of both treatment groups compared to contralateral controls.

Joint space mineralisation is a measure of OA severity, as detailed in a paper by Ramos-Mucci et al. (2022). Quantification of joint space mineralisation using µCT revealed significantly increased ($p \leq 0.001$) mineralisation in the loaded limbs of both the miR-378a-3p and control treated groups, compared to un-loaded contralateral controls (figure 4.12(a)). However, when the difference between the non-loaded and loaded limbs were expressed as a ratio, there was no differences in joint space mineralisation between the miR-378a-3p and control miRNA treated groups (figure 4.12(b)).

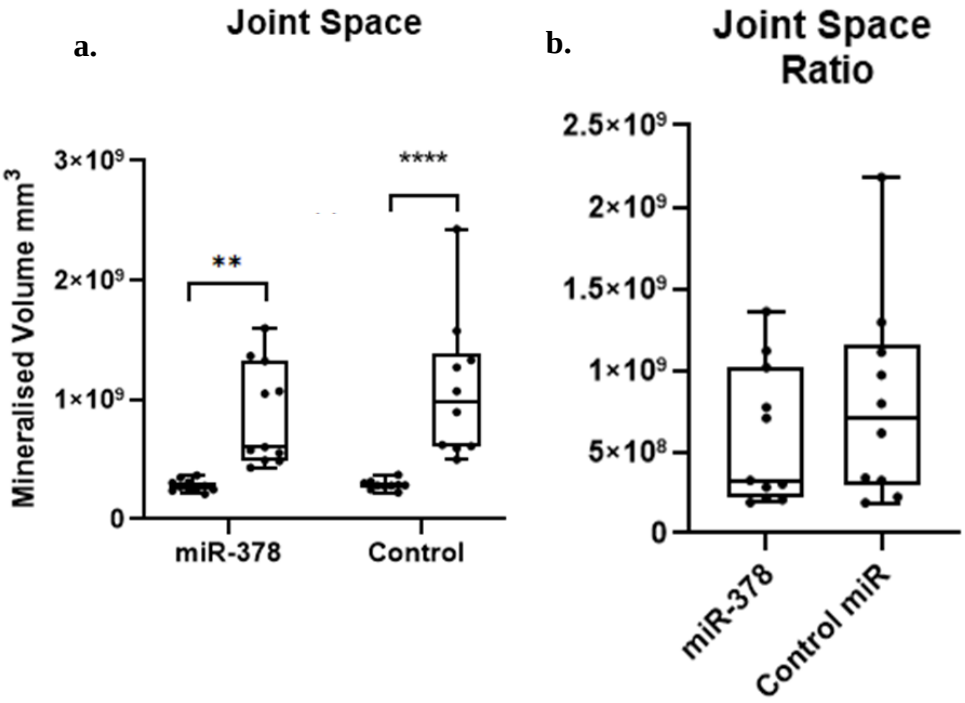

Figure 4.9: (a) µCT analysis of joint space mineralisation in the miR-378a-3p and control miRNA treated mice. *Shaded boxes indicate non-loaded limbs. Non-shaded boxes represent loaded limbs. (b) Joint space mineralisation in the miR-378a-3p (n=11)and control miRNA (n=10) treated groups expressed as a ratio of non-loaded:loaded values **p<0.01 ****0.0001. Data is displayed graphically as mean ± range with all data points per group included.*

4.4.8. Subchondral bone thickness in the lateral and medial femur is significantly increased in the loaded limb of the mice treated with a miR-378a-3p mimic.

Quantification of subchondral bone thickness using µCT, and expression of the thickness as a ratio of loaded:contralateral limb, showed a significant reduction in femoral subchondral bone thickness in the mice treated with a control miRNA. This was the case for both the lateral and medial femoral compartments (p=0.0151 and p=0.0156, respectively; figure 4.13. However, in the lateral tibia, the subchondral bone was significantly thicker in the mice treated with a control miRNA (p=0.0236). A positive value indicates that the subchondral thickness of the loaded limb is larger than that of the non-loaded. Conversely, a negative value indicates that the subchondral bone of the non-loaded limb is thicker than that of the loaded.

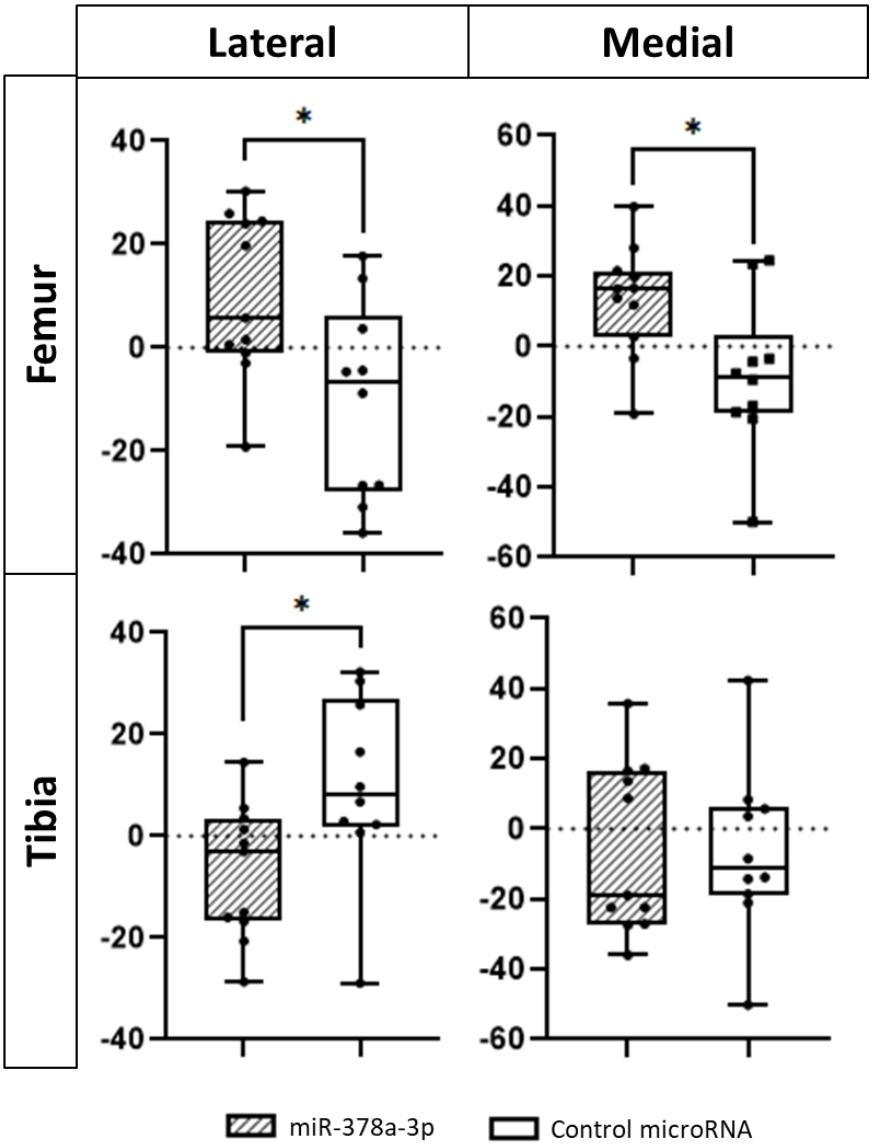

Figure 4.10: µCT analysis of subchondral bone thickness in the miR-378a-3p and control miRNA treated mice*. Differences between the loaded and contralateral control limbs within each treatment group was expressed as a ratio. A positive value indicates that the loaded limb has thicker subchondral bone than the non-loaded limb. *p<0.05. Data is displayed graphically as mean ± range with all data points per group included.*

4.4.9. miR-378a-3p treatment results in a significant reduction in trabecular thickness and increase in trabecular separation in the lateral tibia.

When quantifying epiphyseal bone pathology, namely: trabecular bone volume, number, thickness, and separation, there were no significant differences in the loaded: non-loaded ratio between the two treatment groups in any joint compartment (figures 4.14-4.17).

The only significant response to loading (i.e. the difference between left and right limbs within each treatment group) was found in the lateral tibia. There was a significant increase in lateral tibia trabecular separation in the loaded limb compared to the non-loaded limb in the group treated with a control miRNA (p=0.0236). There was also a significant reduction in trabecular thickness in the same joint compartment in the loaded limb of mice treated with the miR-378a-3p mimic (p=0.0098). These effects of loading are shown by a '#' symbol in figures 4.14-4.17.

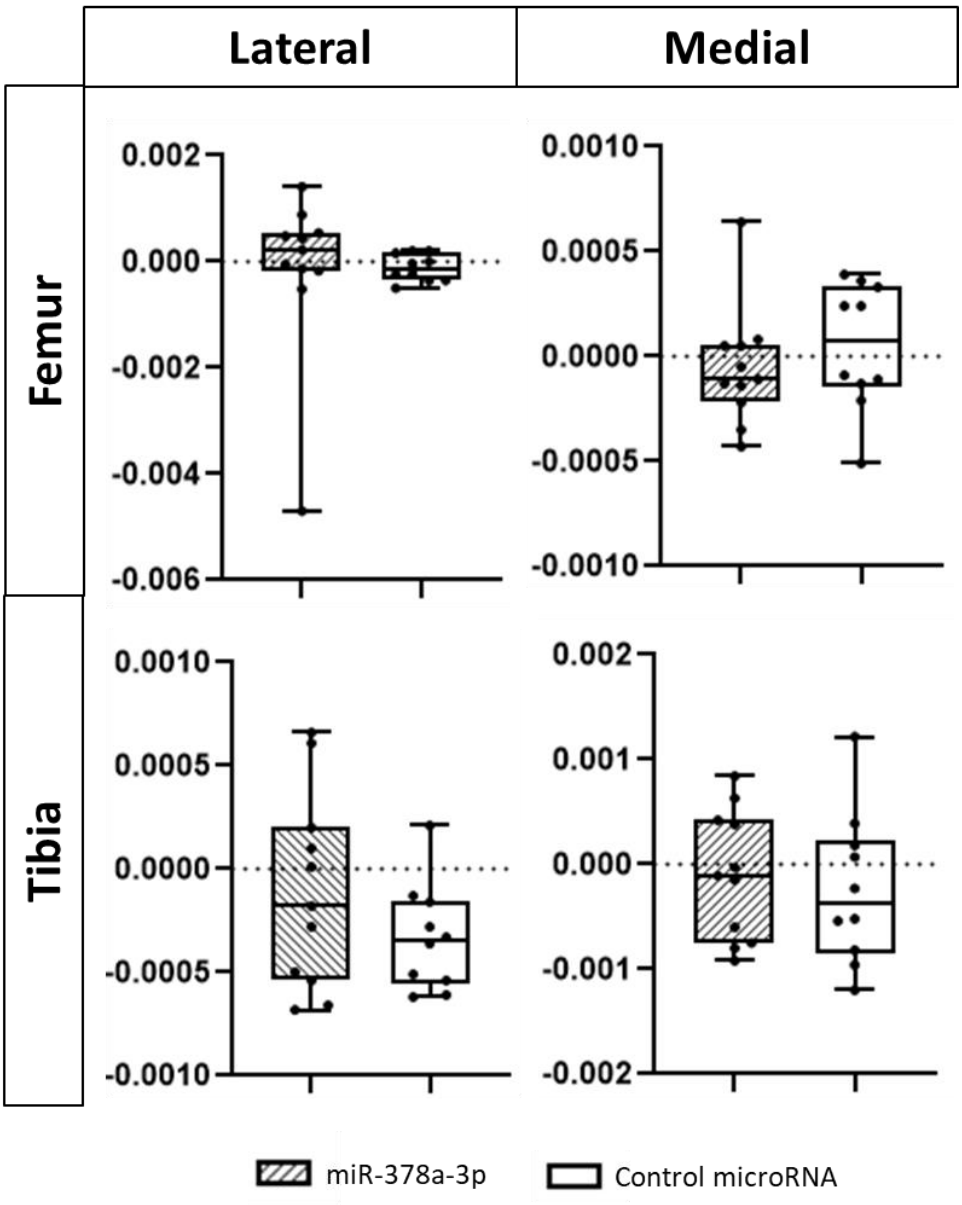

Figure 4.11: µCT analysis of trabeculae number in the miR-378a-3p and control miRNA treated mice. *Differences between the loaded and contralateral control limbs within each treatment group was expressed as a ratio. A positive value indicates that the loaded limb has thicker subchondral bone than the non-loaded limb. Data is displayed graphically as mean ± range with all data points per group included.*

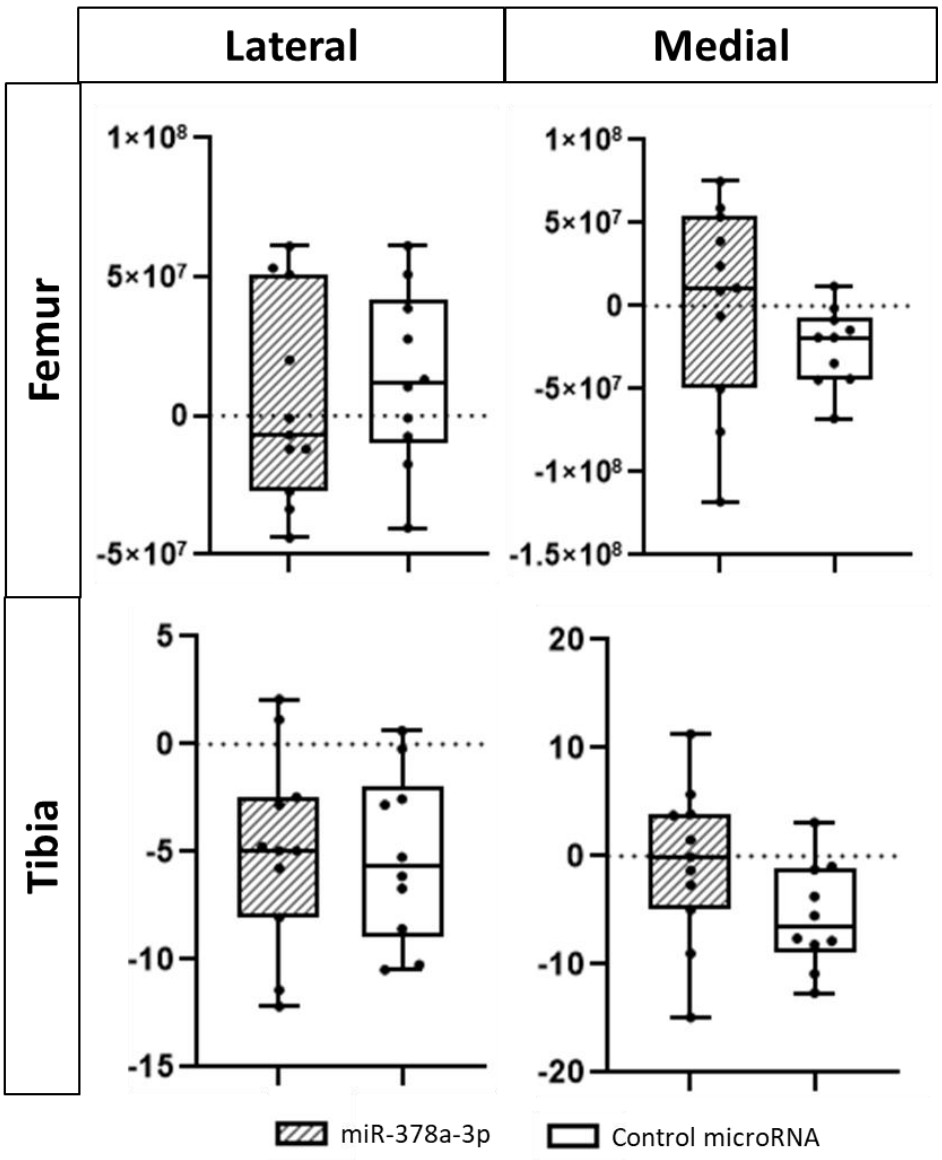

Figure 4.12: µCT analysis of trabeculae bone volume in the miR-378a-3p and control miRNA treated mice. *Differences between the loaded and contralateral control limbs within each treatment group was expressed as a ratio. A positive value indicates that the loaded limb has more trabecular bone volume than the non-loaded limb. Data is displayed graphically as mean ± range with all data points per group included.*

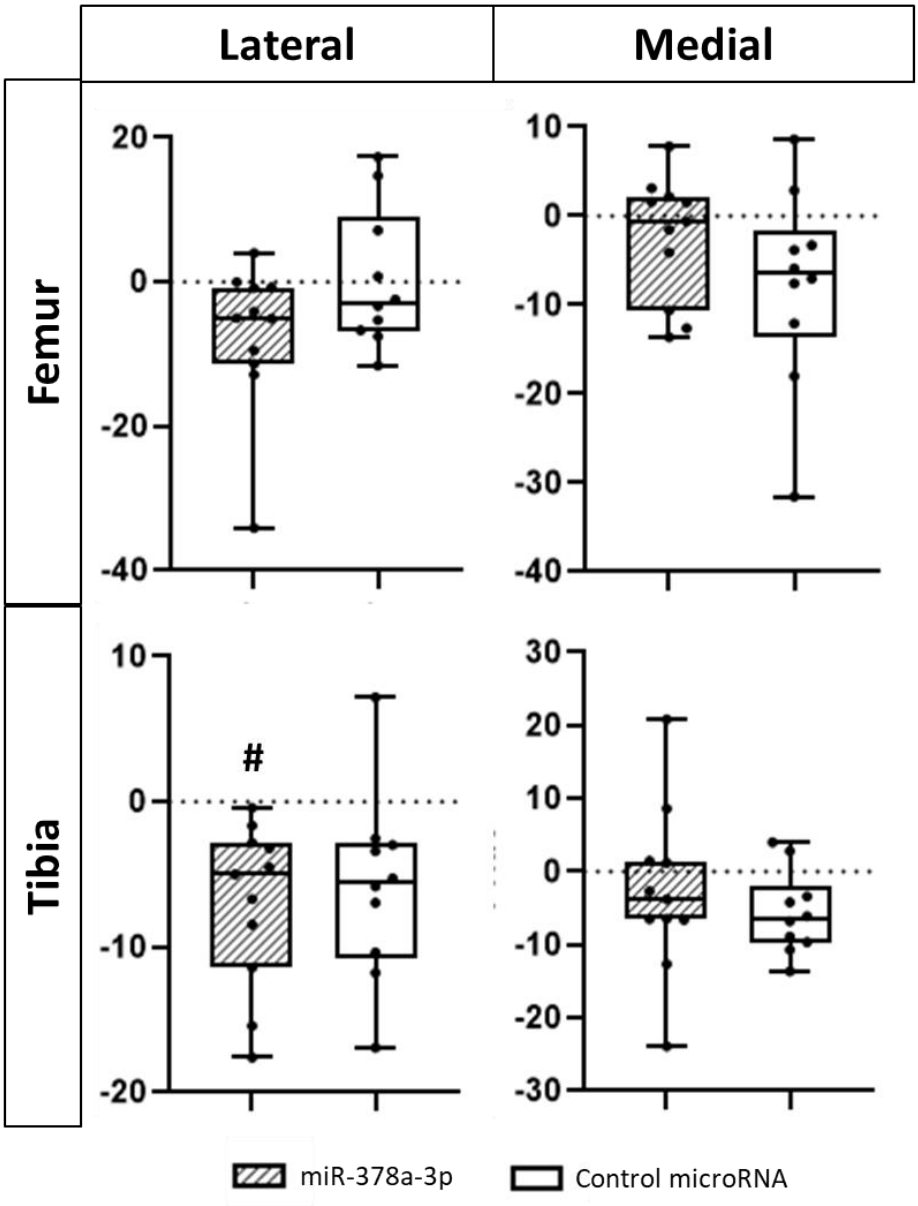

Figure 4.13: µCT analysis of trabecular thickness in the miR-378a-3p and control miRNA treated mice. *Differences between the loaded and contralateral control limbs within each treatment group was expressed as a ratio. A positive value indicates that the loaded limb has thicker trabeculae than the non-loaded limb. Any significant response to loading (i.e. the difference between left and right limbs within each treatment group) is shown with a '#' symbol. Significance was determined via a two-way ANOVA. Data is displayed graphically as mean ± range with all data points per group included.*

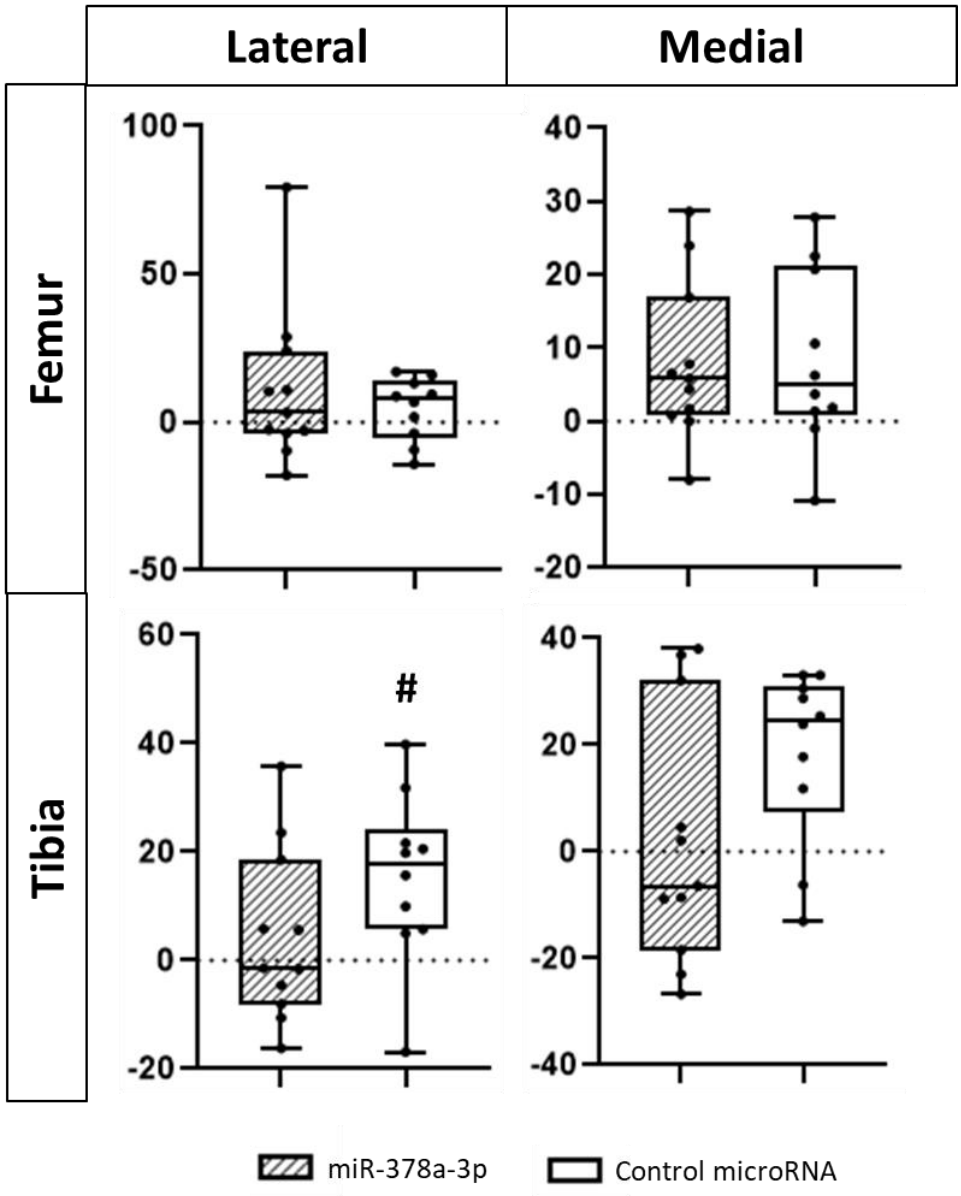

Figure 4.14: µCT analysis of trabecular separation in the miR-378a-3p and control miRNA treated mice. *Differences between the loaded and contralateral control limbs within each treatment group was expressed as a ratio. A positive value indicates that the loaded limb has more trabecular separation than the non-loaded limb. Any significant response to loading (i.e. the difference between left and right limbs within each treatment group) is shown with a '#' symbol. Data is displayed graphically as mean ± range with all data points per group included.*

4.4.10. Ex vivo knee joints treated with miR-378a-3p or a control miRNA show no changes in miRNA target genes or OA markers.

To assess the potential direct effects of miR-378a-3p on the joint, expression of OA markers 'TIMP3' and 'MMP13' were quantified in mouse knee joints that were cultured *ex vivo* and treated with the same miR-378a-3p mimic or control miR used in the *in vivo* study. The joints were dissected sagittally to allow for more efficient penetration of the mimic into the joint tissues. Moreover, the expression of two target genes of miR-378a-3p, 'NRF1' and 'P62' was assessed. qRT-PCR analysis revealed no difference in expression of any of the genes with 24 hours of treatment with the miR-378a-3p mimic compared to the control miRNA (figure 4.18).

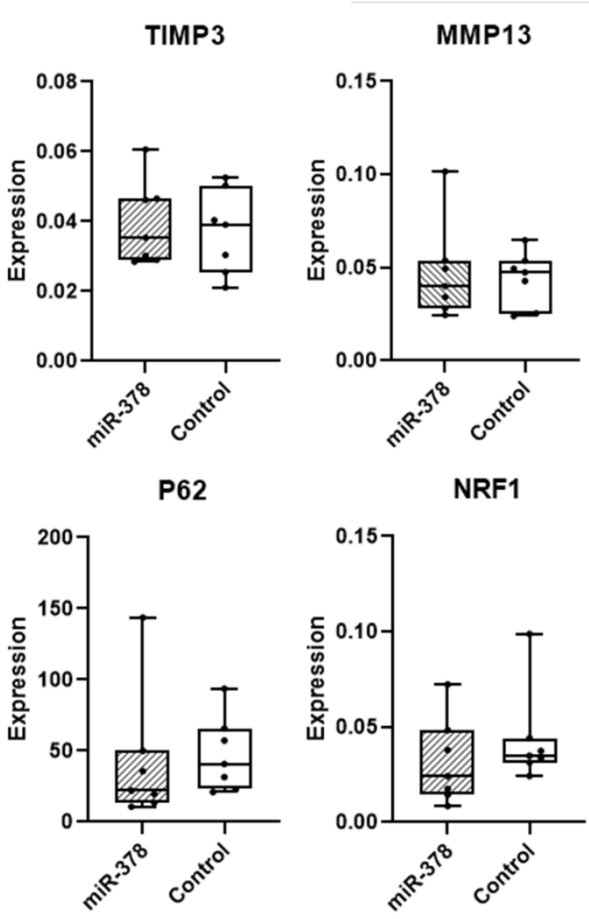

Figure 4.15: TIMP3, MMP13, P62, and NRF1 expression in ex vivo murine knee joints after 24 hours of treatment with either a miR-378a-3p mimic or control miRNA. *'Expression' refers to the CT expression value of the mRNA relative to the housekeeping gene '18S'. Student's unpaired t-test. Data is displayed graphically as mean ± range with all data points per group included. Data is displayed graphically as mean ± range with all data points per group included.*

4.5. Discussion

This study utilised a mechanical loading model of murine OA to investigate the histological and molecular effects of a miR-378a-3p mimic on multiple tissues of the musculoskeletal system. This model has been shown previously to induce muscle changes in the quadriceps of C57/BL6 mice subjected to mechanical joint loading (see previous chapter). There was also a significant increase in miR-378a-3p expression, as well as downregulation of its target genes, in the quadriceps of mice with mechanical load-induced. This, along with other studies implicating it in in muscle and bone homeostasis (Proctor et al., 2017; Zhang et al., 2018), highlighted its potential as a therapeutic molecule for the treatment of musculoskeletal dysfunction.

As expected from the previous experiments examining the effects of the loading model on peri-articular muscle health, there was a significant reduction in fiber cross-sectional area in the mechanically loaded quadriceps of the mice treated with a control microRNA. This was not the case for those treated with the miR-378a-3p mimic, where there was a smaller and non-significant decrease in quadriceps fiber CSA in the loaded limb compared to contralateral controls. There was a 9% and 12% increase in fiber CSA in the gastrocnemius and quadriceps, respectively, regardless of loading, suggesting that miR-378a-3p not only partially restores some of the muscle loss caused by the loading, but improves muscle phenotype with age. Despite the fact that downregulation of this miRNA has been implicated in muscle atrophy (Drummond et al., 2008), this research is novel in that it investigates its therapeutic benefit on muscle health *in vivo.* The importance of this microRNA in muscle is supported by the fact that a patent for the regulation of metabolism by miR-378 was made in 2012 where the authors disclose methods of treating or preventing pathologic cardiac hypertrophy, remodelling, myocardial infarction and heart failure, along with other disorders of the metabolic system (WO2011153542A3).

The improvement in muscle phenotype of the miR-378a-3p treated group, observed histologically as increased fiber CSA, was also reflected behaviourally with improved grip strength. The results of this study show a drastic reduction in grip strength two weeks after the loading regimen and is the first time this has been demonstrated in this model. This reduction occurs in both the miR-378a-3p and control microRNA treated

groups, though they had only received one injection of the treatment when the first post-loading grip strength was assessed. Subsequent assessment of grip strength throughout the 12 weeks that the mice were aged post-loading show a reduction in strength in both treatment groups, though this is more drastic in the control group.

A reduction in grip strength is an ageing-associated phenomenon, with studies showing a large reduction between 8 and 12-months-old in mice (Ge et al., 2016). Therefore, to investigate whether the reduction in grip strength observed in this study was due to the loading or ageing, non-loaded groups subjected to treatment with the same miR-378a-3p mimic or control miR were analysed. This showed that there was no initial drastic decrease in grip strength after the first injection of the treatment, as was the case in the loaded groups, suggesting that this is directly due to loading rather than ageing. There was however a steady decrease in grip strength in the non-loaded mice between the 2nd and 4th injections in both treatment groups (i.e. between ages 42 and 46 weeks-old). There were no significant differences in grip strength between the miR-378a-3p or control treated groups in the non-loaded mice, unlike in the loaded groups where the miR-378a-3p treatment resulted in significantly higher grip strength from the 3rd injection onwards. This suggests that potentially miR-378a-3p protects against loss of grip strength that occurs subsequent to mechanical overloading, but not ageing.

Contrary to expectation, treatment with miR-378a-3p appears to increase the expression of muscle atrophy marker 'ATROGIN1' in both the loaded and non-loaded limbs. Increases in protein degradation are generally associated with the loss of muscle mass, i.e., atrophy, and occur in response to decreased loading, inactivity, and a variety of pathological conditions. The rapid and sustained increase in ATROGIN-1 expression is associated with protein degradation in the muscle. This ligase, along with MURF-1, are thought to target specific proteins for degradation by the 26S proteasome (Bodine et al., 2001). The fact that we see an upregulation of these in both the loaded and non-loaded limb of the miR-378a-3p treated group shows it's not due to the loading regimen or any reduced load bearing caused by the induction of OA. This suggests that it is treatment with the miR-378a-3p mimic itself that is causing this overexpression. However, it should be noted that these mRNAs have complicated expression patterns and therefore investigation of their expression at the protein level,

as well as their post-translational modifications, would be required to fully understand this effect.

MURF-1 has been suggested to promote disassembly of the sarcomere by ubiquitinating the myosin stabilizing proteins myosin-binding protein C (MyBP-C), myosin essential light chain 1 (MyLC1), and myosin regulatory light chain 2 (MyLC2) (Cohen et al., 2009). The complete set of substrates that are targeted for ubiquitination by MURF-1/ATROGIN-1 remains poorly defined, and thus the mechanisms by which upregulation of these ligases contributes to muscle atrophy are not well understood. Recent research has found that these atrophy-related ubiquitin ligases, as well as protein breakdown in general, are blocked by the growth-promoting IGF1/AKT pathway (Milan et al., 2015). Interestingly, IGF1 is a predicted target gene of miR-378a-3p (though not experimentally validated). As such, treatment with this miRNA may downregulate IGF1, thus preventing the 'block' of ATROGIN-1 and MURF-1 expression. Target genes of miR-378a-3p were not increased in the group treated with this miRNA, compared to the control. The lack of significance in this data could be easily explained by the time points that we used. Mice were culled two weeks after the last round of injections, by which point the microRNA would have degraded. Thus, the assumed downregulation of its target genes may have returned to a more physiological normal expression level as the miRNA degraded. However, the fiber CSA and grip strength improvement demonstrated in the mice treated with the miR-378a-3p mimic is indicative of its penetration into the muscle tissue and success as a therapeutic agent. This is also supported by research by Whysall et al. (2020) who used the same injection protocol and mimic design in their study on miR-181a, and who found effective penetration of the miRNA into the muscle.

Ex vivo treatment of mouse joints (including the articular cartilage, synovium, ligaments, and meniscus) with the miRNA mimic showed no difference in OA markers or miR-378a-3p target genes as measured by qRT-PCR expression. This suggests that miR-378a-3p may not play a role in OA protection in the joint tissues directly. This is of course not entirely comprehensive as only a couple of markers and target genes were assessed. Ideally, some of these joints would have been processed for histology to investigate the OA phenotype after treatment with the mimic. However, the nature of *ex vivo* tissue culture means that you cannot keep the knee joints for more than a couple of weeks and whether there would be any changes at all

to the phenotype after so little time is dubious. The fact that the two experimentally validated miR-378a-3p target genes – that have been shown in the previous chapter to be upregulated in the muscle where you see downregulation of the miRNA – have no changes in expression after treatment with the mimic is an indicator that this microRNA is not having an effect in the joint tissues. However, there is a need for a positive control that, due to time and financial constraints, was unable to be included. For example, treatment with a microRNA known to be expressed in the joint – to prove that it is possible for a microRNA treatment to penetrate the tissue. The RNA from these miR-378a-3p and control treated joints has been stored so that RNA sequencing can potentially be performed in the future. This will enable a more thorough analysis of its effect on miR-378a-3p targets (of which there are over 100) as well as OA-associated genes such as: MMPs, TIMPs, ADAMTS, collagens etc.

Assuming this microRNA is not affecting the joint tissues directly, the 25% decrease in OA severity in the miR-378a-3p treated groups can potentially be attributed to the increase in muscle size also seen in the mice treated with the microRNA mimic (9-12% increase depending on the muscle). This provides supporting evidence for the idea that muscle atrophy is, at least partially, linked to the development of OA in the joint. Moreover, that by increasing the size of the muscle – in this case via microRNA treatment – you can potentially prevent the development of load-induced OA in the joint.

This is supported by research into exercise interventions to maintain muscle mass and function during OA. For example, the examination of modifications in low impact exercise, such as swimming and cycling, has shown a beneficial reduction in pain, stiffness and functional deficits in patients with knee OA (Alkatan et al., 2016; Al-Khlaifat et al., 2016). In a 12-week study examining swimming and cycling as exercise therapy for moderate knee OA, patients from both groups showed increased distance achieved in a 6-minute walk test, as well as increased isokinetic knee extensor and flexor strength. Additionally, in the swimming cohort, there was an approximately 40% reduction in joint pain, as assessed by the Western Ontario and McMaster Universities Osteoarthritis Index (WOMAC) (Alkatan et al., 2016). Other areas of research have evaluated similar low-load (20-50% of one-repetition maximum) exercise training in knee OA patients utilising a partial vascular occlusion approach, wherein a pressure cuff or tourniquet is applied to the upper thigh, with similar results

in pain reduction and functional improvements as compared with the conventional strength-training group (i.e., 70% of one-repetition maximum), yet with reduced knee pain whilst exercising (Bryk et al., 2016). The assumption is that this technique provides greater type II fibre activation via a generated anaerobic environment or increased intracellular metabolites (e.g., H+ protons, lactate and adenosine monophosphate), which in turn may stimulate growth hormone secretion (Bryk et al., 2016; Laurentino et al., 2008). Despite the fact that increasing peri-articular muscle strength via exercise is beneficial for the treatment and prevention of OA, meta-analyses show that no specific protocol is deemed the best and current guidelines are ambiguous in recommending exercise programs (Bartholdy et al., 2017). Moreover, there is often low adherence by the individual to the exercise programme as well as a need for graded adjustments to load and volume to provide tolerance to enable consistent progression over time. Though currently in its infancy, the use of miRNA-based therapeutics in OA, including but not limited to regulating muscle mass and function, is a promising avenue of research, with many recent studies suggesting that their use may overcome these limitations associated with many traditional therapies.

As well as increasing muscle mass, miR-378a-3p appears to also have an effect on the subchondral and trabecular bone in these mice with mechanical load-induced OA. Subchondral bone deterioration is commonly associated with articular cartilage defects (Madry et al., 2010) and subchondral bone sclerosis, together with progressive cartilage degradation, is widely considered as a hallmark of OA. However, direct evidence for a critical role of bony remodelling in OA etiology has not been proven. Recent research has demonstrated increased subchondral bone resorption is associated with early development of cartilage lesions, which precedes significant cartilage thinning and subchondral bone sclerosis (Hayami et al., 2006). Arising from subchondral bone plate is the supporting trabeculae, which comprises subchondral trabecular bone, together with deeper bone structure (Madry et al., 2010; Castaneda et al., 2012). Subchondral trabecular bone exerts important shock-absorbing and supportive functions in normal joints and may also be important for cartilage nutrient supply and metabolism (Layton et al., 1988). More recent studies have documented acceleration of subchondral bone turnover accompanied by specific architectural changes in the subchondral trabecular bone of OA joints (Pastoreau et al., 2003).

In this study, we demonstrate an increase in subchondral bone thickness in the medial and lateral femur in the loaded limb of mice treated with the miR-378a-3p mimic. However, the subchondral thickness did not correlate with OARSI severity in the joint, nor did any other subchondral bone pathology measures, suggesting that the changes in the subchondral bone may not be due to the development of cartilage lesions. There was, as expected, a large increase in joint space mineralisation in the loaded limb compared to the non-loaded contralateral control. It seems that miR-378a-3p may protect slightly against joint space mineralisation in load-induced OA, but not to any significant degree. This increase in joint space mineralisation in OA joints, and its correlation with OA severity, has been demonstrated by our group in both the Str/ort spontaneous and post-traumatic DMM models of OA (Ramos-Mucci et al., 2020). This study, as well as those investigating other OA models, suggest that there is a strong relationship between articular cartilage degeneration and pathological joint tissue mineralisation. This research therefore provides further supports the use of μCT imaging as a measure of OA disease progression. Further studies should determine the cellular basis of this pathological joint mineralisation, including in ligaments, and whether these could be potential disease targets.

There were no observed differences between the miR-378a-3p or control mimic treated groups in measures of trabecular bone pathology (thickness, number, trabecular separation, or volume). There was however a highly significant positive and negative correlation between OARSI severity in the loaded limb and trabecular separation and bone volume in the medial femur, respectively. As such, these measures of trabecular bone pathology may be helpful markers of OA progression for future studies. Moreover, it suggests that the medial femur may be more affected than previously thought in this particular model of mechanical load-induced OA.

4.5.1 Future Directions

This research proposes that miR-378a-3p may be a good therapeutic agent for the treatment of OA-associated muscle atrophy. We show that 12 weeks of treatment with this microRNA results in a 25% decrease in OA severity and a 9-12% increase in muscle fiber CSA. Moreover, grip strength results indicate that this apparent improvement in joint and muscle phenotypes may be responsible for improvement of function in these tissues. There are a few limitations and future directions that have

apparent from this research. For example, a more thorough view of all the transcriptome and proteome in the joint, muscle, and bone tissues may help to elucidate some of the molecular mechanisms underlying the observed histological and functional changes in these mice after treatment with the microRNA. This could be achieved by RNA sequencing or mass spectrometry of the relevant tissue. Moreover, longer time points may be required to assess the long-term effects of treatment with this microRNA. As the microRNA was injected intravenously, there may be more systemic effects outside of the musculoskeletal tissues that may need to be assessed and research should investigate the benefit of intramuscular or intraarticular injections. Blood plasma, skin, kidney, and sciatic nerves of these mice have been stored for future research, but time constraints prevented their analysis for this thesis. Another limitation is the fact that we only used male mice for this study. The effects of this loading model on female mice is less well known, but any sex differences in mechanical load-induced or microRNA treatment should be investigated using aged-matched unloaded controls.

4.5.2 Conclusions

Despite these limitations, this study demonstrates the potential therapeutic benefit of miR-378a-3p and its physiologically relevant consequences on myofiber size and muscle strength. This ultimately highlights the potential of microRNA-based therapies for age-related musculoskeletal diseases. Moreover, suggests that one treatment strategy may be used to target multiple diseases simultaneously.

Chapter 5:

Systematic meta-analyses identify osteoarthritis-associated genes and miRNAs in human cartilage

5.1. Introduction

Osteoarthritis (OA) is the most common musculoskeletal disorder and cause of chronic disability in adults (Lu et al., 2014). The main characteristic of OA is the deterioration of the articular cartilage, of which chondrocytes are the only cell type. The primary function of chondrocytes is to maintain homeostasis of the extracellular matrix (ECM). During OA, chondrocytes show aberrant phenotypes and actively produce cartilage-degrading enzymes, such as matrix metalloproteinases (MMPs) and aggrecanases, which result in the destruction of the ECM (Dreier et al., 2010). This change in phenotype is reflected in the cartilage transcriptome, with various studies having identified a number of differentially expressed genes, some of which can also be seen at the protein level (Guo et al., 2007; Haag et al., 2008; Oiu et al., 2021). Despite research having identified a number of key genes and cellular pathways associated with the pathogenesis of OA, their potential as therapeutic targets remain largely undetermined. This is evident in the fact that there is currently no treatment option for the disease beyond total joint replacement. This puts a large demand on research to prioritise which genes, and their regulators, are most important to the disease pathogenesis and thus may act present as candidate targets for therapy.

Micro-RNAs (miRNAs) are a class of small non-coding RNA molecules, approximately 22 nucleotides long, which bind to messenger RNAs (mRNA) and induce their degradation or inhibit protein translation. They play a major role in regulating post-transcriptional gene expression and therefore protein levels. miRNA dysregulation has been implicated with OA development (Malemud et al., 2018) and they are emerging as powerful regulatory molecules and potential novel therapeutic agents. miRNAs often have hundreds of experimentally verified and/or predicted target genes, that can be accessed via public databases such as miRTarBase (Huang et al., 2022) and TargetScan (McGeary et al., 2019), and can therefore target multiple genes involved in a specific disease process. It is thought that restoring physiological levels of miRNAs, via mimics or inhibitors, will allow for restoration of joint homeostasis and function.

The prominent role that miRNAs may play for the integrity of the musculoskeletal system is exemplified by experiments inducing a selective depletion of Dicer, the enzyme that cleaves precursor forms of miRNAs (pre-miRNAs) into mature miRNAs. Depletion of this protein in chondrocytes results in defective cell proliferation and differentiation (Ng et al., 2019). In the muscle, a satellite cell–specific Dicer knockout resulted in mild muscle fibre atrophy over time (Gaur et al., 2010). However, identifying specific miRNAs that may play important roles in OA and sarcopenia development and progression remains a challenge. In humans, several studies have reported on differential miRNA expression in OA patients compared to controls, but results have been inconclusive. This is, in part, attributed to the fact that sample sizes tend to be comparatively small and that studies often analyze different tissues (such as synovium, cartilage, bone, plasma etc.). Moreover, healthy tissue that can be used as a control group is often hard to obtain, with research often resorting to using 'histologically normal' tissue from the same patients as a control. This, along with the lack of statistical power often achieved in individual studies, has hindered the discovery of robust biosignatures. Therefore, the results of these transcriptomic studies have often proven difficult to interpret. Moreover, for gene expression studies, combining published data in the form of a meta-analysis is a particularly challenging task because of the non-standardised fashion that data are reported across publications. However, the integration of multiple related transcriptomic data sets into a single analysis has improved the power to confirm/detect novel biosignatures in other diseases, such as cancer and diabetes (Rasche et al., 2008; Rhodes et al., 2005). It is anticipated that performing this type of analysis with OA data could allow us to prioritise under studied genes that are important to OA pathogenesis, which will enable future research to investigate these as a potential therapeutic targets or biomarkers.

5.2. Aims

The aim of this study was to overcome these difficulties and identify consistently differentially expressed miRNAs and mRNAs in OA based on published evidence. To do so, a systematic literature search was performed to identify all relevant mRNA and miRNA expression studies comparing osteoarthritis cartilage versus healthy control cartilage. Subsequently, data extraction was performed from all eligible articles using

a standardized protocol optimized for the extraction of expression data. A p-value–based meta-analyses was conducted to identify miRNAs and mRNAs that are consistently differentially expressed in OA. Ingenuity pathway analysis was also employed to determine significantly enriched pathways in the genes identified from the meta-analysis. Results were also compared with a recently published systematic meta-analysis on genes dysregulated in muscle atrophy. It is anticipated that this research will help to prioritise genes that are important to OA pathogenesis, for future research to investigate as a potential therapeutic target or biomarker. Moreover, overlap analyses with skeletal muscle data will enable the discovery of genes/pathways that could be potential targets for both OA and muscle atrophy, presenting ways to treat both disorders simultaneously.

5.3. Materials and Methods

5.3.1. Literature Search and Eligibility Criteria

A systematic literature search for miRNA and mRNA expression studies in human OA cartilage was performed using PubMed (http://www.pubmed.gov), applying the search terms "(miRNA OR miRNA OR miR OR micro-RNA) AND (OA OR Osteoarthritis)" for the miRNA analysis, and "(OA OR osteoarthritis) AND (mRNA OR gene) AND (expression) AND (human) AND (knee) NOT (synovium) NOT (murine) NOT (meniscus)" for the mRNA analysis. Papers were assessed for eligibility using the title, abstract, or full text, as necessary. Only articles published in peer-reviewed journals and in English were considered. Papers were not filtered for publication date and were only considered for eligibility provided they: (1) used human knee articular cartilage tissue for analysis, (2) used control cartilage from non-OA amputee patients, and (3) provided the number of patients and significant p-values. A summary of eligible studies can be found in supplementary tables 3 and 4 and an overview of the study design is depicted in figure 5.1.

5.3.2. Data Extraction and Quality Control

For each eligible paper, the first author's name, year of publication, PubMed link, city/country of origin, source of specimen, number of OA and control samples, p-values, miRNA/mRNA names, and direction of dysregulation was extracted. For quality control, the list of the extracted miRNAs was compared to those included on miRbase (v22; http://www.mirbase.org). Any miRNAs that were not listed on miRbase, had insufficient annotation, or corresponded with expired/non-human entries, were excluded from further analysis.

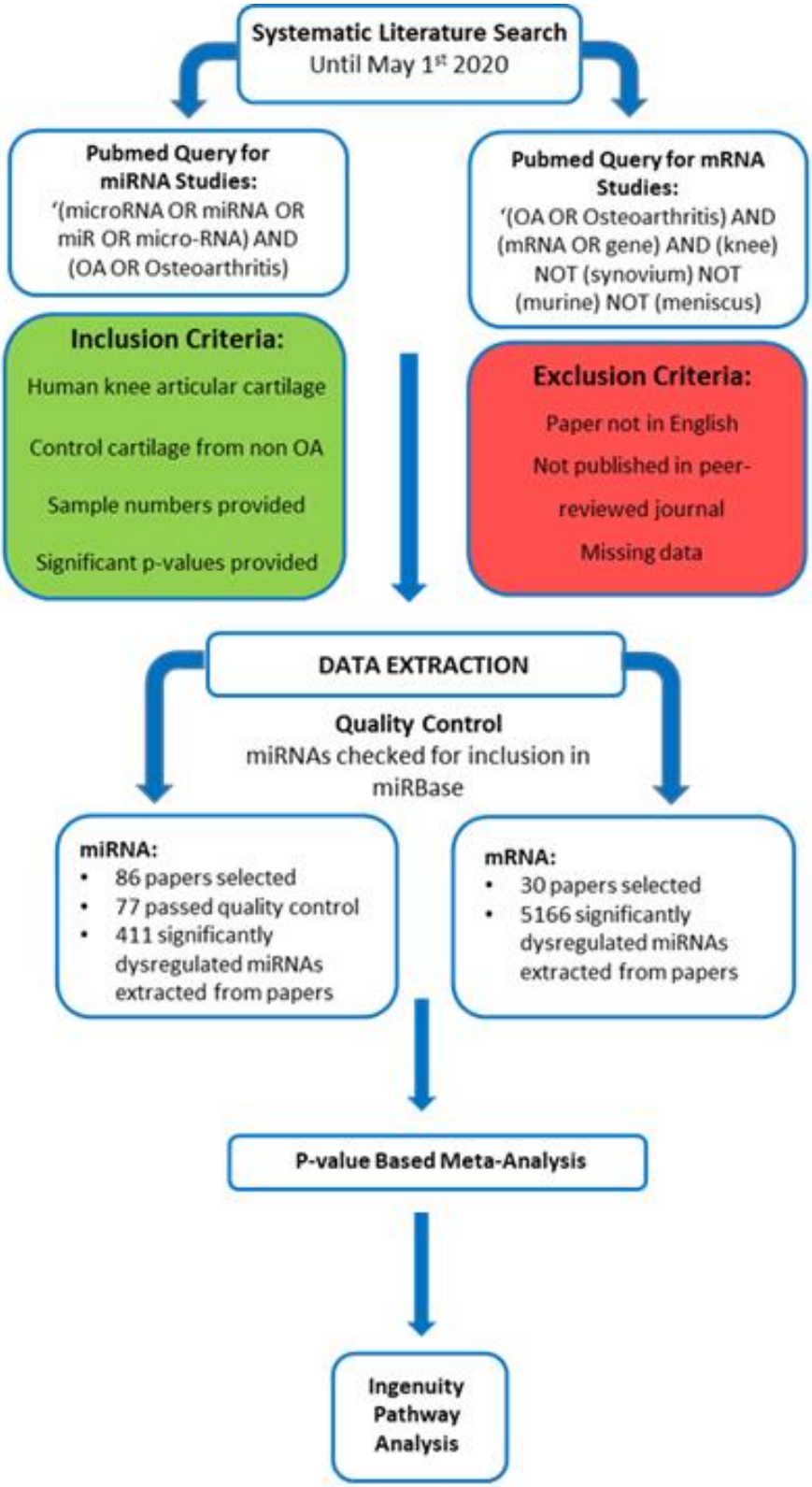

Figure 5.1: A flow chart overview of the methodology used in this study.

5.2.3. P-value based meta-analyses

A p-value based method was used as it enables the combination of results when effect size estimates and/or standard errors from individual studies are not freely available. Meta-analyses were performed on p-values and directions of effects, providing the miRNA or mRNA was identified as being significantly dysregulated in ≥3 independent studies, as previously described (Schulz et al., 2019). To do so, a customised R studio script was used to transform p values into signed z-scores using Stouffer's method (Stouffer et al., 1949; Zaykin et al., 2011) which were then converted to positive or negative values depending on the direction of expression (R script can be found in supplementary table 5). Z-scores for each miRNA/mRNA were combined by calculating a weighted sum, with weights being proportional to the square root of the effective sample size of the study.

5.3.4. Overlap of meta-analysis data with miRNA targets, muscle atrophy-associated genes, and CellAge genes.

CellAge is a database of genes that can drive the senescence process (Avelar et al., 2020). Build 2 of CellAge (Tejada-Martinez et al., 2022) was overlapped with differentially expressed genes identified from the OA meta-analysis. To compare the genes found to be significantly dysregulated in our meta-analysis and those associated with muscle atrophy, data was downloaded from a recent meta-analysis (Deane et al., 2021). Comparisons between the meta-analysis data and miRNA target genes (the 6 miRNAs identified from the meta-analysis as well as miR-3781-3p) used experimentally validated target gene lists obtained from miRTarBase (Huang et al., 2022).

All overlap analyses were performed using the R package ‘GeneOverlap’ (Shen et al., 2022). Given two gene lists, this package tests the significance of their overlap in comparison with a genomic background. In this case, all human protein coding genes were used as background for the analysis. Significance was assessed using a two-tailed Fisher’s exact test with Benjamini-Hochberg false discovery rate (FDR) correction.

5.3.5. Ingenuity Pathway Analysis

Qiagen's Ingenuity Pathway Analysis (IPA) was used to find significantly enriched pathways in 1) The list of mRNAs identified as dysregulated from the meta-analysis 2) validated target genes of the miRNAs shown to be dysregulated in the meta-analysis 3) miR-378a-3p target genes. IPA is a web-based bioinformatics application that allows for functional analysis and integration of gene lists. For IPA, core expression analysis is selected and only experimentally observed interactions are used. Species is set to human only and tissues and cell lines set to tissues and primary cells.

5.3.6. Confirmation of Results with Mass Spectrometry Analysis

Results of the meta-analysis were compared with label-free mass spectrometry proteomics data of human OA articular cartilage compared to healthy controls (manuscript in preparation). The mass spectrometry data have been deposited to the ProteomeXchange Consortium via the PRIDE (Perez-Riverol et al., 2019) partner repository with the dataset identifier PXD029116 and 10.6019/PXD029116.

5.4. Results

5.4.1. P-value based meta-analyses identify 6 miRNAs and 207 mRNAs differentially expressed in OA cartilage.

The PubMed search for studies on mRNA and miRNA expression in OA yielded 936 and 622 papers respectively. Of these initial papers, 86 on miRNA expression and 30 on mRNA expression met our eligibility criteria (see Literature Search and Eligibility Criteria in Methods). Studies on miRNA expression were subject to quality control based on the inclusion of the miRNA in miRbase, resulting in 77 papers that were suitable for the meta-analysis. From these papers, 411 miRNAs and 5,166 mRNAs were extracted. The p-value based meta-analysis identified 6 miRNAs and 207 mRNAs as being significantly dysregulated in OA cartilage compared to healthy tissue in 3 or more independent studies. The 20 top mRNAs and all miRNAs are shown

below (table 5.1) and the full list can be found in supplementary table 6. All miRNAs shown to be dysregulated in or more independent studies can be found in supplementary table 7.

Table 5.1: *The top 20 mRNAs, and all the miRNAs, found to be significantly dysregulated in the meta-analysis.*

miRNA/mRNA	Summed z score	p value
DDIT4	-10.63912988	9.80E-27
GADD45A	-9.671426964	1.99E-22
TXNIP	-9.159840611	2.60E-20
RPL23AP1	-8.608480816	3.70E-18
C10orf10	-8.302559066	5.09E-17
ANG	8.070197563	3.51E-16
APOD	-7.769000282	3.96E-15
GPX3	-7.67384789	8.35E-15
CEBPD	-7.448716407	4.71E-14
DLX5	-7.351922828	9.77E-14
HOXA5	-7.319143505	1.25E-13
GDF15	-7.277596172	1.70E-13
PDK4	-7.26107927	1.92E-13
CISH	-7.150042437	4.34E-13
SCNN1A	6.872376244	3.16E-12
RND1	-6.869197998	3.23E-12
CSNK2A2	-6.803140204	5.12E-12
KLF15	-6.746554293	7.57E-12
DCXR	-6.740626982	7.89E-12
HSD17B14	-6.662116002	1.35E-11
miR-149	-4.31654501	7.92E-06
miR-150-5p	-3.679922531	0.000116652
miR-140	-3.628394273	0.000142595
miR-140-5p	-3.598588637	0.000159974
miR-424-3p	-3.396430809	0.000341354
miR-26a	-3.099660248	0.000968714

5.4.2. Ingenuity Pathway Analysis (IPA) of significant mRNAs and miRNA target genes reveals 12 shared chondrocyte pathways linked to OA, of which senescence is the most significant.

To determine the most significant cellular pathways linked to these dysregulated mRNA and miRs, I performed pathway analysis (IPA) on the 207 dysregulated mRNAs and on the target genes of the miRNAs identified from the meta-analysis. I identified 4 common pathways between the dysregulated mRNA genes and miRNA target genes, including senescence, p53 signalling, BEX2 signalling and unfolded protein response (Figure 5.2). All significantly enriched pathways identified by IPA are detailed in supplementary tables 8 and 9. Further investigation of the most significant pathway - senescence - and showed that our lists of miRNA target genes, mRNAs, and their upstream regulators overlapped with genes shown to induce or inhibit senescence *in vitro* (CellAge genes) (Tejada-Martinez et al., 2022). The most significant overlap was between predicted upstream regulators of the differentially expressed mRNAs identified in the meta-analysis and inducers of senescence (43% overlap). Moreover, there was a 33.3% overlap between inhibitors of senescence and predicted upstream regulators of miRNA target genes (Figure 5.3).

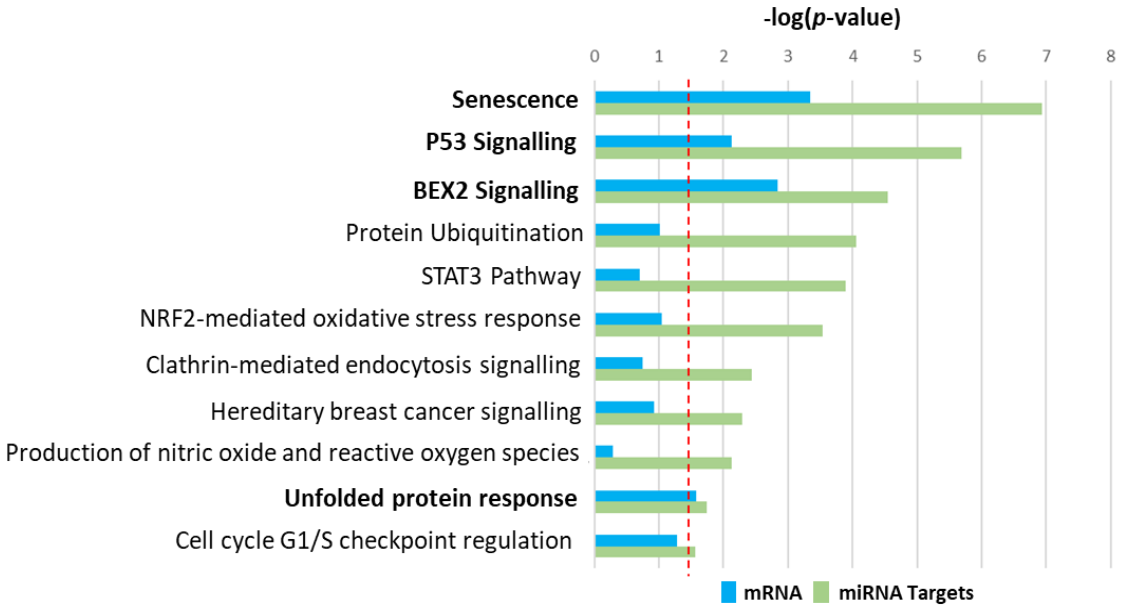

Figure 5.2: The 12 canonical pathways, determined by Ingenuity Pathway Analysis (IPA), that were enriched for both the list of predicted miRNA target genes (green) and list of dysregulated mRNAs (blue) identified from the meta-analysis*. The red dotted line indicates a significant p-value (p=0.05).*

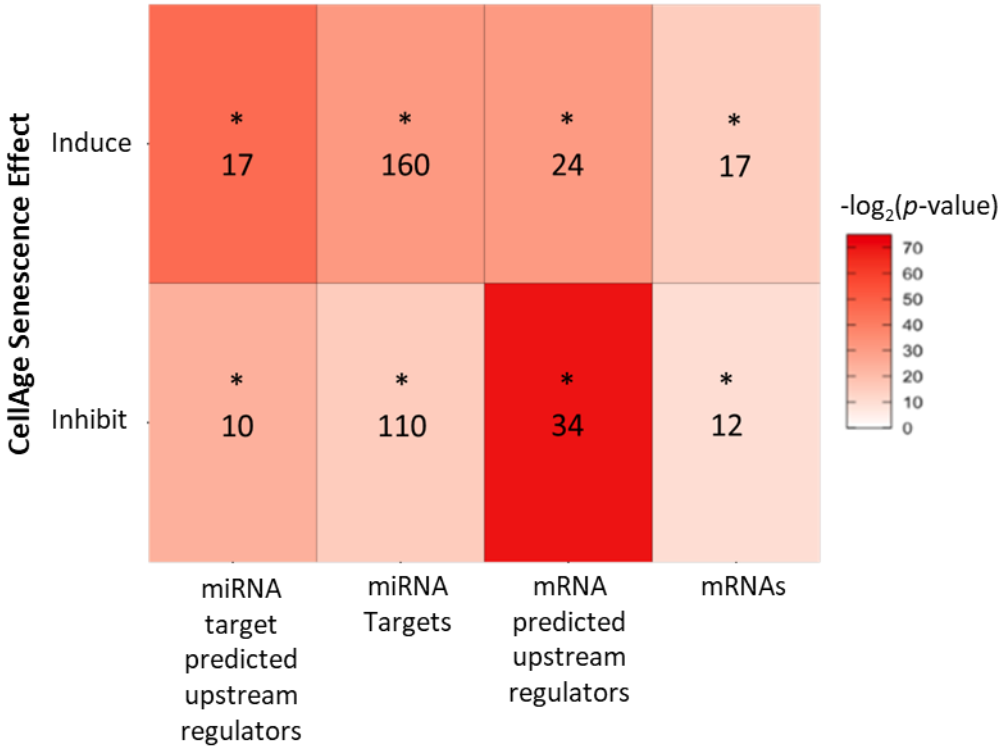

Figure 5.3: A heatmap showing the overlap between miRNA target genes, mRNAs, and their predicted upstream regulators, with genes that have been shown in vitro to either induce or inhibit cellular senescence (CS). *Numbers of overlapped genes are indicated in each cell. *p>0.01 Fisher's exact test with Benjamini-Hochberg false discovery rate correction.*

5.4.3. Mitochondrial dysfunction is the most significantly enriched pathway from a list of muscle-atrophy-associated genes

IPA was used to determine the most significantly enriched pathways in a list of genes found to be dysregulated in muscle atrophy in a recent meta-analysis by Deane et al. (2021). From the 393 pathways that resulted from this analysis, mitochondrial dysfunction was the most significant. 72 genes from the muscle atrophy gene list were associated with mitochondrial dysfunction (figure 5.4).

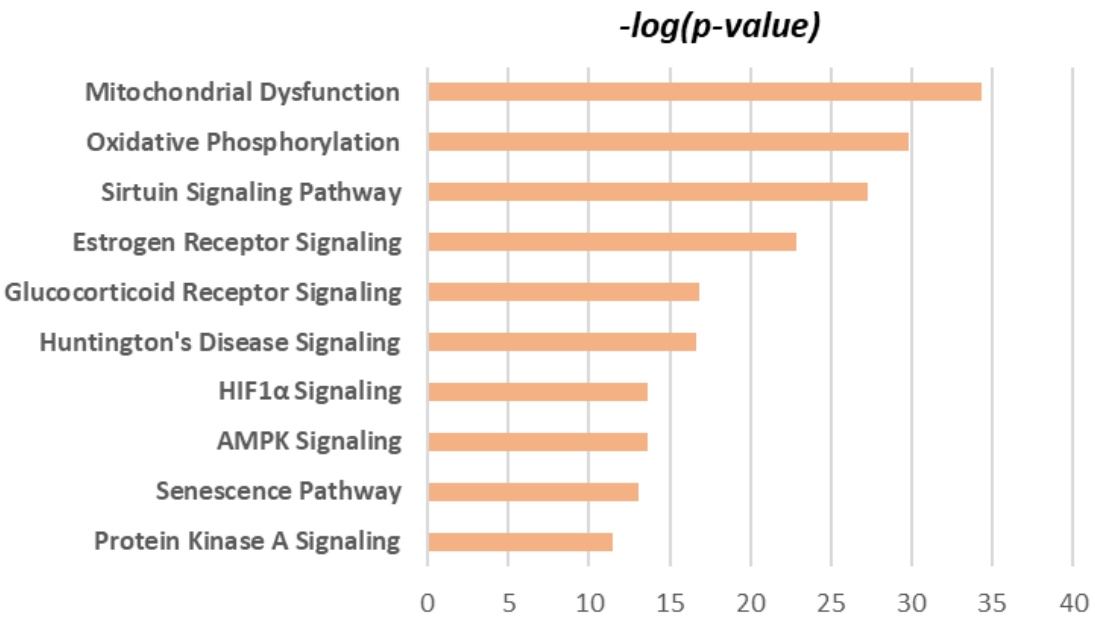

***Figure 5.4**: The top 10 canonical pathways, determined by Ingenuity Pathway Analysis (IPA), that were significantly enriched in a list of muscle-atrophy associated genes from Deane et al. (2021).*

5.4.4. Overlap analyses finds a highly significant overlap between meta-analysis-identified mRNAs and validated target genes of the 6 meta-analysis-identified miRNAs.

Overlap analyses (Fisher's exact test with Bonferroni correction) of the 207 meta-analysis-identified mRNAs and validated target genes (obtained from miRTarBase) of the 6 meta-analysis-identified miRNAs revealed a highly significant overlap (Figure 5.5(a)) with almost double the number of genes being shared between the two lists than expected by chance (p=5.078696e-06). These 55 overlapping genes are detailed in table 5.2 Moreover, when overlapping the genes found by Deane et al. (2021) as significantly differentially expressed in muscle atrophy and target genes of microRNAs identified from the meta-analysis, there was also a highly significant overlap. This was also the case for comparisons between muscle atrophy genes and genes found to be dysregulated in the OA meta-analysis (figure 5.5(b) and table 5.3).)

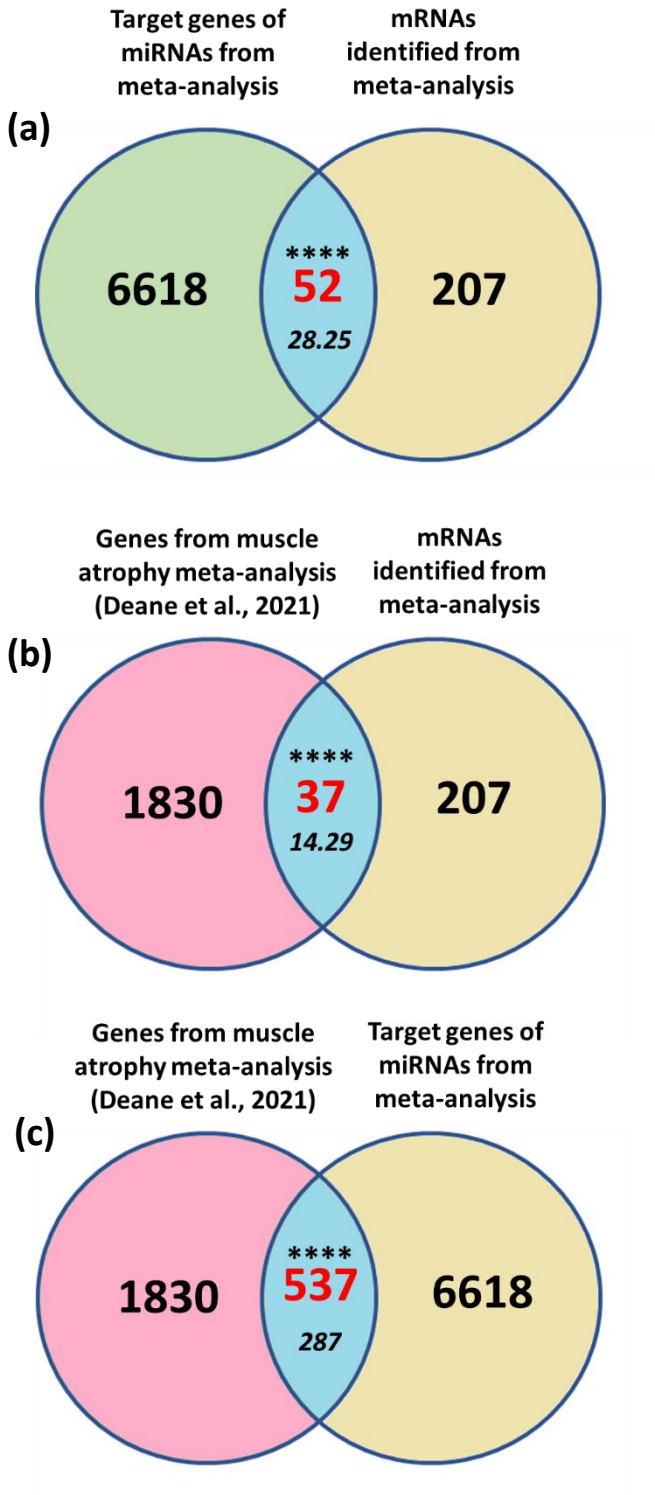

Figure 5.5: Overlap analyses of genes found to be differentially expressed from OA and muscle meta-analyses. ***(a)*** *Overlap between mRNAs identified as significantly dysregulated from the meta-analysis of genes dysregulated in OA and validated target genes of miRNAs found to be dysregulated from the OA meta-analysis.* ***(b)*** *Overlap between mRNAs identified as significantly dysregulated from the meta-analysis of genes dysregulated in OA and mRNAs identified as dysregulated in human muscle atrophy.* ***(c)*** *Overlap between validated target genes of miRNAs found to be dysregulated from the OA meta-analysis and genes identified as dysregulated in human muscle atrophy. Red numbers indicate number of genes found to overlap between the two groups. Numbers in italics represent the expected number of genes to overlap between the two ****p>0.0001 Fisher's exact test.*

Table 5.2: *Genes that overlap between those identified as significantly dysregulated from the meta-analysis and validated target genes of miRNAs found to be dysregulated from the OA meta-analysis.*

Genes overlapping between mRNAs and miRNA targets				
ADAD2	BTG2	CDKN1A	DEK	HIST1H1C
ADM	C20orf24	CLDND1	DMKN	HNRNPD
ANAPC5	CASP8AP2	CMPK1	EEF1D	HOXA5
BACE2	CAST	CTH	ERGIC3	HSPA8
BOD1	CCDC43	DDIT4	FUT3	ID1
IFI6	MYL6	PIM1	RPL5	ST13
KLC1	NEK6	PLIN5	RTN4	TBRG4
KLF6	PCBP2	PRLR	SDC4	TGIF1
LIF	PDP1	RAB37	SLC3A2	TIMP4
MAPK8	PFDN5	RNF39	SSFA2	TXNIP
UBE2D2	UTY	VGLL4	ZNF207	ZNF44

Table 5.3: *Genes that overlap between those identified as significantly dysregulated from the OA and muscle atrophy meta-analyses*

Genes Overlapping Between OA and Muscle Atrophy Meta-Analyses		
GADD45A	BTG2	ANXA11
CD99	TXNIP	HSD11B1
ADM	PIM1	TIMP4
KLF6	TGIF1	ACAA1
STAG2	CD151	RALY
HLA-F	NSFL1C	CLDND1
EXOC7	LGALS3	HOXA5
GPX3	SLC25A11	RTN4
CSNK2A2	IDH3B	ABCC1
VGLL4	DBI	TPM2
CHI3L1	PDHA1	PCBP2
ZNF207	LDHA	HAX1
NPM1		

5.4.5. Overlap analyses reveal a highly significant overlap between genes identified as significantly dysregulated in a recent meta-analysis of differentially expressed genes in human muscle atrophy and miR-378a-3p target genes.

Overlap analyses of mRNAs from our meta-analysis of dysregulated genes in OA and validated miR-378a-3p target genes – obtained from miRTarBase – revealed no significant overlap (Figure 5.6(a)). However, when overlapping validated target genes of miR-378a-3p and target genes of miRNAs from meta-analysis, there was a very significant overlap (p= 6.764667e-101). Moreover, analyses between the genes found by Deane et al. (2021) as significantly differentially expressed in muscle atrophy and miR-378a-3p validated target genes revealed a highly significant overlap (p=1.73906e-17; figure 5.6(b)). Of the 1830 muscle atrophy-associated genes and the 949 OA-associated genes, there was 147 genes that overlapped (table 5.4)

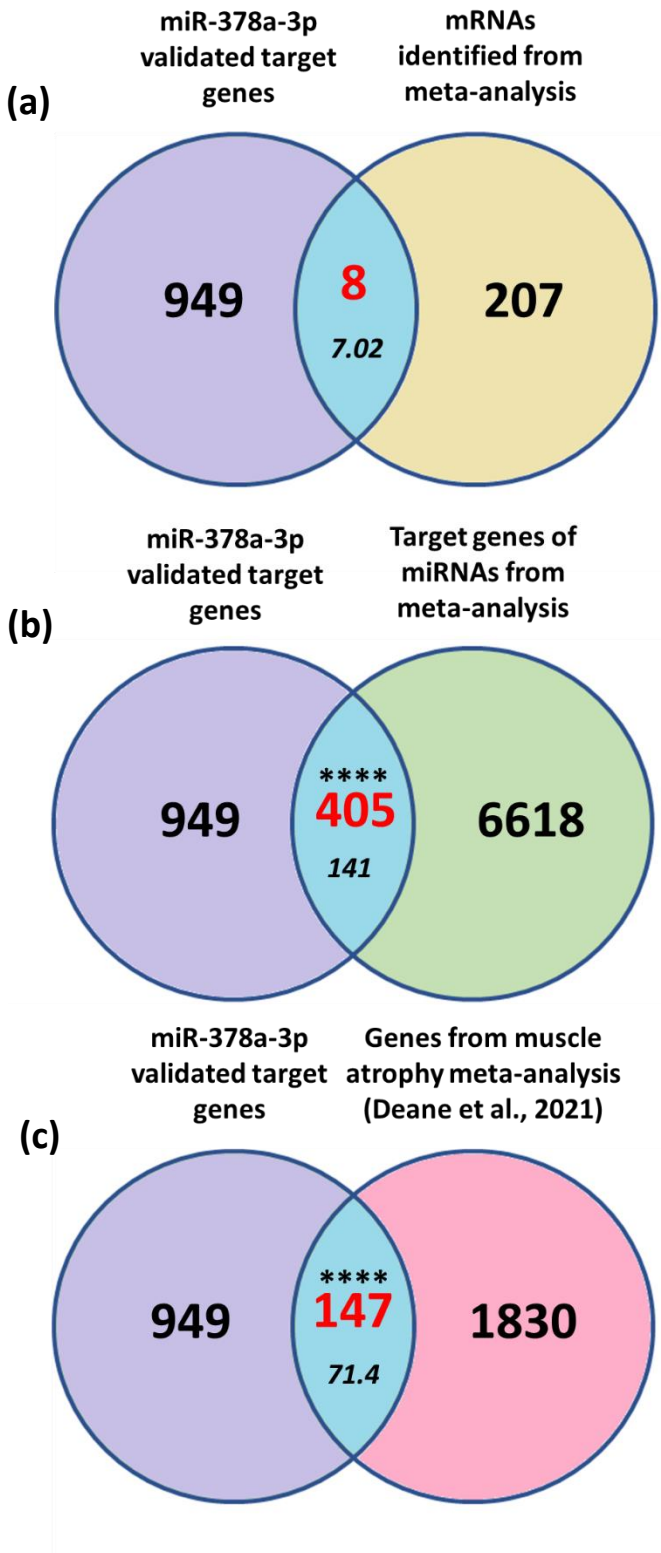

Figure 5.6: Overlap analyses of genes found to be differentially expressed from OA and muscle meta-analyses and miR-378a-3p validated target genes. ***(a)*** *Overlap between mRNAs identified as significantly dysregulated from the meta-analysis of genes dysregulated in OA and validated target genes of miR-378a-3p.* ***(b)*** *Overlap between validated target genes of miR-378a-3p and target genes of miRNAs from meta-analysis.* ***(c)*** *Overlap between validated target genes of miR-378a-3p and genes found to be dysregulated in a meta-analysis of muscle atrophy genes (Deane et al., 2021). Red numbers indicate number of genes found to overlap between the two groups. Numbers in italics represent the expected number of genes to overlap between the two ****p>0.0001 Fisher's exact test.*

Table 5.4: *Genes that overlap between those identified as significantly dysregulated from the meta-analysis of genes associated with muscle atrophy and validated target genes of miR-378a-3p.*

Overlapping genes between miR-378a-3p targets and mRNAs associated with muscle atrophy					
PAFAH1B1	EPM2A	TGOLN2	MZF1	LDLR	BCL2
ZNF207	VEGFA	ZFP36L2	MAPK1	SLC6A8	RPS7
SEMA3B	AMOTL2	FARP1	USP14	IMMT	BSG
RNF10	MRPL3	PPP2R5E	KLF5	PER2	DCP2
AKAP11	NKTR	SLC16A1	NFAT5	SERINC3	DHCR7
CCDC28A	RTN4	EIF4A2	MCM4	CDK8	IQCB1
FOXC1	SRSF4	EIF5B	ECH1	MEIS2	DAG1
WNK1	SFPQ	IFNAR2	DMPK	LDHA	GNG5
HIPK2	SRM	PSKH1	PLIN3	ARHGAP32	COX8A
SLK	C1orf21	ABR	MET	MDM2	ULK1
PKM	PRRC2C	CSTB	LSM5	SUCLA2	JUN
RHOA	RCN2	SQSTM1	YKT6	NDUFB5	TMEM11
CFAP20	SGK1	RPL8	RGP1	MDC1	TUFM
ZFYVE26	TGIF2	NIPBL	PPP3CB	SEC24B	KPNA2
HSD17B10	WBP4	DLC1	EZH1	RPS2	P4HB
KDM5A	TMPO	PEX2	LUC7L3	PRPSAP2	ZFP36L1
PPP2R3A	AMD1	PSMC3	IFT20	TOB1	PPP1CC
WDR62	AGO2	NOLC1	GRPEL1	ARNT	MAPT
APLP2	NCOA3	BLCAP	CCND1	POGZ	PTMA
TXLNA	USP9X	URM1	DDX6	PARP1	ARL4C
HUWE1	AHNAK	THAP11	RSRC2	PIK3R1	SF3B3
TXNL1	ABCC4	PCBP1	CAND1	TNFRSF21	DYNC1H1
ESR1	RAP1B	ROBO1	LDHB	NFIB	BAZ1A
ARCN1	TTBK2	ASXL1	ASF1A	ALDOA	RBM14
E2F3	MAGI1	CYFIP1			

5.4.6. Confirmation of meta-analysis data with mass spectrometry data reveals 7 significantly dysregulated proteins in the superficial, middle, and deep zones of human osteoarthritic knee cartilage.

Results of the OA meta-analysis were overlapped with label-free mass spectrometry proteomics data of human OA articular cartilage compared to healthy controls. The mass spectrometry data have been deposited to the ProteomeXchange Consortium via the PRIDE (Perez-Riverol et al., 2019) partner repository with the dataset identifier PXD029116 and 10.6019/PXD029116. This revealed 7 proteins that were found to be differentially expressed in the superficial zone of the cartilage. Of these 7 proteins, two were also dysregulated in the middle zones and four were dysregulated in the deep zones (table 5.5). Of these proteins, Lactate Dehydrogenase A (LDHA) was found to be an experimentally validated miR-378a-3p target gene as well as one of the genes dysregulated in muscle atrophy (Deane et al., 2021). Parkinsonism Associated Deglycase (PARK7) was one of the 7 meta-analysis genes, validated by mass spectrometry, that was also found to be a CellAge gene (Tejada-Martinez et al., 2022). None of the 7 genes/proteins were target genes of the 6 miRNAs that were found to be significantly dysregulated in our meta-analysis.

Table 5.5: *Mass-spectrometry comparison of mRNAs found to be significantly dysregulated from the meta-analysis.*

Gene Name	Included in cellage?	Included in muscle atrophy meta-analysis?	Validated target of miR-378a-3p?	Target of 6 miRs from miRs from meta-analysis?	Mass spec OA cartilage vs control		
					Superficial zone fold change	Middle Zone fold change	Deep Zone fold change
APOD	FALSE	FALSE	FALSE	FALSE	-1.259817494	-2.410027844	-2.146022337
SERPINA1	FALSE	FALSE	FALSE	FALSE	-3.737089031	-2.102085205	
PARK7	TRUE	FALSE	FALSE	FALSE	-2.178129473		
ACAN	FALSE	FALSE	FALSE	FALSE	-1.918704064		
LDHA	FALSE	TRUE	TRUE	FALSE	-1.375252605		1.052821799
HIST1H1E	FALSE	FALSE	FALSE	FALSE	-1.872258114		-1.688485375
TRPV4	FALSE	FALSE	FALSE	FALSE	-1.49270102		1.776227668

5.5. Discussion

Following a systematic literature search and data extraction, this study performed a p-value based meta-analysis of data from all eligible miRNA and mRNA expression studies in human OA cartilage versus healthy control tissue. I have identified a list of OA-associated genes and miRNAs, seven of which were also confirmed to be modified at the protein level. Overlap analyses revealed significantly more overlap than expected by chance between the 207 mRNAs that I identified from the meta-analysis and experimentally validated target genes of the OA-associated miRNAs that were also found to be differentially expressed in the meta-analysis. The enrichment of the meta-analysis genes in the miRNA target list provides further support as to their importance in OA. It also suggests that these miRNAs may have a potential therapeutic benefit that future research should investigate further.

As senescence was one of the most significantly OA-associated pathways shared between both the miRNA target genes and mRNAs, overlap analysis was performed with genes included in the CellAge database (Tejada-Martinez et al., 2022). These CellAge genes were compiled by a systematic literature search of genetic manipulation studies whereby direct *in vitro* manipulation of the gene in question resulted in induction or inhibition of cellular senescence. Results of this analysis revealed highly significant overlaps, the most significant being with predicted upstream inhibitors of the differentially expressed mRNAs and inducers of cellular senescence. Senescent cells accumulate later in life and at sites of age-related pathologies, where they contribute to disease onset and progression through complex cell autonomous and non-autonomous effects (Childs et al., 2015). Previous research has shown that senescent chondrocytes not only accumulate with age but are present at higher numbers in human OA cartilage compared with age-matched healthy controls (Jeon et al., 2017). In fact, a clinical trial investigating whether the senolytic supplement fisetinA reduces OA- associated pain and cartilage breakdown is due to begin in 2022 (NCT04770064). A key characteristic that distinguishes senescent cells from other cell types is the upregulation of a combination of factors known as the ‘senescence-associated secretory phenotype’ (SASP) (van Deursen et al., 2014). The SASP contributes to fuel a state of chronic, systemic, low-grade inflammation, known

as ‘inflammaging’, and compromises a subset of genes whose encoded secreted proteins include proinflammatory cytokines and chemokines, growth factors, and proteases that can digest the ECM (Rodier et al., 2009). Previous work measuring senescent cell accumulation and telomere attrition with age in chondrocytes indicates that chondrocyte cellular senescence occurs *in vivo* with age and may have a causal or aggravating role in OA development (Martin and Buckwalter, 2001) (Toh et al., 2016). Moreover, excessive loading of articular surfaces caused by acute joint trauma or posttraumatic joint instability can cause a release of reactive oxygen species in chondrocytes. This can induce senescence through activation of p38 MAPK and PI3K/Akt signaling and subsequent stimulation of the SASP (Jeon et al., 2018). Overall, results of the overlap analyses corroborate this research, suggesting a strong association between OA and cellular senescence.

The overlap between the 207 meta-analysis-identified mRNAs and validated target genes of the 6 meta-analysis-identified miRNAs was investigated. This revealed a highly significant overlap, with 52 genes being shared between the two lists. This suggests that miRNAs, and their dysregulation, are at least partially responsible for the differential gene expression observed in the OA. Moreover, when comparing the results of the OA meta-analysis with data from the muscle-atrophy meta-analysis, there were more genes that overlapped than expected by chance. This suggests that the genes/pathways involved in OA development may be the same that occur in muscle atrophy. This is particularly interesting result as it raises the potential to target both tissues simultaneously. For example, one of the genes that were found to be dysregulated in both OA and muscle atrophy is TIMP-4. The TIMP gene family consists of four members, which have matrix metalloproteinases (MMPs)-inhibiting, anti-angiogenic, growth-promoting and proapoptotic activities (Baker et al., 2002). TIMP-3 is well studied in OA (Arpino et al., 2015), as it is the only TIMP family member that can inhibit both ADAMTSs and MMPs, making it a key chondro-protective inhibitor (Doherty et al., 2016). TIMP-4 is less well-studied in OA, however, it does target MMP-13 – the classic matrix metalloproteinase implicated in arthritic tissue damage (Melendez-Zajgla et al., 2008). It’s role in skeletal muscle is even more elusive, with the majority of research investigating it in the context of cardiac muscle. For example, research has demonstrated its downregulation in heart disease (Nakano et al., 2017), suggesting that it inhibits cardiac fibroblast cell

migration (Tummalapalli et al., 2001). Future research should therefore investigate the less-studied family members of genes that are typically associated with OA development/muscle atrophy. Doing so may allow the simultaneous targeting of multiple musculoskeletal disorders. Moreover, the similar sequence/structure of genes/proteins of the same family may enable the repurposing of pre-existing drugs.

In addition, several of the putative targets are known to be mechanoresponsive and interestingly all feed back into Ca2+ signaling, for example TRPV4 and NFAT5 (Gilchrist et al., 2019). As such, one of the possible mechanisms behind OA and muscle atrophy may be Ca2+ dependent, an important pathway in both tissues. In the joint articular cartilage, intracellular calcium signaling is among the earliest responses of chondrocytes to physical stimuli (Han et al., 2012). In muscle, cytosolic Ca2+ plays a critical role in the activation/deactivation of contractile proteins (Cho et al., 2017).

Interestingly, overlap between miR-378a-3p target genes and the mRNAs found to be differentially expressed in OA from the meta-analysis revealed no significant overlap – with only 8 genes appearing in both lists. This is further supporting evidence that this microRNA may not exert its effects on the joint directly, as discussed in the previous chapter. Though it should be noted that this meta-analysis was conducted using studies that investigated OA cartilage only, excluding all other joint tissues. As such, miR-378a-3p may have an effect on the synovium or ligaments and contribute to OA in the joint via these tissues. As research has previously detected miR-378-5p in synovium in late-stage OA patients (Li et al., 2018; Cheng et al., 2017), it is not out of the question that its dysregulation in this tissue may contribute to OA. Though, experiments with *ex vivo* knee joints – including the synovium – showed no effect of a miR-378a-3p mimic on OA markers (detailed in the previous chapter). There was, however, a significant overlap between miR-378a-3p target genes and validated targets of the microRNAs found to be dysregulated in the OA meta-analysis. This could suggest that miR-378a-3p may regulate genes that were not necessarily detected from the meta-analysis of mRNAs dysregulated in OA, but that may still play a role in the disease pathogenesis.

One of the strengths of this study is that it increased the sample size by combining all eligible data into one statistical test. This is particularly important as sample sizes of

individual miRNA studies are often small, especially as control healthy cartilage is notoriously difficult to obtain. I have also confirmed our list of OA-associated genes at the protein level using mass spectrometry data. It is known that articular cartilage can be separated into distinct zones, namely superficial, intermediate, and deep, in which chondrocytes show distinct gene expression profiles and behaviours (Grogan et al., 2013). Thus, separating these zones for proteomics analysis ensures location-specific changes in protein levels is not under-represented compared to whole cartilage samples. The comparison of this mass spectrometry data with the meta-analysis results revealed 7 differentially expressed proteins that were all down-regulated in the superficial zone of the osteoarthritic cartilage vs healthy control cartilage. Of these 7 proteins, LDHA was the only one that was also in the list of experimentally validated miR-378a-3p targets, the OA-meta-analysis, and the list of genes dysregulated in muscle atrophy – where it was also found to be downregulated. LDHA is primarily found in skeletal muscles and codes for the lactate dehydrogenase-A enzyme. Lactate dehydrogenase catalyzes the interconversion of pyruvate and lactate, which are critical fuel metabolites of skeletal muscle particularly during exercise (Liang et al., 2016). In the joint, research has shown that LDHA binds to NADH, promoting reactive oxygen species, and inducing catabolic changes through stabilization of IκB kinase, a critical pro-inflammatory mediator in chondrocytes (Arra et al., 2020). Inhibition of LDHA activity therefore has anti-catabolic properties via increasing degradation of IκB kinase by the proteasome. The fact that LDHA was found to be a significantly dysregulated gene in both muscle atrophy and OA suggests that it may make a good target gene for therapeutic intervention for both disorders. However, as the direction of expression appears to be opposite in OA and muscle atrophy, targeting it in both tissues simultaneously may prove complicated. As detailed in chapter 4 of this thesis - *ex vivo* treatment of mice knee joints with miR-378a-3p had no effect on target genes or OA markers. Moreover, overlap analyses in this chapter revealed no significant enrichment of miR-378a-3p target genes in the meta-analysis data. This suggests that the miRNA is not penetrating or having an effect on the joint tissues. There was, however, a highly significant overlap between miR-378a-3p targets and muscle atrophy-associated genes (obtained from Deane et al., 2021). As such, miR-378a-3p could be potentially used to target muscle atrophy. The fact that there are more than double the expected number of overlapping genes between data from the muscle

atrophy meta-analysis and validated miR-378a-3p targets also demonstrates the miRNAs critical role in muscle atrophy.

It should be noted that different methods of RNA extraction, miRNA expression measurements, and statistical methods, were not considered in this analysis. Hypothetically, the impact of these variables could be investigated systematically, for example, by performing sensitivity or meta-regression analyses. However, the current number of independent studies is too small to allow for this kind of analysis. Most of the studies used in this analysis also did not report specific p-values in relation to the miRNA dysregulation. Rather, the values were reported as "less than" a certain significance level (typically <0.05 or <0.001). In these instances, the largest possible p-value was used (i.e., if it was reported at <0.05, the p-value used in the analysis was 0.05). This conservative method may have prevented some miRNAs that were on the verge of significance from being included in the study. Although the sample size of analysis for each miRNA was increased by the me-ta-analysis method used, ultimately the quality of the analysis is only as strong as the original publications. As mentioned in the methods, quality control was conducted whereby some miRNAs and publications were filtered out based on certain criteria. However, errors or limitations of analysis in the original publications may remain. Moreover, research has suggested that there are reporting biases of differential gene expression in literature, including: preferential reporting of overexpressed rather than underexpressed genes as well as genes that are popular in the biomedical literature at large (Rodriguez-Esteban et al., 2017). As such, a critical mRNA that is investigated by only one group worldwide may not make the cut in the present analysis despite its potential importance to the disease pathogenesis. This bias is evident in the results of this study. For example, miR-140 is probably the most researched and established miRNA to date in terms of its relation to OA (Araldi et al., 2010; Miyaki et al., 2010). As its dysregulation has been very well classified, research will often include it as a positive control. This is reflected in the results of this meta-analysis, where miR-140, miR-140-3p, and miR-140-5p were all found to be significantly dysregulated. However, miR-140 has also been shown to attenuate OA progression via the inhibition of senescence in a recent study by (Si et al., 2019). This provides further support for the downregulation of the miRNA observed in this meta-analysis, as well as the association of its target genes with senescence.

A possible weakness of this study is that eligible studies often did not specify the stage of OA of the tissue donor. As many of the samples came from total joint replacements, it is assumed that a lot of the samples were from late-stage patients. Studies have shown that different stages of OA development and severity have distinct gene and miRNA expression patterns (Zhong et al., 2016). As such, the results may not adequately represent miRNA dysregulation in early-stage OA.

5.6. Conclusion

OA is a progressive and debilitating disease and the most common cause of chronic disability in adults. This study identifies 6 dysregulated miRNAs in human OA cartilage which may present as good candidates for replacement or inhibition therapy, as well as 207 differentially expressed mRNAs. Results of IPA and overlap analyses suggests a strong association between OA and senescence, corroborating the idea that the accumulation of senescent cells in cartilage contributes to the ECM degradation characteristic of OA. Further integrated assessment of our bioinformatic analyses, using mass spectrometry data, revealed 7 proteins that are significantly differentially expressed in human OA cartilage. Ultimately, this will allow for future research to focus on genes that may be of higher importance to OA pathogenesis and assess their suitability as drug targets or disease biomarkers. This is particularly important given that pain management and total joint replacement procedures are the only current treatment

Chapter 6:

General Discussion and Future Directions

Musculoskeletal tissue dysfunction is the leading cause of frailty, falls, and decreased quality of life in older people (Greco et al., 2019). Osteoarthritis (OA), the most common chronic joint disorder, was initially characterised by deterioration of the articular cartilage, though it is now considered to be a disease of the entire joint. Linked to the joint, periarticular muscles also play a major role in joint function and stability. The loss of muscle mass, strength, and function during ageing, known collectively as sarcopenia, is a major factor in the frailty of the elderly, and is a condition that is becoming increasingly prevalent as the population distribution shifts towards an older mean age (Cesari et al., 2014). Despite the high prevalence of both muscle atrophy and OA in older populations, little is known about the interaction between these two disorders, as discussed in a recent review by Shorter et al. (2019). Research has previously suggested that muscle atrophy directly affects joint stability, with loss of mobility leading to gradual degeneration of articular cartilage (Bennell et al., 2013). Conversely, it has been proposed that the disuse of an OA affected joint, due to the pain of movement, may be the primary cause of the reduction in muscle strength associated with OA (Pisters et al., 2014). Whether muscle atrophy precedes OA, or *vice versa*, changes in gene expression and epigenetic modifications are anticipated to be important contributors to the process.

The aim of this project was to characterise muscle phenotypes in OA by utilizing mechanical load-induced and spontaneous models of the disease. Moreover, to explore the role of microRNAs in their interaction, and whether a particular microRNA (-378a-3p) that we identified as being downregulated in OA-associated muscle atrophy could be used as a therapeutic agent to treat both tissues simultaneously. Finally, to use a range of bioinformatic analyses to identify genes/pathways that could be potential biomarkers or targets for OA and muscle atrophy in humans.

These results confirmed significant muscle atrophy in the peri-articular muscles subsequent to the induction of OA via non-invasive mechanical loading of the joint. Moreover, we proposed the CD1 strain of mice as a potential novel model of spontaneous OA, showing significant increase in OA severity by 6-months-old. The

OA severity in these mice also correlates with a reduction in fiber cross-sectional area – indicative of muscle atrophy. Expression analyses of the gastrocnemius and quadricep muscles in these models confirmed miR-378a-3p is downregulated in both muscle atrophy associated with spontaneous and load-induced OA. Treatment with a miR-378a-3p mimic in older mice with load-induced OA resulted in significantly less muscle atrophy in the quadriceps muscles, as well as 25% less OA severity in the loaded limb. Pathway analyses identified autophagy as the most enriched pathway in a list of validated miR-378a-3p target genes. This, together with an increase in autophagy markers in the muscles of these OA models, highlights the importance of this pathway in OA-associated muscle atrophy. Results of meta-analyses of microRNA and mRNA dysregulation in human OA identified 6 dysregulated miRNAs in human OA cartilage which may present as good candidates for replacement or inhibition therapy, as well as 207 differentially expressed mRNAs. Experimental confirmation of these bioinformatic analyses, using mass spectrometry data, revealed 7 proteins that are significantly differentially expressed in human OA cartilage. Overlap with data from a human muscle-atrophy meta-analysis also finds potential targets to treat both disorders simultaneously. Overall, this research is the first to characterise muscle atrophy in non-surgical murine models of OA and provides evidence that OA and muscle atrophy are intricately linked. Moreover, it demonstrates the potential of microRNA-based therapies for age-related musculoskeletal diseases.

6.1 Musculoskeletal System: Mice vs Humans

In this study, murine load-induced and spontaneous OA models were chosen to explore OA pathology in the various musculoskeletal tissues. Despite differences in gait and weight distribution, the murine knee joint ligaments have a similar function and anatomy to the human knee joint. Furthermore, murine spontaneous OA models offer many similarities to human OA disease pathology (Mason et al., 2001). The non-invasive mechanical loading model used in this study has benefits over other surgically induced models of OA in that it does not permanently alter the joint mechanics (in contrast to models such as destabilisation of the medial meniscus). Instead, the loading regime is controllable, adjustable, and more temporary, making the model very versatile (Poulet et al., 2011). Despite this, translating these findings into human OA

should be taken with caution. Size, weight, gait, ontogeny, immunology, and biomechanics are a few key differences between humans and mice.

A large obstacle to the translation of mouse studies to human patients is the time points used to study the disease pathogenesis *in vivo*. Many OA treatments that have shown promise in animal models produce disappointing results in humans, which is attributed to the fact that the treatments are started so late in the disease course (Bingham et al., 2006). When people seek treatment for OA, it is typically when the disease is late-stage – with the estimated median age of knee OA diagnosis being 55 years old (Losina et al., 2013). Determining the age relation between mice and humans is therefore necessary for setting up experimental murine models more analogous to humans (Dutta and Sengupta, 2016). Taking this into consideration, *in vivo* studies, especially ones that are testing drug efficacies, should utilize mice that are at least 1.5 years old. However, time constraints and the large expense of conducting long-term *in vivo* studies often prevent these older time points being investigated.

Limitations surrounding the translation of murine research to the clinic does not stop at OA – research into skeletal muscle and its associated disease also have many hurdles to overcome. For example, of specific interest to muscle repair and regeneration are satellite cells which typically exist in a quiescent state but become activated and proliferate upon injury. During this process of proliferation and differentiation into myofibers post-injury, the satellite cell recapitulates the myogenic program similar to that of muscle development in terms of the expression of myogenic regulatory factors: Myf5, MyoD, MRF4, and myogenin (Boldrin et al., 2010). The inherent challenges in identifying and isolating satellite cells, and the practical difficulties in obtaining human muscle biopsies, means that most of the research conducted on the role of satellite cells in disease and ageing has been focused on rodents, particularly mice. It has, therefore, proven hard to determine whether the phenotype and functions of satellite cells in humans and mice are equivalent. An example of where research seems to be disparate between human and mice is the fact that Pax7 has been shown to be a reliable mouse satellite cell marker (Seale et al. 2000). However, in human muscle it appears not to identify all satellite cells; in addition, it may also stain myonuclei (Reimann et al., 2004). Moreover, new data shows that satellite cells may protect

against muscle ageing in active more so than sedentary mice, something which hasn´t been explored in humans (Arpke et al., 2021).

Biomechanical differences between mice and humans may also be responsible for the different phenotype appearing in mouse models of musculoskeletal diseases. A lot of research into skeletal muscle dysfunction has been conducted in murine models of Duchenne Muscular Dystrophy (DMD), a genetic, progressive degenerative disorder of muscles. The limb muscles of these mice have a much milder phenotype, potentially owing to the differences in daily locomotion between humans and mice. For example, mouse muscles stretch less during movement than human muscles, so stretch induced damage would be minimized in the mouse model compared to patients with the disease (Moens et al., 1993). Stretch-induced muscle damage is also more severe in older animals (Brooks and Faulkner, 1996) and may have a role in the decline of muscle function seen in the elderly (Allen et al., 2005). Despite its potential detrimental effect on the muscle, the change in fiber length with locomotion – known as fiber excursion – is very hard to measure *in vivo*, due to the small size body size of the mice. Therefore, whether the relative muscle excursions of mice during daily locomotion are smaller than those of humans remains relatively unknown. To overcome this, recent research has developed a 3D musculoskeletal model of a mouse's hindlimb based on detailed anatomical measurements from microCT scanning, digital segmentation, and microdissection (Charles et al., 2016). Since then, further studies have created simulations of fiber excursions of 25 muscle homologs in humans and mice. These simulation results demonstrated biomechanical differences that could contribute to different disease states between mouse models of neuromuscular diseases and human patients. These disparities – such as limb posture and musculoskeletal stiffness - may diminish the utility of pre-clinical studies for predicting the efficacy of new therapeutic treatments for muscle atrophy in humans.

Overall, despite having many great uses for musculoskeletal research, the mouse OA models currently used, regardless of whether they are load-induced, surgically induced, or spontaneous, all have consistent problems that hinder our understanding of the disease pathogenesis. As such, it may be necessary to develop a 'gold standard' model of OA. This will make it easier to compare data between different research groups, test pre-clinical drugs, and identify biomarkers.

6.2 Sex Differences in OA

It is well known that the prevalence, incidence, and severity of OA are different in women than in men, with women being more likely to have higher incidence, and more severe, OA of the knee (Srikanth et al., 2005; Tschon et al., 2021). This discrepancy is due to both genetics and anatomy. For example, research has shown that patients heterozygous for polymorphisms in the estrogen receptor-alpha gene have significantly more radiographic OA of the knee (Bergink et al., 2003) and that transcriptionally functional estrogen receptors are present in adult articular cartilage (Richmond et al., 2000). Moreover, anatomical differences in female knee anatomy – such as a narrower femur, thinner patella, and larger quadriceps angle - may all contribute to the increased incidence of OA in women (Mary, 2007). Despite this discrepancy, experimental OA is predominantly modelled in male animals, who show a higher incidence both in spontaneous and post-traumatic OA models (Malfait and Miller, 2020). In fact, male mice are overwhelmingly used for the most common model of OA – the DMM model – even though female mice are less susceptible to OA after DMM surgery unless they have been ovarectomized (Blanchet et al., 2007). The fact that male mice have more severe OA is often why they are used, though this then presents obvious problems when translating the findings to humans, where women have more severe OA. It is also possible that sex hormones can induce behavior and activity changes in weight, activity levels, and diet, that can ultimately influence the progression of OA, rather than having direct effects on the joint tissues (Brismar et al., 2003). Interestingly, our analyses of OA and muscle meta-analyses datasets (chapter 5) show estrogen receptor pathways as being enriched, supporting the idea of sex differences in these tissues. Whatever the reasons underlying these differences, it is clear that more in-depth and mechanistic studies are required in order to discover biomarker differential expressions, molecular pathways, and transcriptomic/proteomic profiles. This will allow us to direct preclinical and clinical research towards more sex-oriented protocols and treatments.

6.3 Pain in OA

Chronic pain and discomfort are hallmarks of OA; thus, its evaluation is an integral part of understanding the disease pathogenesis as well as developing successful treatment options. Pain is the major clinical symptom in osteoarthritis of the knee and a key determinant for seeking medical care - it is also the leading cause of mobility impairment in the elderly population (Guccione et al., 1994). There are any subjective factors that contribute to a person's pain experience, such as: genetic predisposition, mood, and analgesic tolerance. This, along with an apparent discrepancy in OA pathophysiology and the onset of pain, especially in early stage OA (Hadler et al., 1994), makes its treatment a lot more complex. Several investigators have found that little correlation exists between the objective measures of OA (e.g., radiologic or pathologic changes) and the degree of chronic pain experienced by the individual. For example, people with clearly abnormal joint radiographs may have no or only mild pain whereas others with pain may not have radiographic osteoarthritis (Hannan et al., 2000). Neogi et al. (2009) attempted to investigate the relationship between pain and radiographic knee OA by utilising patients who had knees that were discordant for pain (that is, one knee had pain but the other did not) - a method that minimizes between-person confounding. This study revealed a strong dose-response relation between severity of radiographic knee osteoarthritis and knee pain. They concluded that radiographic severity and individual radiographic features, particularly joint space narrowing, is a strong risk factor for the presence, consistency, and severity of knee pain and accurately reflect the presence of painful pathology. Interestingly – a cation channel that is involved in the development of neuropathic pain (TRPV4) was found to be dysregulated in both muscle atrophy and OA meta-analyses, as well as the proteomic cartilage dataset (chapter 5).

Pain assessment in murine models of OA is often difficult to achieve. Indirect measures of pain in mice include: static or dynamic weight-bearing, foot posture, gait analysis, spontaneous movement, and mechanical/thermal/cold sensitivity (Piel et al., 2015). In the experiments in this thesis where mice were treated with a miR-378a-3p

mimic (chapter 4), gait measurement was attempted along-side grip strength. However, the level of non-compliance after loading was extreme (around 85% of the mice refused to walk at any speed). Previous research has indicated that paw area and treadmill compliance may be the most useful tools to longitudinally monitor nonpainful OA development in STR/Ort mice (Poulet et al., 2014). However, with only two mice actually complying with the regime at the end of the study, we were unable to perform any kind of statistical analysis on measures of gait, paw area, or compliance. This may be an indicator that the mice were experiencing pain in association with the OA, but this is conjecture and would require further assessment to fully deduce.

Ultimately, there is a vast number of papers investigating animal models of OA, but studies that incorporate pain as an outcome are sparse (Miller and Malfait, 2017). Testing the efficacy and mechanisms of novel analgesics will require the use of sophisticated animal models and behavioral assays. Malfait et al., (2013) reviewed the most effective ways of modelling OA pain in small animals – concluding that, in mice, reduced locomotion during forced exercise (Whitehead et al., 2012) and mechanical hypersensitivity (Ogbona et al., 2013), were the most commonly reported outcomes of pain. Future research would benefit from exploring these pain outcomes when studying OA *in vivo*. Moreover, when researching analgesics, their influence on joint structure should also be investigated.

6.4 The OARSI Grading System

It should be noted that this project primarily quantified articular cartilage lesions to determine OA severity, with some subchondral bone analysis in chapter 4. To do so, the OARSI grading system was used. This was first proposed by the Osteoarthritis Research Society International (OARSI) as a histopathology assessment system to define new standards in the assessment of OA (Pritzker et al., 2006). Each compartment within the joint must be graded individually, with a grade 0 indicating morphologically intact cartilage, and grade 6 being complete loss of articular cartilage and exposed subchondral bone. It has since been widely used in OA research, and has been an incredibly useful and simple tool for standardizing OA severity. However, its

simplicity is also a limitation, as detail and subtle differentiation between the different OARSI grades can be lost when there are only 6 grades to encompass type, depth, and extent of cartilage damage. We also know that there are many other facets to a diseased osteoarthritic joint and research has suggested that combining osteophyte/synovial grades and histomorphometry features with the OARSI cartilage lesion score gives the best overview of the disease severity and extent (Armstrong et al., 2021).

Subchondral bone analysis is also important in determining OA severity as accumulating research suggests that alterations in bone remodeling are not merely secondary manifestations, but are part of a more active component of OA. Excessive bone remodeling has been linked to cartilage degeneration and pain from early on in disease (Koh et al., 2010; Kaukinen et al., 2016), but the nature of the relationship between both tissues and how lesions progress over time remains unclear (Kwan et al., 2010). This is partly because cartilage loss frequently progresses prior to development of symptoms and partly because available tools are insensitive and do not permit early diagnosis (Das Neves Borges et al., 2017). Moreover, the majority of data on OA changes of subchondral bone is acquired from meniscectomy and anterior cruciate ligament transection models, which might be influenced by biomechanical effects (Calvo et al., 2004; Chappard et al., 2006). The experiments in chapter 4 assessed different measures of bone pathology and correlated these with OA severity, finding that trabecular separation, bone volume, and joint space mineralization are highly correlated with OA severity, and thus may be the most suitable bone pathology parameters to assess OA severity in this mechanical loading model of load-induced OA.

6.5 Methods of Analysing Muscle Atrophy

There are many ways to assess muscle quality *in vivo* or *ex vivo* when determining levels of atrophy in mouse skeletal muscles. The methods used in this thesis include: determination of fiber cross-sectional area (CSA) and Feret´s diameter, centralized myonuclei assessment, atrogene expression, and measurement of grip strength. All of these methods have associated merits and limitations. Fiber CSA analysis is a gold-standard histological approach to determining levels of muscle atrophy. This involves

sectioning the muscle and staining for sarcolemma proteins to visualise the circumference of the muscle fiber. Images of the cross-sections are then analysed with various software (ImageJ, myovision etc.). This analysis is often manual and therefore is reliant on researcher expertise and can often lead to human error and variation. As such, standardised and automated quantitative assessment of histopathological parameters is desirable to allow an objective comparison between laboratories. This is an area that research is working on with the creation of novel web-based methods of muscle analysis (Pertl et al., 2013; Stevens et al., 2020; Gilda et al., 2021). Minimum Feret´s diameter is another parameter to measure atrophy and involves calculating the closest possible distance between the two parallel tangents of the fiber. This is often a preferred measurement to fiber CSA as s it is the least affected by distortion due to oblique cross-sectioning of muscle tissue (Briguet et al., 2004).

Grip strength was used in chapter 4 of this project and is considered a valuable preclinical method to study muscle physiology in disease and aging by directly determining changes in muscle force generation *in vivo* (Munier et al., 2022). Despite this, there are limitations to its use. For example, it is often not possible to assess the limbs independently, with resulting force measurements being that of all limbs combined. This may introduce problems in experiments whereby only one limb is subject to a treatment (such as the mechanical loading used in this project). Moreover, results may be affected by: relative amount of lean/fat mass, motivation of the mice and neuromuscular/circulatory health. Therefore, a positive value observed for a treatment in this test should be confirmed by another more specific test (e.g., specific force measurements).

Fiber type analysis is another way of assessing a muscle phenotype with age or disease. This often involves staining of muscle sections using antibodies against myosin heavy chain proteins class I, IIA and IIB and appropriate secondary fluorescent antibodies (Bergmeister et al., 2017). Muscle atrophy can occur through multiple distinct signaling pathways with differential sensitivity between fiber subtypes (Wang and Pessin, 2017). As such, future research would benefit from assessing the fiber type

proportions in the mouse models used in this project to understand the specific pathways involved in the observed atrophy.

6.6 Meta-analyses use in medical research

Meta-analyses are a quantitative, formal, epidemiological studies used to systematically assess previous research. These kinds of systematic analyses are often used to obtain a broader estimate of the effect of a treatment or risk factor in different populations by pooling all relevant research into one statistical analysis. It can also help to consolidate research that has conflicting results. For example, in chapter 5, some of the studies used for the meta-analysis of genes dysregulated in OA were found to have different directions of expression in different studies. Meta-analysis can therefore be important tools to inform clinical decision making, where the results of one independent study may not be sufficiently conclusive. This is reflected in the fact that meta-analyses are the most frequently cited form of clinical research, receiving more citations than randomized trials. (Patsopoulos et al., 2005). Despite having proven value to medical research, these types of analysis have been subject to criticism in the past, mainly for poor quality and heterogeneity of included studies, and failing to address publication bias (Imrey, 2020; Esterhuizen and Thabane, 2016). These are limitations that we sought to address in this project, with many transcriptomic studies being excluded on the basis of failing the strict criteria. As such, the included studies were fairly homogenous and comparable. Publication bias is much harder to overcome, and is something that was briefly mentioned in the discussion of chapter 5. Publication bias is a well-known phenomenon where studies that showed little or no effect, or were not statistically significant, are not likely to be published and therefore do not appear in meta-analyses. Conversely, and in the case of the meta-analysis in this project, genes that are known to be important to a disease process are often included in transcriptomic studies as a kind of positive control. The effect of this publication bias was observed in the results of the meta-analysis, where classic OA genes and microRNAs were found to be significantly differentially expressed, presumably because their dysregulation was identified in many, if not all, of the

included papers. To overcome this, unpublished material should also be sourced for inclusion, though this may also be problematic in that the results would have not gone through peer review. Moreover, the effect of publication bias can be seen by conducting sensitivity analysis, though there was not enough data in this meta-analysis to conduct such as test. A strength of this study was that the results were further interrogated with proteomics data, which a lot of bioinformatics research fails to do.

Ultimately, no single piece of research will provide the definitive understanding of the influence of risk factors on a disease process. Despite the limitations outlined above, these types of bioinformatic approaches have demonstrated significant benefits in addressing the limitations of study size and can provide a more broad understanding of a disease process.

6.7 Limitations and Future Directions

Future directions of this research have been discussed throughout this thesis. One of the most important future directions is exploration of the mechanistic studies of pathways and microRNAs involved in OA-associated muscle atrophy. This project is quite exploratory, the main findings of which propose novel *in vivo* models of OA and highlight the importance of peri-articular muscle health in the protection of the joint tissues. Some microRNAs and pathways were explored – for example we found autophagy, and its regulation by miR-378a-3p, was significantly dysregulated in OA-associated muscle atrophy. It was also the most significantly enriched pathway in a list of validated miR-378a-3p target genes. Research has already investigated the role of autophagy in skeletal muscle ageing – as reviewed by Li et al. (2021) – and this research therefore provides further support for this. There was, however, a discrepancy in the expression of these atrogenes depending on the model used. In the spontaneous model of OA (the CD1 mouse strain) there was a near-significant increase in both ATROGIN-1 and MURF-1 in the quadriceps and gastroc muscles of the older mice, with ATROGIN-1 being significantly increased in the quadriceps of 6- and 8-month old mice compared to their 3- and 4-month old counterparts. This was not reflected in the model of load-induced OA in either chapter 4 or 5, where there was no change in expression in the loaded limb despite having other atrophy-associated phenotypic

markers (such as reduced fiber CSA). The CD1 mice with increased ATROGIN-1 expression were older than the load-induced OA mice used in chapter 4, and younger than those in chapter 5. This, and the fact that they are a different strain of mouse, makes it hard to make comparisons between the two models. Potentially these atrogenes may have cyclical expression with ageing which could explain the discrepancy. Alternatively, these atrogenes may be regulated by mechanoresponsive elements that were induced upon the loading regime used. There are many extenuating factors that can cause differences in gene expression, and future research should consider using matched time points and mouse strains to investigate atrogene expression in different mouse models of OA.

In this project, we looked at two key autophagy-associated miR-378a-3p target genes – P62 and NRF1 – showing their dysregulation in OA-associated muscle atrophy. Quantification of other genes (such as LC3b) was attempted in this project, but low primer efficiencies prevented their analysis. Autophagy signaling is mediated by activation of the ULK/Atg1 complex, which consists of four gene members in mammals (ULK1/2, ATG13, FIP200/RB1CC1, and ATG101) and is under tight regulation by several signaling inputs (Xia et al., 2021). Therefore, the expression of these autophagy-associated genes in *in vivo* models of spontaneous and post-traumatic OA would be beneficial for a more in depth understanding of the role of muscle autophagy in OA development.

Future studies would also benefit from looking at other joints and musculoskeletal tissues in these OA models. The hip and ankle joints would be of particular interest considering their interaction with the recus femoris muscle of the quadriceps and gastrocnemius, respectively. This may also help to explain some of the discrepancies observed in which muscles are more effected in the load-induced and spontaneous OA models. For example, in the CD1 model of spontaneous OA, the gastrocnemius - the main plantarflexor of the ankle joint - was the most impacted by age/OA. It would therefore be interesting to correlate measures of sarcopenia in the gastrocnemius with OA severity in the ankle.

Although fiber cross-sectional area and centralized myonuclei were analyzed in the peri-articular muscles in these mouse models, other parameters, such as fiber size and

type should also be explored. As mentioned before, proliferation and differentiation potentials of satellite cells are reduced with increasing age and sarcopenia development. Therefore, quantification of satellite cells, via techniques such as immunofluorescence, should also be considered. Moreover, methods of analyzing ECM composition, fibrosis an adipose infiltration should be examined in these models. Taken together, this would allow for a more comprehensive understanding of the processes driving muscle atrophy specifically in relation to OA development.

It should also be noted that the experiments looking at muscle atrophy and OA *in vivo* only quantified gene dysregulation at the mRNA level, not protein. Immunofluorescence for P62 and NRF1 was attempted, but the protocol has not yet been fully optimized, and therefore the results were not included in this thesis. Mass spectrometry analysis of the periarticular muscles of mice treated with the miR-378a-3p mimic or control microRNA was considered. However, limitations with the methodology (i.e. the inability to detect small proteins) and time constraints prevented this. Future investigations into OA-associated muscle atrophy should confirm some of the dysregulated pathways and genes identified in this project at the protein level, as well as at different time points. Moreover, localizations of said proteins could be evaluated with immunohistochemistry.

The results of *in vivo* studies into OA pathogenesis, disease mechanisms, and treatments, including those detailed in this thesis, are incredibly promising. Animal models have been used to successfully elucidate key biochemical and physiologic disease processes for decades. However, research into musculoskeletal disease and ageing ultimately needs to be confirmed in human tissues. This was addressed in chapter 5 of this project, where gene and microRNA dysregulation in human OA was investigated. As outlined above, there are many challenges involved in the translation of data from *in vivo* murine models. OA and sarcopenia are both debilitating and painful conditions that, with the exception of total joint replacement, have little to no treatment options. Therefore, going forward, clinical translation needs to be at the focus and forefront of OA research in order to provide hope for patients suffering with the diseases.

References

Abulhasan JF, Grey MJ. Anatomy and Physiology of Knee Stability. Journal of Functional Morphology and Kinesiology. 2017; 2(4):34. https://doi.org/10.3390/jfmk2040034

Aigner, T., & Schmitz, N. (2011). 173 - Pathogenesis and pathology of osteoarthritis. Rheumatology.

Alexander MS, Kawahara G, Motohashi N, Casar JC, Eisenberg I, Myers JA, Gasperini MJ, Estrella EA, Kho AT, Mitsuhashi S, Shapiro F, Kang PB, Kunkel LM. MicroRNA-199a is induced in dystrophic muscle and affects WNT signaling, cell proliferation, and myogenic differentiation. Cell Death Differ. 2013 Sep;20(9):1194-208. doi: 10.1038/cdd.2013.62. Epub 2013 Jun 14. PMID: 23764775; PMCID: PMC3741500.

Alexander, M. S., & Kunkel, L. M. (2015). Skeletal Muscle MiRNAs: Their Diagnostic and Therapeutic Potential in Human Muscle Diseases. Journal of Neuromuscular Diseases, 2(1), 1–11.

Alkatan M, Baker JR, Machin DR, Park W, Akkari AS, Pasha EP, et al. Improved function and reduced pain after swimming and cycling training in patients with osteoarthritis. J Rheumatol. 2016;43(3):666–672. doi: 10.3899/jrheum.151110.

Al-Khlaifat L, Herrington LC, Hammond A, Tyson SF, Jones RK. The effectiveness of an exercise programme on knee loading, muscle co-contraction, and pain in patients with medial knee osteoarthritis: a pilot study. Knee. 2016;23(1):63–69. doi: 10.1016/j.knee.2015.03.014.

Allen DG, Whitehead NP, Yeung EW. Mechanisms of stretch-induced muscle damage in normal and dystrophic muscle: role of ionic changes. J Physiol. 2005 Sep 15;567(Pt 3):723-35. doi: 10.1113/jphysiol.2005.091694. Epub 2005 Jul 7. PMID: 16002444; PMCID: PMC1474216.

Amirthalingam, H., Cicuttini, F. M., Wang, Y., Chou, L., Wluka, A. E., Hussain, S. Association between sarcopenia and osteoarthritis-related knee structural changes: a systematic review, Osteoarthritis and Cartilage, Volume 27, Supplement 1, 2019

Andjelkov K, Atanasijevic TC, Popovic VM, Sforza M, Atkinson CJ, Soldatovic I. Anatomical aspects of the gastrocnemius muscles: A study in 47 fresh cadavers. J Plast Reconstr Aesthet Surg. 2016 Aug;69(8):1102-8. doi: 10.1016/j.bjps.2016.04.002. Epub 2016 May 4. PMID: 27292288.

Araldi, E., & Schipani, E. (2010). MiRNA-140 and the silencing of osteoarthritis. Genes & Development, 24(11), 1075–1080. https://doi.org/10.1101/GAD.1939310

Armstrong AR, Carlson CS, Rendahl AK, Loeser RF. Optimization of histologic grading schemes in spontaneous and surgically-induced murine models of osteoarthritis. Osteoarthritis Cartilage. 2021 Apr;29(4):536-546. doi: 10.1016/j.joca.2021.01.006. Epub 2021 Feb 6. PMID: 33561541; PMCID: PMC8038967.

Arokoski MH, Arokoski JP, Haara M, Kankaanpää M, Vesterinen M, Niemitukia LH, Helminen HJ. Hip muscle strength and muscle cross sectional area in men with and without hip osteoarthritis. J Rheumatol. 2002 Oct;29(10):2185-95. PMID: 12375331.

Arpino V, Brock M, Gill SE. The role of TIMPs in regulation of extracellular matrix proteolysis. Matrix Biol. 2015 May-Jul;44-46:247-54. doi: 10.1016/j.matbio.2015.03.005. Epub 2015 Mar 21. PMID: 25805621.

Arpke, R. W., Shams, A. S., Collins, B. C., Larson, A. A., Lu, N., Lowe, D. A., & Kyba, M. (2021). Preservation of satellite cell number and regenerative potential with age reveals locomotory muscle bias. Skeletal muscle, 11(1), 22. https://doi.org/10.1186/s13395-021-00277-2

Avelar, R. A., Ortega, J. G., Tacutu, R., Tyler, E. J., Bennett, D., Binetti, P., Budovsky, A., Chatsirisupachai, K., Johnson, E., Murray, A., Shields, S., Tejada-Martinez, D., Thornton, D., Fraifeld, V. E., Bishop, C. L., & De Magalhães, J. P. (2020). A mul-tidimensional systems biology analysis of cellular senescence in aging and disease. Genome Biology, 21(1), 91.

Bader, D. L., Salter, D. M., & Chowdhury, T. T. (2011). Biomechanical influence of cartilage homeostasis in health and disease. Arthritis, 2011, 979032. https://doi.org/10.1155/2011/979032

Baltgalvis KA, Call JA, Cochrane GD, Laker RC, Yan Z, Lowe DA. Exercise training improves plantar flexor muscle function in mdx mice. Med Sci Sports Exerc. 2012 Sep;44(9):1671-9. doi: 10.1249/MSS.0b013e31825703f0. PMID: 22460476; PMCID: PMC3470762.

Bartholdy C, Juhl C, Christensen R, Lund H, Zhang W, Henriksen M. The role of muscle strengthening in exercise therapy for knee osteoarthritis: a systematic review and meta-regression analysis of randomized trials. Semin Arthritis Rheum. 2017;47(1):9–21. doi: 10.1016/j.semarthrit.2017.03.007.

Bergink AP, van Meurs JB, Loughlin J, Arp PP, Fang Y, Hofman A, van Leeuwen JP, van Duijn CM, Uitterlinden AG, Pols HA. Estrogen receptor alpha gene haplotype is associated with radiographic osteoarthritis of the knee in elderly men and women. Arthritis Rheum. 2003 Jul;48(7):1913-22. doi: 10.1002/art.11046. PMID: 12847685.

Bergmeister, K. D., Gröger, M., Aman, M., Willensdorfer, A., Manzano-Szalai, K., Salminger, S., & Aszmann, O. C. (2017). A Rapid Automated Protocol for Muscle Fiber Population Analysis in Rat Muscle Cross Sections Using Myosin Heavy Chain Immunohistochemistry. Journal of visualized experiments : JoVE, (121), 55441. https://doi.org/10.3791/55441

Bikram, M., Lee, M., Chang, C.-W., Janát-Amsbury, M.-M., Kern, S. E., & Kim, S. W. (2005). Long-circulating DNA-complexed biodegradable multiblock copolymers for gene delivery: degradation profiles and evidence of dysopsonization. Journal of Controlled Release, 103(1), 221–233.

Bingham CO, Buckland-Wright JC, Garnero P, et al. Risedronate decreases biochemical markers of cartilage degradation but does not decrease symptoms or slow radiographic progression in patients with medial compartment osteoarthritis of the knee: results of the two-year multinational knee osteoarthritis structural arthritis study. Arthritis & Rheumatism. 2006;54(11):3494–3507.

Blanchet TJ, Peluso D, Hopkins B, Morris EA, Glasson SS. Osteoarthritis severity is sex dependent in a surgical mouse model. Osteoarthritis Cartilage. 2007 Jun;15(6):695-700. doi: 10.1016/j.joca.2006.11.005. Epub 2007 Jan 3. PMID: 17207643.

Blanco-Bose, W. E. , Yao, C. C. , Kramer, R. H. , & Blau, H. M. (2001). Purification of mouse primary myoblasts based on alpha 7 integrin expression. Experimental Cell Research, 265(2), 212–220. 10.1006/excr.2001.5191

Bodine SC, Latres E, Baumhueter S, Lai VK, Nunez L, Clarke BA, Poueymirou WT, Panaro FJ, Na E, Dharmarajan K, Pan ZQ, Valenzuela DM, DeChiara TM, Stitt TN, Yancopoulos GD, Glass DJ. Identification of ubiquitin ligases required for skeletal muscle atrophy. Science. 2001 Nov 23;294(5547):1704-8. doi: 10.1126/science.1065874. Epub 2001 Oct 25. PMID: 11679633.

Boldrin L, Muntoni F, Morgan JE. Are human and mouse satellite cells really the same? J Histochem Cytochem. 2010 Nov;58(11):941-55. doi: 10.1369/jhc.2010.956201. Epub 2010 Jul 19. PMID: 20644208; PMCID: PMC2958137.

Bottinelli R, Reggiani C. Human skeletal muscle fibres: molecular and functional diversity. Prog Biophys Mol Biol. 2000;73(2-4):195-262. doi: 10.1016/s0079-6107(00)00006-7. PMID: 10958931.

Bren-Mattison, Y., Hausburg, M., & Olwin, B. B. (2011). Growth of limb muscle is dependent on skeletal-derived Indian hedgehog. Developmental biology, 356(2), 486–495. https://doi.org/10.1016/j.ydbio.2011.06.002

Briguet, A., Courdier-Fruh, I., Foster, M., Meier, T., & Magyar, J. P. (2004). Histological parameters for the quantitative assessment of muscular dystrophy in the mdx-mouse. Neuromuscular disorders : NMD, 14(10), 675–682. https://doi.org/10.1016/j.nmd.2004.06.008

Brismar BH, Lei W, Hjerpe A, Svensson O. The effect of body mass and physical activity on the development of guinea pig osteoarthrosis. Acta Orthop Scand. 2003 Aug;74(4):442-8. doi: 10.1080/00016470310017767. PMID: 14521296.

Broderick, J. A., & Zamore, P. D. (2011). MiRNA therapeutics. Gene Therapy, 18(12), 1104–1110. https://doi.org/10.1038/gt.2011.50

Brooks SV, Faulkner JA. The magnitude of the initial injury induced by stretches of maximally activated muscle fibres of mice and rats increases in old age. J Physiol. 1996;497:573–580

Brown DM, Goljanek-Whysall K. miRNAs: Modulators of the underlying pathophysiology of sarcopenia? Ageing Res Rev. 2015;24(Pt B):263–273. doi: 10.1016/j.arr.2015.08.007.

Bryk FF, Dos Reis AC, Fingerhut D, Araujo T, Schutzer M, Cury Rde P, et al. Exercises with partial vascular occlusion in patients with knee osteoarthritis: a randomized clinical trial. Knee Surg Sports Traumatol Arthrosc. 2016;24(5):1580–1586. doi: 10.1007/s00167-016-4064-7.

Burnett JC, Rossi JJ. RNA-based therapeutics: current progress and future prospects. Chem Biol. 2012 Jan 27;19(1):60-71. doi: 10.1016/j.chembiol.2011.12.008. PMID: 22284355; PMCID: PMC3269031.

Cairns DM, Lee PG, Uchimura T, Seufert CR, Kwon H, Zeng L. The role of muscle cells in regulating cartilage matrix production. J Orthop Res. 2010 Apr;28(4):529-36. doi: 10.1002/jor.21014. PMID: 19813241; PMCID: PMC2826581.

Calvo E, Palacios I, Delgado E, Sanchez-Pernaute O, Largo R, Egido J et al (2004) Histopathological correlation of cartilage swelling detected by magnetic resonance imaging in early experimental osteoarthritis. Osteoarthr Cartil 12:878–886

Camerino, C., Zayzafoon, M., Rymaszewski, M., Heiny, J., Rios, M., & Hauschka, P. V. (2012). Central depletion of brain-derived neurotrophic factor in mice results in high bone mass and metabolic phenotype. Endocrinology, 153(11), 5394–5405. https://doi.org/10.1210/en.2012-1378

Canepari M, Pellegrino MA, D'Antona G, Bottinelli R. Skeletal muscle fibre diversity and the underlying mechanisms. Acta Physiol (Oxf). 2010 Aug;199(4):465-76. doi: 10.1111/j.1748-1716.2010.02118.x. Epub 2010 Mar 24. PMID: 20345415.

Chakraborty C, Sharma AR, Sharma G, Lee SS. Therapeutic advances of miRNAs: A preclinical and clinical update. J Adv Res. 2020 Aug 29;28:127-138. doi: 10.1016/j.jare.2020.08.012. PMID: 33364050; PMCID: PMC7753224.

Chang SH, Mori D, Kobayashi H, Mori Y, Nakamoto H, Okada K, Taniguchi Y, Sugita S, Yano F, Chung UI, Kim-Kaneyama JR, Yanagita M, Economides A, Canalis E, Chen D, Tanaka S, Saito T. Excessive mechanical loading promotes osteoarthritis through the gremlin-1-NF-κB pathway. Nat Commun. 2019 Mar 29;10(1):1442. doi: 10.1038/s41467-019-09491-5. PMID: 30926814; PMCID: PMC6441020.

Chappard C, Peyrin F, Bonnassie A, Lemineur G, Brunet-Imbault B, Lespessailles E et al (2006) Subchondral bone micro-architectural alterations in osteoarthritis: a synchrotron micro-computed tomography study. Osteoarthr Cartil 14:215–223

Charles JP, Cappellari O, Spence AJ, Wells DJ, Hutchinson JR. Muscle moment arms and sensitivity analysis of a mouse hindlimb musculoskeletal model. J Anat. 2016;229:514–35.

Chen, Y., Gao, D.-Y., & Huang, L. (2015). In vivo delivery of miRNAs for cancer therapy: Challenges and strategies. Advanced Drug Delivery Reviews, 81, 128–141.

Chen, Z., Zhao, F., Liang, C., Hu, L., Li, D., Zhang, Y., Yin, C., Chen, L., Wang, L., Lin, X., Su, P., Ma, J., Yang, C., Tian, Y., Zhang, W., Li, Y., Peng, S., Chen, W., Zhang, G., & Qian, A. (2020). Silencing of miR-138-5p sensitizes bone anabolic action to mechanical stimuli. Theranostics, 10(26), 12263–12278. https://doi.org/10.7150/thno.53009

Cheng NT, Meng H, Ma LF, Zhang L, Yu HM, Wang ZZ, et al. Role of autophagy in the progression of osteoarthritis: the autophagy inhibitor, 3-methyladenine, aggravates the severity of experimental osteoarthritis. Int J Mol Med. 2017;39(5):1224–1232. doi: 10.3892/ijmm.2017.2934.

Chevalier X. Fibronectin, cartilage, and osteoarthritis. Semin Arthritis Rheum. 1993 Apr;22(5):307-18. doi: 10.1016/s0049-0172(05)80010-1. PMID: 8511595.

Childs, B. G., Durik, M., Baker, D. J., & van Deursen, J. M. (2015). Cellular senescence in aging and agerelated disease: from mechanisms to therapy. Nature Medicine, 21(12), 1424–1435.

Cho CH, Woo JS, Perez CF, Lee EH. A focus on extracellular Ca2+ entry into skeletal muscle. Exp Mol Med. 2017 Sep 15;49(9):e378. doi: 10.1038/emm.2017.208. PMID: 28912570; PMCID: PMC5628281.

Cohen S, Brault JJ, Gygi SP et al. During muscle atrophy, thick, but not thin, filament components are degraded by MuRF1-dependent ubiquitylation. J Cell Biol. 2009;185(6):1083–1095.

Conroy MB, Kwoh CK, Krishnan E, Nevitt MC, Boudreau R, Carbone LD, et al. Muscle strength, mass, and quality in older men and women with knee osteoarthritis. Arthritis Care Res. 2012;64(1):15–21. doi: 10.1002/acr.20588.

Courties A, Gualillo O, Berenbaum F, Sellam J. 2015. Metabolic stress-induced joint inflammation and osteoarthritis. Osteoarthritis Cartilage 23(11):1955–1965.

Cruz-Jentoft AJ, Bahat G, Bauer J, Boirie Y, Bruyère O, Cederholm T, Cooper C, Landi F, Rolland Y, Sayer AA, Schneider SM, Sieber CC, Topinkova E, Vandewoude M, Visser M, Zamboni M; Writing Group for the European Working Group on Sarcopenia in Older People 2 (EWGSOP2), and the Extended Group for EWGSOP2. Sarcopenia: revised European consensus on definition and diagnosis. Age Ageing. 2019 Jan 1;48(1):16-31. doi: 10.1093/ageing/afy169. Erratum in: Age Ageing. 2019 Jul 1;48(4):601. PMID: 30312372; PMCID: PMC6322506.

Das Neves Borges P, Vincent TL, Marenzana M. Automated assessment of bone changes in cross-sectional micro-CT studies of murine experimental osteoarthritis. PLoS One. 2017 Mar 23;12(3):e0174294. doi: 10.1371/journal.pone.0174294. PMID: 28334010; PMCID: PMC5363908.

Dave HD, Shook M, Varacallo M. Anatomy, Skeletal Muscle. [Updated 2021 Sep 5]. In: StatPearls [Internet]. Treasure Island (FL): StatPearls Publishing; 2022 Jan-.

Deane CS, Willis CRG, Phillips BE, Atherton PJ, Harries LW, Ames RM, Szewczyk NJ, Etheridge T. Transcriptomic meta-analysis of disuse muscle atrophy vs. resistance exercise-induced hypertrophy in young and older humans. J Cachexia Sarcopenia Muscle. 2021 Jun;12(3):629-645. doi: 10.1002/jcsm.12706. Epub 2021 May 5. PMID: 33951310; PMCID: PMC8200445.

Deleavey, G. F., & Damha, M. J. (2012). Designing Chemically Modified Oligonucleotides for Targeted Gene Silencing. Chemistry & Biology, 19(8), 937–954.

Ding, Y., Wang, L., Zhao, Q., Wu, Z., & Kong, L. (2019). MiRNA-93 inhibits chondrocyte apoptosis and inflammation in osteoarthritis by targeting the TLR4/NF-κB signaling pathway. International Journal of Molecular Medicine, 43(2), 779–790. https://doi.org/10.3892/ijmm.2018.4033

Doherty CM, Visse R, Dinakarpandian D, Strickland DK, Nagase H, Troeberg L. Engineered Tissue Inhibitor of Metalloproteinases-3 Variants Resistant to Endocytosis Have Prolonged Chondroprotective Activity. J Biol Chem. 2016 Oct 14;291(42):22160-22172. doi: 10.1074/jbc.M116.733261. Epub 2016 Aug 31. PMID: 27582494; PMCID: PMC5063997.

Dreier, R. Hypertrophic differentiation of chondrocytes in osteoarthritis: the developmental aspect of degenerative joint disorders. Arthritis Res Ther 12, 216 (2010). https://doi.org/10.1186/ar3117

Drummond MJ, McCarthy JJ, Fry CS, Esser KA, Rasmussen BB. Aging differentially affects human skeletal muscle miRNA expression at rest and after an anabolic stimulus of resistance exercise and essential amino acids. Am J Physiol Endocrinol Metab. 2008;295(6):E1333–E1340. doi: 10.1152/ajpendo.90562.2008.

Duan R, Xie H, Liu ZZ. The Role of Autophagy in Osteoarthritis. Front Cell Dev Biol. 2020 Nov 25;8:608388. doi: 10.3389/fcell.2020.608388. PMID: 33324654; PMCID: PMC7723985.

Duan, L., Liang, Y., Xu, X. et al. Recent progress on the role of miR-140 in cartilage matrix remodelling and its implications for osteoarthritis treatment. Arthritis Res Ther 22, 194 (2020). https://doi.org/10.1186/s13075-020-02290-0

Dumont, N. A. , Wang, Y. X. , & Rudnicki, M. A. (2015). Intrinsic and extrinsic mechanisms regulating satellite cell function. Development, 142(9), 1572–1581.

Dunn, W., DuRaine, G., & Reddi, A. H. (2009). Profiling microRNA expression in bovine articular cartilage and implications for mechanotransduction. Arthritis and rheumatism, 60(8), 2333–2339. https://doi.org/10.1002/art.24678

Dutta S, Sengupta P. Men and mice: Relating their ages. Life Sci. 2016 May 1;152:244-8. doi: 10.1016/j.lfs.2015.10.025. Epub 2015 Oct 24. PMID: 26596563.

Ebert, M. S., Neilson, J. R., & Sharp, P. A. (2007). MiRNA sponges: competitive inhibitors of small RNAs in mammalian cells. Nature Methods, 4(9), 721–726.

Esterhuizen TM, Thabane L. Con: Meta-analysis: some key limitations and potential solutions. Nephrol Dial Transplant. 2016 Jun;31(6):882-5. doi: 10.1093/ndt/gfw092. PMID: 27217394.

Falah M, Nierenberg G, Soudry M, Hayden M, Volpin G. Treatment of articular cartilage lesions of the knee. Int. Orthop. 2010;34:621–630. Journal of biological chemistry, 291(49), 25306–25318.

Fariyike B, Singleton Q, Hunter M, Hill WD, Isales CM, Hamrick MW, et al. Role of MiRNA-141 in the aging musculoskeletal system: a current overview. Mech Ageing Dev. 2019;178:9–15. doi: 10.1016/j.mad.2018.12.001.

Felekkis, K., Touvana, E., Stefanou, C., & Deltas, C. (2010). miRNAs: a newly described class of encoded molecules that play a role in health and disease. Hippokratia, 14(4), 236–240. Retrieved from http://www.ncbi.nlm.nih.gov/pubmed/21311629

Fisher NM, White SC, Yack HJ, Smolinski RJ, Pendergast DR. Muscle function and gait in patients with knee osteoarthritis before and after muscle rehabilitation. Disabil Rehabil. 1997;19(2):47–55. doi: 10.3109/09638289709166827.

Fox SAJ, Bedi A, Rodeo SA. The basic science of articular cartilage: structure, composition, and function. Sports Health. 2009 Nov;1(6):461-8. doi: 10.1177/1941738109350438. PMID: 23015907; PMCID: PMC3445147.

Frank, C.B., Ligament structure, physiology and function. J Musculoskelet Neuronal Interact, 2004. 4(2): p. 199-201.

Fujita N, Matsushita T, Ishida K, Kubo S, Matsumoto T, Takayama K, Kurosaka M, Kuroda R. Potential involvement of SIRT1 in the pathogenesis of osteoarthritis through the modulation of chondrocyte gene expressions. J Orthop Res. 2011 Apr;29(4):511-5. doi: 10.1002/jor.21284. Epub 2010 Oct 26. PMID: 21337390.

Gao Y, Liu S, Huang J, Guo W, Chen J, Zhang L, Zhao B, Peng J, Wang A, Wang Y, Xu W, Lu S, Yuan M, Guo Q. The ECM-cell interaction of cartilage extracellular matrix on chondrocytes. Biomed Res Int. 2014;2014:648459. doi: 10.1155/2014/648459. Epub 2014 May 18. PMID: 24959581; PMCID: PMC4052144.

Gardlík, R., Pálffy, R., Hodosy, J., Lukács, J., Turna, J., & Celec, P. (2005). Vectors and delivery systems in gene therapy. Medical Science Monitor : International Medical Journal of

Experimental and Clinical Research, 11(4), RA110-21. Retrieved from http://www.ncbi.nlm.nih.gov/pubmed/15795707

Garlich MW, Baltgalvis KA, Call JA, Dorsey LL, Lowe DA. Plantarflexion contracture in the mdx mouse. Am J Phys Med Rehabil. 2010 Dec;89(12):976-85. doi: 10.1097/PHM.0b013e3181fc7c9e. PMID: 21403594; PMCID: PMC3392333.

Gaur T, Hussain S, Mudhasani R, Parulkar I, Colby JL, Frederick D, Kream BE, van Wijnen AJ, Stein JL, Stein GS, Jones SN, Lian JB. Dicer inactivation in osteoprogenitor cells compromises fetal survival and bone formation, while excision in differentiated osteoblasts increases bone mass in the adult mouse. Dev Biol. 2010 Apr 1;340(1):10-21. doi: 10.1016/j.ydbio.2010.01.008. Epub 2010 Jan 15. PMID: 20079730; PMCID: PMC2840721.

Ge X, Cho A, Ciol MA, Pettan-Brewer C, Snyder J, Rabinovitch P, Ladiges W. Grip strength is potentially an early indicator of age-related decline in mice. Pathobiol Aging Age Relat Dis. 2016 Sep 8;6:32981. doi: 10.3402/pba.v6.32981. Erratum in: Pathobiol Aging Age Relat Dis. 2016 Oct 24;6:33718. PMID: 27613499; PMCID: PMC5018066.

Gilda, J. E., Ko, J. H., Elfassy, A. Y., Tropp, N., Parnis, A., Ayalon, B., Jhe, W., & Cohen, S. (2021). A semiautomated measurement of muscle fiber size using the Imaris software. American journal of physiology. Cell physiology, 321(3), C615–C631. https://doi.org/10.1152/ajpcell.00206.2021

Glasson SS, Chambers MG, Van Den Berg WB, Little CB. The OARSI histopathology initiative - recommendations for histological assessments of osteoarthritis in the mouse. Osteoarthritis Cartilage. 2010 Oct;18 Suppl 3:S17-23. doi: 10.1016/j.joca.2010.05.025. PMID: 20864019.

Goljanek-Whysall K, Soriano-Arroquia A, McCormick R, Chinda C, McDonagh B. miR-181a regulates p62/SQSTM1, parkin, and protein DJ-1 promoting mitochondrial dynamics in skeletal muscle aging. Aging Cell. 2020 Apr;19(4):e13140. doi: 10.1111/acel.13140. Epub 2020 Apr 15. PMID: 32291905; PMCID: PMC7189996.

Gregory, R. I., Chendrimada, T. P., Cooch, N., & Shiekhattar, R. (2005). Human RISC Couples MiRNA Biogenesis and Posttranscriptional Gene Silencing. Cell, 123(4), 631–640. https://doi.org/10.1016/J.CELL.2005.10.022

Grogan SP, Duffy SF, Pauli C, et al. Zone-specific gene expression patterns in articular cartilage. Arthritis Rheum. 2013;65(2):418-428. doi:10.1002/art.37760

Guan YJ, Yang X, Wei L, Chen Q. MiR-365: a mechanosensitive miRNA stimulates chondrocyte differentiation through targeting histone deacetylase 4. FASEB J. 2011 Dec;25(12):4457-66. doi: 10.1096/fj.11-185132. Epub 2011 Aug 19. PMID: 21856783; PMCID: PMC3236620.

Guccione AA, Felson DT, Anderson JJ, Anthony JM, Zhang Y, Wilson PW, Kelly-Hayes M, Wolf PA, Kreger BE, Kannel WB. The effects of specific medical conditions on the functional limitations of elders in the Framingham Study. Am J Public Health. 1994 Mar;84(3):351-8. doi: 10.2105/ajph.84.3.351. PMID: 8129049; PMCID: PMC1614827.

Guilak, F., Nims, R. J., Dicks, A., Wu, C. L. & Meulenbelt, I. Osteoarthritis as a disease of the cartilage pericellular matrix. Matrix Biol 71-72, 40–50 (2018).

Guo D, Tan W, Wang F, Lv Z, Hu J, Lv T, Chen Q, Gu X, Wan B, Zhang Z. Proteomic analysis of human articular cartilage: identification of differentially expressed proteins in knee osteoarthritis. Joint Bone Spine. 2008 Jul;75(4):439-44. doi: 10.1016/j.jbspin.2007.12.003. Epub 2008 May 12. PMID: 18468937.7. Alexander, M. S., & Kunkel, L. M. (2015). Skeletal Muscle MiRNAs: Their Diagnostic and Therapeutic Potential in Human Muscle Diseases. Journal of Neuromuscular Diseases, 2(1), 1–11. https://doi.org/10.3233/JND-140058

Guo Y, Wang Y, Liu Y, Liu Y, Zeng Q, Zhao Y, Zhang X, Zhang X. MiRNA-218, miRNA-191*, miRNA-3070a and miRNA-33 are responsive to mechanical strain exerted on osteoblastic cells. Mol Med Rep. 2015 Aug;12(2):3033-8. doi: 10.3892/mmr.2015.3705. Epub 2015 Apr 30. PMID: 25937096.

Gupta RC, Lall R, Srivastava A, Sinha A. Hyaluronic Acid: Molecular Mechanisms and Therapeutic Trajectory. Front Vet Sci. 2019;6:192. Published 2019 Jun 25. doi:10.3389/fvets.2019.00192

Haag J, Gebhard PM, Aigner T. SOX gene expression in human osteoarthritic cartilage. Pathobiology. 2008;75(3):195-199. doi:10.1159/000124980

Hadler NM. Knee pain is the malady—not osteoarthritis. Ann Intern Med1992;116:598-9.

Han SK, Wouters W, Clark A, Herzog W. Mechanically induced calcium signaling in chondrocytes in situ. J Orthop Res. 2012 Mar;30(3):475-81. doi: 10.1002/jor.21536. Epub 2011 Aug 22. PMID: 21882238.

Hannan MT, Felson DT, Pincus T. Analysis of the discordance between radiographic changes and knee pain in osteoarthritis of the knee. J Rheumatol. 2000 Jun;27(6):1513-7. PMID: 10852280.

He Z, Nie P, Lu J, Ling Y, Guo J, Zhang B, Hu J, Liao J, Gu J, Dai B, Feng Z. Less mechanical loading attenuates osteoarthritis by reducing cartilage degeneration, subchondral bone remodelling, secondary inflammation, and activation of NLRP3 inflammasome. Bone Joint Res. 2020 Oct;9(10):731-741. doi: 10.1302/2046-3758.910.BJR-2019-0368.R2. PMID: 33399476; PMCID: PMC7640939.

Heijink, A., Gomoll, A. H., Madry, H., Drobnič, M., Filardo, G., Espregueira-Mendes, J., & Van Dijk, C. N. (2012). Biomechanical considerations in the pathogenesis of osteoarthritis of the knee. Knee Surgery, Sports Traumatology, Arthroscopy, 20(3), 423–435.

Hermann, W., Lambova, S., & Müller- Ladner, U. (2018). Current Treatment Options for Osteoarthritis. Current Rheumatology Reviews, 14(2), 108–116.

Hernández-Hernández, J. M., García-González, E. G., Brun, C. E., & Rudnicki, M. A. (2017). The myogenic regulatory factors, determinants of muscle development, cell identity and regeneration. Seminars in cell & developmental biology, 72, 10–18. https://doi.org/10.1016/j.semcdb.2017.11.010

Hill C, James RS, Cox VM, Seebacher F, Tallis J. Age-related changes in isolated mouse skeletal muscle function are dependent on sex, muscle, and contractility mode. Am J Physiol Regul Integr Comp Physiol. 2020 Sep 1;319(3):R296-R314. doi: 10.1152/ajpregu.00073.2020. Epub 2020 Jul 22. PMID: 32697655.

Hirschmann, M.; Müller, W. Complex function of the knee joint: The current understanding of the knee. Knee Surg. Sports Traumatol. Arthrosc. 2015, 23, 2780–2788.

Hong, B.-K., You, S., Yoo, S.-A., Park, D., Hwang, D., Cho, C.-S., & Kim, W.-U. (2017). MiRNA-143 and -145 modulate the phenotype of synovial fibroblasts in rheumatoid arthritis. Experimental & Molecular Medicine, 49(8), e363.

Horak, M., Novak, J., & Bienertova-Vasku, J. (2016). Muscle-specific miRNAs in skeletal muscle development. Developmental Biology, 410(1), 1–13.

House, L., Bou-Gharios, G., Peffers, M., Clegg, P. D., Young, D. A., Whysall, K. A. (2016). The role of microRNAs in osteoarthritis and ageing-related functional decline in joint tissue homeostasis. Osteoarthritis and Cartilage, doi.org/10.1016/j.joca.2016.01.141

Huang HY, Lin YC, Cui S, Huang Y, Tang Y, Xu J, Bao J, Li Y, Wen J, Zuo H, Wang W, Li J, Ni J, Ruan Y, Li L, Chen Y, Xie Y, Zhu Z, Cai X, Chen X, Yao L, Chen Y, Luo Y, LuXu S, Luo M, Chiu CM, Ma K, Zhu L, Cheng GJ, Bai C, Chiang YC, Wang L, Wei F, Lee TY, Huang HD. miRTarBase update 2022: an informative resource for experimentally validated miRNA-target interactions. Nucleic Acids Res. 2022 Jan 7;50(D1):D222-D230. doi: 10.1093/nar/gkab1079. PMID: 34850920; PMCID: PMC8728135.

Hussain, N., Zhu, W., Jiang, C., Xu, J., Wu, X., Geng, M., … Lu, S. (2018). Down-regulation of miR-10a-5p in synoviocytes contributes to TBX5-controlled joint inflammation. Journal of Cellular and Molecular Medicine, 22(1), 241–250. https://doi.org/10.1111/jcmm.13312

Hwang HS, Park SJ, Cheon EJ, Lee MH, Kim HA. Fibronectin fragment-induced expression of matrix metalloproteinases is mediated by MyD88-dependent TLR-2 signaling pathway in human chondrocytes. Arthritis Res Ther. 2015 Nov 12;17:320. doi: 10.1186/s13075-015-0833-9. PMID: 26563875; PMCID: PMC4643537.

Ikeda S, Tsumura H, Torisu T. Age-related quadriceps-dominant muscle atrophy and incident radiographic knee osteoarthritis. J Orthop Sci. 2005;10(2):121-6. doi: 10.1007/s00776-004-0876-2. PMID: 15815857.

Imrey PB. Limitations of Meta-analyses of Studies With High Heterogeneity. JAMA Netw Open. 2020 Jan 3;3(1):e1919325. doi: 10.1001/jamanetworkopen.2019.19325. PMID: 31922554.

Isaac C, Wright A, Usas A, Li H, Tang Y, Mu X, et al. Dystrophin and utrophin "double knockout" dystrophic mice exhibit a spectrum of degenerative musculoskeletal abnormalities. J Orthop Res. 2013;31(3):343–349. doi: 10.1002/jor.22236.

Isaacson J, Brotto M. Physiology of Mechanotransduction: How Do Muscle and Bone "Talk" to One Another? Clinical Reviews in Bone and Mineral Metabolism. 2014 Jun;12(2):77-85. DOI: 10.1007/s12018-013-9152-3. PMID: 25838800; PMCID: PMC4380142.

Jeon, O., Kim, C., Laberge, R. et al. Local clearance of senescent cells attenuates the development of post-traumatic osteoar-thritis and creates a pro-regenerative environment. Nat Med 23, 775–781 (2017). https://doi.org/10.1038/nm.4324

Jin W, Peng J, Jiang S. The epigenetic regulation of embryonic myogenesis and adult muscle regeneration by histone methylation modification. Biochem Biophys Rep. 2016 Apr 20;6:209-219. doi: 10.1016/j.bbrep.2016.04.009. PMID: 28955879; PMCID: PMC5600456.

Jiwlawat, N., Lynch, E., Jeffrey, J., Van Dyke, J. M., & Suzuki, M. (2018). Current Progress and Challenges for Skeletal Muscle Differentiation from Human Pluripotent Stem Cells Using Transgene-Free Approaches. Stem cells international, 2018, 6241681. https://doi.org/10.1155/2018/6241681

Jo MH, Shin S, Jung SR, Kim E, Song JJ, Hohng S. Human Argonaute 2 Has Diverse Reaction Pathways on Target RNAs. Mol Cell. 2015 Jul 2;59(1):117-24. doi: 10.1016/j.molcel.2015.04.027. PMID: 26140367.

Johnson, V. L., & Hunter, D. J. (2014). The epidemiology of osteoarthritis. Best Practice & Research Clinical Rheumatology, 28(1), 5–15. https://doi.org/10.1016/j.berh.2014.01.004

Jonas S, Izaurralde E. Towards a molecular understanding of microRNA-mediated gene silencing. Nat Rev Genet. 2015 Jul;16(7):421-33. doi: 10.1038/nrg3965. Epub 2015 Jun 16. PMID: 26077373.

Jones SW, Watkins G, Le Good N, Roberts S, Murphy CL, Brockbank SM, Needham MR, Read SJ, Newham P. The identification of differentially expressed microRNA in osteoarthritic tissue that modulate the production of TNF-alpha and MMP13. Osteoarthritis Cartilage. 2009 Apr;17(4):464-72. doi: 10.1016/j.joca.2008.09.012. Epub 2008 Oct 11. PMID: 19008124.

Ju JS, Varadhachary AS, Miller SE, Weihl CC. Quantitation of "autophagic flux" in mature skeletal muscle. Autophagy. 2010 Oct;6(7):929-35. doi: 10.4161/auto.6.7.12785. Epub 2010 Oct 24. PMID: 20657169; PMCID: PMC3039739.

Ju, J. S., Varadhachary, A. S., Miller, S. E., & Weihl, C. C. (2010). Quantitation of "autophagic flux" in mature skeletal muscle. Autophagy, 6(7), 929–935. https://doi.org/10.4161/auto.6.7.12785

Judex S, Rubin CT. Is bone formation induced by high-frequency mechanical signals modulated by muscle activity? J Musculoskelet Neuronal Interact. 2010 Mar;10(1):3-11. PMID: 20190375; PMCID: PMC2919567.

Jung HJ, Lee KP, Milholland B, Shin YJ, Kang JS, Kwon KS, Suh Y. Comprehensive miRNA Profiling of Skeletal Muscle and Serum in Induced and Normal Mouse Muscle Atrophy During Aging. J Gerontol A Biol Sci Med Sci. 2017 Oct 12;72(11):1483-1491. doi: 10.1093/gerona/glx025. PMID: 28329037; PMCID: PMC5861915.

Kahn J, Shwartz Y, Blitz E, Krief S, Sharir A, Breitel DA, et al. Muscle contraction is necessary to maintain joint progenitor cell fate. Dev Cell. 2009;16(5):734–743. doi: 10.1016/j.devcel.2009.04.013

Kanakis I, Alameddine M, Folkes L, Moxon S, Myrtziou I, Ozanne SE, Peffers MJ, Goljanek-Whysall K, Vasilaki A. Small-RNA Sequencing Reveals Altered Skeletal Muscle miRNAs and snoRNAs Signatures in Weanling Male Offspring from Mouse Dams Fed a Low Protein Diet during Lactation. Cells. 2021 May 11;10(5):1166. doi: 10.3390/cells10051166. PMID: 34064819; PMCID: PMC8150574.

Kapoor, M., Martel-Pelletier, J., Lajeunesse, D., Pelletier, J.-P., & Fahmi, H. (2011). Role of proinflammatory cytokines in the pathophysiology of osteoarthritis. Nature Reviews Rheumatology, 7(1), 33–42.

Kaukinen P, Podlipská J, Guermazi A, Niinimäki J, Lehenkari P, Roemer FW, Nieminen MT, Koski JM, Arokoski JP, Saarakkala S. Associations between MRI-defined structural pathology and generalized and localized knee pain - the Oulu Knee Osteoarthritis study. Osteoarthritis Cartilage. 2016 Sep;24(9):1565-76. doi: 10.1016/j.joca.2016.05.001. Epub 2016 May 10. PMID: 27174007.

Keenan CM, Ramos-Mucci L, Kanakis I, Milner PI, Leask A, Abraham D, Bou-Gharios G, Poulet B. Post-traumatic osteoarthritis development is not modified by postnatal chondrocyte deletion of Ccn2. Dis Model Mech. 2020 Jul 14;13(7):dmm044719. doi: 10.1242/dmm.044719. PMID: 32616521; PMCID: PMC7375478.

Kim HJ, Hong YH. Age-related low skeletal muscle mass correlates with joint space narrowing in knee osteoarthritis in a South Korean population: a cross-sectional, case-control study. J Yeungnam Med Sci. 2022 Feb 3. doi: 10.12701/jyms.2021.01536. Epub ahead of print. PMID: 35108762.

Kim KM, Jang HC, Lim S. Differences among skeletal muscle mass indices derived from height-, weight-, and body mass index-adjusted models in assessing sarcopenia. Korean J Intern Med. 2016 Jul;31(4):643-50. doi: 10.3904/kjim.2016.015. Epub 2016 Jun 22. PMID: 27334763; PMCID: PMC4939509.

Kim, V. N., Han, J., & Siomi, M. C. (2009). Biogenesis of small RNAs in animals. Nature Reviews Molecular Cell Biology, 10(2), 126–139. https://doi.org/10.1038/nrm2632

Kitajima Y, Yoshioka K, Suzuki N. The ubiquitin-proteasome system in regulation of the skeletal muscle homeostasis and atrophy: from basic science to disorders. J Physiol Sci. 2020 Sep 16;70(1):40. doi: 10.1186/s12576-020-00768-9. PMID: 32938372.

Klionsky DJ. Autophagy: from phenomenology to molecular understanding in less than a decade. Nat Rev Mol Cell Biol. 2007 Nov;8(11):931-7. doi: 10.1038/nrm2245. PMID: 17712358.

Ko, J.-Y., Lee, M. S., Lian, W.-S., Weng, W.-T., Sun, Y.-C., Chen, Y.-S., & Wang, F.-S. (2017). MiRNA-29a Counteracts Synovitis in Knee Osteoarthritis Pathogenesis by Targeting VEGF. Scientific Reports, 7(1), 3584. https://doi.org/10.1038/s41598-017-03616-w

Koh, Y.H., Hong, S.H., Kang, H.S. et al. The effects of bone turnover rate on subchondral trabecular bone structure and cartilage damage in the osteoarthritis rat model. Rheumatol Int 30, 1165–1171 (2010). https://doi.org/10.1007/s00296-009-1118-x

Kozomara A, Birgaoanu M, Griffiths-Jones S. miRBase: from miRNA sequences to function. Nucleic Acids Res. 2019 Jan 8;47(D1):D155-D162. doi: 10.1093/nar/gky1141. PMID: 30423142; PMCID: PMC6323917.

Krishnasamy P, Hall M, Robbins SR. The role of skeletal muscle in the pathophysiology and management of knee osteoarthritis. Rheumatology. 2018;57(suppl_4):iv124. doi: 10.1093/rheumatology/key039.

Krützfeldt, J., Rajewsky, N., Braich, R., Rajeev, K. G., Tuschl, T., Manoharan, M., & Stoffel, M. (2005). Silencing of miRNAs in vivo with ‘antagomirs.’ Nature, 438(7068), 685–689. https://doi.org/10.1038/nature04303

Kuo, S.-J., Yang, W.-H., Liu, S.-C., Tsai, C.-H., Hsu, H.-C., & Tang, C.-H. (2017). Transforming growth factor β1 enhances heme oxygenase 1 expression in human synovial fibroblasts by inhibiting miRNA 519b synthesis. PloS One, 12(4), e0176052.

Kwan Tat S, Lajeunesse D, Pelletier JP, Martel-Pelletier J. Targeting subchondral bone for treating osteoarthritis: what is the evidence? Best Pract Res Clin Rheumatol. 2010 Feb;24(1):51-70. doi: 10.1016/j.berh.2009.08.004. PMID: 20129200; PMCID: PMC5250505.

Lam, J. K. W., Chow, M. Y. T., Zhang, Y., & Leung, S. W. S. (2015). siRNA Versus miRNA as Therapeutics for Gene Silencing. Molecular Therapy. Nucleic Acids, 4(9), e252. https://doi.org/10.1038/mtna.2015.23

Lamon S, Zacharewicz E, Butchart LC, Orellana L, Mikovic J, Grounds MD, Russell AP. MicroRNA expression patterns in post-natal mouse skeletal muscle development. BMC Genomics. 2017 Jan 7;18(1):52. doi: 10.1186/s12864-016-3399-2. PMID: 28061746; PMCID: PMC5219731.

Larsson L, Degens H, Li M, Salviati L, Lee YI, Thompson W, et al. Sarcopenia: aging-related loss of muscle mass and function. Physiol Rev. 2019;99(1):427–511. doi: 10.1152/physrev.00061.2017.

Laurentino G., Ugrinowitsch C., Aihara A., Fernandes A., Parcell A., Ricard M., Tricoli V. Effects of Strength Training and Vascular Occlusion. International Journal of Sports Medicine. 2008;29(08):664–667. doi: 10.1055/s-2007-989405.

Le, L., Swingler, T. E., Crowe, N., Driscoll, C., Vincent, T. L., Barter, M. J., … Clark, I. M. (2014). The miRNA-29 family in osteoarthritis. Osteoarthritis and Cartilage, 22, S41–S42.

Lee SY, Ro HJ, Chung SG, Kang SH, Seo KM, Kim DK. Low skeletal muscle mass in the lower limbs is independently associated to knee osteoarthritis. PLoS One. 2016;11(11):e0166385. doi: 10.1371/journal.pone.0166385.

Lefebvre V, Dvir-Ginzberg M. SOX9 and the many facets of its regulation in the chondrocyte lineage. Connect Tissue Res. 2017 Jan;58(1):2-14. doi: 10.1080/03008207.2016.1183667. Epub 2016 Apr 29. PMID: 27128146; PMCID: PMC5287363.

Levinger I, Levinger P, Trenerry MK, Feller JA, Bartlett JR, Bergman N, McKenna MJ, Cameron-Smith D. Increased inflammatory cytokine expression in the vastus lateralis of patients with knee osteoarthritis. Arthritis Rheum. 2011 May;63(5):1343-8. doi: 10.1002/art.30287. PMID: 21538317.

Li C, Zheng Z. Identification of Novel Targets of Knee Osteoarthritis Shared by Cartilage and Synovial Tissue. Int J Mol Sci. 2020;21(17):6033. Published 2020 Aug 22. doi:10.3390/ijms21176033

Li P, Ma Y, Yu C, Wu S, Wang K, Yi H, Liang W. Autophagy and Aging: Roles in Skeletal Muscle, Eye, Brain and Hepatic Tissue. Front Cell Dev Biol. 2021 Oct 28;9:752962. doi: 10.3389/fcell.2021.752962. PMID: 34778264; PMCID: PMC8581214.

Li Y, Jiang J, Liu W, Wang H, Zhao L, Liu S, et al. miRNA-378 promotes autophagy and inhibits apoptosis in skeletal muscle. Proc Natl Acad Sci U S A. 2018;115(46):E10849–E10E58. doi: 10.1073/pnas.1803377115.

Li YH, Tavallaee G, Tokar T, Nakamura A, Sundararajan K, Weston A, et al. Identification of synovial fluid miRNA signature in knee osteoarthritis: differentiating early- and late-stage knee osteoarthritis. Osteoarthritis Cartilage. 2016;24(9):1577–1586. doi: 10.1016/j.joca.2016.04.019.

Li, J., Huang, J., Dai, L., Yu, D., Chen, Q., Zhang, X., & Dai, K. (2012). miR-146a, an IL-1β responsive miRNA, induces vascular endothelial growth factor and chondrocyte apoptosis by targeting Smad4. Arthritis Research & Therapy, 14(2), R75. https://doi.org/10.1186/ar3798

Li, Y.-H., Tavallaee, G., Tokar, T., Nakamura, A., Sundararajan, K., Weston, A., … Kapoor, M. (2016). Identification of synovial fluid miRNA signature in knee osteoarthritis: differentiating early- and late-stage knee osteoarthritis. Osteoarthritis and Cartilage, 24(9), 1577–1586.

Liang, X., Liu, L., Fu, T., Zhou, Q., Zhou, D., Xiao, L., Liu, J., Kong, Y., Xie, H., Yi, F., Lai, L., Vega, R. B., Kelly, D. P., Smith, S. R., & Gan, Z. (2016). Exercise Inducible Lactate Dehydrogenase B Regulates Mitochondrial Function in Skeletal Muscle.

Lin EA, Kong L, Bai XH, Luan Y, Liu CJ. miR-199a, a bone morphogenic protein 2-responsive MiRNA, regulates chondrogenesis via direct targeting to Smad1. J Biol Chem. 2009 Apr 24;284(17):11326-35. doi: 10.1074/jbc.M807709200. Epub 2009 Feb 27. PMID: 19251704; PMCID: PMC2670138.

Liu WJ, Ye L, Huang WF, Guo LJ, Xu ZG, Wu HL, Yang C, Liu HF. p62 links the autophagy pathway and the ubiqutin-proteasome system upon ubiquitinated protein degradation. Cell Mol Biol Lett. 2016 Dec 13;21:29. doi: 10.1186/s11658-016-0031-z. PMID: 28536631; PMCID: PMC5415757.

Livak KJ, Schmittgen TD. Analysis of relative gene expression data using real-time quantitative PCR and the 2(-Delta Delta C(T)) Method. Methods. 2001 Dec;25(4):402-8. doi: 10.1006/meth.2001.1262. PMID: 11846609.

Loeser, R. F., Goldring, S. R., Scanzello, C. R., & Goldring, M. B. (2012). Osteoarthritis: a disease of the joint as an organ. Arthritis and Rheumatism, 64(6), 1697–1707.

Losina E, Weinstein AM, Reichmann WM, Burbine SA, Solomon DH, Daigle ME, Rome BN, Chen SP, Hunter DJ, Suter LG, Jordan JM, Katz JN. Lifetime risk and age at diagnosis of symptomatic knee osteoarthritis in the US. Arthritis Care Res (Hoboken). 2013 May;65(5):703-11. doi: 10.1002/acr.21898. PMID: 23203864; PMCID: PMC3886119.

Lu H, Yang Y, Ou S, Qi Y, Li G, He H, Lu F, Li W, Sun H. The silencing of miR-199a-5p protects the articular cartilage through MAPK4 in osteoarthritis. Ann Transl Med. 2022 May;10(10):601. doi: 10.21037/atm-22-2057. PMID: 35722355; PMCID: PMC9201181.

Lu: G. S., & Mologhianu, G. (2014). Osteoarthritis pathogenesis - a complex process that involves the entire joint. Journal of Medicine and Life, 7(1), 37–41

Mackie, E. J., Tatarczuch, L. & Mirams, M. The skeleton: a multi-functional complex organ: the growth plate chondrocyte and endochondral ossification. J. Endocrinol. 211, 109–121 (2011).

Maeda, Y., Farina, N. H., Matzelle, M. M., Fanning, P. J., Lian, J. B., & Gravallese, E. M. (2017). Synovium-Derived MiRNAs Regulate Bone Pathways in Rheumatoid Arthritis. Journal of Bone and Mineral Research : The Official Journal of the American Society for Bone and Mineral Research, 32(3), 461–472. https://doi.org/10.1002/jbmr.3005

Maldonado M, Nam J. The role of changes in extracellular matrix of cartilage in the presence of inflammation on the pathology of osteoarthritis. Biomed Res Int. 2013;2013:284873. doi:10.1155/2013/284873

Malemud C. J. (2018). MiRNAs and Osteoarthritis. Cells, 7(8), 92. https://doi.org/10.3390/cells7080092

Malfait AM, Miller RE. Why we should study osteoarthritis pain in experimental models in both sexes. Osteoarthritis Cartilage. 2020 Apr;28(4):397-399. doi: 10.1016/j.joca.2019.12.008. Epub 2020 Jan 9. PMID: 31926266; PMCID: PMC7108964.

Man, G. S., & Mologhianu, G. (2014). Osteoarthritis pathogenesis - a complex process that involves the entire joint. Journal of Medicine and Life, 7(1), 37–41.

Mandillo S, Tucci V, Hölter SM, Meziane H, Banchaabouchi MA, Kallnik M, Lad HV, Nolan PM, Ouagazzal AM, Coghill EL, Gale K, Golini E, Jacquot S, Krezel W, Parker A, Riet F,

Martin, J. A., & Buckwalter, J. A. (2001). Telomere erosion and senescence in human articular cartilage chondrocytes. Journals of Gerontology - Series A Biological Sciences and Medical Sciences, 56(4). https://doi.org/10.1093/gerona/56.4.B172

Marzetti E, Lees HA, Wohlgemuth SE, Leeuwenburgh C. Sarcopenia of aging: underlying cellular mechanisms and protection by calorie restriction. Biofactors. 2009 Jan-Feb;35(1):28-35. doi: 10.1002/biof.5. PMID: 19319843; PMCID: PMC5992495.

Mason, R.M., et al., The STR/ort mouse and its use as a model of osteoarthritis. Osteoarthritis and Cartilage, 2001. 9(2): p. 85-91

Maurer B, Stanczyk J, Jüngel A, Akhmetshina A, Trenkmann M, Brock M, Kowal-Bielecka O, Gay RE, Michel BA, Distler JH, Gay S, Distler O. MicroRNA-29, a key regulator of collagen expression in systemic sclerosis. Arthritis Rheum. 2010 Jun;62(6):1733-43. doi: 10.1002/art.27443. PMID: 20201077.

McCulloch K, Litherland GJ, Rai TS. Cellular senescence in osteoarthritis pathology. Aging Cell. 2017 Apr;16(2):210-218. doi: 10.1111/acel.12562. Epub 2017 Jan 26. PMID: 28124466; PMCID: PMC5334539.

McGeary SE, Lin KS, Shi CY, Pham TM, Bisaria N, Kelley GM, Bartel DP. The biochemical basis of miRNA targeting effi-cacy. Science. 2019 Dec 20;366(6472):eaav1741. doi: 10.1126/science.aav1741. Epub 2019 Dec 5. PMID: 31806698; PMCID: PMC7051167.

Melendez-Zajgla J, Del Pozo L, Ceballos G, Maldonado V. Tissue inhibitor of metalloproteinases-4. The road less traveled. Mol Cancer. 2008 Nov 21;7:85. doi: 10.1186/1476-4598-7-85. PMID: 19025595; PMCID: PMC2599898.

Messner, K. and J. Gao, The menisci of the knee joint. Anatomical and functional characteristics, and a rationale for clinical treatment. J Anat, 1998. 193 (Pt 2): p. 161-78.

Miao, G., Zang, X., Hou, H., Sun, H., Wang, L., Zhang, T., … Zha, Z. (2019). Bax Targeted by miR-29a Regulates Chondrocyte Apoptosis in Osteoarthritis. BioMed Research International, 2019, 1–9. https://doi.org/10.1155/2019/1434538

Milan, G., Romanello, V., Pescatore, F. et al. Regulation of autophagy and the ubiquitin–proteasome system by the FoxO transcriptional network during muscle atrophy. Nat Commun 6, 6670 (2015).

Miller RE, Malfait AM. Osteoarthritis pain: What are we learning from animal models? Best Pract Res Clin Rheumatol. 2017 Oct;31(5):676-687. doi: 10.1016/j.berh.2018.03.003. Epub 2018 Apr 26. PMID: 30509413; PMCID: PMC6284232.

Misra D, Fielding RA, Felson DT, Niu J, Brown C, Nevitt M, et al. Risk of knee osteoarthritis with obesity, sarcopenic obesity, and sarcopenia. Arthritis Rheum. 2019;71(2):232–237. doi: 10.1002/art.40692.

Miyaki, S., Sato, T., Inoue, A., Otsuki, S., Ito, Y., Yokoyama, S., … Asahara, H. (2010). MiRNA-140 plays dual roles in both cartilage development and homeostasis. Genes & Development, 24(11), 1173–1185. https://doi.org/10.1101/gad.1915510

Moens P, Baatsen P, Maréchal G. Increased susceptibility of EDL muscles from mdx mice to damage induced by contractions with stretch. J Muscle Res Cell Motil. 1993;14:446–51.

Molina T, Fabre P, Dumont NA. Fibro-adipogenic progenitors in skeletal muscle homeostasis, regeneration and diseases. Open Biol. 2021 Dec;11(12):210110. doi: 10.1098/rsob.210110. Epub 2021 Dec 8. PMID: 34875199; PMCID: PMC8651418.

Moreno, P. M. D., & Pêgo, A. P. (2014). Therapeutic antisense oligonucleotides against cancer: hurdling to the clinic. Frontiers in Chemistry, 2, 87. https://doi.org/10.3389/fchem.2014.00087

Mukund K, Subramaniam S. Skeletal muscle: A review of molecular structure and function, in health and disease. Wiley Interdiscip Rev Syst Biol Med. 2020 Jan;12(1):e1462. doi: 10.1002/wsbm.1462. Epub 2019 Aug 13. PMID: 31407867; PMCID: PMC6916202.

Munier, J. J., Pank, J. T., Severino, A., Wang, H., Zhang, P., Vergnes, L., & Reue, K. (2022). Simultaneous monitoring of mouse grip strength, force profile, and cumulative force profile distinguishes muscle physiology following surgical, pharmacologic and diet interventions. Scientific reports, 12(1), 16428. https://doi.org/10.1038/s41598-022-20665-y

Narici MV, Maffulli N. Sarcopenia: characteristics, mechanisms and functional significance. Br Med Bull. 2010;95:139–159. doi: 10.1093/bmb/ldq008.

Noehren B, Kosmac K, Walton RG, Murach KA, Lyles MF, Loeser RF, Peterson CA, Messier SP. Alterations in quadriceps muscle cellular and molecular properties in adults with moderate knee osteoarthritis. Osteoarthritis Cartilage. 2018 Oct;26(10):1359-1368. doi: 10.1016/j.joca.2018.05.011. Epub 2018 May 23. PMID: 29800621; PMCID: PMC7050996.

Nogimori T, Furutachi K, Ogami K, Hosoda N, Hoshino SI. A novel method for stabilizing microRNA mimics. Biochem Biophys Res Commun. 2019 Apr 2;511(2):422-426. doi: 10.1016/j.bbrc.2019.02.075. Epub 2019 Feb 21. PMID: 30799083.

Noyes FR, Cummings JF, Grood ES, Walz-Hasselfeld KA, Wroble RR (1991) The diagnosis of knee motion limits, subluxations, and ligament injury. Am J Sports Med 19:163–171

O'Reilly SC, Jones A, Muir KR, Doherty M. Quadriceps weakness in knee osteoarthritis: the effect on pain and disability. Ann Rheum Dis. 1998;57(10):588–594. doi: 10.1136/ard.57.10.588.

Obayashi, T., & Kinoshita, K. (2009). Rank of correlation coefficient as a comparable measure for biological significance of gene coexpression. DNA Research, 16(5), 249–260. https://doi.org/10.1093/dnares/dsp016

O'Brien J, Hayder H, Zayed Y, Peng C. Overview of MicroRNA Biogenesis, Mechanisms of Actions, and Circulation. Front Endocrinol (Lausanne). 2018 Aug 3;9:402. doi: 10.3389/fendo.2018.00402. PMID: 30123182; PMCID: PMC6085463.

O'Brien J, Hayder H, Zayed Y, Peng C. Overview of MiRNA Biogenesis, Mechanisms of Actions, and Circulation. Front Endocrinol (Lausanne). 2018 Aug 3;9:402. doi: 10.3389/fendo.2018.00402. PMID: 30123182; PMCID: PMC6085463.

Ohlendieck K. Proteomic Profiling of Fast-To-Slow Muscle Transitions during Aging. Front Physiol. 2011 Dec 26;2:105. doi: 10.3389/fphys.2011.00105. PMID: 22207852; PMCID: PMC3245893.

Okada Y: Proteinase and matrix degradation. In Kelly's Textbook of Rheumatology. Edited by: Ruddy S, Harris ED Jr, Sledge CB. 2001, Philadelphia: WB Saunders Company, 55-72.

Okugawa Y, Toiyama Y, Hur K, Yamamoto A, Yin C, Ide S, Kitajima T, Fujikawa H, Yasuda H, Koike Y, Okita Y, Hiro J, Yoshiyama S, Araki T, Miki C, McMillan DC, Goel A, Kusunoki M. Circulating miR-203 derived from metastatic tissues promotes myopenia in colorectal cancer patients. J Cachexia Sarcopenia Muscle. 2019 Jun;10(3):536-548. doi: 10.1002/jcsm.12403. Epub 2019 Mar 25. PMID: 31091026; PMCID: PMC6596405.

O'Reilly SC, Jones A, Muir KR, Doherty M. Quadriceps weakness in knee osteoarthritis: the effect on pain and disability. Ann Rheum Dis. 1998 Oct;57(10):588-94. doi: 10.1136/ard.57.10.588. PMID: 9893569; PMCID: PMC1752483.

Panagopoulos PK, Lambrou GI. The Involvement of MiRNAs in Osteoarthritis and Recent Developments: A Narrative Review. Mediterr J Rheumatol. 2018 Jun 29;29(2):67-79. doi: 10.31138/mjr.29.2.67. PMID: 32185303; PMCID: PMC7046075.

Papalia R, Zampogna B, Torre G, Lanotte A, Vasta S, Albo E, Tecame A, Denaro V. Sarcopenia and its relationship with osteoarthritis: risk factor or direct consequence? Musculoskelet Surg. 2014 Jun;98(1):9-14. doi: 10.1007/s12306-014-0311-6. Epub 2014 Jan 31. PMID: 24482109.

Parker MH. The altered fate of aging satellite cells is determined by signaling and epigenetic changes. Front Genet. 2015 Feb 20;6:59. doi: 10.3389/fgene.2015.00059. PMID: 25750654; PMCID: PMC4335604.

Patsopoulos NA, Analatos AA, Ioannidis JP. Relative citation impact of various study designs in the health sciences. JAMA. 2005 May 18;293(19):2362-6. doi: 10.1001/jama.293.19.2362. PMID: 15900006.

Pearle, A. D., Warren, R. F., & Rodeo, S. A. (2005). Basic science of articular cartilage and osteoarthritis. Clinics in sports medicine, 24(1), 1–12. https://doi.org/10.1016/j.csm.2004.08.007

Perez-Riverol Y, Csordas A, Bai J, Bernal-Llinares M, Hewapathirana S, Kundu DJ, Inuganti A, Griss J, Mayer G, Eisenacher M, Pérez E, Uszkoreit J, Pfeuffer J, Sachsenberg T, Yilmaz S, Tiwary S, Cox J, Audain E, Walzer M, Jarnuczak AF, Ternent T, Brazma A, Vizcaíno JA. The PRIDE database and related tools and resources in 2019: improving support for quantification data..

Nucleic Acids Res. 2019 Jan 8;47(D1):D442-D450. doi: 10.1093/nar/gky1106. PubMed ID:30395289.

Pertl, C., Eblenkamp, M., Pertl, A., Pfeifer, S., Wintermantel, E., Lochmüller, H., Walter, M. C., Krause, S., & Thirion, C. (2013). A new web-based method for automated analysis of muscle histology. BMC musculoskeletal disorders, 14, 26. https://doi.org/10.1186/1471-2474-14-26

Piel MJ, Kroin JS, van Wijnen AJ, Kc R, Im HJ. Pain assessment in animal models of osteoarthritis. Gene. 2014 Mar 10;537(2):184-8. doi: 10.1016/j.gene.2013.11.091. Epub 2013 Dec 10. PMID: 24333346; PMCID: PMC3950312.

Pisters MF, Veenhof C, van Dijk GM, Dekker J, Group CS Avoidance of activity and limitations in activities in patients with osteoarthritis of the hip or knee: a 5 year follow-up study on the mediating role of reduced muscle strength. Osteoarthritis Cartilage. 2014;22(2):171–177. doi: 10.1016/j.joca.2013.12.007

Pollard, T. C. B., Gwilym, S. E., & Carr, A. J. (2008). The assessment of early osteoarthritis. The Journal of Bone and Joint Surgery. British Volume, 90–B(4), 411–421.

Poulet B, de Souza R, Knights CB, Gentry C, Wilson AM, Bevan S, Chang YM, Pitsillides AA. Modifications of gait as predictors of natural osteoarthritis progression in STR/Ort mice. Arthritis Rheumatol. 2014 Jul;66(7):1832-42. doi: 10.1002/art.38616. PMID: 24623711; PMCID: PMC4271671.

Poulet B, Westerhof TA, Hamilton RW, Shefelbine SJ, Pitsillides AA. Spontaneous osteoarthritis in Str/ort mice is unlikely due to greater vulnerability to mechanical trauma. Osteoarthritis Cartilage. 2013;21(5):756–763. doi: 10.1016/j.joca.2013.02.652

Pritzker KP, Gay S, Jimenez SA, Ostergaard K, Pelletier JP, Revell PA, Salter D, van den Berg WB. Osteoarthritis cartilage histopathology: grading and staging. Osteoarthritis Cartilage. 2006 Jan;14(1):13-29. doi: 10.1016/j.joca.2005.07.014. Epub 2005 Oct 19. PMID: 16242352.

Proctor, C.J., Goljanek-Whysall, K. Using computer simulation models to investigate the most promising miRNAs to improve muscle regeneration during ageing. Sci Rep 7, 12314 (2017).

Punzi L, Galozzi P, Luisetto R, Favero M, Ramonda R, Oliviero F, Scanu A. Post-traumatic arthritis: overview on pathogenic mechanisms and role of inflammation. RMD Open. 2016 Sep 6;2(2):e000279. doi: 10.1136/rmdopen-2016-000279. PMID: 27651925; PMCID: PMC5013366.

Ramos-Mucci L, Elsheikh A, Keenan C, Eliasy A, D'Aout K, Bou-Gharios G, Comerford E, Poulet B. The anterior cruciate ligament in murine post-traumatic osteoarthritis: markers and mechanics. Arthritis Res Ther. 2022 May 30;24(1):128. doi: 10.1186/s13075-022-02798-7. PMID: 35637500; PMCID: PMC9150328.

Ramos-Mucci L, Javaheri B, van 't Hof R, Bou-Gharios G, Pitsillides AA, Comerford E, Poulet B. Meniscal and ligament modifications in spontaneous and post-traumatic mouse models of osteoarthritis. Arthritis Res Ther. 2020 Jul 16;22(1):171. doi: 10.1186/s13075-020-02261-5. PMID: 32678020; PMCID: PMC7364489.

Rasche A, Al-Hasani H, Herwig R. Meta-analysis approach identifies candidate genes and associated molecular networks for type-2 diabetes mellitus. BMC Genomics. 2008 Jun 30;9:310. doi: 10.1186/1471-2164-9-310. PMID: 18590522; PMCID: PMC2515154.

Reimann J, Brimah K, Schroder R, Wernig A, Beauchamp JR, Partridge TA (2004) Pax7 distribution in human skeletal muscle biopsies and myogenic tissue cultures. Cell Tissue Res 315:233–242

Rhodes DR, Chinnaiyan AM. Integrative analysis of the cancer transcriptome. Nat Genet. 2005 Jun;37 Suppl:S31-7. doi: 10.1038/ng1570. PMID: 15920528.

Richmond RS, Carlson CS, Register TC, Shanker G, Loeser RF. Functional estrogen receptors in adult articular cartilage: estrogen replacement therapy increases chondrocyte synthesis of proteoglycans and insulin-like growth factor binding protein 2. Arthritis Rheum. 2000 Sep;43(9):2081-90. doi: 10.1002/1529-0131(200009)43:9<2081::AID-ANR20>3.0.CO;2-I. PMID: 11014360.

Rodier, F., Coppé, J.-P., Patil, C. K., Hoeijmakers, W. A. M., Muñoz, D. P., Raza, S. R., … Campisi, J. (2009). Persistent DNA damage signaling triggers senescence-associated inflammatory cytokine secretion

Rodriguez-Esteban R, Jiang X. Differential gene expression in disease: a comparison between high-throughput studies and the literature. BMC Med Genomics. 2017 Oct 11;10(1):59. doi: 10.1186/s12920-017-0293-y. PMID: 29020950; PMCID: PMC5637346.

Rothschild, S. I. (2014). miRNA therapies in cancer. Molecular and Cellular Therapies, 2, 7. https://doi.org/10.1186/2052-8426-2-7

Rupaimoole, R., & Slack, F. J. (2017). MiRNA therapeutics: towards a new era for the management of cancer and other diseases. Nature Reviews Drug Discovery, 16(3), 203–222.

Rupaimoole, R., Han, H.-D., Lopez-Berestein, G., & Sood, A. K. (2011). MiRNA therapeutics: principles, expectations, and challenges. Chinese Journal of Cancer, 30(6), 368.

Sanchez AM, Candau RB, Bernardi H. FoxO transcription factors: their roles in the maintenance of skeletal muscle homeostasis. Cell Mol Life Sci. 2014 May;71(9):1657-71. doi: 10.1007/s00018-013-1513-z. PMID: 24232446.

Schiaffino S, Reggiani C. Fiber types in mammalian skeletal muscles. Physiol Rev. 2011 Oct;91(4):1447-531. doi: 10.1152/physrev.00031.2010. PMID: 22013216.

Schulz J, Takousis P, Wohlers I, Itua IOG, Dobricic V, Rücker G, Binder H, Middleton L, Ioannidis JPA, Perneczky R, Ber-tram L, Lill CM. Meta-analyses identify differentially expressed miRNAs in Parkinson's disease. Ann Neurol. 2019 Jun;85(6):835-851. doi: 10.1002/ana.25490. PMID: 30990912.

Scott D, Blizzard L, Fell J, Jones G. Prospective study of self-reported pain, radiographic osteoarthritis, sarcopenia progression, and falls risk in community-dwelling older adults. Arthritis Care Res (Hoboken). 2012 Jan;64(1):30-7. doi: 10.1002/acr.20545. PMID: 21739619.

Seale P, Sabourin LA, Girgis-Gabardo A, Mansouri A, Gruss P, Rudnicki MA (2000) Pax7 is required for the specification of myogenic satellite cells. Cell 102:777–786

Segal NA, Glass NA, Torner J, Yang M, Felson DT, Sharma L, et al. Quadriceps weakness predicts risk for knee joint space narrowing in women in the MOST cohort. Osteoarthritis Cartilage. 2010;18(6):769–775. doi: 10.1016/j.joca.2010.02.002.

Segal NA, Glass NA, Torner J, Yang M, Felson DT, Sharma L, Nevitt M, Lewis CE. Quadriceps weakness predicts risk for knee joint space narrowing in women in the MOST cohort. Osteoarthritis Cartilage. 2010 Jun;18(6):769-75. doi: 10.1016/j.joca.2010.02.002. Epub 2010 Feb 11. PMID: 20188686; PMCID: PMC2873062.

Shah, M. Y., Ferrajoli, A., Sood, A. K., Lopez-Berestein, G., & Calin, G. A. (2016). miRNA Therapeutics in Cancer — An Emerging Concept. EBioMedicine, 12, 34–42.

Shang, X., Böker, K. O., Taheri, S., Lehmann, W., & Schilling, A. F. (2021). Extracellular Vesicles Allow Epigenetic Mechanotransduction between Chondrocytes and Osteoblasts. International journal of molecular sciences, 22(24), 13282. https://doi.org/10.3390/ijms222413282

Shen L, Sinai ISoMaM (2022). GeneOverlap: Test and visualize gene overlaps. R package version 1.32.0, http://shenlab-sinai.github.io/shenlab-sinai/.

Shen, J., Li, S., & Chen, D. (2014). TGF-β signaling and the development of osteoarthritis. Bone research, 2, 14002–

Shorter, E., Sannicandro, A.J., Poulet, B. et al. Skeletal Muscle Wasting and Its Relationship With Osteoarthritis: a Mini-Review of Mechanisms and Current Interventions. Curr Rheumatol Rep 21, 40 (2019).

Si HB, Yang TM, Li L, Tian M, Zhou L, Li DP, Huang Q, Kang PD, Yang J, Zhou ZK, Cheng JQ, Shen B. miR-140 Attenuates the Progression of Early-Stage Osteoarthritis by Retarding Chondrocyte Senescence. Mol Ther Nucleic Acids. 2020 Mar 6;19:15-30. doi: 10.1016/j.omtn.2019.10.032. Epub 2019 Nov 9. PMID: 31790972; PMCID: PMC6909049.

Si, H. -b., Zeng, Y., Liu, S. -y., Zhou, Z. -k., Chen, Y. -n., Cheng, J. -q., … Shen, B. (2017). Intra-articular injection of miRNA-140 (miRNA-140) alleviates osteoarthritis (OA) progression by modulating extracellular matrix (ECM) homeostasis in rats. Osteoarthritis and Cartilage, 25(10), 1698–1707

Silva JMS, Alabarse PVG, Teixeira VON, Freitas EC, de Oliveira FH, Chakr RMDS, Xavier RM. Muscle wasting in osteoarthritis model induced by anterior cruciate ligament transection. PLoS One. 2018 Apr 30;13(4):e0196682. doi: 10.1371/journal.pone.0196682. PMID: 29709011; PMCID: PMC5927423.

Smith, M.D., The normal synovium. Open Rheumatol J, 2011. 5: p. 100-6.

Smyth A, Callaghan B, Willoughby CE, O'Brien C. The Role of miR-29 Family in TGF-β Driven Fibrosis in Glaucomatous Optic Neuropathy. Int J Mol Sci. 2022 Sep 6;23(18):10216. doi: 10.3390/ijms231810216. PMID: 36142127; PMCID: PMC9499597.

Soares RJ, Cagnin S, Chemello F, Silvestrin M, Musaro A, De Pitta C, Lanfranchi G, Sandri M. Involvement of microRNAs in the regulation of muscle wasting during catabolic conditions. J Biol Chem. 2014 Aug 8;289(32):21909-25. doi: 10.1074/jbc.M114.561845. Epub 2014 Jun 2. PMID: 24891504; PMCID: PMC4139209.

Soriano-Arroquia A, Gostage J, Xia Q, Bardell D, McCormick R, McCloskey E, Bellantuono I, Clegg P, McDonagh B, Goljanek-Whysall K. miR-24 and its target gene Prdx6 regulate viability and senescence of myogenic progenitors during aging. Aging Cell. 2021 Oct;20(10):e13475. doi: 10.1111/acel.13475. Epub 2021 Sep 24. PMID: 34560818; PMCID: PMC8520721.

Srikanth VK, Fryer JL, Zhai G, Winzenberg TM, Hosmer D, Jones G. A meta-analysis of sex differences prevalence, incidence and severity of osteoarthritis. Osteoarthritis Cartilage. 2005 Sep;13(9):769-81. doi: 10.1016/j.joca.2005.04.014. PMID: 15978850.

Staines KA, Poulet B, Wentworth DN, Pitsillides AA. The STR/ort mouse model of spontaneous osteoarthritis - an update. Osteoarthritis Cartilage. 2017 Jun;25(6):802-808. doi: 10.1016/j.joca.2016.12.014. Epub 2016 Dec 11. PMID: 27965138; PMCID: PMC5446355.

Stevens, C. R., Berenson, J., Sledziona, M., Moore, T. P., Dong, L., & Cheetham, J. (2020). Approach for semi-automated measurement of fiber diameter in murine and canine skeletal muscle. PloS one, 15(12), e0243163. https://doi.org/10.1371/journal.pone.0243163

Stouffer, S. A., Suchman, E. A., Devinney, L. C., Star, S. A., & Williams, R. M., Jr. (1949). The American soldier: Adjustment during army life. (Studies in social psychology in World War II). Princeton Univ. Press.

Suzuki T, Chino K, Fukashiro S. Gastrocnemius and soleus are selectively activated when adding knee extensor activity to plantar flexion. Hum Mov Sci. 2014 Aug;36:35-45. doi: 10.1016/j.humov.2014.04.009. Epub 2014 Jun 10. PMID: 24922619.

Tagliaferri C, Wittrant Y, Davicco MJ, Walrand S, Coxam V. Muscle and bone, two interconnected tissues. Ageing Res Rev. 2015 May;21:55-70. doi: 10.1016/j.arr.2015.03.002. Epub 2015 Mar 21. PMID: 25804855.

Takayama K, Ishida K, Matsushita T, Fujita N, Hayashi S, Sasaki K, Tei K, Kubo S, Matsumoto T, Fujioka H, Kurosaka M, Kuroda R. SIRT1 regulation of apoptosis of human chondrocytes. Arthritis Rheum. 2009 Sep;60(9):2731-40. doi: 10.1002/art.24864. PMID: 19714620.

Tavallaee G, Rockel JS, Lively S, Kapoor M. MicroRNAs in Synovial Pathology Associated With Osteoarthritis. Front Med (Lausanne). 2020 Aug 11;7:376. doi: 10.3389/fmed.2020.00376. PMID: 32850892; PMCID: PMC7431695.

Tejada-Martinez, D., Avelar, R. A., Lopes, I., Zhang, B., Novoa, G., de Magalhães, J. P., Trizzino, M. Positive Selection and Enhancer Evolution Shaped Lifespan and Body Mass in Great Apes, Molecular Biology and Evolution, Volume 39, Issue 2, February 2022, msab369,

Toda Y, Kobayashi T. The usefulness of walking for preventing sarcopenia in dieting postmenopausal women complaining of knee pain. Ann N Y Acad Sci. 2000;904:610–613. doi: 10.1111/j.1749-6632.2000.tb06524.x.

Toh, W. S., Brittberg, M., Farr, J., Foldager, C. B., Gomoll, A. H., Hui, J. H. P., Richardson, J. B., Roberts, S., & Spector, M. (2016). Cellular senescence in aging and osteoarthritis: Implications for cartilage repair. Acta Orthopaedica, 87(sup363), 6–14. https://doi.org/10.1080/17453674.2016.1235087

Troeberg, L., & Nagase, H. (2012). Proteases involved in cartilage matrix degradation in osteoarthritis. Biochimica et Biophysica Acta, 1824(1), 133–145.

Tuddenham, L., Wheeler, G., Ntounia-Fousara, S., Waters, J., Hajihosseini, M. K., Clark, I., & Dalmay, T. (2006). The cartilage specific miRNA-140 targets histone deacetylase 4 in mouse cells. FEBS Letters, 580(17), 4214–4217.

Tummalapalli CM, Heath BJ, Tyagi SC. Tissue inhibitor of metalloproteinase-4 instigates apoptosis in transformed cardiac fibroblasts. J Cell Biochem. 2001;80(4):512-21. doi: 10.1002/1097-4644(20010315)80:4<512::aid-jcb1005>3.0.co;2-n. PMID: 11169735.

Van Deursen, J. M. (2014). The role of senescent cells in ageing. Nature, 509(7501), 439–446.

Vasudevan, S. (2012). Posttranscriptional Upregulation by MiRNAs. Wiley Interdisciplinary Reviews: RNA, 3(3), 311–330. https://doi.org/10.1002/wrna.121

Veronese N, Stefanac S, Koyanagi A, Al-Daghri NM, Sabico S, Cooper C, Rizzoli R, Reginster JY, Barbagallo M, Dominguez LJ, Smith L, Maggi S. Lower Limb Muscle Strength and Muscle Mass Are Associated With Incident Symptomatic Knee Osteoarthritis: A Longitudinal Cohort Study. Front Endocrinol (Lausanne). 2021 Dec 16;12:804560. doi: 10.3389/fendo.2021.804560. PMID: 34975772; PMCID: PMC8716541.

Wahid, F., Shehzad, A., Khan, T., & Kim, Y. Y. (2010). MiRNAs: Synthesis, mechanism, function, and recent clinical trials. Biochimica et Biophysica Acta (BBA) - Molecular Cell Research, 1803(11), 1231–1243.

Waligora AC, Johanson NA, Hirsch BE. Clinical anatomy of the quadriceps femoris and extensor apparatus of the knee. Clin Orthop Relat Res. 2009 Dec;467(12):3297-306. doi: 10.1007/s11999-009-1052-y. Epub 2009 Aug 19. PMID: 19690926; PMCID: PMC2772911.

Walston JD. Sarcopenia in older adults. Curr Opin Rheumatol. 2012 Nov;24(6):623-7. doi: 10.1097/BOR.0b013e328358d59b. PMID: 22955023; PMCID: PMC4066461.

Walton M. Degenerative joint disease in the mouse knee; radiological and morphological observations. J Pathol. 1977 Oct;123(2):97-107. doi: 10.1002/path.1711230206. PMID: 592018.

Wang XH. MiRNA in myogenesis and muscle atrophy. Curr Opin Clin Nutr Metab Care. 2013 May;16(3):258-66. doi: 10.1097/MCO.0b013e32835f81b9. PMID: 23449000; PMCID: PMC3967234.

Wang Y, Wluka AE, Berry PA, Siew T, Teichtahl AJ, Urquhart DM, et al. Increase in vastus medialis cross-sectional area is associated with reduced pain, cartilage loss, and joint replacement risk in knee osteoarthritis. Arthritis Rheum. 2012;64(12):3917–3925. doi: 10.1002/art.34681.

Wang Y, Zhang G, Huang W. MiR-300 promotes the proliferation, migration and invasion of fibroblast-like synoviocytes in rheumatoid arthritis by targeting IL-37. Autoimmunity. 2022 Sep;55(6):371-377. doi: 10.1080/08916934.2022.2081842. Epub 2022 Jun 6. PMID: 35658770.

Wang, X., Li, X., Li, J., Zhai, L., Liu, D., Abdurahman, A., Zhang, Y., Yokota, H., & Zhang, P. (2021). Mechanical loading stimulates bone angiogenesis through enhancing type H vessel formation and downregulating exosomal miR-214-3p from bone marrow-derived mesenchymal stem cells. FASEB journal : official publication of the Federation of American Societies for Experimental Biology, 35(1), e21150.

Wang, Y., & Pessin, J. E. (2013). Mechanisms for fiber-type specificity of skeletal muscle atrophy. Current opinion in clinical nutrition and metabolic care, 16(3), 243–250. https://doi.org/10.1097/MCO.0b013e328360272d

Wang, Y., Li, Y., Ma, Z., Yang, W., & Ai, C. (2010). Mechanism of MiRNA-Target Interaction: Molecular Dynamics Simulations and Thermodynamics Analysis. PLoS Computational Biology, 6(7), e1000866. https://doi.org/10.1371/journal.pcbi.1000866

Weaver RE, Sharif M, Livingston LA, Andrews KL, Fuller CJ. Microscopic change in macroscopically normal equine cartilage from osteoarthritic joints. Connect Tissue Res. 2006;47(2):92-101. doi: 10.1080/03008200600584165. PMID: 16754515.

Wen Y, Murach KA, Vechetti IJ, Jr., Fry CS, Vickery CD, Peterson CA, McCarthy JJ, and Campbell KS. MyoVision: Software for Automated High-Content Analysis of Skeletal Muscle Immunohistochemistry. J Appl Physiol. jap 00762 02017, 2017.

Whitehead RA, Puil E, Ries CR, Schwarz SK, Wall RA, Cooke JE, Putrenko I, Sallam NA, MacLeod BA. GABA(B) receptor-mediated selective peripheral analgesia by the non-proteinogenic amino acid, isovaline. Neuroscience. 2012 Jun 28;213:154-60. doi: 10.1016/j.neuroscience.2012.04.026. Epub 2012 Apr 21. PMID: 22525135.

Whitesides, T.E. Orthopaedic Basic Science: Biology and Biomechanics of the Musculoskeletal System, 2nd ed.; American Academy of Orthopaedic Surgeons: Rosemont, IL, USA, 2001; Volume 83, p. 481.

Williams, J., Smith, F., Kumar, S., Vijayan, M., & Reddy, P. H. (2017). Are miRNAs true sensors of ageing and cellular senescence? Ageing Research Reviews, 35, 350–363. https://doi.org/10.1016/j.arr.2016.11.008

Woo SL, Abramowitch SD, Kilger R, Liang R. Biomechanics of knee ligaments: injury, healing, and repair. J Biomech. 2006;39(1):1-20. doi: 10.1016/j.jbiomech.2004.10.025. Epub 2005 Jan 7. PMID: 16271583.

Woods, S., Charlton, S., Cheung, K., Hao, Y., Soul, J., Reynard, L. N., … Young, D. A. (2020). miRNA-seq of cartilage reveals an over-abundance of miR-140-3p which contains functional isomiRs. BioRxiv, 2020.01.29.925206.

Xia Q, Huang X, Huang J, Zheng Y, March ME, Li J, Wei Y. The Role of Autophagy in Skeletal Muscle Diseases. Front Physiol. 2021 Mar 25;12:638983. doi: 10.3389/fphys.2021.638983. PMID: 33841177; PMCID: PMC8027491.

Xue H, Tu Y, Ma T, Wen T, Yang T, Xue L, Cai M, Wang F, Guan M. miR-93-5p attenuates IL-1β-induced chondrocyte apoptosis and cartilage degradation in osteoarthritis partially by targeting TCF4. Bone. 2019 Jun;123:129-136. doi: 10.1016/j.bone.2019.03.035. Epub 2019 Mar 28. PMID: 30930294.

Xue, H., Tu, Y., Ma, T., Wen, T., Yang, T., Xue, L., … Guan, M. (2019). miR-93-5p attenuates IL-1β-induced chondrocyte apoptosis and cartilage degradation in osteoarthritis partially by targeting TCF4. Bone, 123, 129–136.

Yamasaki, K., Nakasa, T., Miyaki, S., Ishikawa, M., Deie, M., Adachi, N., … Ochi, M. (2009). Expression of MiRNA-146a in osteoarthritis cartilage. Arthritis and Rheumatism, 60(4), 1035–1041.

Yan, X.-T., Ji, L.-J., Wang, Z., Wu, X., Wang, Q., Sun, S., … Zhang, Y. (2017). MiRNA-93 alleviates neuropathic pain through targeting signal transducer and activator of transcription 3. International Immunopharmacology, 46, 156–162. https://doi.org/10.1016/J.INTIMP.2017.01.027

Yanai K, Kaneko S, Ishii H, Aomatsu A, Ito K, Hirai K, Ookawara S, Ishibashi K, Morishita Y. MicroRNAs in Sarcopenia: A Systematic Review. Front Med (Lausanne). 2020 May 28;7:180. doi: 10.3389/fmed.2020.00180. PMID: 32549041; PMCID: PMC7270169.

Yang, N. (2015). An overview of viral and nonviral delivery systems for miRNA. International Journal of Pharmaceutical Investigation, 5(4), 179–81.

Yin, C.-M., Suen, W.-C.-W., Lin, S., Wu, X.-M., Li, G., & Pan, X.-H. (2017). Dysregulation of both miR-140-3p and miR-140-5p in synovial fluid correlate with osteoarthritis severity. Bone & Joint Research, 6(11), 612–618.

Yu XM, Meng HY, Yuan XL, Wang Y, Guo QY, Peng J, Wang AY, Lu SB. MiRNAs' Involvement in Osteoarthritis and the Prospects for Treatments. Evid Based Complement Alternat Med. 2015;2015:236179. doi: 10.1155/2015/236179. Epub 2015 Oct 26. PMID: 26587043; PMCID: PMC4637488.

Zaykin D. V. (2011). Optimally weighted Z-test is a powerful method for combining probabilities in meta-analysis. Jour-nal of evolutionary biology, 24(8), 1836–1841. https://doi.org/10.1111/j.1420-9101.2011.02297.x

Zeng P, Han W, Li C, Li H, Zhu D, Zhang Y, Liu X. miR-378 attenuates muscle regeneration by delaying satellite cell activation and differentiation in mice. Acta Biochim Biophys Sin (Shanghai). 2016 Sep;48(9):833-9. doi: 10.1093/abbs/gmw077. Epub 2016 Aug 25. PMID: 27563005.

Zhang B, Li Y, Yu Y, Zhao J, Ou Y, Chao Y, et al. MiRNA-378 promotes osteogenesis-angiogenesis coupling in BMMSCs for potential bone regeneration. Anal Cell Pathol (Amst) 2018;2018:8402390. doi: 10.1155/2018/8402390.

Zhang, R., Ma, J., & Yao, J. (2013). Molecular mechanisms of the cartilage-specific miRNA-140 in osteoarthritis. Inflammation Research, 62(10), 871–877.

Zhang, Y., Wang, Z., & Gemeinhart, R. A. (2013). Progress in miRNA delivery. Journal of Controlled Release : Official Journal of the Controlled Release Society, 172(3), 962–974.

Zheng YL, Song G, Guo JB, Su X, Chen YM, Yang Z, Chen PJ, Wang XQ. Interactions Among lncRNA/circRNA, miRNA, and mRNA in Musculoskeletal Degenerative Diseases. Front Cell Dev Biol. 2021 Oct 11;9:753931. doi: 10.3389/fcell.2021.753931. PMID: 34708047; PMCID: PMC8542847.

Zhong, L., Huang, X., Karperien, M., & Post, J. N. (2016). Correlation between Gene Expression and Osteoarthritis Progres-sion in Human. International journal of molecular sciences, 17(7), 1126. https://doi.org/10.3390/ijms17071126

Zhu J, Zhu Y, Xiao W, Hu Y, Li Y. Instability and excessive mechanical loading mediate subchondral bone changes to induce osteoarthritis. Ann Transl Med. 2020 Mar;8(6):350. doi: 10.21037/atm.2020.02.103. PMID: 32355794; PMCID: PMC7186756.Het

Supplementary Materials

S1: All pathways that were found by IPA to be significantly enriched in the list of validated miR-378a-3p target genes

Ingenuity Canonical Pathways	-log(p-value)
Autophagy	9.11
Senescence Pathway	8.88
Ribonucleotide Reductase Signaling Pathway	8.34
EIF2 Signaling	6.31
CSDE1 Signaling Pathway	5.75
Kinetochore Metaphase Signaling Pathway	5.68
Inhibition of ARE-Mediated mRNA Degradation Pathway	5.65
Epithelial Adherens Junction Signaling	5.29
AMPK Signaling	5.27
Axonal Guidance Signaling	5.04
ERB2-ERBB3 Signaling	5.04
ATM Signaling	4.97
Clathrin-mediated Endocytosis Signaling	4.96
Huntington's Disease Signaling	4.94
14-3-3-mediated Signaling	4.88
Renal Cell Carcinoma Signaling	4.84
HER-2 Signaling in Breast Cancer	4.8
Role of CHK Proteins in Cell Cycle Checkpoint Control	4.78
Estrogen Receptor Signaling	4.63
Cell Cycle: G2/M DNA Damage Checkpoint Regulation	4.61
Coronavirus Pathogenesis Pathway	4.59
Molecular Mechanisms of Cancer	4.56
Cyclins and Cell Cycle Regulation	4.48
HIF1α Signaling	4.45
mTOR Signaling	4.27
Protein Kinase A Signaling	4.24
MiRNA Biogenesis Signaling Pathway	4.17
Mitotic Roles of Polo-Like Kinase	4.17
Polyamine Regulation in Colon Cancer	4.03
Cell Cycle Regulation by BTG Family Proteins	3.96
Semaphorin Neuronal Repulsive Signaling Pathway	3.94
Regulation of eIF4 and p70S6K Signaling	3.89
Ephrin B Signaling	3.88
p53 Signaling	3.83
Insulin Receptor Signaling	3.79
ERK/MAPK Signaling	3.79
PI3K/AKT Signaling	3.77
Hereditary Breast Cancer Signaling	3.72
CLEAR Signaling Pathway	3.64
PI3K Signaling in B Lymphocytes	3.61
Sumoylation Pathway	3.61
fMLP Signaling in Neutrophils	3.6
Superpathway of Inositol Phosphate Compounds	3.59
3-phosphoinositide Biosynthesis	3.52
HOTAIR Regulatory Pathway	3.51
3-phosphoinositide Degradation	3.47

p70S6K Signaling	3.46
Actin Cytoskeleton Signaling	3.44
Cell Cycle: G1/S Checkpoint Regulation	3.44
Integrin Signaling	3.44
Estrogen-Dependent Breast Cancer Signaling	3.42
RAN Signaling	3.37
D-myo-inositol-5-phosphate Metabolism	3.36
Glioma Signaling	3.34
RHOA Signaling	3.34
Ephrin Receptor Signaling	3.28
Pancreatic Adenocarcinoma Signaling	3.27
Endometrial Cancer Signaling	3.21
HIPPO signaling	3.19
Semaphorin Signaling in Neurons	3.16
Protein Ubiquitination Pathway	3.14
Pulmonary Fibrosis Idiopathic Signaling Pathway	3.13
Hypoxia Signaling in the Cardiovascular System	3.05
Tight Junction Signaling	3.04
Cardiac β-adrenergic Signaling	3.01
Ceramide Signaling	2.98
Prolactin Signaling	2.98
PTEN Signaling	2.97
Pyridoxal 5'-phosphate Salvage Pathway	2.96
IL-7 Signaling Pathway	2.96
D-myo-inositol (1,4,5,6)-Tetrakisphosphate Biosynthesis	2.94
D-myo-inositol (3,4,5,6)-tetrakisphosphate Biosynthesis	2.94
Signaling by Rho Family GTPases	2.92
IL-3 Signaling	2.92
Chronic Myeloid Leukemia Signaling	2.91
Telomerase Signaling	2.88
Role of BRCA1 in DNA Damage Response	2.87
Reelin Signaling in Neurons	2.87
Gαq Signaling	2.85
Remodeling of Epithelial Adherens Junctions	2.82
Spermidine Biosynthesis I	2.79
BEX2 Signaling Pathway	2.79
BER (Base Excision Repair) Pathway	2.76
Production of Nitric Oxide and Reactive Oxygen Species in Macrophages	2.73
GM-CSF Signaling	2.73
TR/RXR Activation	2.71
PEDF Signaling	2.71
BAG2 Signaling Pathway	2.71
CDK5 Signaling	2.65
PDGF Signaling	2.63
CCR3 Signaling in Eosinophils	2.54
Virus Entry via Endocytic Pathways	2.52
ILK Signaling	2.5
CXCR4 Signaling	2.49
Estrogen-mediated S-phase Entry	2.47
RAC Signaling	2.45
Melanoma Signaling	2.44
Sirtuin Signaling Pathway	2.42
Role of NFAT in Cardiac Hypertrophy	2.42
Glioblastoma Multiforme Signaling	2.42

ERBB Signaling	2.39
MSP-RON Signaling In Cancer Cells Pathway	2.37
Glucocorticoid Receptor Signaling	2.37
Thrombin Signaling	2.36
Fcγ Receptor-mediated Phagocytosis in Macrophages and Monocytes	2.35
Non-Small Cell Lung Cancer Signaling	2.35
Cardiac Hypertrophy Signaling	2.35
WNT/β-catenin Signaling	2.35
Inosine-5'-phosphate Biosynthesis II	2.33
N-acetylglucosamine Degradation I	2.33
IL-8 Signaling	2.31
Endocannabinoid Developing Neuron Pathway	2.29
DNA Methylation and Transcriptional Repression Signaling	2.27
ERBB4 Signaling	2.24
Breast Cancer Regulation by Stathmin1	2.24
Prostate Cancer Signaling	2.21
EGF Signaling	2.21
April Mediated Signaling	2.2
Gap Junction Signaling	2.2
Endocannabinoid Cancer Inhibition Pathway	2.2
Cell Cycle Control of Chromosomal Replication	2.16
FAT10 Signaling Pathway	2.16
HGF Signaling	2.16
Ferroptosis Signaling Pathway	2.16
B Cell Activating Factor Signaling	2.15
Neuregulin Signaling	2.13
RHOGDI Signaling	2.11
Dopamine-DARPP32 Feedback in cAMP Signaling	2.11
IGF-1 Signaling	2.05
Sertoli Cell-Sertoli Cell Junction Signaling	2.04
N-acetylglucosamine Degradation II	2.04
Relaxin Signaling	2.01
Unfolded protein response	2
RANK Signaling in Osteoclasts	1.97
Inhibition of Angiogenesis by TSP1	1.96
Ephrin A Signaling	1.96
IL-2 Signaling	1.96
Apelin Endothelial Signaling Pathway	1.94
Role Of Osteoclasts In Rheumatoid Arthritis Signaling Pathway	1.88
Thyroid Cancer Signaling	1.86
Interferon Signaling	1.86
Dopamine Receptor Signaling	1.83
Death Receptor Signaling	1.82
TGF-β Signaling	1.82
Salvage Pathways of Pyrimidine Ribonucleotides	1.8
Role of PI3K/AKT Signaling in the Pathogenesis of Influenza	1.79
UVA-Induced MAPK Signaling	1.77
JAK/STAT Signaling	1.77
Acute Phase Response Signaling	1.76
VEGF Signaling	1.74
NAD Signaling Pathway	1.73
Androgen Signaling	1.72
Cardiac Hypertrophy Signaling (Enhanced)	1.71
Pyruvate Fermentation to Lactate	1.66

Glycolysis I	1.66
Apoptosis Signaling	1.62
Leukocyte Extravasation Signaling	1.62
Chondroitin Sulfate Degradation (Metazoa)	1.61
Hepatic Fibrosis / Hepatic Stellate Cell Activation	1.6
CNTF Signaling	1.58
Regulation of Cellular Mechanics by Calpain Protease	1.58
Aryl Hydrocarbon Receptor Signaling	1.57
Sonic Hedgehog Signaling	1.56
Immunogenic Cell Death Signaling Pathway	1.55
Oncostatin M Signaling	1.55
Cancer Drug Resistance By Drug Efflux	1.55
Dermatan Sulfate Degradation (Metazoa)	1.54
Sperm Motility	1.54
α-Adrenergic Signaling	1.53
Acute Myeloid Leukemia Signaling	1.53
G Protein Signaling Mediated by Tubby	1.51
GP6 Signaling Pathway	1.49
ID1 Signaling Pathway	1.49
GDNF Family Ligand-Receptor Interactions	1.49
Retinoic acid Mediated Apoptosis Signaling	1.48
PCP (Planar Cell Polarity) Pathway	1.48
IL-4 Signaling	1.48
Coronavirus Replication Pathway	1.48
IL-6 Signaling	1.47
Antiproliferative Role of Somatostatin Receptor 2	1.46
G Beta Gamma Signaling	1.45
Hepatic Fibrosis Signaling Pathway	1.45
Neurotrophin/TRK Signaling	1.43
HMGB1 Signaling	1.43
Aldosterone Signaling in Epithelial Cells	1.41
Small Cell Lung Cancer Signaling	1.41
IL-1 Signaling	1.41
iNOS Signaling	1.4
Thio-molybdenum Cofactor Biosynthesis	1.4
Thrombopoietin Signaling	1.39
Chemokine Signaling	1.38
Germ Cell-Sertoli Cell Junction Signaling	1.38
Gα12/13 Signaling	1.38
Apelin Muscle Signaling Pathway	1.37
PFKFB4 Signaling Pathway	1.37
Melanocyte Development and Pigmentation Signaling	1.36
Role of Tissue Factor in Cancer	1.36
STAT3 Pathway	1.34
Apelin Cardiomyocyte Signaling Pathway	1.34
FLT3 Signaling in Hematopoietic Progenitor Cells	1.33
Role of PKR in Interferon Induction and Antiviral Response	1.32

S2: Additional details for microCT analysis of mice joints

C. Task list performed on Batman for SCB thickness

Step	Name	Detail
1	Thresholding	Mode global, lower grey threshold 55 and upper grey threshold 250
2	Despeckle	Remove white speckles in an area with less than 40 voxels
3	Bitwise operations	
4	Reload	Reload images
5	3D Analysis	Provides spreadsheet of values for mean thickness (Tb.Th)

D. Task list performed on Batman for trabecular thickness, number and separation

Step	Name	Detail
1	Thresholding	Mode global, lower grey threshold 55 and upper grey threshold 255
2	ROI shrink-wrap	Stretch over holes with a diameter equal to or less than 12 voxels
3	Reload	Reload images
4	Thresholding	Mode global, lower grey threshold 55 and upper grey threshold 255
5	Despeckle	Remove black speckles in an area with less than 30 voxels
6	Despeckle	Remove white speckles in an area with less than 30 voxels
7	3D Analysis	Provides spreadsheet of values for bone volume (Bv), and trabecular thickness (Tb.Th), number (Tb.N) and separation (Tb.Sp)

E. Task list performed on Batman for joint space mineralisation

Step	Name	Detail
1	Thresholding	Mode global, lower grey threshold 55 and upper grey threshold 255
2	Despeckle	Remove white speckles in an area with less than 40 voxels
3	Despeckly	Remove black speckles in an area with less than 20 voxels
4	ROI shrink-wrap	Stretch over holes with a diameter equal to or less than 12 voxels
5	3D Analysis	Provides spreadsheet of values for tissue volume

S3: All eligible miRNA papers selected for data-extraction for the meta-analysis

Paper	OA Sample Number	Control Nu	Tissue
Aigner et al., 2001	6	9	Articular Cartilage
Akagi et al. 2016	16	23	Articular Cartilage
Akagi et al., 2007	16	6	Articular Cartilage
Aref-Eshghi et al., 2015	32	21	Articular Cartilage
Aref-Eshghi et al., 2016	58	55	Articular Cartilage
Attur et al., 2015	19	13	Articular Cartilage
Bonnelye et al., 2011	46	10	Articular Cartilage
Chanalaris et al. 2019	12	12	Articular Cartilage
Collins-Racie, et al. 2009	20	10	Articular Cartilage
Cucchiarini et al., 2014	52	13	Articular Cartilage
Fisch et al., 2019	20	18	Articular Cartilage
Fu et al., 2015	6	5	Articular Cartilage
Fuijita et al., 2006	15	10	Articular Cartilage
Gebhard et al., 2002	14	21	Articular Cartilage
Haag et al., 2008	9	8	Articular Cartilage
Higashiyama et al., 2009	10	6	Articular Cartilage
Karlsson et al., 2010	5	8	Articular Cartilage
Li et al., 2005	8	7	Articular Cartilage
Li et al., 2009	10	10	Articular Cartilage
Li et al., 2016	38	9	Articular Cartilage
Martin et al., 2001	21	18	Articular Cartilage
Mokuda et al., 2019	10	8	Articular Cartilage
Orfanidou et al., 2012	40	10	Articular Cartilage
Söder et al., 2006	9	8	Articular Cartilage
Soul et al., 2018	60	10	Articular Cartilage
Tanaka et al., 2019	10	9	Articular Cartilage
Thorfve et al., 2012	5	8	Articular Cartilage
Wang et al., 2014	5	3	Articular Cartilage
Yang et al., 2016	6	3	Articular Cartilage
Zhu et al., 2018	23	20	Articular Cartilage

S4: All eligible mRNA papers selected for data-extraction for the meta-analysis

Paper	OA Sample Number	Control Sample Number
Akhtar et al. 2010	3	3
An et al,. 2020	30	20
Balaskas et al. 2017	6	6
Cai et al. 2019	20	10
Cao et al. 2018	10	10
Chang et al. 2016	11	7
Chang et al. 2018	9	12
Chen and Tian. 2016	15	6
Chen et al. 2017	8	9
Chen et al. 2018	20	20
Chen et al. 2019	12	12
Cheng et al. 2019	23	23
Dai et al. 2019	30	30
Díaz-Prado et al. 2012	6	4
Gu et al. 2016	25	10
He et al. 2017	10	10
Hou et al. 2020	12	10
Hu et al. 2016	20	20
Hu et al. 2017	50	16
Hu et al. 2018	80	12
Hu et al. 2019	6	7
Huang et al. 2017	15	10
Hwang et al. 2017	10	10
Iliopoulos et al. 2008	33	10
Jin et al. 2017	15	15
Jones et al. 2009	3	3
Kang et al. 2016	10	10
Kostopoulou et al. 2015	14	9
Li et al. 2015	10	10
Li et al. 2016	25	25
Li et al. 2016	9	9
Li et al. 2018	5	5
Lu et al. 2016	10	13
Lui et al. 2019	30	30
Lui et al. 2019	24	11

Paper	OA Sample Number	Control Sample Number
Lui et al. 2019	24	11
Luo et al. 2019	46	28
Matsukawa et al. 2013	7	3
Miyaki et al. 2009	11	8
Nakamura et al. 2019	5	5
Ni et al. 2018	30	30
Ntoumou et al. 2017	12	7
Papathanasiou et al. 2019	20	15
Park et al. 2013	20	6
Park et al. 2013	20	20
Park et al. 2016	7	10
Qiu et al. 2019	3	3
Ren et al. 2020	30	30
Shi et al. 2018	25	25
Shu et al. 2019	30	30
Steck et al. 2012	25	10
Tardif et al. 2009	6	6
Tardif et al. 2013	48	8
Tu et al. 2016	16	16
Vonk et al. 2014	7	7
Wang et al. 2015	10	10
Wang et al. 2016	25	25
Wang et al. 2019	40	20
Wang et al. 2019	43	35
Wu et al. 2017	27	14
Xiang et al. 2020	**4**	4
Yan et al. 2016	12	10
Yang et al. 2014	11	5
Yang et al. 2016	15	12
Yang et al. 2018	10	10
Yang et al. 2019	20	20
Yin et al. 2017	33	15
Yuan et al. 2016	16	6
Zhang et al. 2018	48	20
Zhang et al. 2018	7	8
Zhang et al. 2019	42	20
Zhao et al. 2019	10	10
Zheng et al. 2017	86	59

S5: R code used to transform p values into signed z-scores

```
p_to_z=function(z_score){
  z_score_copy=z_score
  pvals=z_score$P.value
  zscores=qnorm(pvals/2,lower.tail=FALSE)
  z_score_copy$Z.score=zscores

z_score_copy$Z.score[z_score_copy$direction=='down']=z_score_copy$Z.score[z_s
core_copy$direction=='down']*-1
  return(z_score_copy)
}

mrnas=p_to_z(mrnas)
View(mrnas)
```

S6: All mRNAs identified from the meta-analysis as being significantly dysregulated in OA cartilage vs controls

mRNA	Summed z score	p value
DDIT4	-10.63912988	9.80E-27
GADD45A	-9.671426964	1.99E-22
TXNIP	-9.159840611	2.60E-20
RPL23AP1	-8.608480816	3.70E-18
C10orf10	-8.302559066	5.09E-17
ANG	8.070197563	3.51E-16
APOD	-7.769000282	3.96E-15
GPX3	-7.67384789	8.35E-15
CEBPD	-7.448716407	4.71E-14
DLX5	-7.351922828	9.77E-14
HOXA5	-7.319143505	1.25E-13
GDF15	-7.277596172	1.70E-13
PDK4	-7.26107927	1.92E-13
CISH	-7.150042437	4.34E-13
SCNN1A	6.872376244	3.16E-12
RND1	-6.869197998	3.23E-12
CSNK2A2	-6.803140204	5.12E-12
KLF15	-6.746554293	7.57E-12
DCXR	-6.740626982	7.89E-12
HSD17B14	-6.662116002	1.35E-11
BTG2	-6.614946494	1.86E-11
ADM	-6.488272437	4.34E-11
HIST1H1C	-6.265497585	1.86E-10
CRTAP	-6.254358385	2.00E-10
G0S2	-6.217016854	2.53E-10
CNN2	-6.191152903	2.99E-10
PIM1	-6.185370273	3.10E-10
CDKN1A	-6.080006425	6.01E-10
TIMP4	-5.820668058	2.93E-09
SRCIN1	5.746293702	4.56E-09
ACPP	-5.65306975	7.88E-09
SOD2	-5.590312621	1.13E-08

mRNA	Summed z score	p value
MMP3	-5.567283735	1.29E-08
C16orf13	-5.367823528	3.98E-08
GNMT	-5.36138865	4.13E-08
PQBP1	-5.331634408	4.87E-08
UQCR10	-5.311542887	5.44E-08
HSD11B1	-5.306034699	5.60E-08
SERPINA1	5.194803932	1.02E-07
PLIN5	-5.146962961	1.32E-07
MFAP1	-5.054563643	2.16E-07
CALCA	-5.049295177	2.22E-07
SDC4	-4.975628021	3.25E-07
CHI3L1	-4.953928846	3.64E-07
HNRNPH3	-4.921586662	4.29E-07
GCH1	-4.753863268	9.98E-07
AGTRAP	-4.635522946	1.78E-06
CEACAM4	-4.594819737	2.17E-06
U2AF1L4	-4.577709365	2.35E-06
ANXA11	-4.562537858	2.53E-06
BEX2	-4.493820208	3.50E-06
LIF	-4.453026189	4.23E-06
ASL	-4.409596632	5.18E-06
RXR	-4.370248438	6.21E-06
MRPL24	-4.369665552	6.22E-06
NSFL1C	-4.340088509	7.12E-06
ERR?	-4.318819079	7.84E-06
HNRNPAB	-4.251285608	1.06E-05
ACAN	-4.240826463	1.11E-05
ATP6V1E1	-4.223253345	1.20E-05
ATP5H	-4.219846621	1.22E-05
CYB561D1	4.191736351	1.38E-05
AKR7L	-4.144232135	1.70E-05
PDHA1	-4.143058085	1.71E-05

mRNA	Summed z score	p value
IDH3B	-4.14165412	1.72E-05
ANAPC11	-4.139962774	1.74E-05
HYI	-4.12422655	1.86E-05
RAB37	-4.104569213	2.03E-05
RPL5	-4.100230622	2.06E-05
ID1	-4.079272868	2.26E-05
TGIF1	-4.04082079	2.66E-05
UBB	-4.037016135	2.71E-05
RALY	-4.035569336	2.72E-05
CD151	-3.994388796	3.24E-05
COPE	-3.957659184	3.78E-05
RNF39	-3.946595268	3.96E-05
ZNF44	-3.937353848	4.12E-05
FOXA2	-3.927425915	4.29E-05
BAT3	-3.902448575	4.76E-05
MYL12B	-3.882079111	5.18E-05
PARK7	-3.873008436	5.38E-05
DHPS	-3.859712885	5.68E-05
ACAA1	-3.855718682	5.77E-05
C8orf40	-3.817105274	6.75E-05
SFTPA1	-3.815007272	6.81E-05
SLC41A3	-3.813012118	6.86E-05
BACE2	-3.74806202	8.91E-05
GSTK1	-3.737045174	9.31E-05
HIST1H1E	-3.726646446	9.70E-05
HAX1	-3.722015361	9.88E-05
UTY	-3.691928121	0.000111
NPM1	-3.687492029	0.000113
BOD1	-3.684683411	0.000114
RAMP1	-3.684486402	0.000115
PRLR	-3.677683716	0.000118
CASP8AP2	-3.675796998	0.000119
VGLL4	-3.673893166	0.000119

mRNA	Summed z score	p value
UBL5	-3.666449551	0.000123
SMTN	-3.655342725	0.000128
DBI	3.647605454	0.000132
FUT3	-3.645163508	0.000134
STAG2	-3.6403718	0.000136
KLF6	-3.632987912	0.00014
DMKN	-3.631560004	0.000141
STAG3L1	-3.617241064	0.000149
RAB34	-3.592217418	0.000164
UBE2D2	-3.551911218	0.000191
PRMT1	-3.537854184	0.000202
C1orf43	-3.537581729	0.000202
PKD1	-3.51307406	0.000221
SENP8	-3.462372298	0.000268
ROBLD3	-3.462059883	0.000268
SPINT2	-3.459411027	0.000271
HNRNPD	-3.455884216	0.000274
LDHA	-3.453792604	0.000276
EEF1D	-3.452769128	0.000277
NME1-NME	-3.433550459	0.000298
WIPI2	-3.419582791	0.000314
TPM2	-3.414984899	0.000319
C6orf48	-3.406588038	0.000329
CCDC43	-3.391458422	0.000348
PARL	-3.389790167	0.00035
ASB3	-3.378066465	0.000365
GCOM1	-3.376414761	0.000367
ARTN	-3.37534228	0.000369
COQ6	-3.36577859	0.000382
MAPK8	-3.361514629	0.000388
PCID2	-3.357722983	0.000393
LXR?	-3.348211373	0.000407
PPAR?	-3.348211373	0.000407

mRNA	Summed z score	p value
TATDN3	-3.317950429	0.000453
PDP1	-3.307411121	0.000471
PCBP2	-3.302349937	0.000479
PER1	-3.298156614	0.000487
CES2	-3.288052631	0.000504
PFDN5	-3.280387646	0.000518
LDB1	-3.271729236	0.000534
DEK	-3.257268209	0.000562
CTH	-3.25654647	0.000564
RTN4	-3.253666275	0.00057
SLC25A11	-3.202020042	0.000682
IFI6	-3.19835639	0.000691
HSPA5	-3.195109758	0.000699
TNFSF13	-3.173901511	0.000752
SPG21	-3.161655525	0.000784
TMEM91	-3.159357489	0.000791
CLDND1	-3.149459197	0.000818
ANAPC5	-3.148372035	0.000821
C21orf33	-3.132759556	0.000866
WWP2	-3.132206109	0.000867
ZNF37A	-3.126133896	0.000886
ITM2C	-3.08679376	0.001012
EXOC7	-3.085758887	0.001015
TRPV4	-3.056094602	0.001121
C5orf45	-3.048254565	0.001151
ST13	-3.045768194	0.00116
AP2S1	-3.044376395	0.001166
CCND3	-3.026774599	0.001236
NEK6	-3.024195976	0.001246
PSMA3	-3.024135387	0.001247
PKM2	-3.018993864	0.001268
MLL5	-3.017100778	0.001276
KDM4C	-3.00773361	0.001316
TM2D2	-3.004420615	0.00133
PPM1M	-3.003859626	0.001333
SYF2	-3.001289233	0.001344
TSPAN4	-3.000655453	0.001347
CAST	-2.996302248	0.001366

mRNA	Summed z score	p value
CIDEA	-2.983550277	0.001425
TMEM14C	-2.979457542	0.001444
PILRB	-2.944923556	0.001615
MYL6	-2.921419467	0.001742
C22orf39	-2.921180407	0.001744
LGALS3	-2.91351412	0.001787
HLA-F	-2.894161415	0.001901
SLC3A2	-2.888726099	0.001934
ERGIC3	-2.886152556	0.00195
CD99	-2.881593393	0.001978
CMPK1	-2.875579362	0.002016
HSPA8	-2.874665859	0.002022
ADAD2	-2.874624586	0.002023
WDR45	-2.864843389	0.002086
TMEM14B	-2.855273782	0.00215
BMAL1	-2.852071956	0.002172
AMZ2	-2.83819244	0.002268
MYD88	-2.828466986	0.002339
IMPDH2	-2.825598216	0.00236
RHCE	-2.824613028	0.002367
RAD51L1	-2.821236781	0.002392
API5	-2.817748765	0.002418
ARMCX6	-2.810982904	0.00247
ABCC1	-2.79285506	0.002612
HIST1H3D	-2.762004393	0.002872
ZNF669	-2.755302745	0.002932
S1PR1	-2.744840741	0.003027
DYNC1I1	-2.74413764	0.003034
SSFA2	-2.711065866	0.003353
ZNF83	-2.708999369	0.003374
HIST2H2AB	-2.698962216	0.003478
KLC1	-2.676244231	0.003723
TBRG4	-2.648830781	0.004039
ATXN10	-2.632148286	0.004242
NM_019102	-2.61925335	0.004406
C20orf24	-2.617883348	0.004424
ZNF207	-2.575493688	0.005005
LHPP	-2.525844367	0.005771
C16orf92	-2.474488605	0.006671

S7: miRNAs that were found via the meta-analysis to be differentially expressed in two or more independent studies

miRNA	Summed z score	p value
miR-107a	-2.868900156	0.00206
miR-127-5p	-2.65717017	0.00394
miR-138-5p	-3.198721	0.00069
miR-140-3p	2.993918362	0.001377
miR-145	-3.281048373	0.000517
miR-146a	-2.317784362	0.010231
miR-17-5p	-2.653813654	0.003979
miR-203a	-3.458399795	0.000272
miR-216a-5p	-2.326174307	0.010005
miR-221-3p	-2.326174307	0.010005
miR-26b	3.058968133	0.001111
miR-27a-3pa	-2.307633992	0.01051
miR-29a	-2.313010609	0.010361
miR-30a-3p	-2.092645318	0.01819
miR-337-3p	-2.81276118	0.002456
miR-338-3p	-2.909450105	0.00181
miR-373	-2.243824737	0.012422
miR-378f	-2.304561032	0.010596
miR-378i	-2.304561032	0.010596
miR-424-5p	-2.552690196	0.005345
miR-4428	-3.487387465	0.000244
miR-4716-3p	3.624771935	0.000145
miR-542-5p	-2.326174307	0.010005
miR-675-5p	-2.092645318	0.01819
miR-6795-5p	-2.615306935	0.004457
miR-6830-5p	-2.185978969	0.014409
miR-6833-5p	-2.567843907	0.005117

S8: All pathways that were found by IPA to be significantly enriched in the list of mRNAs that were differentially expressed from the meta-analysis

Ingenuity Canonical Pathways	-log(p-value)
GADD45 Signaling	3.09
Mitochondrial Dysfunction	2.9
Sirtuin Signaling Pathway	2.69
Unfolded protein response	2.68
HIF1α Signaling	2.41
Protein Ubiquitination Pathway	2.28
Role of PKR in Interferon Induction and Antiviral Response	2.26
Toll-like Receptor Signaling	2.19
Urate Biosynthesis/Inosine 5'-phosphate Degradation	2.15
BEX2 Signaling Pathway	2.13
FXR/RXR Activation	2.1
BAG2 Signaling Pathway	2.09
Hepatic Cholestasis	2.06
Cdc42 Signaling	2.04
L-cysteine Degradation II	2.01
Parkinson's Signaling	1.97
Granzyme A Signaling	1.92
Clathrin-mediated Endocytosis Signaling	1.92
Purine Nucleotides Degradation II (Aerobic)	1.88
p53 Signaling	1.79
Kinetochore Metaphase Signaling Pathway	1.78
Endoplasmic Reticulum Stress Pathway	1.75
Senescence Pathway	1.73
Glutathione Redox Reactions I	1.71
Cysteine Biosynthesis/Homocysteine Degradation	1.71
Cysteine Biosynthesis III (mammalia)	1.71
Mitotic Roles of Polo-Like Kinase	1.61
Cell Cycle: G1/S Checkpoint Regulation	1.56
Tetrahydrobiopterin Biosynthesis I	1.53
D-glucuronate Degradation I	1.53
Hypusine Biosynthesis	1.53
Tetrahydrobiopterin Biosynthesis II	1.53
Semaphorin Neuronal Repulsive Signaling Pathway	1.46
Production of Nitric Oxide and Reactive Oxygen Species in Macrophages	1.44
NRF2-mediated Oxidative Stress Response	1.43
IL-12 Signaling and Production in Macrophages	1.4
Leukocyte Extravasation Signaling	1.37
Apelin Adipocyte Signaling Pathway	1.36
STAT3 Pathway	1.35
Superpathway of Methionine Degradation	1.33
Aryl Hydrocarbon Receptor Signaling	1.33
Hereditary Breast Cancer Signaling	1.33
Pyruvate Fermentation to Lactate	1.32
Citrulline-Nitric Oxide Cycle	1.32

S8: All pathways that were found by IPA to be significantly enriched in the list of validated target genes of the miRNAs that were significantly differentially expressed from the meta-analysis

Ingenuity Canonical Pathways	-log(p-value)
Ribonucleotide Reductase Signaling Pathway	12.8
p53 Signaling	11.5
Cell Cycle: G2/M DNA Damage Checkpoint Regulation	10.8
Senescence Pathway	10.3
Molecular Mechanisms of Cancer	10.2
HIPPO signaling	9.88
Epithelial Adherens Junction Signaling	9.35
ILK Signaling	8.18
HER-2 Signaling in Breast Cancer	8.18
Protein Ubiquitination Pathway	7.61
Pulmonary Fibrosis Idiopathic Signaling Pathway	7.52
Estrogen Receptor Signaling	7.38
ID1 Signaling Pathway	7.37
Amyotrophic Lateral Sclerosis Signaling	7.04
Synaptogenesis Signaling Pathway	7
Hepatic Fibrosis Signaling Pathway	6.85
Kinetochore Metaphase Signaling Pathway	6.68
ATM Signaling	6.56
DNA Methylation and Transcriptional Repression Signaling	6.56
IGF-1 Signaling	6.55
Protein Kinase A Signaling	6.48
HOTAIR Regulatory Pathway	6.48
MiRNA Biogenesis Signaling Pathway	6.29
ERK/MAPK Signaling	6.21
Inhibition of ARE-Mediated mRNA Degradation Pathway	6.17
Colorectal Cancer Metastasis Signaling	6.17
Pyridoxal 5'-phosphate Salvage Pathway	6.1
Cell Cycle Regulation by BTG Family Proteins	5.94
IL-8 Signaling	5.89
Regulation Of The Epithelial Mesenchymal Transition By Growth Factors Pathway	5.88
PD-1, PD-L1 cancer immunotherapy pathway	5.84
Estrogen-mediated S-phase Entry	5.83
Unfolded protein response	5.82
Mitotic Roles of Polo-Like Kinase	5.79
Actin Cytoskeleton Signaling	5.77
Ferroptosis Signaling Pathway	5.74
Caveolar-mediated Endocytosis Signaling	5.73
Virus Entry via Endocytic Pathways	5.6
Role of CHK Proteins in Cell Cycle Checkpoint Control	5.46
Cyclins and Cell Cycle Regulation	5.45
Huntington's Disease Signaling	5.4
HGF Signaling	5.33
Sumoylation Pathway	5.26
CSDE1 Signaling Pathway	5.19

Mouse Embryonic Stem Cell Pluripotency	5.15
Role of BRCA1 in DNA Damage Response	5.08
RAN Signaling	5.08
Integrin Signaling	5.08
Cardiac β-adrenergic Signaling	5.05
Salvage Pathways of Pyrimidine Ribonucleotides	5.01
IL-4 Signaling	4.99
3-phosphoinositide Biosynthesis	4.97
RAC Signaling	4.88
Ephrin A Signaling	4.87
Role of Tissue Factor in Cancer	4.8
Ephrin Receptor Signaling	4.8
Reelin Signaling in Neurons	4.8
Clathrin-mediated Endocytosis Signaling	4.78
Telomerase Signaling	4.74
Pancreatic Adenocarcinoma Signaling	4.69
Regulation of the Epithelial-Mesenchymal Transition Pathway	4.64
Insulin Receptor Signaling	4.63
MSP-RON Signaling In Cancer Cells Pathway	4.63
TR/RXR Activation	4.61
Cell Cycle: G1/S Checkpoint Regulation	4.59
Docosahexaenoic Acid (DHA) Signaling	4.57
Endocannabinoid Cancer Inhibition Pathway	4.43
Iron homeostasis signaling pathway	4.43
JAK/STAT Signaling	4.38
IL-7 Signaling Pathway	4.36
Insulin Secretion Signaling Pathway	4.36
Oxytocin Signaling Pathway	4.35
Neuroinflammation Signaling Pathway	4.34
Regulation of eIF4 and p70S6K Signaling	4.32
Prolactin Signaling	4.32
Renal Cell Carcinoma Signaling	4.25
TGF-β Signaling	4.24
EGF Signaling	4.23
AMPK Signaling	4.11
Superpathway of Inositol Phosphate Compounds	4.06
Glioblastoma Multiforme Signaling	4.04
Chronic Myeloid Leukemia Signaling	4.03
RHOGDI Signaling	3.97
Glucocorticoid Receptor Signaling	3.9
D-myo-inositol (1,4,5,6)-Tetrakisphosphate Biosynthesis	3.88
D-myo-inositol (3,4,5,6)-tetrakisphosphate Biosynthesis	3.88
NRF2-mediated Oxidative Stress Response	3.85
Small Cell Lung Cancer Signaling	3.84
CDK5 Signaling	3.74
Hypoxia Signaling in the Cardiovascular System	3.68
Interferon Signaling	3.67
Renin-Angiotensin Signaling	3.63
UVB-Induced MAPK Signaling	3.59
Aryl Hydrocarbon Receptor Signaling	3.58
Granzyme B Signaling	3.58
Sirtuin Signaling Pathway	3.56
FGF Signaling	3.55
PDGF Signaling	3.55

Semaphorin Neuronal Repulsive Signaling Pathway	3.55
WNT/β-catenin Signaling	3.54
Endocannabinoid Developing Neuron Pathway	3.52
BEX2 Signaling Pathway	3.52
Hepatic Fibrosis / Hepatic Stellate Cell Activation	3.51
Opioid Signaling Pathway	3.5
RAR Activation	3.5
Coronavirus Pathogenesis Pathway	3.5
Germ Cell-Sertoli Cell Junction Signaling	3.49
mTOR Signaling	3.49
ERK5 Signaling	3.46
3-phosphoinositide Degradation	3.45
Role of p14/p19ARF in Tumor Suppression	3.45
PI3K/AKT Signaling	3.45
Human Embryonic Stem Cell Pluripotency	3.44
RHOA Signaling	3.4
Autophagy	3.38
CCR3 Signaling in Eosinophils	3.36
Ovarian Cancer Signaling	3.34
Role of OCT4 in Mammalian Embryonic Stem Cell Pluripotency	3.34
Axonal Guidance Signaling	3.33
CXCR4 Signaling	3.32
Leukocyte Extravasation Signaling	3.29
PAK Signaling	3.24
Antigen Presentation Pathway	3.22
Apelin Endothelial Signaling Pathway	3.21
Cardiac Hypertrophy Signaling	3.16
Mitochondrial Dysfunction	3.15
GADD45 Signaling	3.15
Hereditary Breast Cancer Signaling	3.14
Glioma Invasiveness Signaling	3.14
Prostate Cancer Signaling	3.12
Signaling by Rho Family GTPases	3.12
Role of JAK1 and JAK3 in γc Cytokine Signaling	3.1
EIF2 Signaling	3.08
Role of JAK family kinases in IL-6-type Cytokine Signaling	3.07
Phagosome Maturation	3.05
Regulation of Actin-based Motility by Rho	3.05
IL-2 Signaling	3.04
Nitric Oxide Signaling in the Cardiovascular System	3.03
Cleavage and Polyadenylation of Pre-mRNA	3
Tumor Microenvironment Pathway	2.98
D-myo-inositol-5-phosphate Metabolism	2.97
Paxillin Signaling	2.95
Growth Hormone Signaling	2.92
Role of PKR in Interferon Induction and Antiviral Response	2.92
Angiopoietin Signaling	2.87
GDNF Family Ligand-Receptor Interactions	2.87
Melanoma Signaling	2.87
Role of JAK2 in Hormone-like Cytokine Signaling	2.84
Remodeling of Epithelial Adherens Junctions	2.79
HIF1α Signaling	2.78
Type II Diabetes Mellitus Signaling	2.78
Neurotrophin/TRK Signaling	2.71

Cell Cycle Control of Chromosomal Replication	2.69
Circadian Rhythm Signaling	2.64
Semaphorin Signaling in Neurons	2.63
Thyroid Cancer Signaling	2.63
NAD Signaling Pathway	2.62
Tumoricidal Function of Hepatic Natural Killer Cells	2.61
eNOS Signaling	2.61
Role of NFAT in Cardiac Hypertrophy	2.61
CLEAR Signaling Pathway	2.59
CNTF Signaling	2.59
Endothelin-1 Signaling	2.58
Regulation of Cellular Mechanics by Calpain Protease	2.57
Fcγ Receptor-mediated Phagocytosis in Macrophages and Monocytes	2.55
Apelin Cardiomyocyte Signaling Pathway	2.53
Endoplasmic Reticulum Stress Pathway	2.5
Pulmonary Healing Signaling Pathway	2.49
MSP-RON Signaling In Macrophages Pathway	2.48
Glioma Signaling	2.47
Tight Junction Signaling	2.47
Thrombopoietin Signaling	2.45
FAT10 Cancer Signaling Pathway	2.42
Role of NANOG in Mammalian Embryonic Stem Cell Pluripotency	2.42
Death Receptor Signaling	2.41
Relaxin Signaling	2.41
PTEN Signaling	2.41
Apelin Pancreas Signaling Pathway	2.39
Multiple Sclerosis Signaling Pathway	2.39
1D-myo-inositol Hexakisphosphate Biosynthesis V (from Ins(1,3,4)P3)	2.39
Lymphotoxin β Receptor Signaling	2.37
Amyloid Processing	2.33
14-3-3-mediated Signaling	2.3
ERB2-ERBB3 Signaling	2.29
UVA-Induced MAPK Signaling	2.28
IL-3 Signaling	2.28
Aldosterone Signaling in Epithelial Cells	2.27
Adrenomedullin signaling pathway	2.27
PEDF Signaling	2.26
BAG2 Signaling Pathway	2.26
IL-6 Signaling	2.25
Osteoarthritis Pathway	2.25
Androgen Signaling	2.22
IL-9 Signaling	2.21
Dopamine-DARPP32 Feedback in cAMP Signaling	2.2
LPS-stimulated MAPK Signaling	2.19
Vitamin-C Transport	2.19
Macropinocytosis Signaling	2.16
Dilated Cardiomyopathy Signaling Pathway	2.16
NGF Signaling	2.14
Ephrin B Signaling	2.11
Cardiac Hypertrophy Signaling (Enhanced)	2.1
fMLP Signaling in Neutrophils	2.09
Antiproliferative Role of Somatostatin Receptor 2	2.09
Th1 and Th2 Activation Pathway	2.09
FLT3 Signaling in Hematopoietic Progenitor Cells	2.07

GABA Receptor Signaling	2.04
VDR/RXR Activation	2.02
NF-κB Activation by Viruses	2.02
MYC Mediated Apoptosis Signaling	2.02
PPARα/RXRα Activation	2
P2Y Purigenic Receptor Signaling Pathway	2
Endometrial Cancer Signaling	1.96
PCP (Planar Cell Polarity) Pathway	1.96
Production of Nitric Oxide and Reactive Oxygen Species in Macrophages	1.95
VEGF Family Ligand-Receptor Interactions	1.95
Activation of IRF by Cytosolic Pattern Recognition Receptors	1.94
Apoptosis Signaling	1.93
VEGF Signaling	1.93
Role of Macrophages, Fibroblasts and Endothelial Cells in Rheumatoid Arthritis	1.92
Role of Osteoblasts, Osteoclasts and Chondrocytes in Rheumatoid Arthritis	1.91
p70S6K Signaling	1.9
Gap Junction Signaling	1.89
Corticotropin Releasing Hormone Signaling	1.88
Role Of Chondrocytes In Rheumatoid Arthritis Signaling Pathway	1.86
Inhibition of Angiogenesis by TSP1	1.86
Estrogen-Dependent Breast Cancer Signaling	1.83
Oxidative Phosphorylation	1.83
Ceramide Signaling	1.82
IL-1 Signaling	1.82
RANK Signaling in Osteoclasts	1.82
Breast Cancer Regulation by Stathmin1	1.82
Apelin Muscle Signaling Pathway	1.81
CD40 Signaling	1.8
IL-17A Signaling in Airway Cells	1.8
GP6 Signaling Pathway	1.79
Th1 Pathway	1.79
Polyamine Regulation in Colon Cancer	1.76
Endocannabinoid Neuronal Synapse Pathway	1.74
Spliceosomal Cycle	1.73
Melanocyte Development and Pigmentation Signaling	1.72
Actin Nucleation by ARP-WASP Complex	1.71
ERBB Signaling	1.71
Phosphatidylglycerol Biosynthesis II (Non-plastidic)	1.69
NER (Nucleotide Excision Repair, Enhanced Pathway)	1.67
Adipogenesis pathway	1.67
Cardiomyocyte Differentiation via BMP Receptors	1.66
DNA damage-induced 14-3-3σ Signaling	1.64
GM-CSF Signaling	1.61
Chemokine Signaling	1.6
Dopamine Receptor Signaling	1.6
Sertoli Cell-Sertoli Cell Junction Signaling	1.6
β-alanine Degradation I	1.59
Cysteine Biosynthesis/Homocysteine Degradation	1.59
Th2 Pathway	1.58
FAT10 Signaling Pathway	1.57
Role Of Osteoblasts In Rheumatoid Arthritis Signaling Pathway	1.56
Acute Myeloid Leukemia Signaling	1.56
Xenobiotic Metabolism General Signaling Pathway	1.55
IL-22 Signaling	1.55

Leptin Signaling in Obesity	1.55
Neuregulin Signaling	1.54
Natural Killer Cell Signaling	1.51
FcγRIIB Signaling in B Lymphocytes	1.5
Regulation Of The Epithelial Mesenchymal Transition In Development Pathway	1.5
Glutamate Degradation III (via 4-aminobutyrate)	1.5
Gαi Signaling	1.46
Cholecystokinin/Gastrin-mediated Signaling	1.46
STAT3 Pathway	1.45
Macrophage Classical Activation Signaling Pathway	1.45
CDP-diacylglycerol Biosynthesis I	1.44
Inhibition of Matrix Metalloproteases	1.42
Factors Promoting Cardiogenesis in Vertebrates	1.42
SNARE Signaling Pathway	1.41
Non-Small Cell Lung Cancer Signaling	1.41
GNRH Signaling	1.38
Agrin Interactions at Neuromuscular Junction	1.38
Xenobiotic Metabolism Signaling	1.38
1D-myo-inositol Hexakisphosphate Biosynthesis II (Mammalian)	1.37
Calcium Signaling	1.37
IL-13 Signaling Pathway	1.36
Cholesterol Biosynthesis I	1.36
Cholesterol Biosynthesis II (via 24,25-dihydrolanosterol)	1.36
Cholesterol Biosynthesis III (via Desmosterol)	1.36
Apelin Adipocyte Signaling Pathway	1.31
Superpathway of D-myo-inositol (1,4,5)-trisphosphate Metabolism	1.3
IL-15 Production	1.3